Modeling the emission, transport, and fate of key micropollutants and their treatment using novel titanium dioxide nanomaterials

by

Maricor Jane Arlos

A thesis
presented to the University of Waterloo
in fulfillment of the
thesis requirement for the degree of
Doctor of Philosophy
in
Biology

Waterloo, Ontario, Canada, 2018

Examining Committee Membership

The following served on the Examining Committee for this thesis. The decision of the Examining Committee is by majority vote.

External Examiner	Dr. Graham Gagnon Professor, Department of Civil and Resource Engineering, Dalhousie University
Supervisors	Dr. Mark Servos Professor, Department of Biology, University of Waterloo
	Dr. Susan Andrews Professor, Department of Civil Engineering, University of Toronto
Internal Member	Dr. Paul Craig Professor, Department of Biology, University of Waterloo
Internal-External Member	Dr. Wayne Parker Professor, Department of Civil and Environmental Engineering, University of Waterloo
Other Member(s)	Dr. Carol Ptacek Professor, Department of Earth and Environmental Sciences, University of Waterloo

AUTHOR'S DECLARATION

This thesis consists of material all of which I authored or co-authored: see Statements of Contributions included in the thesis. This is a true copy of the thesis, including any required final revisions, as accepted by my examiners.

I understand that my thesis may be made electronically available to the public.

Statement of Contributions

The findings of this thesis are presented as co-authored papers. Chapters 2, 4, 5, and 6 have been published and Chapter 3 has been submitted to a peer-reviewed journal. I am the lead author of each paper and was responsible for the research execution and manuscript preparation and submission. My supervisors, Dr. Mark Servos and Dr. Susan Andrews, served as the anchor authors and provided significant inputs, support, and direction for each paper. All the co-authors assisted in the revision of the article for intellectual content. The specific contributions of several co-authors are presented below:

Chapter 2: Wayne Parker was involved in the analysis and interpretation of the results. Patricija Marjan provided the historical datasets required for model assumptions. Pam Law and José Bicudo from the Region of Waterloo provided the treatment plant datasets and contributed to the data interpretation.

Chapter 3: Wayne Parker was involved in the analysis and interpretation of the results. Keegan Hicks and Meghan Fuzzen provided the biological effects data. Pam Law and José Bicudo from the Region of Waterloo provided the treatment plant datasets and contributed to the data interpretation.

Chapter 4. Robert Liang was responsible for the photoreactor setup, material synthesis, and characterization. Carol Ptacek provided a significant suggestion in the experimental design. Lena Li Chun Fong completed the experiments and contributed to the drafting of the manuscript under my supervision.

Chapter 5. Robert Liang and Melisa Hatat-Fraile were responsible for the material synthesis, and characterization. Leslie Bragg provided direction in the analysis of samples via LC-MS/MS. I executed the experiments with the help of Melisa Hatat-Fraile.

Chapter 6. Robert Liang and Melisa Hatat-Fraile were responsible for the material synthesis and characterization. Leslie Bragg provided direction in the analysis of samples via LC-MS/MS. I executed the experiments with the help of Melisa Hatat-Fraile.

Abstract

Endocrine disruptive effects in fish have been observed in many watersheds worldwide. The presence of intersex (ova-testes) in particular is well-documented in the Grand River watershed in southern Ontario, and is associated with estrogenic compounds discharged from wastewater treatment plants (WWTP). However, this linkage is hard to establish since no exposure data are available to suggest the relationship. In addition, the presence of estrogens in trace amounts has become a major challenge in their analytical detection and this problem is often intensified by matrix effects. Bioassays can be employed to determine the total estrogenicity in environmental samples, but the identification of specific chemicals causing the activity is still often required. In the absence of chemical and biological activity data, modeling can be used to predict the concentrations of estrogenic compounds and estimate the exposure-response relationship in fish.

A model was employed to determine the spatial and temporal distribution of estrone (E1), estradiol (E2), and ethinylestradiol (EE2), key estrogens that are associated with intersex. The emission, transport, and fate (ETF) of these compounds were simulated in ~80-km reach of the Grand River from 2007-2015. The modeled section included the two major WWTPs in the watershed (Kitchener and Waterloo WWTPs), one of which (Kitchener) underwent major process updates (nitrification) in 2012. The emissions of estrogens from the WWTPs were first estimated using population demographics, excretion rates, and removals through the plant. Their transport and fate in the receiving water were then predicted using a mechanistic water quality model (WASP).

The model estimated relatively high emissions of E1 from both WWTPs. E1 was also predicted as the most abundant in the Grand River followed by E2 and EE2. The transport of the estrogens (advection) was observed as the primary mechanism for their distribution in the river and, therefore, flow was an important factor that influenced the environmental exposure. The highest predicted total estrogenicity in the river was associated with the Kitchener WWTP during the pre-upgrade with a low-flow (≤ 11 m^3/s) average concentration of 3.4 ± 0.9 ng/L E2 eq. The average concentration dropped to 0.7 ± 0.1 ng/L E2 eq. when the upgrades were implemented. The simulated average total estrogenicity was 0.45 ± 0.1 ng/L E2 eq. below the Waterloo WWTP

and the river concentrations were predicted to persist during low flows, such that they may influence the total exposure below the Kitchener outfall located ~20 km downstream.

The ETF model was extended to explore the relationship of predicted total estrogenicity and field-observed intersex in rainbow darter (*Etheostoma caerulum*). The distribution of intersex in the Grand River was adequately described using the four-parameter Hill equation for dose-response relationship (R^2 of 0.76 and 0.80 for incidence and severity respectively). High occurrence and severity of intersex were associated with fish exposure to ≥10 ng/L E2 eq. while concentrations that are ≤0.1 ng/L E2 eq. were predicted to cause minimal expression of intersex. The model projects that low levels of intersex will be observed after upgrades at both WWTPs are implemented. This study also predicted that estrogenicity levels associated with the currently proposed thresholds of exposure do not lead to adverse effects in rainbow darter, thus verifying the applicability of such recommendations.

The presence of estrogens and other organic micropollutants (OMPs) in water remains a major challenge as conventional treatment processes are not designed to remove these contaminants. Innovative approaches are needed to protect the public and environment health from these chemicals. Titanium dioxide (TiO_2) is a potential advanced treatment option for OMPs that has recently attracted worldwide attention. Upon photoactivation by UV, highly reactive hydroxyl radicals that can degrade organic compounds are produced. Unfortunately, studies that employ TiO_2 for the removal of OMPs require the use of solvents such as methanol to dissolve the compounds in the test solutions (i.e., resolve solubility issues). Although these carrier solvents can act as hydroxyl radical scavengers, it was found that up to 0.002 % methanol v/v could be added without having a major effect on treatment performance for the selected OMPs. Despite this result, removal of the use of carrier solvents from future studies is desirable.

Two TiO_2-based membrane materials were tested for their efficiency to remove a mixture of OMPs using UV-LED as the light source (under 0.002% methanol v/v). The materials were synthesized and immobilized onto different membrane supports using the (1) sol-gel, dip-coating method with quartz fiber membranes (QFT) and (2) thermal-chemical oxidation of porous titanium sheets (PTT). The resulting treatments were selective such that negatively charged compounds were well-removed by PTT, while the positively charged ones were degraded

efficiently by QFT. Neutral compounds remained recalcitrant during the treatment. The study suggested that for these materials, surface charge interactions play a major role in the removal of OMPs. This result is advantageous if specificity in treatment is required and may be optimized by simply adjusting the pH conditions.

PTT was additionally tested for its efficiency to remove estrogens (E1, E2, EE2, estriol [E3], and bisphenol A [BPA]) and reduce their estrogenic activity under different pH conditions (pH 4, 8, and 11). All compounds were removed efficiently (except E2) with treatments at pH 4 and 11 showing the most and least efficient removals respectively. Although E2 was poorly degraded, the total estrogenicity of the mixture was substantially reduced and followed a similar trend as for chemical removal. Although the experiments were completed at bench-scale, the results suggest that UV/TiO_2 is a promising new approach for the removal of OMPs.

In summary, this thesis estimated the emission, transport, and fate of key estrogens (E1, E2, and EE2) in the Grand River via modeling. It also provided an exposure-response relationship between estrogenicity and intersex that verified the thresholds recommended by several studies in Europe and North America. Although additional work is required to improve the predictions, the model can be employed to investigate future exposure conditions and management actions. This thesis also demonstrated the potential of UV/TiO_2 as a remediation option to treat surface waters contaminated with estrogens and a mixture of OMPs. Further investigations on the material synthesis and UV/TiO_2 treatment configurations are essential for future large-scale operation.

Acknowledgements

I would like to extend my heartfelt gratitude to many individuals who helped me throughout my PhD studies. I would like to first thank my supervisors, Dr. Mark Servos and Dr. Susan Andrews, for their unwavering support, encouragement, and guidance. You have been truly helpful during this journey and your excellent supervision has brought my PhD research to its successful conclusions. My regular interactions with you have been transformative and I am grateful for these productive relationships.

I also would like to thank my committee members, Dr. Carol Ptacek and Dr. Paul Craig, for their motivation, thought-provoking questions, and advice. A special thank you to Dr. Wayne Parker for his helpful feedback and heavy involvement while I was completing the water quality modeling project. I also would like to acknowledge the help of Dr. José Bicudo and Pam Law from the Region of Waterloo for their willingness to assist with my data needs.

I appreciate the help from the Centre for Advanced Materials Joining, especially Dr. Norman Zhou, for giving me access to his laboratory facilities. Thank you, Robert Liang, for many stimulating discussions and a very fruitful TiO_2 project collaboration. Thank you to Melisa Hatat-Fraile for sharing her expertise in TiO_2 nanomaterial synthesis and for spending long days with me in the lab. I also would like to thank the graduate students from the Drinking Water Research Group at the University of Toronto with whom I exchanged ideas during the early years of my PhD. A big thank you to Leslie Bragg for being a very effective lab manager. To all the graduate students from the Servos Lab, thank you! You have been a very positive influence and you made my four years of PhD easier.

I also would like to acknowledge the following organizations for their financial support:

- Natural Sciences and Engineering Research Council of Canada (NSERC) Postgraduate Scholarship;
- President's Graduate Scholarship – University of Waterloo;
- Waterloo Institute for Nanotechnology – Nanofellowship;
- Golder Associates Scholarship through the Water Institute;
- RBC Entrance Scholarship through the Collaborative Water Program;

- Allan Holmes Scholarship through the Grand River Conservation Foundation; and
- Conference travel funding from the Society of Environmental Toxicology and Chemistry-North America (SETAC-NA) and UW Graduate Student and Postdoc Association.

Thank you to my parents, Jena and Felipe Arlos, my sister Marie de la Pena and her family, Joed and Jared, and my brother Philip Arlos for their moral support. Thank you for being available during the difficult times. My genuine thanks to my Aunt Nina Arlos, Sue and Konrad Hahnelt, and Angele and Al Genterola for all the encouragement. I also would like to sincerely thank my in-laws, Angelika (Angi) and David Malar, for their steadfast reassurance and motivation to pursue my dreams. Also, thank you Angi for proofreading this thesis. Many thanks to the friends who helped me slow down and gave me a life outside of grad school.

Finally, I owe a heartfelt gratitude to my husband, Malcolm Jardine, for always believing in me and giving me the liberty to choose what I desired. You uplift my spirit during the toughest parts of this journey and thank you for all the support and love.

Table of Contents

List of Figures

List of Tables

Chapter 1

Introduction

Although the impacts of organic pollutants in the environment have been documented since the post-world war and the industrialization era, it was Rachel Carson's *Silent Spring* published in 1962 that ignited a movement in environmental science. The book called for scientific experts to investigate the unintended consequences and environmental implications of anthropogenic chemicals, and to support their potential regulation. Indeed, significant regulatory advances were made particularly for pesticides, and many legal measures have been developed to minimize the environmental risks associated with their use (Pimentel, 2012).

Fifty-five years later, the challenges of anthropogenic chemical regulation and remediation still haunt the modern environmental field. In particular, the presence and the potential impacts of organic micropollutants (OMPs) such as pharmaceuticals and personal care products have been articulated in several studies since the late 1990s (Daughton and Ternes, 1999; Ternes et al., 1999; Williams, 2005). OMPs span a diverse group of compounds that are present in trace amounts and may have the potential to induce adverse impacts on exposed organisms. These compounds also represent "emerging" issues in water research since the consequences of their exposure are still unknown (Petrovic et al., 2016). Furthermore, the concerns are not necessarily linked with persistence *per se*, but with the high potency of several OMPs at low concentrations. Pharmaceutical ingredients, for instance, are made to be biologically active in the target organisms (e.g. humans, livestock), and non-target species such as fish or invertebrates may not have the physiological functions to eliminate or modulate these compounds in the body (Arnold et al., 2014).

The advancements in the analytical detection of OMPs have increased the understanding of their fate and distribution in environmental compartments. A recent online database of over 120,000 entries compiled by the Federal Environmental Agency in Germany (https://www.umweltbundesamt.de) determined a total of over 600 unique pharmaceuticals detected across the globe (Figure 1.1). Of these compounds, 17 were found in all five United Nations (UN) regions, suggesting the ubiquity of OMPs in various environmental matrices worldwide.

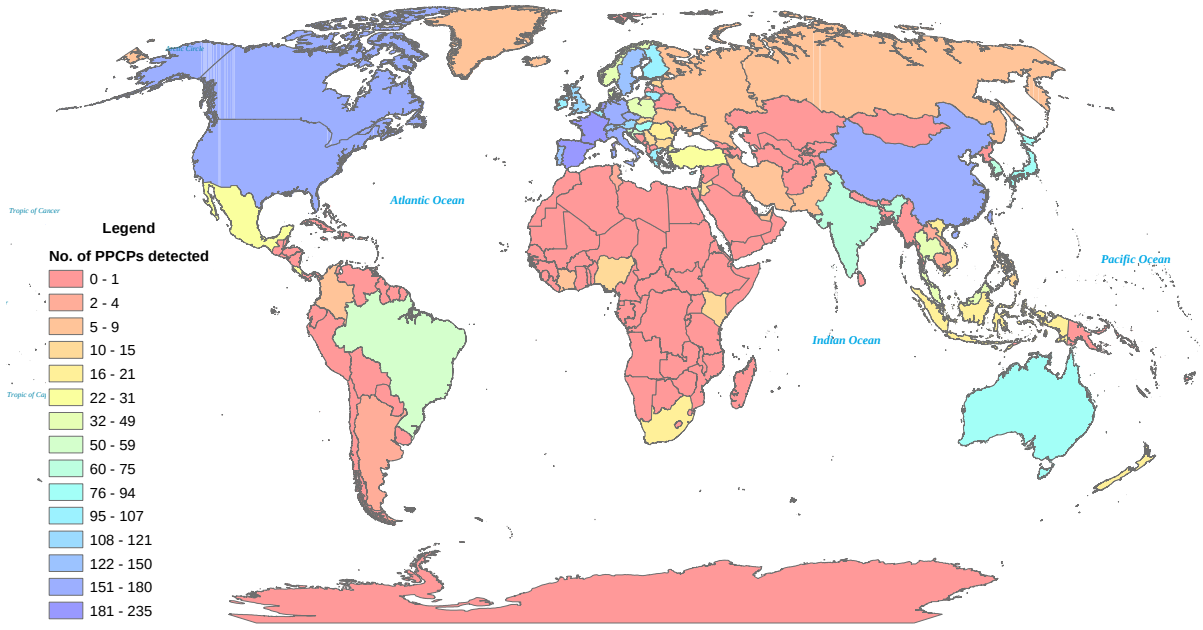

Figure 1.1 Pharmaceutical detections in surface water, groundwater, and wastewater around the globe. Raw data were taken from https://www.umweltbundesamt.de.

Threats to humans via environmental exposure are expected to be minimal due to the presence of OMPs at extremely low concentrations in most drinking water supplies (Schwab et al., 2005). However, considering the diversity of emerging contaminants and their potential mechanisms of action, it is difficult to ignore their potential risk. Jones et al. (2005) further reiterated that the future water quality may be compromised, as distances between wastewater discharge points and drinking water sources are reduced. Also, drinking waterworks may be pressured to implement process changes due to issues related to public trust rather than actual risk (i.e., users unwilling to consume water with trace chemicals) (Houtman et al., 2014). By upgrading their wastewater treatment systems to tertiary level, Switzerland is one of the countries that exemplified a proactive approach toward the reduction of OMP loadings. This work is being completed with no directives from any existing regulations and is deeply rooted in Switzerland's strong commitment to protecting their water resources (Eggen et al., 2014). In situations where many uncertainties exist while making decisions, applying precautionary measures can be a prudent approach in responding to emerging water quality issues.

Impacts of OMPs on aquatic ecosystems highlighted in many recent studies (Bean et al., 2014; Corcoran et al., 2010; Sumpter, 2009) include their effect on organism’s physiology and

behavior (Arnold et al., 2014). However, uncertainties still remain pertaining to the uptake, metabolism, and excretion of OMPs within the non-target organisms (Boxall et al., 2012; Brodin et al., 2014). Furthermore, environmental regulatory work associated with OMPs necessitates evidence of population effects (Arnold et al., 2014), but translating the individual-level observations to higher levels is difficult to implement. Evidently, more scientific work and policy debates are required to make such connections.

1.1 Sources, fate, and distribution of OMPs in the aquatic environment

The continuously growing human population has driven the use and demand for chemicals (e.g., prescription drugs) that support society (Kümmerer, 2008). As a result, municipalities and industries release a cocktail of hundreds to thousands of chemicals in wastewaters that include both the parent compounds and their transformation byproducts. Wastewater treatment plants (WWTPs) are effective barriers and have long been utilized for macropollutant removals such as nutrients (ammonia, phosphorus) and suspended solids. Although some OMPs such as ibuprofen (anti-inflammatory) and atorvastatin (antibiotic) are removed by these systems, some (e.g., carbamazepine) are recalcitrant to wastewater treatments (Salveson et al., 2012). The removal of OMPs in WWTPs are heavily reliant on microbial degradation that mainly occurs in activated sludge systems, but the exact processes associated with biodegradation are not clearly understood. However, it is widely accepted that OMPs can be eliminated via direct metabolism or co-metabolism that can result in either chemical structure alteration (e.g., conjugation, deconjugation) or complete breakdown of molecules to simpler compounds (carbon dioxide, methane, nitrate/ammonium, water). Since OMP concentrations are typically lower than other available organic compounds, co-metabolism likely plays a vital role (Ternes et al., 2004). The overall quality of the influent and WWTP operational parameters can significantly influence the processes in bioreactors, likely resulting in the co-existence of both direct and co-metabolic processes (Quintana et al., 2005; Ternes and Joss, 2007). Sorption also plays an important function in the elimination of compounds in WWTPs. It is typically influenced by the characteristics of both the treatment matrix (sludge characteristics) and the chemical's sorption potential (partition coefficient, log K_d).

The combined biodegradation and sorption characteristics of the OMPs have been used to predict their removal in WWTPs. Salveson et al. (2012), for example, developed a matrix using log K_d and biotransformation rates of select OMPs to indicate their likely removal through the plant (Figure 1.2). The behavior of WWTP operational parameters, such as the solids retention time (Clara et al., 2005), mix liquor suspended solids (MLSS) (Cao et al., 2008), and the biological oxygen demand (BOD) removal (Dotan et al., 2017) have been used as alternatives. However, there are large uncertainties surrounding these predictive tools and, when available, site-specific datasets must be employed.

Sorption, Log Kd		Biodegradation, k_b (L/g-d)			Sorption, Log Kd
		Slow <0.1	Moderate 0.1-10	Rapid 10	
	Low <2.5	0-30%	0-100% (70-90%)	70-100% (95%)	
	Moderate 2.5-3	0-60%	0-100% (30-50%)	60-100% (70%)	
	High >3	0-95%	-	0-100%	
		Biodegradation, k_b (L/g-d)			

Figure 1.2 Removal matrix of OMPs in WWTPs as suggested by Salveson et al. (2012). Numbers in parentheses represent the typical removals observed.

Although wastewater is a major point source, the pathways of OMPs into receiving waters are very diverse (Figure 1.3). For example, direct disposal from household and industries (e.g., spills) and runoff from agriculture and urban sites can also be significant sources of OMPs (Figure 1.3). The influx of OMPs from these diffuse sources can be additionally intensified by rainfall events (Wittmer et al., 2016). Regardless of the source, a dissolved contaminant that enters the aquatic environment is transported by the system through various mechanisms such as advection and dispersion. These processes are typically influenced by many factors including water flows and river hydrogeometry (e.g., roughness, bed slope). Furthermore, the contaminant can be converted into its daughter by-products during mass transformation processes via biodegradation, photolysis, and hydrolysis. It can also simultaneously partition to different environmental compartments depending on its affinity to the sediment, water, and air. The

combined processes of mass transport, transformation, and transfer make up the overall fate and distribution of the organic chemicals in the aquatic environment and are dependent on the conditions within the environmental compartment as well as the physical-chemical properties of the compound (Chapra, 1997; Mandaric et al., 2016).

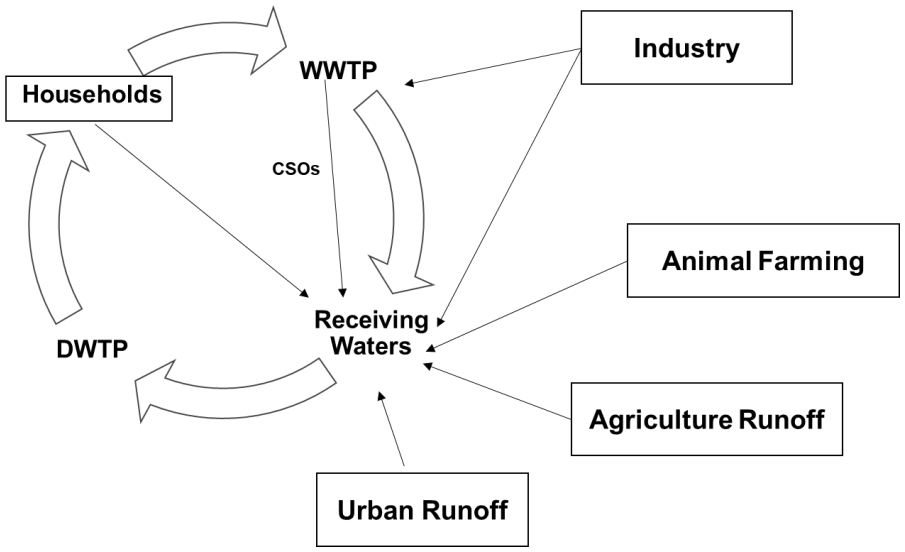

Figure 1.3 Major pathway of OMPs into the receiving water. DWTP=drinking water treatment plant, CSOs = combined sewer overflows. Adapted from Mandaric et al. (2016).

The fate of an OMP in WWTPs is often reflective of its behavior in the aquatic environment. When compounds are poorly degraded in a WWTP, they are also not well removed via biodegradation in the aquatic systems. Hence, their assimilation relies on transport conditions and other chemical transformations such as photolysis and hydrolysis. In general, photolysis has been considered an important removal process for photolabile compounds such as naproxen and triclosan (Andreozzi et al., 2003; Arlos et al., 2014; Boreen et al., 2003; Lin and Reinhard, 2005). It has been suggested, however, that transport processes (i.e., dilution) mostly contribute to the reduction of OMP concentrations in the environment (Arlos et al., 2014; Jurgens et al., 1999). Hence, flow conditions are important drivers of contaminant distribution in a water body, especially in lotic systems (rivers and streams). As residence times in river segments are much shorter than in lakes and ponds, there is less opportunity for loss via partitioning and internal

transformations since the reaction half-lives are typically in the same range or lower than the contaminant residence times (Jurgens et al., 1999). Also, loss via sorption to suspended and bed sediments of chemicals with low or moderate K_d is minimal in rivers when systems have suspended solids from 1-50 mg/L (Chapra, 1997). However, biodegradation for some OMPs could be important during periods when flows are low (typically summer) and the concentrations are not well diluted (Jurgens et al., 1999). Therefore, the distribution of OMPs in the environment can be influenced by several factors and the understanding of these processes can largely impact the assessment of their exposure.

1.2 Major classes of OMPs

OMPs can be roughly grouped as: pharmaceuticals and hormones; personal care products (PCPs); perfluorinated compounds (PFCs); plasticizers; anticorrosive agents; surfactants; emerging pesticides; and nanomaterials (Table 1.1) (Mandaric et al., 2016). Pharmaceuticals are chemicals with medicinal properties (typically synthesized to a molecular weight of <500 Da), and are moderately soluble or lipophilic depending on their targeted pharmacologic action (Petrovic et al., 2016; Williams, 2005). It is projected that newer active pharmaceutical ingredients will be manufactured as medical science continues to advance (Bound and Voulvoulis, 2005). The natural and synthetic hormones are considered potent endocrine disrupting chemicals (EDCs) and specific attention has been given to the estrogens, estrone (E1), estradiol (E2), estriol (E3), ethinylestradiol (EE2), and progestogens, due to their potential to cause endocrine disruptive effects in exposed organisms (e.g., intersex in fish) (Kidd et al., 2007; Kime, 1999). Personal care products are consumer chemicals generally intended for hygienic purposes whereas perfluorinated compounds (PFCs) are major components of consumer goods designed to repel water and oil. A few examples of PFCs are non-stick pans (Teflon), stain repellants, and food packaging. Anticorrosive agents such as benzotriazole and toltriazole are found in dishwasher tablets, and surfactants are major ingredients in laundry detergents. Plasticizers are additives in plastic materials that are commonly used in many types of food and drink containers (e.g., bisphenol A). Emerging pesticides are less toxic, highly soluble, and more biodegradable than the earlier types of pesticides (e.g., organochlorines) but their potential to exhibit sub-lethal chronic effects in exposed organisms is not yet fully understood.

Nanomaterials were added to the list because of their widespread use in consumer products (e.g., silver nanoparticles in clothing) and unknown environmental impacts (Mandaric et al., 2016). For instance, nanopharmaceuticals is an emerging trend in the pharmaceutical industry and their uses may have some unintended health consequences on non-target organisms.

Table 1.1 Major classes and examples of OMPs

OMP Group	Use	Examples
Pharmaceuticals and hormones	Medicinal properties, endocrine function	Anti-inflammatory, antidepressants, anti-epileptic, lipid-lower agent, antidiabetics, estrogens
Personal care products	Hygiene	Ingredients in fragrances, UV-filters
Perfluorinated compounds	Water and oil repellent	Perfluorooctanoic acid (Teflon)
Plasticizers	Various Industrial applications	Bisphenol A, phthalates
Anticorrosive agents	Corrosion inhibition	Dishwasher tablets
Surfactants	Reduce surface tension in water	Detergents, alkylphenols
Emerging pesticides	Pest control	Organophosphates
Nanomaterials	Various uses such as antimicrobial	Titanium oxide, zinc oxide, nanomedicines

The diversity of OMPs in the environment makes it difficult to monitor these compounds, let alone regulate their use. Many prioritization studies for assessing environmental risk and focused testing and monitoring of OMPs have been completed, but to date, clear regulatory measures related to their environmental release have not been widely applied. There has also been a call to reduce the sole reliance on end-of-pipe solutions (additional treatment processes) and to develop measures that control micro-pollution straight from the source (Metz and Ingold, 2014; Schwarzenbach et al., 2006). For example, the US Food and Drug Administration (FDA) recently banned the use of triclosan, a major ingredient in many antibacterial soaps (https://www.fda.gov/newsevents/newsroom/pressannouncements/ucm517478.htm). A popular Canadian retailer (Loblaw Companies Ltd.) made a commitment to phase out the use of microplastics, triclosan, and phthalates in the products it manufactures by the end of 2018 (http://www.cbc.ca/news/). This approach is still proven to be extremely difficult since changing the behavior of a target group on the use of OMPs does not happen rapidly (Metz and Ingold, 2014). It has been additionally suggested that the key to reducing the risk of these chemicals in the environment is to modify the current water quality policies to accommodate this complex and diverse group of compounds (Metz and Ingold, 2014). However, only a few policy frameworks

have recommended guidelines for OMPs in water. Under the Water Framework Directive, the European Union (EU) has proposed environmental quality standards for key OMPs (E2, EE2, and diclofenac) and mandated its member countries to monitor these compounds (European Commission, 2012). In Canada, only the province of British Columbia has approved a water quality guideline for a pharmaceutically-active compound in freshwater (i.e., EE2). The absence of benchmarks for other OMPs is likely associated with the lack of strong mechanistic linkages that relate stressor concentrations (exposure) to higher level effects (e.g., population and ecosystem level effects). It is then advisable to conduct further research and monitoring to characterize the potential risks of these compounds to the aquatic environment.

1.3 Monitoring of OMPs: To measure or to model?

Currently, the monitoring of trace organic contaminants in the environment relies heavily on chemical analyses. Over the years, sophisticated chemical analyses such as the high resolution/tandem mass spectrometry have improved the understanding of the fate and transport of OMPs in the aquatic environment (de Witte et al., 2011). However, the chemical monitoring of these trace chemicals only quantifies the presence of individually known contaminants (Escher and Leusch, 2012). Some studies have utilized biological assessments (i.e., bioassays) to detect the presence of total biological activity that chemical analyses cannot directly identify (Coleman et al., 2004; Marinho et al., 2013; Ohko et al., 2002). These techniques examine the combined biological activity in a mixture, and can provide an indication of the potential biological responses in organisms exposed to complex mixtures (without identifying the specific chemicals).

A number of bioassays have recently become available to monitor the water quality of different water matrices ranging from surface water to municipal and industrial wastewater effluents (Escher and Leusch, 2012). Yeast-based assays transfected with a selected response element (e.g., estrogen receptor) have been designed for screening and testing for endocrine disrupting responses (i.e., compounds) in water and effluents for some time. Although the emphasis in the past has been on hormone-mimicking activity (e.g., estrogen and androgen agonists), there are numerous mechanisms or adverse outcome pathways that can alter the organism performance (Ankley et al., 2010).

Site-specific chemical and bioassay monitoring are desirable, but the large number and diversity of OMPs, and the cost and technical issues of measuring them, make the exposure assessment difficult. For example, the data gaps can be associated with past exposures which can no longer be monitored. The use of modeling techniques has been suggested as an alternative tool in situations when chemical and bioanalytical data are unavailable or are not feasible to implement. As a cost-effective approach to predicting environmental concentrations, models can evaluate the current and future strategies to mitigate the OMP discharge into the environment. Many studies also advocate the use of models to design hypothesis-based monitoring frameworks that can evaluate the exposure to newly synthesized chemicals.

1.3.1 Modeling approaches used in OMP fate and transport

Models can be used to estimate emissions from sources and predict the fate and transport of OMPs in aquatic systems. Point source emission models rely heavily on population demographics, usage rates or sales data, excretion rates, and removal through WWTP. Elaborate work has also been completed to include emissions from diffuse sources (e.g., urban and agricultural runoff) by quantifying runoff dynamics during rain events (Wittmer et al 2016). This modeling approach is a critical aspect in exposure assessment as it quantifies the loadings of target OMPs into the receiving environment.

Fate and transport modeling involves the prediction of OMP concentrations in the aquatic system following its release. Several models with varying complexities and applications are currently available. For example, the Mackay Level III and the European Union System for the Evaluation of Substance Modelling (EUSES) apply the fugacity principles that quantify the transfer of contaminants in various environmental compartments (Roig and D'Aco, 2016). GIS-based or catchment models such as GREAT-ER and PhATE have been increasingly used due to their direct applications in risk assessment. However, catchment-based models may not have accurate predictions at the local scale (specific river reach) since they are rather focused on the gross prediction of OMP distribution in catchments. Small-scale models that use hydrodynamics such as the Water Quality Simulation Program (WASP) and MARS 3D can be applied to investigate the near-field exposure to OMPs (e.g., downstream of WWTPs).

Considering the diversity of the models for OMP exposure assessment, it is critical to identify their limitations when making predictions. Models are often simplified versions of the environmental system and the estimates they provide have associated uncertainties. Whenever possible, it is often recommended to have a few measured data to validate their applicability when assessing exposure conditions.

1.4 Assessment of sub-lethal effects associated with OMP exposure

It is widely accepted that OMP exposure will likely result in sub-lethal effects in many organisms. Environmental concentrations of OMPs occur at low concentrations (ppb to ppt), with acute effects only resulting upon exposure to high concentrations. Exposure conditions in the environment are also characterized by long durations (e.g., WWTP effluent exposure), sometimes occurring over the organism's entire life cycle. Also, changes in biological functions can occur at very low exposure to one or more chemicals acting on specific and sensitive mechanisms (e.g., endocrine disruption). As a result, the observed effects in the environment are often associated with exposure to complex mixtures that are challenging to link to a specific contaminant or pollution source (Arnold et al., 2013).

Sub-lethal effects are often quantified based on five fitness-related endpoints: growth, behavior, reproduction, development, and physiology. An extensive body of literature now exists that documents these effects in response to OMP exposure for many invertebrate and vertebrate species (reviewed in Corcoran et al., Fent et al., 2006, Hamilton et al, 2015). For example, laboratory exposure studies of several fish species to antidepressants have shown behavioral changes with regard to territorial aggression and predation behavior (Gaworecki and Klaine, 2008; Perreault et al., 2003) Several field surveys across the globe have observed the widespread occurrence of feminized male fish (intersex) collected downstream of a WWTP effluent outfall (Fuzzen et al., 2015; Hicks et al., 2017; Jobling et al., 1998; Jobling et al., 2006). Many studies further associated this effect to the presence of potent estrogens such as EE2 (Desbrow et al., 1998). Interestingly, Kidd et al. (2007) demonstrated the collapse of fathead minnow population when exposed to only 4-6 ng/L of EE2. However, despite the overwhelming evidence that associates estrogen exposure to endocrine disruption, there is still difficulty in linking stressor concentrations to individual/population level effects. For example, Johnson and

Sumpter (2016) argued that the sewage effluent concentration of estrogens is typically ~0.5 ng/L in Europe and 95% of their rivers contain <0.1 ng/L. Effects on population are highly unlikely considering that it requires 5 ng/L to initiate a population collapse (Kidd et al., 2007). Johnson and Chen (2017) followed up on this hypothesis by predicting the mean total estrogenicity in five UK rivers, and found that there is no relationship between the average predicted estrogenicity and the fish density observed for 17 years. However, they recognize that there are situations when much higher concentrations may have been (or continue to be) discharged and adverse impacts could conceivably have happened. Although male fish with some intersex can still reproduce (Hamilton et al., 2014) and fish populations are relatively resilient to chronic exposure to WWTP effluents (Johnson and Chen, 2017), subtle changes in reproductive performance in fish are still a concern.

The effects analysis for chemicals is reliant on standardized laboratory tests that determines the lowest observed effect concentration (LOEC) through hypothesis-testing or an effective concentration (ECx) using a regression-based approach (point estimate). When sufficient data are available for all species, the LOECs and/or point estimates (typically EC10) can be used to generate a species sensitivity distribution (SSD) to calculate the predicted no effects concentration (PNEC). In typical risk assessment, PNECs are compared to predicted effects concentrations (PECs). The ratio of PNEC to PEC known as the risk quotient (RQ) is then calculated. When RQ is >1 then there is a potential adverse impact and if RQ<1, then the compound concentration is considered ‘safe’ or ‘acceptable’. However, it has been debated that this classical method of environmental risk assessment is lacking the ability to resolve the time-varying predictions from fate models – i.e., toxicity is not necessarily described by a single value, but by the dynamics of environmental exposure (Ashauer et al., 2011; Jager, 2016). In addition, fish species that are used in laboratory studies have been selected for practical reasons and may not be representative of the target species of concern. Laboratory studies are also conducted in optimal conditions and, in some cases, have been completed over a short duration, while some adverse effects can manifest at later life stages (Lange et al., 2009) or after several generations (Jeong et al., 2015). Hence, whenever possible, it is advisable to link the measured or predicted concentrations to the field-observed effects (as opposed to laboratory effects) that

occurred over a reasonable spatial and temporal scale. Obviously, this is a difficult approach and often very resource intensive, but realistic conclusions and causal linkages cannot be drawn without complementing laboratory effects data with field-based information.

1.5 Available treatment processes for the removal of OMPs

Over the past decade, advancements have been made in understanding the degradation of OMPs in drinking water and wastewater. It is now well understood that conventional treatment systems only remove OMPs partially; some compounds exhibit relatively high resistance to treatment (e.g., carbamazepine). Considering that direct potable water reuse is becoming more accepted globally, the removal of OMPs from water and wastewater to protect human and environmental health will remain a priority for researchers and water managers. Many approaches are being investigated and employed to remove OMPs. Advanced oxidation processes (AOPs) are considered to be a viable option. They use reactive oxygen species (e.g., hydroxyl radicals [·OH] and superoxide ions [$\cdot O_2^-$]) to oxidize and potentially mineralize organic compounds. Widely investigated AOPs include processes using ozone (O_3), ultraviolet/hydrogen peroxide (UV/H_2O_2) processes, Fenton and photo-Fenton processes (Fe^{2+}), and heterogenous AOPs that incorporate adsorptive and oxidative properties of photocatalysts such as titanium dioxide (TiO_2) (Muruganandham et al., 2014; Naddeo et al., 2010).

Ozonation is widely used because of its high oxidation power (Silva et al., 2017). Ozone can be coupled with H_2O_2, UV, or both, and the combined processes of $O_3/UV/H_2O_2$ have been shown to be effective in the treatment of highly polluted effluents (Muruganandham et al., 2014). When paired with UV, O_3 is considered more stoichiometrically efficient than H_2O_2 as it produces more hydroxyl radicals for the same oxidant concentration. However, UV/O_3 has higher energy requirements than UV/H_2O_2. Fenton processes can be combined with H_2O_2 to generate radicals, and the oxidation process happens via the following steps: pH adjustment, oxidation reaction, neutralization/coagulation, and precipitation (Muruganandham et al., 2014). Organic compounds are typically removed during the oxidation and coagulation steps.

1.5.1 Titanium dioxide (TiO_2) photocatalysis as an advanced oxidation process

UV/TiO_2 treatment has been viewed favorably in water treatment studies because of its excellent ability to remove persistent OMPs (Friedmann et al., 2010). TiO_2 acts as a photocatalyst: when activated by light, an electron from the valence band moves to the conduction band, adding a free electron (e^-) in the conduction band but leaving an electron hole (h^+) in the valence band (Figure 1.4). This excitation creates an ideal condition for redox reactions upon the contact of the charge carriers (e^- and h^+) with electron acceptors (e.g., oxygen) and donors. Reactive oxygen species (ROS) are often produced that can attack organic molecules. Ultimately, complete mineralization may be achieved where carbon dioxide and water are produced. However, if there are no available compounds that can interact with the energy carriers (h^+ and e^-) the energy is dissipated as heat via charge recombination.

TiO_2 in nanoscale forms can be synthesized in several ways, producing different crystal structures, such as anatase and rutile. These crystalline structures have different reactivities, but anatase is superior to rutile because of its more open structure and larger band gap. P25 is a commercial form of TiO_2 containing mostly anatase and is typically used as the standard material against which newly synthesized TiO_2 nanomaterials are compared.

Many studies have demonstrated the effectiveness of UV/TiO_2 in the removal of OMPs including steroidal estrogens (Benotti et al., 2009; Coleman et al., 2004; Frontistis et al., 2012), analgesics (Benotti et al., 2009), and antibiotics (Elmolla and Chaudhuri, 2010). The TiO_2 nanoparticles used for photocatalytic degradation can be structurally modified to improve their efficiency and specificity in removing target pollutants (Lu and Pichat, 2013). Several studies have evaluated different experimental parameters to optimize treatment efficiency (Kanakaraju et al., 2014), such as the impact of TiO_2 loading, the initial concentration of OMPs, solution pH, and water matrix. The possible use of sunlight as an energy source to drive the OMP degradation process has also made TiO_2 photocatalysis a favorable option especially when economic savings are a priority.

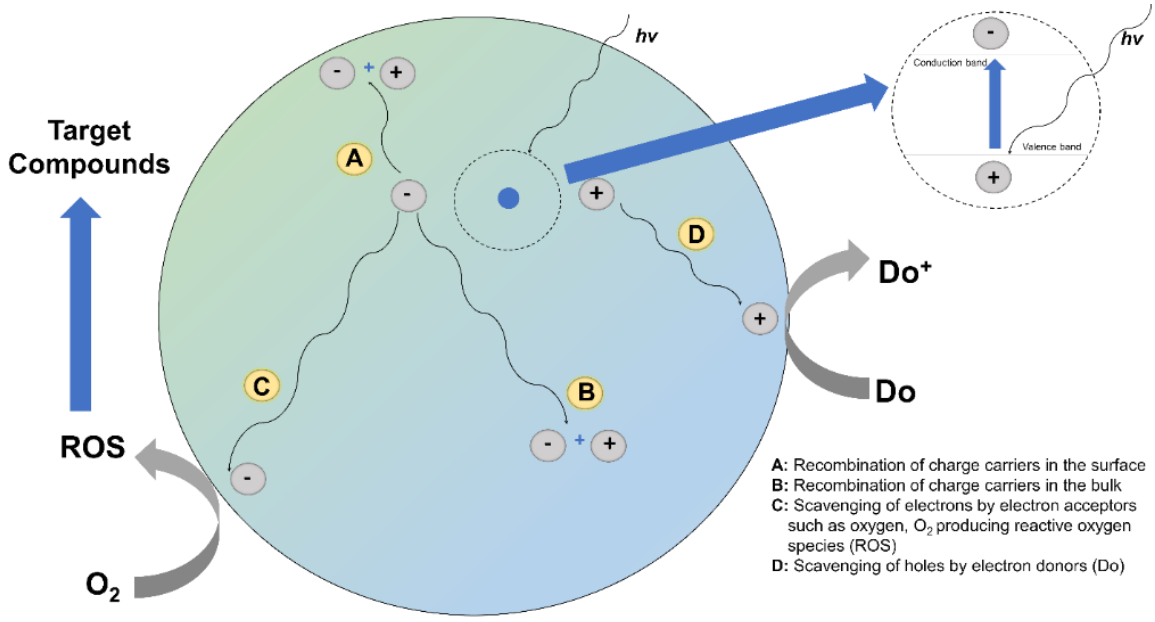

Figure 1.4 Photocatalytic degradation mechanism of organic compounds using TiO_2. Photon energy (*hv*) equal to or greater than the bandgap energy of TiO_2 excites the electron in the valence band and migrates to the conduction band. This process creates an electron-hole pair which can interact in the surface or bulk via mechanisms described in A to D.

1.5.2 The potential application of immobilized TiO_2 in water treatment

Photocatalytic activity mainly occurs on the surface of TiO_2. As a result, it is highly recommended that nanomaterials be synthesized with a smaller particle size and a high surface-to-volume ratio. However, the potential application of TiO_2 in large-scale water treatment operations is limited, because TiO_2 must be recovered or else it may eventually find its way into wastewater, surface water, and drinking water. Immobilization of TiO_2 on/in supports is a good option. There are several ways to do this (Table 1.2), each having advantages and disadvantages. The annealing stage of the immobilization process is crucial to enhancing the photocatalytic activity of the new material. It has not yet been determined which technique(s) is (are) superior, primarily because of the variability in the synthesis optimization processes and experimental designs in the studies conducted to date (Varshney et al., 2016).

Table 1.2 Techniques for TiO_2 immobilization. Text taken from Varshney et al. (2016) with permission from Elsevier.

Method	Advantages	Disadvantages
Sol-gel	- Simple and produces homogeneous material - Good bonding of TiO_2 to support - Suitable for different substrates including silica/glass, stainless steel, and aluminum plates	- Deposition requires a long period - Requires high temperature to anneal anatase form - Difficult to attach thick layer of TiO_2 nanoparticles
Doctor-blade	- Simple and requires fewer materials - Low cost and straightforward - Mass production of electro-ceramic thick films is possible	- Slow evaporation - Can aggregate or crystallize easily
Chemical vapour deposition (CVD)	- Uniform and reproducible films - Can be deposited to any substrate shape - Can be used for inner pipe surface or on flexible substrates	- High cost and reaction temperature - Low deposition rates - Safety conditions during synthesis (corrosive gas)
Plasma enhanced CVD	- Low temperature synthesis - Good adhesion and high deposition rate - Good on multilayer films	- High equipment cost - Toxic by-products
Hydrothermal	- Simple operation - Can grow large high-quality crystals during operation	- Autoclaves required - Difficult to observe crystals while they are being synthesized
Electrophoretic deposition	- Simple and cheap - Homogeneous material - Thick and uniform films can be produced	- High electric field strength required to deposit particles toward electrode - Flammable and volatile process (toxicity)
Sputtering deposition	- High-quality and uniform films - Process can be manipulated easily - Low melting point material can be used as substrates	- Porous, grainy material - Substrate damage because of ionic bombardment
Spray pyrolysis	- Well controlled stoichiometry and homogenous material - Low operational cost	- Non-uniform coating

1.5.2.1 Photocatalytic membrane reactor configurations

The synthesized nanomaterials can be incorporated in a photocatalytic membrane reactor (PMR). A PMR is a hybrid reactor that is characterized by both separation (membrane) and photocatalytic oxidation capabilities. PMRs can be coupled in various configurations, such as those presented in Figure 1.5. These PMRs are not limited to immobilized TiO_2; some have TiO_2 in slurry. Slurry PMRs must be coupled with separate membrane filtration techniques such as ultrafiltration or nanofiltration.

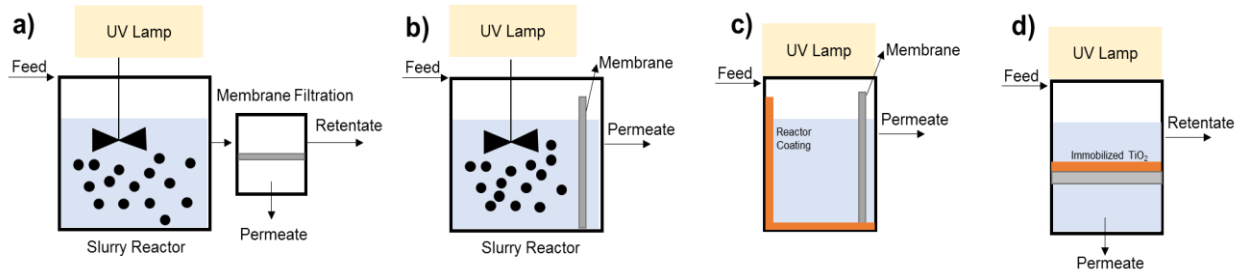

Figure 1.5 Different configurations for PMRs: (a) slurry reactor followed by a membrane filtration system (photocatalyst not immobilized); (b) slurry and membrane filtration within one reactor; (c) photocatalyst-coated reactor and membrane filtration; and (d) immobilized photocatalyst on membrane supports.

PMRs with TiO_2 slurry and those with immobilized TiO_2 each have advantages and disadvantages. PMRs that employ TiO_2 slurry typically have better removals than PMRs with immobilized TiO_2, but passage of TiO_2 through the membrane filtration causes fouling, resulting in low-quality permeate (Mozia, 2010). In PMRs with immobilized TiO_2, fouling can be mitigated by enhancing the hydrophilicity of the membrane (this can be optimized during membrane synthesis). The immobilized membrane also has self-cleaning capabilities during UV irradiation because of the continuous decomposition of organic membrane materials on the surface of TiO_2 (provided that UV exposure is long enough) (Iglesias et al., 2016).

The design configurations of PMRs are limited by the size and type of commercially available UV lamps (Leong et al., 2014; Mozia, 2010). Lamps can be placed outside the reactor with a quartz or Plexiglas window through which the light can penetrate. Alternatively, they can be submerged within the reactor, but this requires the use of borosilicate or glass jackets for additional lamp protection. There have been studies that employed solar light as an energy-efficient alternative to UV light, but the TiO_2 synthesis in these studies required metal or non-metal doping for the material to function well (Charanpahari et al., 2012; Xu et al., 2009). A few studies have employed UV-LED as the light source because it provides flexibility in various configurations (Natarajan et al., 2011). With this many design options, it is important to optimize the reactor configuration before commercialization and provide appropriate strategies for maintaining the reactor and nanomaterial reuse.

1.6 Thesis problem statement

The ubiquity of OMPs in the water cycle is evident. Hence, there is a need to characterize their presence and monitor their potential effects in exposed organisms. Characterization of spatial and temporal variability in exposure is a critical step in understanding the risk posed by these pollutants. In addition, modeling the transport and fate of OMPs in watersheds will enable researchers and water managers to quantify and predict the exposure when chemical and biological measurements are not available. There is also a need for innovative technology to degrade a variety of emerging and priority OMPs from water. TiO_2 photocatalytic degradation is a promising new approach that is currently being developed. However, the effectiveness of TiO_2 for the removal of OMPs remains unknown.

1.7 The Grand River watershed as the model watershed

The Grand River watershed in southern Ontario has a drainage area of ~6,800 km^2 with a population of close to 1 million (Figure 1.6). The watershed drains into the eastern basin of Lake Erie and its land use is 70% agricultural and 30% urban with the following major cities: Kitchener, Waterloo, Cambridge, Guelph, and Brantford. These urban areas are among the fastest growing cities in Canada and the watershed population is projected to increase by 36% by 2040. In addition, the Kitchener and Waterloo WWTPs are two of the main point sources in the watershed, contributing ~10% and ~5% of the total river flow, respectively. The areas downstream of these plants are severely impacted by the high concentrations of nutrients in the wastewater (Loomer and Cooke, 2011) and are exposed to elevated concentrations of pharmaceuticals and personal care products (Arlos et al., 2015; McCann, 2016; Metcalfe et al., 2010). A variety of pharmaceuticals have been identified in tissues of both caged and wild fish downstream of the Kitchener WWTP (Togunde et al., 2012; Wang et al., 2011), suggesting that OMPs can accumulate in fish.

Clear biological responses to WWTP effluent exposure have been documented in fish, including changes in the exposed organism's stress response (Ings et al., 2011) and metabolic performance (Ings et al., 2012). Impacts on higher level endpoints including population

dynamics (Tetreault et al., 2011) and community assemblages (Hicks, 2017; Tetreault et al., 2013) have also been observed in areas downstream of WWTP discharges.

Reproductive effects in male rainbow darter (*Etheosoma caerulum*) from the cellular level to higher levels of biological organization have been documented in the Grand River since 2007. For example, changes in the mRNA expression of vitellogenin (a protein associated with egg-yolk formation in females) have been observed in rainbow darter exposed to Kitchener and Waterloo WWTP effluents (Bahamonde et al., 2014; Fuzzen et al., 2016), along with major transcriptomic responses (Marjan et al., 2017a; Marjan et al., 2017b) and a reduction in *in vitro* steroid production (Marjan et al., 2017c) in male rainbow darter. Intersex, a condition characterized by the simultaneous presence of male and female reproductive physiology, is a consistent endpoint that can be used to evaluate endocrine disruption in the watershed (Fuzzen et al., 2016). Although intersex fish have been shown to reproduce in the lab, severely intersex males have reduced reproductive success (Fuzzen et al. 2015).

Despite the prevalence of reproductive responses to wastewater effluent, the specific chemicals responsible for these effects have not been clearly identified. Natural and synthetic estrogens (e.g., estradiol, ethinylestradiol, bisphenol A, and nonyl/octylphenols) have been linked to endocrine disruption in municipal wastewaters, but measurements of these chemicals in the Grand River are not available. Bioassays (e.g., yeast estrogen screen assays) have been used to measure estrogenicity in WWTP effluents but the data are sporadic and are not sufficiently detailed for a direct comparison with effects data.

The two major WWTP facilities in the Grand River were recently upgraded (Figure 1.7). The Kitchener WWTP was upgraded in August 2012 to include nitrification systems. Minor aeration upgrades at the Waterloo WWTP were completed in 2014 but a major infrastructure upgrade is underway. While recent studies have shown that rainbow darters are recovering (Hicks et al., 2017; Marjan et al., 2017b), the lack of chemical exposure data for estrogens limits the scope of the assessment. Modeling of estrogens is one way to predict exposure concentrations across the watershed and examine the linkages with biological responses.

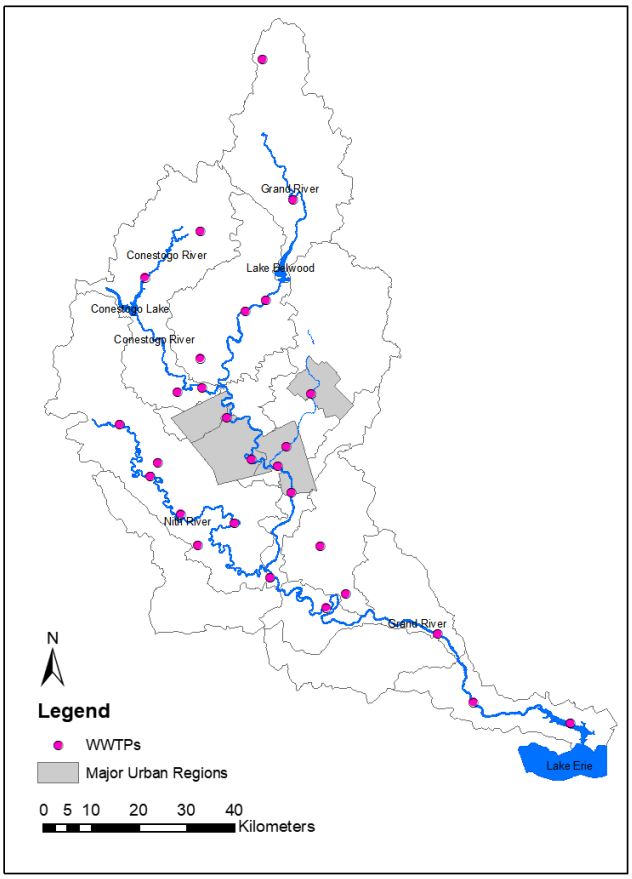

Figure 1.6 Map of the Grand River watershed and WWTPs.

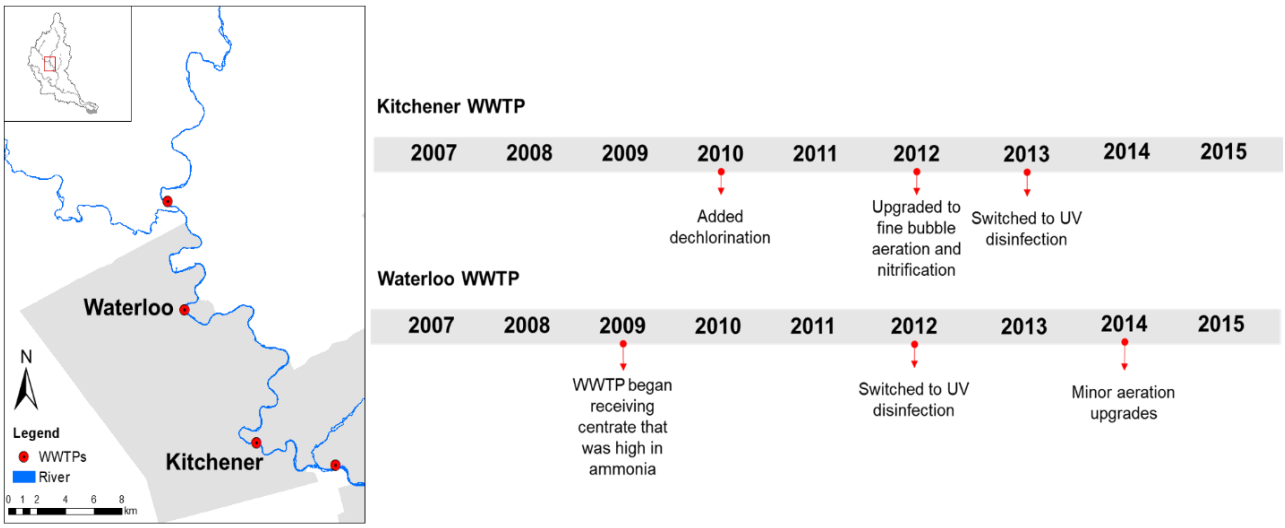

Figure 1.7 WWTP changes and upgrades from 2007 to 2015**.**

1.8 Research objectives

This thesis aims to characterize the presence of key estrogens (estrone, estradiol, and ethinylestradiol) in the WWTP effluents and in the Grand River. The primary goal is to predict the river concentrations of estrogens and link them to the field-reported biological effects (i.e., intersex). Since the concentrations of estrogens are currently below the analytical detection limits in the Grand River, this work was completed using a mechanistic modeling approach that estimated the temporal and spatial variability in effluent and river concentrations. This thesis provides a tool for quantifying the emissions of significant OMPs that can be used as a baseline for future remediation efforts.

There is a potential for UV-irradiated TiO_2 to be employed as a treatment strategy for the removal of OMPs from the Grand River. This thesis also aims to investigate the efficiency of newly synthesized TiO_2 nanomaterials immobilized on/in supports using the sol-gel/dip-coating and thermal-chemical oxidation techniques. Bench-scale experiments were conducted to assess experimental design issues (i.e., the use of carrier solvent) and the reaction kinetics associated with the removal of OMPs and their associated biological activity. The following specific objectives were established:

Objective 1: Predict the estrogen loadings into the Grand River using an emission modeling approach based on population demographics, consumption/usage rates, and removal through the plant (Chapter 2).

Objective 2: Estimate the estrogen concentrations in the Grand River and establish a relationship between the predicted concentrations in the river and the observed effects on rainbow darter (intersex) (Chapter 3).

Objective 3: Describe the effect of carrier solvents (methanol) during TiO_2 photocatalysis when conducting bench-scale experiments (Chapter 4).

Objective 4: Assess the efficiency of two types of immobilized TiO_2 membrane materials in removing a mixture of representative OMPs to provide insights into the mechanisms of chemical removal (Chapter 5).

Objective 5: Determine the ability of the newly synthesized materials to remove a mixture of key estrogens and their associated estrogenic activity (Chapter 6).

The final chapter (Chapter 7) integrates the findings of all the thesis data chapters and discusses the scientific contribution of this thesis to micropollutant research. Perspectives and recommendations for future studies are also provided.

Chapter 2

Multi-year prediction of estrogenicity in municipal wastewater effluents

Modified from the Science of the Total Environment, 610-611, M.J. Arlos, W.J. Parker, J.R. Bicudo, P. Law, P. Marjan, S. A. Andrews, and M.R. Servos. Multi-year prediction of estrogenicity in municipal wastewater effluents, 1103-1112, Copyright 2018, with permission from Elsevier.

2.1 Chapter summary

In this study, the estrogenicity of two major wastewater treatment plant (WWTP) effluents located in the central reaches of the Grand River watershed in southern Ontario was estimated using population demographics, excretion rates, and treatment plant-specific removals. Due to the lack of data on estrogen concentrations from direct measurements at WWTPs, the treatment efficiencies through the plants were estimated using the information obtained from an effects-directed analysis. The results show that this approach could effectively estimate the estrogenicity of WWTP effluents, both before and after major infrastructure upgrades were made at the Kitchener WWTP. The model was then applied to several possible future scenarios including population growth and river low flow conditions. The scenario analyses showed that post-upgrade operation of the Kitchener WWTP will not release highly estrogenic effluent under the 2041 projected population increase (36%) or summer low flows. Similarly, the Waterloo WWTP treatment operation is also expected to improve after the upgrades have been fully implemented and is expected to effectively treat estrogens even under extreme scenarios of population growth and river flows. The developed model may be employed to support decision making on wastewater management strategies designed for environmental protection, especially for reducing the endocrine effects in fish exposed to WWTP effluents.

2.2 Introduction

Human pharmaceutical compounds act on molecular targets (e.g., enzymes and receptors) to produce the desired level of therapeutic effect. These targets are highly conserved across many aquatic vertebrates and invertebrates (fish and mollusks), suggesting that the exposure of non-target species to pharmaceuticals can have damaging effects (Huggett et al., 2005). In particular, some fish species show a large percentage of similarities to the estrogen receptor in humans (Dang, 2010), and their laboratory exposure to estrogenic compounds have been shown to produce endocrine disruptive effects (Tyler et al., 1998).

Endocrine disruption in wild fish species is associated with the presence of estrogenic compounds that can be discharged to receiving environments from municipal wastewater treatment plants (Jobling et al., 2006; Vajda et al., 2008; Woodling et al., 2006). The occurrence

of natural and anthropogenic hormones (e.g., estrone [E1], estradiol [E2] and ethinylestradiol, [EE2]) in wastewater effluents is of foremost concern due to their high potential to induce endocrine abnormalities in fish (Kime, 1999; Nash et al., 2004; Sumpter, 1998). The exposure of male fish to estrogenic compounds has been found to manifest in different levels of biological organization including changes in hormone levels, testicular structure (ova-testis), and male mating ritual behavior as shown in laboratory and field experiments worldwide. Field studies in the U.S. and the U.K. have suggested that endocrine-active chemicals such as EE2 and various alkylphenols detected in wastewater effluent have likely compromised the reproductive health of wild fish species (Jobling et al., 2006; Kime, 1999; Vajda et al., 2008; Woodling et al., 2006).

Although significant advances in analytical chemistry have been made in the last two decades, the detection of estrogens in wastewater matrices remains challenging due to high matrix effects that can either suppress or enhance the analytical signals (Kebarle and Tang, 1993). The annual average environmental quality standards proposed for E2 and EE2 in the European Union (EU) are 0.4 ng/L and 0.035 ng/L respectively for inland surface waters (European Commission, 2012), which are well below the current detection limits of many analytical methods. Since environmental exposure is fundamental to risk assessment, the lack of sufficient data can limit the evaluation of the burden of estrogens on aquatic environments.

The Grand River watershed in southern Ontario, Canada receives discharges from 30 WWTPs and has been employed as a platform to characterize wastewater impacts on wild fish. The watershed has been the subject of many studies that evaluated the responses of rainbow darter (*Etheostoma caeruleum*) to municipal wastewater effluent exposures. Changes in gene expression, stress response, male fish feminization (intersex), and fish community assemblages have been reported (Bahamonde et al., 2014; Fuzzen et al., 2016; Hicks, 2017; Hicks et al., 2017; Ings et al., 2012; Tanna et al., 2013; Tetreault et al., 2011). The severity of these biological responses is typically higher downstream of the two major WWTPs (Kitchener and Waterloo WWTPs; Figure 2.1). However, important and key linkages to biological responses of fish and the stressor concentrations have not been fully established due in part to the lack of consistent measurement of estrogens in both the wastewater effluents and in the receiving water body. Chemical measurements via LC-MS/MS have been attempted but were unsuccessful due to

issues associated with matrix effects (signal suppression). Another approach is to measure estrogenicity using bioassays (YES) as they are more robust. However, bioassays only provide an estimate of total estrogenicity and individual chemicals that cause estrogenicity are not identified.

An alternative to chemical and bioassay measurements is to estimate loadings into the receiving body based on population demographics, drug consumption patterns, excretion rates, and removals through wastewater treatment. Successful approximations of effluent concentrations using this approach have been reported by many studies (Jobling et al., 2006; Johnson and Williams, 2004; Ottmar et al., 2013; Sumpter et al., 2006; Zhao et al., 2013). Furthermore, ter Laak et al. (2014) have shown that pharmaceutical sales data and compound-specific excretion rates are good indicators of most pharmaceutical loadings to Dutch and Belgian WWTPs. Fleming et al. (2016) adopted the model of Johnson and Williams (2004), refined the demographic profiles and associated parameters, and estimated estrogen concentrations at different WWTP process units.

In this study, temporally varying concentrations of target estrogenic compounds E1, E2, and EE2 in Kitchener and Waterloo WWTP effluents were estimated using data on population demographics, consumption patterns, excretion rates, and WWTP treatment efficiency using an approach similar to the work of Johnson and Williams (2004). Since site-specific information on estrogen removals through the plants was not available and the information from the literature on removals is highly variable (Teske and Arnold, 2008), plant-specific treatment efficiencies were estimated using a separate dataset obtained from an effects-directed analysis (EDA) of the WWTP effluents. The predictions were then compared against a multi-year data set (2009 to 2015) including periods when major treatment plant upgrades came into operation to verify the validity of the approach. This study combined currently available datasets including past environmental diagnostics on municipal WWTP effluents and straightforward calculations to estimate the concentrations of target estrogens entering the receiving environment. The overall goal was to develop an approach that can be incorporated into the future decision support systems that facilitate the assessment of WWTP upgrades.

2.3 Materials and methods

2.3.1 Site details

The Kitchener and Waterloo WWTPs are both located in the central Grand River watershed and serve a total population of 219,000 and 98,000 respectively. Both plants were designed for carbonaceous biological oxygen demand (cBOD) and total suspended solids removal through conventional secondary treatment and chemical phosphorus removal. Upgrades have occurred over time and information on the WWTP treatment process is shown in Figure 2.1 and is also described in detail in Hicks et al. (2017).

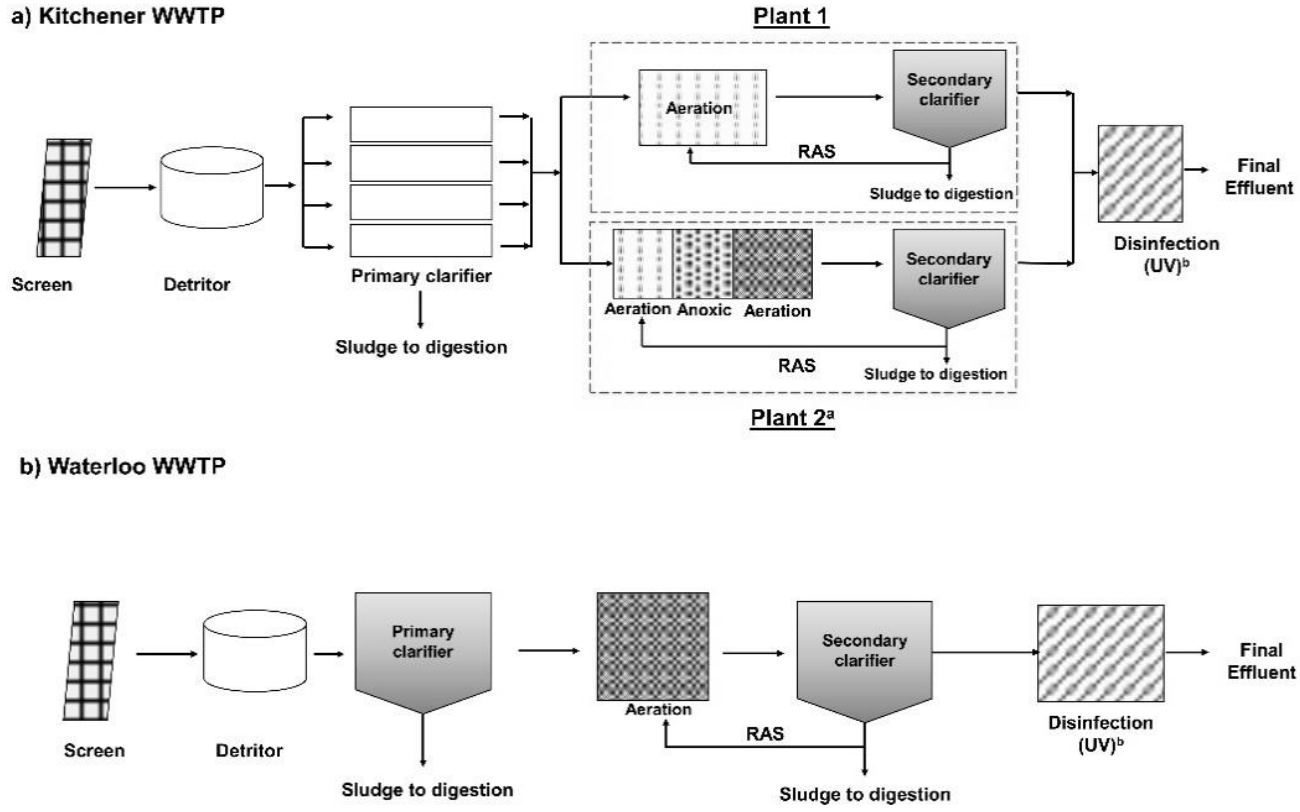

Figure 2.1 Process diagram for wastewater treatment at (a) Kitchener and (b) Waterloo WWTPs. [a]Plant 2 was upgraded in August 2012 (original operation was identical to Plant 1). [b]Kitchener WWTP started using UV disinfection in 2013 and Waterloo WWTP in 2012. No major upgrades were completed at Waterloo WWTP during the study period.

2.3.2 Estimating influent and effluent concentrations

The influent and effluent concentrations of E1, E2, and EE2 at the two plants were estimated using the method of Johnson and Williams (2004) (schematic found in the supplementary material, Figure S2.1, Appendix A). The population data including the partitioning by age groups and gender for Kitchener and Waterloo were taken from the 2011 census compiled by Statistics Canada (http://geodepot.statcan.gc.ca). Demographic profiles that included: (1) males, (2) menstruating females, (3) pregnant females, (4) menopausing females, (5) females undergoing hormone replacement therapy, and (6) females that use birth control pills were then generated (Table 2.1). Data on birth control usage rates were derived from the information collected by Statistics Canada (Rotterman et al. 2015) and it was assumed that additional consumption rates due to the illegal purchase of this drug via online pharmacies were minimal. There are also two major universities located in Waterloo with a total average female population of ~17,000. Since a relatively high percentage of female students in universities use birth control pills (~38%, American College Health Association, http://www.acha-ncha.org/data_highlights.html), a sub-demographic profile was created for Waterloo that incorporated the student population (see supplementary Material, Tables S2.1-S2.3, Appendix A).

Each demographic profile was assigned a compound excretion rate (µg/d) based on literature values (Table 2.1). These excretion rates were used to calculate the total mass entering the sewer and wastewater treatment plant (WWTP) for each target compound and demographic profile. Estrogens are conjugated during the detoxification process in the body. However, many studies suggest that they are transformed back to their parent estrogens either before excretion or by microorganisms present in the sewers (D'Ascenzo et al., 2003; Johnson and Sumpter, 2001; Kumar et al., 2012). Hence, all the estrogens in this model are considered to be in their deconjugated forms (i.e., free form). An adjustment was made to account for the transformation of E2 to E1 in sewers (27 % based on the report of Fleming et al. (2016)). The mass loadings (µg/d) calculated for each estrogen using the information in Table 2.1 were then totaled and converted into influent concentrations (ng/L) using equation 2.1:

$$C_j = \frac{\sum_i^n W_i}{Q_d} \times 1000 \qquad \text{(Equation 2.1)}$$

where $\sum_i^n W_i$ is the total mass loading (µg/d) by all demographic profiles, i represents each demographic profile (n=6), j represents each estrogen (j=3), Q_d is the daily reported flow rate (L/d) at the treatment plant (supplied by the Region of Waterloo, Ontario Canada).

Table 2.1 Breakdown of the population, demographic profile, excretion rates, and calculations used in the model.

Breakdown of female population (P_i)						
	$P_{f,MN}$	$P_{f,MNP}$	$P_{f,PRG}$	$P_{f,HRT}$	$P_{f,BC}$	
E1/E2	females ages 10 to 49 minus $P_{f,PRG}$ [a]	females ages 45 to 54[b]	3.89% of female ages 15-49[c]	22% of females from 45 to 64[d]	-	
EE2	-	-	-	-	Various demographic usage rates[e]	
Excretion Rate (ER_i), µg/d[f]						
	ER_m	$ER_{f,MN}$	$ER_{f,MNP}$	$ER_{f,PRG}$	$ER_{f,HRT}$	$ER_{f,BC}$
E1	2.6	11.7	1.8	550	28.4	-
E2	1.8	3.2	1	393	53	-
EE2	-	-	-	-	-	11.3
Calculation of the loading released per demographic profile (W_i), µg/d							
W_i	W_m	$W_{f,MN}$	$W_{f,MNP}$	$W_{f,PRG}$	$W_{f,HRT}$	$W_{f,BC}$	**Total Loading for each estrogen**
E1	$ER_{m,E1} \times P_m$	$ER_{f,E1} \times P_{f,MN}$	$ER_{f,E1} \times P_{f,MNP}$	$ER_{f,E1} \times P_{f,PRG}$	$ER_{f,E1} \times P_{f,HRT}$	-	$\sum W_{i,E1}$
E2	$ER_{m,E2} \times P_m$	$ER_{f,E2} \times P_{f,MN}$	$ER_{f,E2} \times P_{f,MNP}$	$ER_{f,E2} \times P_{f,PRG}$	$ER_{f,E2} \times P_{f,HRT}$	-	$\sum W_{i,E2}$
EE2	-	-	-	-	-	$ER_{f,EE2} \times P_{f,BC}$	$\sum W_{i,EE2}$

Notes: m=males; f=females; MN=menstruating females; MNP=menopausing females; PRG=pregnant females; BC=birth control; HRT=hormone replacement therapy; "-" = not applicable; *i* represents each demographic profile.
[a]Start of menstruation in females assumed at age 10 and ends at age 49 (end of the reproductive age). [b]Canadian Women's Health Network (http://www.cwhn.ca/en/faq/menopause) suggests a bracket of 42 to 56 as menopausing age but female population breakdown is only available for 45 to 54 (Statistics Canada, http://geodepot.statcan.gc.ca) and was used to calculate $P_{f,MNP}$. [c]Calculated from the data collected by the Region of Waterloo (see Table S2.1 of the supplementary material found in Appendix A). [d]Beaudet et al. (1997) . [e]Rotermann et al. (2015). The prevalence of birth control pill use among Canadian women aged 15-29 is ~30%, 20% for 35-39, 6.4% for 40-45 and 2.8 % for 40-49. [f]The rates shown are the mean values used by Johnson and Williams (2004) and represent total excretion via urine and feces.

To determine the concentrations of an estrogen in the effluent, $C_{e,j}$ (ng/L), was calculated using equation 2.2:

$$C_{e,j} = C_j \times (1 - r) \qquad \text{(Equation 2.2)}$$

where r is the fraction removed. The removal efficiencies of the target estrogens in the Kitchener and Waterloo WWTPs have not been directly measured. Instead, the removals at each plant were estimated using data collected from an EDA completed in 2010 and 2012. The EDA is an environmental diagnostic that combines the biological effects and chemical analysis to determine the analytes that contribute to the total measurable effect (e.g., estrogenicity) in a complex mixture such as municipal wastewater effluent. The procedure followed in the EDA are described in detail in the supplementary material (Appendix A-1). Briefly, effluent grab samples were collected and extracted. The effluent extracts were then fractionated into 60 fractions by liquid chromatography and subjected to biological activity testing using the yeast estrogen screen (YES) assay (Tanna et al., 2013). The estrogenic fractions (Figures S2.4 and S2.5, Appendix A) were then compared to a standard containing 8 estrogens (Figure 2.2) that was also subjected to the same fractionation and estrogenicity analysis. The compounds that displayed estrogenic activity were identified based on the order of elution and retention times observed in the fractionated standard mix. The elution of target compounds occurred in the following order: estriol (E3), bisphenol A (BPA), estradiol (E2), estriol (E1), ethinylestradiol (EE2), diethylbestriol (DES), octylphenol (OP), and nonylphenol (NP) (Figure 2.2). The concentration of the target estrogens (E1, E2, and EE2) in the effluent ($Ce,_{EDA}$) were then calculated using equation 2.3:

$$C_{e,EDA} = \frac{\sum EEQ}{EEF} \qquad \text{(Equation 2.3)}$$

where ∑EEQ (ng/L E2 equivalents) is the sum of the estrogenic fractions associated with each target compound as shown in the YES assay. The estrogenic fractions included in equation 2.3 were based on the patterns displayed by the standard estrogen mixture (Figure 2.2) EEF is the

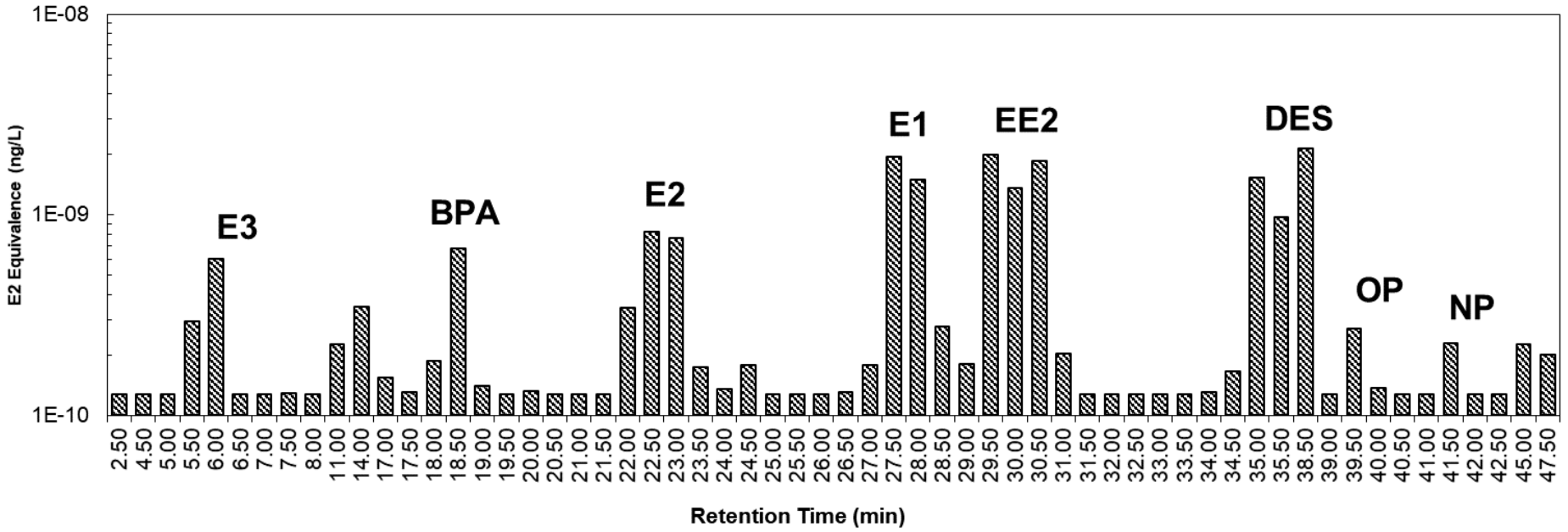

Figure 2.2 Estrogenic profile describing the elution order and retention times of compounds present in the standard mixture. This figure served as the basis for estrogenic compound identification in WWTP effluents. E3 = estriol; BPA = bisphenol A; E2 = estradiol; E1 = estrone; EE2 = ethinylestradiol; DES = diethylbestriol; OP = octylphenol; NP = nonylphenol. The estrogenicity profile of the Kitchener and Waterloo WWTP (2010 and 2012) are found in the supplementary material (Figures S2.4 and S2.5, Appendix A-1).

estradiol equivalency factor. EEF values of 0.3, 1.0, and 1.23 were calculated for E1, E2, and EE2 respectively using the data of Jarošová et al. (2014).

The removals were then calculated using the averaged estimated influent concentrations (equation 2.1) and the effluent concentrations of E1, E2, and EE2 derived from the EDA (equation 2.3). The removals calculated for 2010 at the Kitchener WWTP were used for the pre-upgrade period (2007 to July 2012) while the 2012 results were used for modeling the post-upgrade condition (August 2012 to 2015). Since the Waterloo WWTP did not undergo significant upgrades during the study period, the removals derived from both investigations were averaged.

The model predictions were assessed using a total estrogenicity dataset (E2 equivalents) that was derived from the YES assay conducted at various times over the period of 2009 to 2015 (methodology described in Hicks et al. (2017)). There are other estrogens present in the municipal wastewater effluent such as bisphenol A and nonylphenols that can contribute to the total estrogenicity. However, a previous study (Smith, 2013) suggested that E1, E2, and EE2 dominated the total estrogenicity in the Kitchener and Waterloo WWTPs. In cases when other endocrine active compounds significantly contribute to the total estrogenicity (e.g., BPA), then the influent estimates require an adjustment to include the emissions of these compounds into the WWTPs. In this study, we assumed that E1, E2, and EE2 were the major contributors of estrogenicity in WWTP effluents, and the predicted concentrations were converted into total estrogenicity values as E2 equivalents using equation 2.4:

$$EEQ_{pred} = \sum C_{e,j} \times EEF_j \qquad \text{(Equation 2.4)}$$

where EEQ_{pred} is the predicted total estrogenicity of the WWTP effluent.

The quality of model predictions was evaluated using the Spearman correlation test, a non-parametric test to measure the strength of association between predicted and measured values. Significant differences in the median of the predicted and measured concentrations were evaluated using the Mood non-parametric test (α=0.05). The tests were performed using SigmaPlot 13.0 (Systat Software, Inc).

2.4 Results and discussion

2.4.1 Influent daily loading rates

The mass loadings of estrogens entering the WWTPs were estimated from the population data, demographic profiles, consumption rates (only for EE2), and excretion rates (Figure 2.3). The estrogen loadings were generally 50% higher at the Kitchener WWTP than the Waterloo WWTP primarily due to the higher population serviced by the Kitchener WWTP. The E1 loading was the highest amongst the target estrogens at ~2,600 mg/d and ~1,400 mg/d at Kitchener and Waterloo WWTPs respectively followed by E2 at 1,200 mg/d and ~600 mg/d. EE2 had the lowest loading in the influents (~130 mg/d and 123 mg/d for Kitchener and Waterloo WWTP respectively).

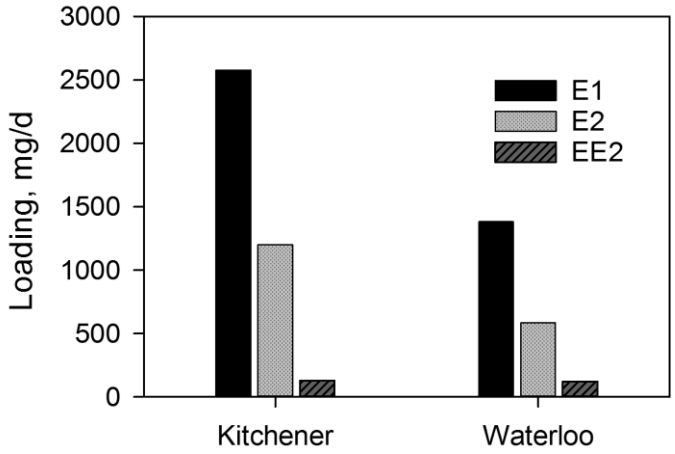

Figure 2.3 Estimated mass loadings of E1, E2, and EE2 into Kitchener and Waterloo WWTP derived using population, demographic profile, and excretion rates.

The average daily concentrations of estrogens, C_j, that corresponded to the estrogen loadings were 37 ± 5 ng/L, 17 ± 2 ng/L, 2 ± 0.2 ng/L for E1, E2, and EE2 respectively for the Kitchener WWTP. These values did not substantially differ from the Waterloo WWTP influent concentrations: 32 ± 7 ng/L, 13 ± 3 ng/L, 3 ± 0.6 ng/L for E1, E2, and EE2 respectively. The fluctuations in these estimates were dependent on the time-varying flows at the WWTPs. These estimates were considered to be within the range of concentrations of E1, E2, and EE2 reported in WWTP influents elsewhere, with EE2 typically occurring in influents at lower concentrations than E1 and E2 (Mohagheghian et al., 2014).

2.4.2 Estimates of estrogen removals through WWTPs

The site-specific removals estimated in this study are shown in Table 2.2 and were calculated using (a) the influent concentrations derived from the use of population demographics, excretion rates, and sewer conversion rate and (b) the effluent estrogen concentrations estimated from the EDA datasets (2010 and 2012). It is evident that during the pre-upgrade period (2010 sample) at the Kitchener WWTP, the treated effluent was highly estrogenic which suggested a relatively poor removal of estrogens through the plant (Table 2.2). The concentration of E1 was found to be the highest in the effluent (23.20 ng/L) but since it is a less potent estrogen (EEF of 0.3), its contribution to the total estrogenicity was similar to E2 and EE2 (Table 2.2). The estimated removals employed for the pre-upgrade conditions at the Kitchener WWTP were 37%, 64%, and 0% for E1, E2, and EE2 respectively. The total estrogenicity in the effluent declined during the post-upgrade period as evident from the EDA dataset collected in 2012 (Table 2.2 and Figure S2.4). The concentration of E1 remained the highest among the target estrogens but was substantially lower than the pre-upgrade condition. The removals also improved with values of 90%, 96%, and 78% for E1, E2, and EE2 respectively.

Table 2.2 Percent removals employed for Kitchener and Waterloo WWTPs. The data were estimated from an EDA completed in 2010 (pre-upgrade) and 2012 (post-upgrade). See Figures S2.4 and S2.5.

	Fractions considered in the calculation (min)	**ΣEEQ**	**EEF**	**Effluent concentration, $C_{e,\ EDA}$ (ng/L)**	**Influent concentration, C_i (ng/L)**	**Percent Removal**
Kitchener – 2010 (pre**)**						
E1	29 to 31	6.961	0.3	23.20	35.0	37%
E2	24 to 25.5	6.202	1	6.20	17.0	64%
EE2	32 to 33	5.294	1.23	4.30	2.0	0%[a]
Kitchener – 2012 (post)						
E1	29 to 30	3.56	0.3	4.27	37.0	90%
E2	23.5	1.55	1	2.31	17.0	96%
EE2	31 to 32	0.44	1.23	0.60	2.0	78%
Waterloo – **2010**						
E1	29 to 31	3.89	0.3	12.96	32	60%
E2	24 to 25.5	1.12	1	1.12	13	91%
EE2	32 to 33	1.92	1.23	1.56	3	48%
Waterloo – **2012**						
E1	29 to 30	4.76	0.3	15.85	32	50%
E2	23.5	0.28	1	0.28	13	98%
EE2	31 to 32	0.34	1.23	0.28	3	91%

[a]The estimated influent concentration was numerically lower than the effluent concentrations resulting to a negative percent removal (-115%). Biological activity measurements can be highly variable and 0% removal was instead adopted.

The total estrogenicity of the Waterloo WWTP effluent was dominated by E1 (Table 2.2). Since the Waterloo WWTP did not undergo significant treatment upgrades between 2010 and 2012, only a single removal value was used for the prediction of effluent concentrations at the Waterloo WWTP and these were obtained by averaging the removals derived from the two separate EDA datasets. The removals employed at the Waterloo WWTP were 55%, 95%, and 69% for E1, E2, and EE2 respectively.

In this study, information on plant-specific removals for each target estrogen was considered a major source of uncertainty due to the lack of direct measurements of estrogens. It is generally known that E2 has the highest removal through the WWTP followed by E1 and then EE2 (Johnson and Sumpter, 2001). However, the removals reported in the literature, especially for E1, (Table 2.3) are highly variable, even for the plants that operate similarly. Clara et al. (2004) recommended the use of solids retention time (SRT) as a gauging parameter to determine the efficiency of estrogen removals in WWTPs. Lower SRTs generally indicate poor removals of estrogens while higher SRTs are correlated with good removals. However, they noted that these estimates do not necessarily apply to EE2 in a high-SRT operating WWTP that have both nitrification and denitrification processes (<20% removal, Table 2.3). The opposite was observed by Muller et al. (2008) and Andersen et al. (2003) in WWTPs that have nitrogen removal processes. High efficiency was observed not only for E1 and E2 but also for EE2 where up to 90% removal was reported in the nitrifying tank by Andersen et al. (2003).

To determine whether nitrogen removal has a direct relationship with the estrogenicity at Kitchener and Waterloo WWTPs, the reported ammonia concentrations and total estrogenicity measurements in the effluent were compared. Although a significant Spearman correlation (r_s =0.525, p<0.001) was found for Kitchener WWTP, a poor and non-significant correlation was determined for Waterloo WWTP (r_s=0.059, p=0.423, Figure S2.6, Appendix A). This clearly suggests that the use of surrogate parameters to measure estrogen concentrations in the effluent may not easily be generalized and site-specific data are more helpful in this regard. Attempts have been made to measure specific estrogens by LC-MS/MS but were confounded by background interferences. Hence, the removals were estimated from the EDA datasets as these are the only site-specific information available for this study.

Table 2.3 Percent removals of target estrogens reported in selected studies[a].

Compound	Geographical Area	Percent removals, % (average or range)	Reference
E1	Rome	61	D'Ascenzo et al. (2003)
	Canada	-55 to 98	Servos et al. (2005)
	Italy	61	Baronti et al. (2000)
	Brazil	83	Ternes et al. (1999)
	Germany	0	Ternes et al. (1999)
	Australia	-223 to 100	Tan et al. (2007)
	Austria	20 to 40[b]	Clara et al. (2005)
	Austria	60 to 80[c]	Clara et al. (2005)
E2	Canada	40 to 99	Servos et al. (2005)
	Rome	85	D'Ascenzo et al. (2003)
	Italy	87	Baronti et al. (2000)
	Brazil	99.9	Ternes et al. (1999)
	Germany	64	Ternes et al. (1999)
	Australia	90-100	Tan et al. (2007)
	Austria	20 to 40[b]	Clara et al. (2005)
	Austria	60 to 80[c]	Clara et al. (2005)
EE2	Italy	85	Baronti et al. (2000)
	Brazil	78	Ternes et al. (1999)
	Austria	40 – 60[b]	Clara et al. (2005)
	Austria	<20[c]	Clara et al. (2005)

[a]Data adapted from Teske and Arnold (2008) and modified to include only WWTPs with activated sludge process. [b]Not listed in Teske and Arnold (2008). WWTP has activated sludge system with anaerobic digestion. [c]Not listed in Teske and Arnold (2008). WWTP has primary settling and activated sludge systems with anaerobic digestion.

2.4.3 Total estrogenicity estimates in Kitchener WWTP

The measured estrogenicity at the Kitchener WWTP, as quantified by the YES assay, agreed well with the predicted concentrations both qualitatively and quantitatively (Figure 2.4, r_S=0.749, p=0.00139, α=0.05). However, the estimated total estrogenicities were slightly over predicted compared to the YES results especially during the post-upgrade period. The YES assay has limitations when estimating the estrogenic activity in wastewater effluents. It has been reported that matrix effects via the interaction of estrogens with particulates in wastewater, binding with dissolved organic matter, and interference with other estrogenic compounds can contribute to the underestimation of the effluent estrogenicity (Huggett et al., 2003; Johnson and Sumpter, 2001; Snyder et al., 2001). The measurements may have been more affected during the post-upgrade period when concentrations of the estrogenic substances were estimated to be low. It is highly likely that some estrogens may have been lost due to the interferences in the bioassay procedure. However, the overprediction was only quantified to be around 1% (percent bias, Table S2.4, Appendix A) and is considered sufficient for the purposes of this study.

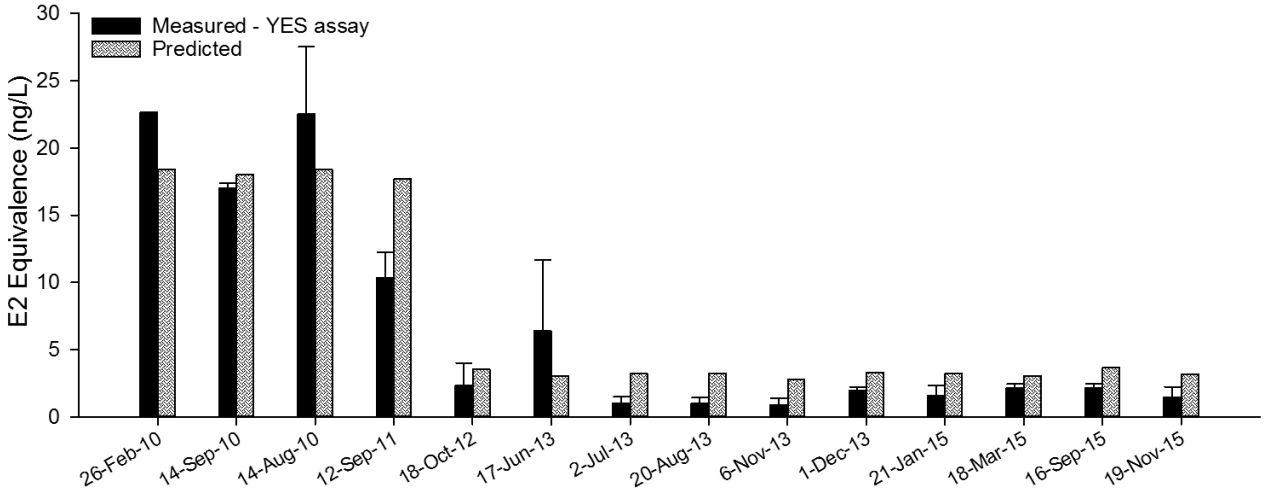

Figure 2.4 Comparison between the measured (YES assay) and predicted estrogenicity at the Kitchener WWTP effluent.

As mentioned previously, one of the major uncertainties in the predictions comes from the use of a single removal for the pre- and post-upgrade conditions. Many studies have shown that there are fluctuations in the removals of estrogens through the plant over time (Fernandez et al., 2008; Jin et al., 2008). The Kitchener WWTP, in particular, has experienced a few process upsets after the aeration upgrades in August 2012. Changes in removals over time must be incorporated into the model to provide better results. However, the good agreement between the observed and predicted data demonstrates that the use of a single removal for the pre- and post-upgrade periods was justified, and temporally specific removals may not be necessary for this particular situation. The overall results (Figure 2.4) at the Kitchener WWTP suggest that the method and the input parameters used in this simulation can be considered conceptually sound and adequate in reflecting the conditions that influenced the source, distribution, and sinks of the target estrogens in the system.

2.4.3.1 Assessment of pre- and post-upgrade estrogenicity at Kitchener WWTP

Process upgrades were introduced starting July 2012 at the Kitchener WWTP resulting in a substantial decrease in effluent ammonia concentrations (Figure 2.5b). These upgrades consisted of providing adequate tankage and aeration capacity for nitrification. The overall improvement was further reflected in the total estrogenicity profile as shown in Figure 2.5a. During the pre-upgrade period, the predicted total estrogenicity averaged at 17 ng/L E2 equivalents (ranging from 7 to 24 ng/L) while predicted post-upgrade estrogenicity levels

dropped to an average of 3.4 ng/L (ranging from 1 to 16 ng/L). Jarošová et al. (2014) derived EEQs between 0.1 and 0.4 ng/L as the allowable range of effluent estrogenicity that is protective of long-term fish exposure (>60 d) to estrogens. To reflect site-specific conditions, dilution factors must be applied since the thresholds are only applicable to effluents contributing to ~100% of the river flow. The Kitchener WWTP on average contributes ~10% and the thresholds were increased to 1 and 4 ng/L to reflect the effluent dilution.

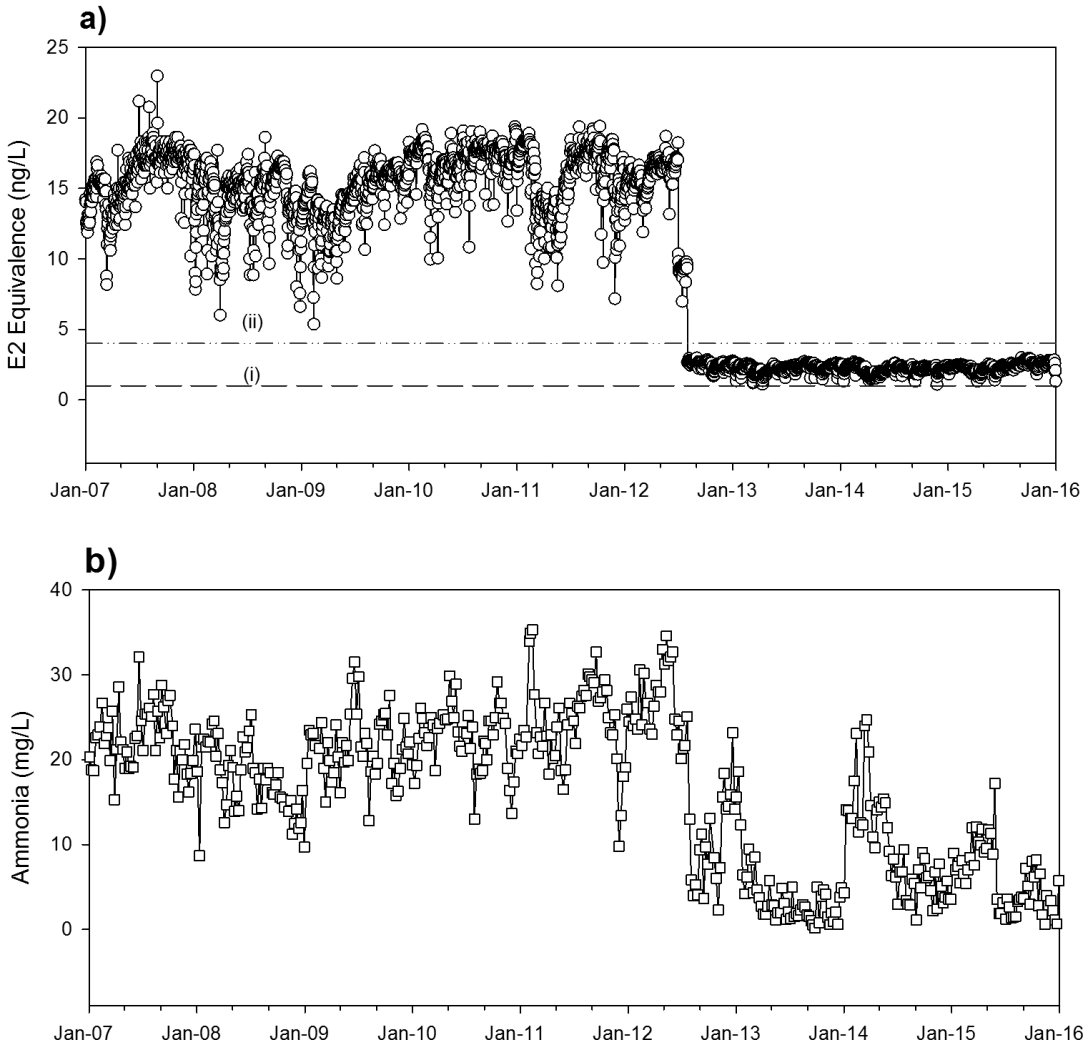

Figure 2.5 (a) Estimated estrogenicity profile and (b) measured ammonia concentrations at Kitchener WWTP effluent. The benchmarks used to determine effluent quality were (i) 1 ng/L (conservative) and (ii) 4 ng/L (maximum allowable EEQ for long-term exposure, derived from Jarošová et al. (2014)).

The predicted EEQs during the pre-upgrade years (2007 to 2012) were consistently above the thresholds, with percent exceedances (i.e., number of times the effluent EEQ exceeded the benchmarks) at 100% for both 1 and 4 ng/L EEQ benchmarks respectively. In terms of estrogen removal, this was indicative of the relatively poor effluent quality discharged by the Kitchener WWTP during that period suggesting that the reproductive health of exposed fish may have been compromised. This effluent quality is reflected in the impaired reproductive health conditions of rainbow darters collected during this period, with one sampling event showing up to 100% fish intersex incidence rate and very high severity (Bahamonde et al., 2014; Fuzzen et al., 2016; Tanna et al., 2013; Tetreault et al., 2011).

The total estrogenicity values predicted in the post-upgrade period (late 2012 to 2015), however, were mostly below the benchmark EEQs for long-term exposure (percent exceedance at 39% and 1% for 1 and 4 ng/L respectively). These results suggest that the operation of the partially upgraded Kitchener WWTP is not expected to impair the reproductive health of fish that might be exposed to its effluent. This finding supports the work of Hicks et al. (2017) that indicate a significant reduction of fish intersex incidence and severity after the upgrades of the Kitchener WWTP.

The results were further analysed to assess the contribution of each compound to the total estrogenicity. The contributions of E1 and E2 to the total estrogenicity during the pre-upgrade were similar (45% and 41% respectively) while EE2 contributed ~14%. The contributions of each compound follow a similar trend during the post-upgrade period (49%, 30% and 21% for E2, E1, and EE2 respectively). Although E1 had higher loads/concentrations in the influent than E2, its contribution to estrogenicity was less than E2 due to its relatively lower potency. Although EE2 is more potent than E1 and E2, it contributed a small fraction to the total estrogenicity. This was consistent with the results of Jarošová et al. (2014) when they examined 14 *in vitro* bioassays that were used to measure estrogenicity in WWTP effluents.

The results of this study show a promising application in quantifying the exposure to estrogenic compounds in WWTP effluents. Although a few limitations exist, the potential extension of the method to other WWTP is warranted. Hence, this method was extended to

predict the estrogenicity at another major treatment plant in the watershed (Waterloo WWTP) and is described in the next section.

2.4.4 Total estrogenicity estimates in Waterloo WWTP

A similar procedure was used to estimate the total estrogenicity of the Waterloo WWTP effluent from 2007 to 2015 and no significant upgrades were completed during this period. The measured total estrogenicity at the Waterloo WWTP was highly variable and did not display an observable temporal pattern (Figure 2.6). The random fluctuations in the measured data were not predicted well by the model since only a single removal was utilized for the prediction (Figure 2.6, r_S=0.373, p=0.245, α=0.050). However, the median concentrations of the measured and predicted values were not statistically different (*p*=0.201, Mood nonparametric test, α=0.05), suggesting that the median conditions were predicted well.

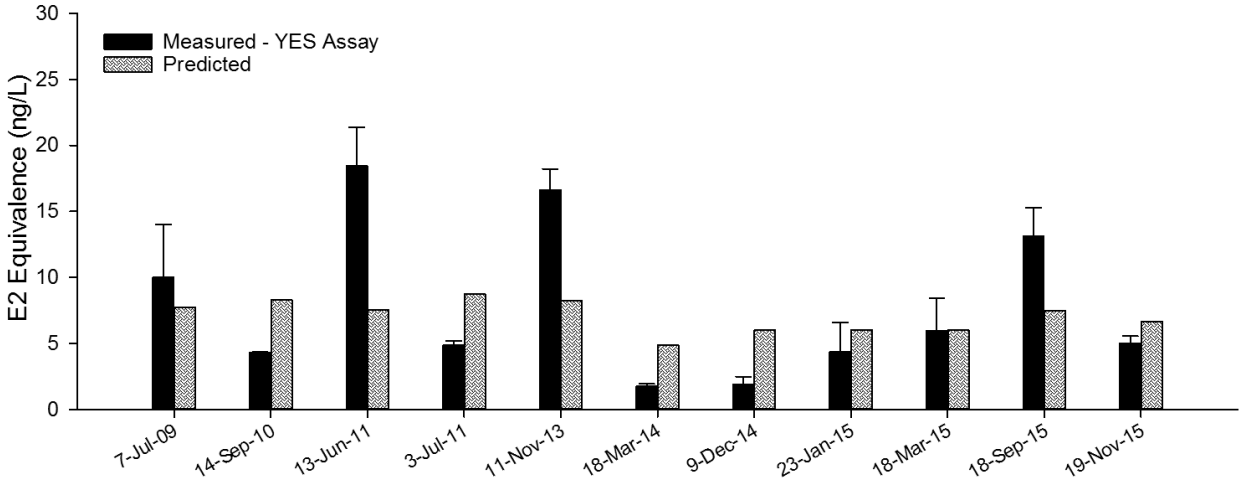

Figure 2.6 Comparison between the measured (YES assay) and predicted estrogenicity at the Waterloo WWTP effluent.

The predicted daily total estrogenicity at the Waterloo WWTP is presented in Figure 2.7. Waterloo's effluent contributes 5% of the total river flow on average, hence the allowable range of EEQs for long-term exposure to estrogens was adjusted as recommended by Jarošová et al. (2014) to 2 ng/L to 8 ng/L. The estrogenicity exceeded the more conservative threshold (2 ng/L) by 100% but only 8% for the 8 ng/L. The exceedances at maximum allowable benchmark (8 ng/L) also occur less often than the pre-upgrade conditions in Kitchener WWTP. This result

further supports the findings by Hicks et al. (2017) that although intersex was prevalent downstream of Waterloo WWTP, intersex incidences were generally lower than downstream of Kitchener WWTP from 2007 to 2015. Note that the Kitchener WWTP services a population that is higher than Waterloo WWTP (Figure 2.3) and the relatively lower estrogen loadings at the Waterloo WWTP primarily accounts for the lower intersex occurrence downstream of its discharge point. It is anticipated that the conditions will substantially improve upon the implementation of process upgrades that are similar to upgrades already implemented at the Kitchener WWTP.

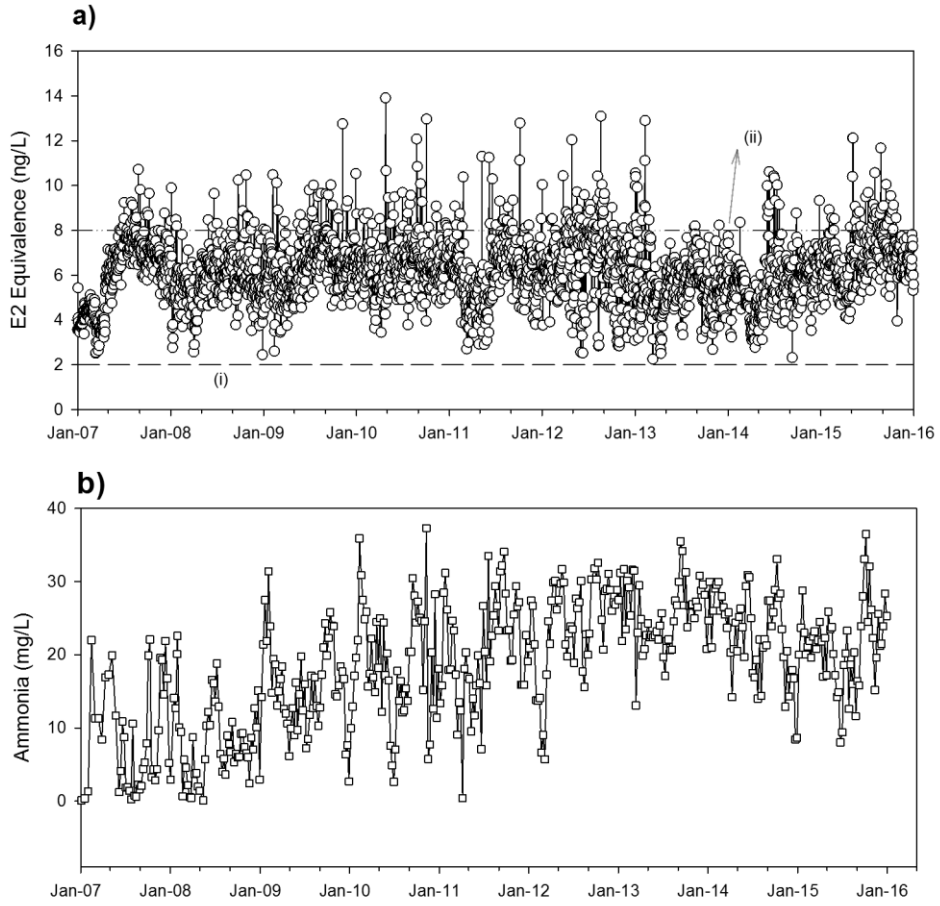

Figure 2.7 (a) Estimated estrogenicity profile and (b) measured ammonia concentrations at Waterloo WWTP effluent. The benchmarks used to determine effluent quality were (i) 2 ng/L (conservative) and (ii) 8 ng/L (maximum allowable EEQ for long-term exposure, derived from Jarošová et al. (2014))

2.5 General implications of the method used

In this study, the predictions were compared against the historical effluent estrogenicity measured by the YES assay (from 2009 to 2015) for two major WWTPs assumed to discharge treated effluent with relatively high levels of estrogens. Given the uncertainty associated with process upgrades and seasonal variations, the adequacy of the predictions was apparent (Figures 2.4 and 2.6), suggesting that the estimation process employed is robust. Our results also support the findings of Hicks et al. (2017a) that suggested the reduction of biological effects when the upgrades at the Kitchener WWTP were implemented. Although more information on site-specific conditions could improve the predictions, this rapid and practical approach is particularly useful for situations where assessment of the risk of exposures to estrogens is desired.

2.6 Effluent estrogenicity characterization under potential future conditions

Scenario analyses were employed to determine the implications of potential future conditions on effluent quality. A base case scenario was first developed using the previously described approach with constant WWTP flow (average daily flows from 2007 to 2015) and removals derived from the EDA dataset. The base case EEQ values calculated were 3 and 5 ng/L E2 equivalents for the Kitchener and Waterloo WWTPs respectively. Three sets of scenarios were compared against the base case condition: (1) impact of population growth; (2) improved WWTP operation (over 95% removal of all estrogens); and (3) lower river flow conditions (e.g., due to the potential impacts of climate change). The results were evaluated against the allowable range of EEQs previously described (1 to 4 ng/L for Kitchener WWTP and 2 to 8 ng/L for Waterloo WWTP).

It is expected that the Region of Waterloo will experience ~36% population growth by 2041 (http://chd.region.waterloo.on.ca/en/researchResourcesPublications/quickstats.asp, retrieved January 8, 2017). The population profiles in the model were increased by 36%, 50%, and 100% to examine the sensitivity of the system to population increase. The predicted Kitchener WWTP effluent values exceeded the allowable EEQs when the population increased by 50%. A similar observation was made for the Waterloo WWTP, but it exceeded the allowable

EEQs with a 36% population growth (Figure 2.8). When high treatment efficiency (95%) was applied for both plants (Figure 2.8), the projected EEQs were always within the "safe" EEQ threshold for all population growth rates, suggesting that the upgrades will likely reduce the reproductive health impacts downstream.

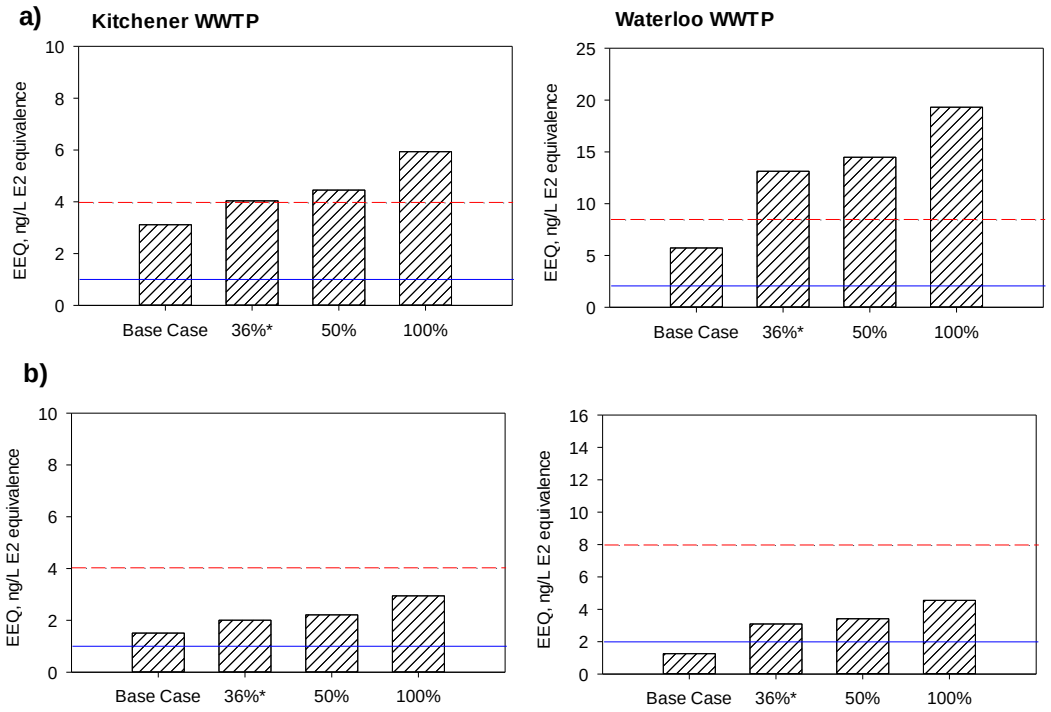

Figure 2.8 Projected EEQ when 36%, 50%, and 100% population growth rate was applied for Kitchener and Waterloo WWTPs with the allowable range ([—] conservative and [---] maximum) of effluent estrogenicity that is protective of long-term exposure. Long-term EEQ benchmarks using the percent removals (a) derived from this study and (b) 95% removals.

The impacts of low flow conditions were conducted with five different percentages of effluent contribution to river flow. Values of 10% and 5% percent contribution were employed as the base case scenario for the Kitchener and Waterloo WWTPs respectively (Table 2.4). These percentages were the calculated averages for WWTP percent contribution to the total Grand River flows from 2007 to 2015 on an annual basis. The results indicate that the Kitchener WWTP effluent will exceed the maximum allowable EEQ (4 ng/L) for long-term exposure when the effluent flow contribution to the river flow is greater than 30%. If the Kitchener WWTP

operates at its maximum design flow capacity (122 MLD) and at a river flow of 10 m^3/s (normal summer low flow), the effluent contribution is only 14%. In addition, the river flow must be extremely low (~5 m^3/s) for the effluent to contribute to greater than 30% of the total flow and to exceed the allowable EEQ. In the Grand River watershed, the flows are regulated from the reservoirs to maintain a flow of 9 m^3/s from May to September. Therefore, the current treatment conditions employed at the plant seem to be acceptable (if fully-mixed) in the future even during summer low flow conditions.

Table 2.4 Scenario analyses – benchmark exceedances resulting from changes in effluent contribution to total river flow (i.e., flow conditions)

Effluent Contribution	Revised EEQ benchmark (maximum allowable)[b]	Exceeds (Yes/No)
Kitchener		
3%	13.33	No
10%[a]	4.00	No
20%	2.00	No
30%	1.33	Yes
50%	0.80	Yes
Waterloo		
5%[a]	8.00	No
10%	4.00	Yes
15%	2.67	Yes
20%	2.00	Yes
50%	0.80	Yes

[a]Base case benchmark EEQ. [b]The EEQ benchmarks were revised based on the work of Jarošová et al. (2014) which derived the estrogenicity benchmark assuming that the WWTP effluent contributes to 100% of the river flow. The analysis assumed that WWTPs are the major contributors of estrogenicity.

The Waterloo WWTP will exceed the maximum allowable EEQ level when it contributes greater than 10% of the river flow under its current treatment operation. If the plant operates at its maximum flow (98 MLD) and the river flow is at 10 m^3/s (summer low flow), the overall effluent contribution to the total flow would be 11%. Therefore, the Waterloo WWTP effluent may continue to pose an impact on fish reproductive health. However, as mentioned earlier, the Waterloo WWTP is currently undergoing upgrades that could significantly improve the removal of estrogens in wastewater. It is further predicted that when the upgrades at the Waterloo WWTP are complete (i.e., 95% removal for all estrogens), the effluent could still be protective even at an extremely low river flow (but not lower than 4 m^3/s).

The exercise detailed above illustrates that models can be easily applied to different water quality management strategies. Although several limitations on their use exist, it is evident overall that this work has shown the potential application of the model employed to inform decisions related to WWTP capital planning and operations.

2.7 Conclusions

The estrogenicity of the effluent discharged by the Kitchener and Waterloo WWTP into the Grand River in southern Ontario Canada was predicted using population demographics, consumption rates, and treatment plant efficiency. The estimates were derived with confidence and were validated by the measured EEQ concentrations. When the model was extended to several future scenarios, it was found that the Kitchener WWTP effluent is considered protective under high rates of population growth and during low-flow conditions while the current operation of Waterloo WWTP may not be protective of the aquatic environment at low-flow conditions. However, treatment upgrades that are being implemented at both WWTPs could significantly improve effluent quality and are predicted to reduce or eliminate the estrogenic responses downstream. Without the upgrades, future population growth may result in endocrine effects in wild fish, especially in low flow periods. Overall, the modeling exercise is a practical approach that can potentially be employed in areas where the risk of environmental exposure to estrogens in wild fish is of concern and can help describe future scenarios to support risk management.

Chapter 3

Modeling the exposure of wild fish to endocrine active chemicals: linkages of total estrogenicity to field-observed intersex

3.1 Chapter summary

Decades of studies on endocrine disruption have suggested the need to manage the release of key estrogens from municipal wastewater treatment plants (WWTP) into receiving aquatic environments. However, the proposed thresholds are below the detection limits of most routine chemical analysis, thereby restricting the ability to assess the environmental exposure appropriately. In this case study, we demonstrated the utility of a mechanistic model to address the data gaps on estrogen exposure. Concentrations of the prominent estrogenic contaminants in wastewaters (estrone, estradiol, and ethinylestradiol) were simulated in the Grand River in southern Ontario (Canada) for 9 years, including a period when major WWTP upgrades occurred. The predicted concentrations expressed as total estrogenicity (E2 equivalent concentrations) were contrasted to a key estrogenic response (i.e., intersex) in rainbow darter (*Etheostoma caeruleum*), a wild sentinel fish species. A predicted total estrogenicity in the river of ≥10 ng/L E2 equivalents can cause high intersex incidence and severity, whereas concentrations <0.1 ng/L E2 equivalents were associated with minimal intersex expression. Exposure to a predicted river concentration of 0.4 ng/L E2 equivalents, the environmental quality standard (EQS) proposed by the European Union for estradiol, was associated with 34% (95% CI:30-38) intersex incidence and a very low severity score of 0.6 (95% CI:0.5-0.7). This exposure is not predicted to cause adverse effects in rainbow darter. Overall, this study illustrates the value of models for exposure assessment and supports the recommended EQS for its use in future environmental assessment and monitoring.

3.2 Introduction

The exposure of fish to a mixture of estrogenic compounds has been shown globally to have deleterious consequences for reproductive health (Brian et al., 2005; Kime, 1999; Nash et al., 2004; Tyler and Routledge, 1998). One of the most frequent observations is the feminization of male fish, with vitellogenin induction (production of estrogen-dependent protein) and intersex (presence of ova-testis) as examples of changes reported (Jordan et al., 2016). Prior studies have associated these effects with the discharge of endocrine active chemicals (EACs) from municipal wastewater treatment plants (WWTPs) (Jobling et al., 1998; Jobling et al., 2006; Tyler and

Routledge, 1998). Estrogenic compounds, including ethinylestradiol (EE2) and natural female hormones (e.g., estradiol [E2] and estrone [E1]), have been linked to endocrine disruption in fish exposed to wastewater effluents and have become targets of many environmental sampling and monitoring surveys worldwide (Agunbiade and Moodley, 2016; Kasprzyk-Hordern et al., 2009; Scott et al., 2014; Servos et al., 2005; Xu et al., 2007).

Progress in analytical chemistry has enabled the detection of EACs at very low concentrations (Benotti et al., 2008; Carballa et al., 2004; López-Roldán et al., 2010). However, the European Union's (EU) proposed environmental quality standards (EQS) for E2 and EE2 are only 0.4 and 0.035 ng/L respectively (European Commission, 2012) , and are below the current detection limits of most routine analytical methods. This issue is further exacerbated by the high levels of matrix interferences during the analysis of water and wastewater samples via liquid chromatography-mass spectrometry (LC-MS/MS) (Čelić et al., 2017). As an alternative to chemical analyses, recent studies have also utilized biological assessments (i.e., bioassays) to detect the presence of total estrogenicity in complex mixtures (Busch et al., 2016; Escher et al., 2013; Neale et al., 2017a; Neale et al., 2017b). Although considerable chemical and bioanalytical monitoring of effluents have been completed worldwide, there is still limited information to assess the spatial or temporal concentrations of estrogens in receiving waters where technical challenges (e.g. detection limits) and cost are important considerations (Roig and D'Aco, 2016). In the absence of such data, the modeling of environmental systems can be used as an alternate approach to characterize exposure of fish to EACs (Roig and D'Aco, 2016; Zhang et al., 2015). Numerous models have been developed to predict the fate and transport of conventional pollutants as well as contaminants of emerging concern such as pharmaceuticals and personal care products (Arlos et al., 2014; Balaam et al., 2010; Dale et al., 2015; Grechi et al., 2016; Kehrein et al., 2015). Models can be further applied to evaluate current and future mitigation strategies for eliminating the target compounds through scenario testing (e.g., high input rates, low flow conditions) (Kehrein et al., 2015) and assist in the design of effective monitoring programs (e.g., refine timing and location of field investigations) (Roig and D'Aco, 2016). Finally, models can be employed to assess the potential relationship of stressor concentrations to observed effects in the wild (Jobling et al., 2009; Jobling et al., 2006).

Field investigations on the occurrence and severity of intersex in male rainbow darter (*Etheosoma caeruleum*) in the Grand River watershed (southern Ontario) have been ongoing since 2007 (Hicks et al., 2017). The presence of severe intersex in rainbow darter has been linked to poor reproductive success (Fuzzen et al., 2015) with potential negative impacts on the fish population. However, due to the lack of consistent chemical measurements, a quantitative link between the exposure to EACs and intersex responses has not been made. In this study, the concentrations of target EACs (E1, E2, and EE2) in ~80-km stretch of the Grand River were simulated using a mechanistic water quality model (Water Quality Simulation Program, WASP). This river section includes sites that are exposed to WWTP effluents which have been previously predicted to have elevated levels of pharmaceuticals, personal care products, and estrogenicity (Grill et al., 2016; Hosseini et al., 2012). A major upgrade in one of the treatment plants (Kitchener WWTP) has also resulted in effluent quality changes during the study period. This represented a unique opportunity to develop and test models for estrogen(icity) exposure in the environment. The overall goals of this study were to (1) estimate the concentrations of EACs in the Grand River through mechanistic water quality modeling and (2) explore the linkages between predicted concentrations and available data on intersex in wild fish observed between 2007 and 2015.

3.3 Methodology

3.3.1 Study site

The Grand River watershed in southern Ontario (~6,800 km^2) drains into Lake Erie and is inhabited by close to 1 million people. In addition to the non-point sources from numerous agricultural activities (~70% of total land use), the watershed also receives inputs from 30 WWTPs. In this study, ~80 km of the Grand River was modeled starting below a regulated water reservoir (Shand Dam) to an area that is ~2 km above the Grand and Speed River confluence (Figure 3.1a). This section captures both agriculture and urban gradients in the watershed and incorporates the inputs from two major (Waterloo and Kitchener) and two smaller (Elora and Fergus) WWTPs (Table 3.1). Grill et al. (2016) also determined in a large-scale modeling study that sections of the Grand River were among the 0.8% of the river courses in Ontario and Quebec

that “triggered” risk of exposure to EE2 under average flow conditions. In a separate water quality modeling study, Hosseini et al. (2012) indicated that the central region of the watershed (heavily urbanized) was predicted to have elevated risk of exposure to pharmaceuticals and personal care products.

The Grand River has been extensively investigated for several biological effect endpoints on fish health since the late 2000s (Bahamonde et al., 2014; Fuzzen et al., 2015; Fuzzen et al., 2016; Tanna et al., 2013; Tetreault et al., 2011; Tetreault et al., 2013) and provided this study with datasets for linking predicted EAC concentrations and field-observed effects, including a transition in findings associated with major process upgrades that were completed at the Kitchener WWTP in 2012 (nitrification and replacement of chlorination/dechlorination with UV effluent disinfection).

3.3.2 Modeling strategy

The water quality modeling included three separate components: (1) source, (2) transport and fate, and (3) effects as outlined in Figure 3.2. The source modeling predicted the effluent concentrations from the target WWTPs and was completed as detailed in Arlos et al. (2018). The transport and fate component simulated the movement and distribution of target EACs in the study area and was completed using a water quality model (WASP). Finally, the effects component evaluated the relationship between the predicted river concentrations derived from the transport and fate model component and field-recorded intersex conditions. Due to their relatively high site fidelity (Hicks and Servos, 2017) and constant exposure to WWTP effluents throughout their life cycle, data on rainbow darter were considered suitable for quantifying the exposure impacts. The intersex data for rainbow darter at 9 sites in the Grand River watershed (2007-2015) were compiled by Hicks et al. (2017) and were used in the concentration-response regression analysis (see section 3.3.6).

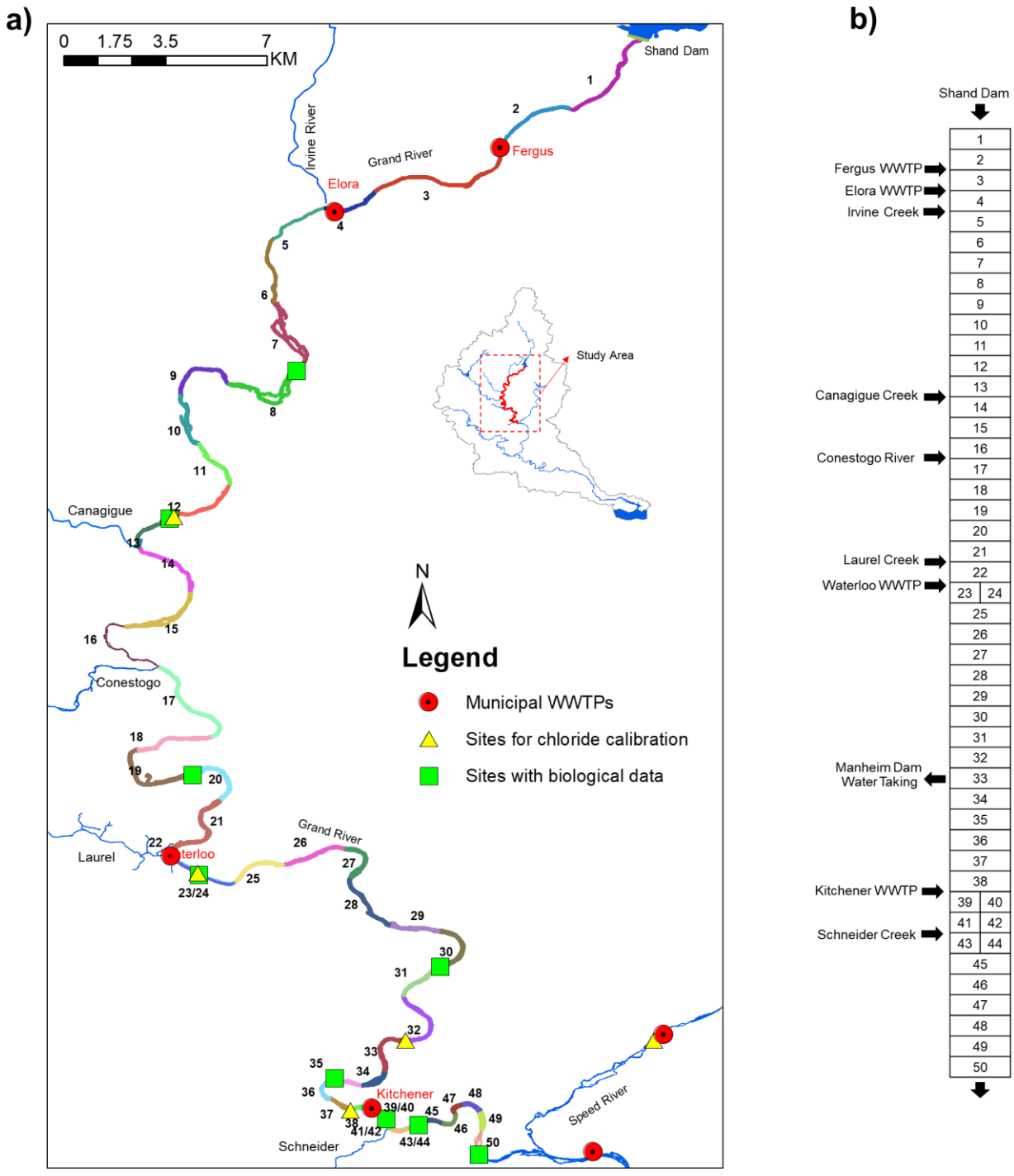

Figure 3.1 (a) Modeled reaches of the Grand River. Sections 23/24, 39/40, 41/42, and 43/44 represent the eastern and western divisions of the single segment. (b) Segmentation profile used in the model.

Table 3.1 Description of the municipal wastewater treatment plants included in the model.

Plant name	Population served	Treatment type (as of 2016)	Average hydraulic contribution to the river flow at low flow conditions
Fergus	19,000	Conventional activated sludge (primary and secondary sludge digesters) with tertiary filters and seasonal UV disinfection	0.9%
Elora	4,000	Conventional activated sludge with tertiary filters and UV disinfection	0.4%
Waterloo	160,000	Conventional activated sludge and partial nitrification with phosphorus removal and UV disinfection	4.8%
Kitchener[a]	232,900	Conventional activated sludge and full nitrification with phosphorus removal and UV disinfection	7.4%

[a]Conditions of the WWTPs prior upgrade are found described in Hicks et al. (2017)

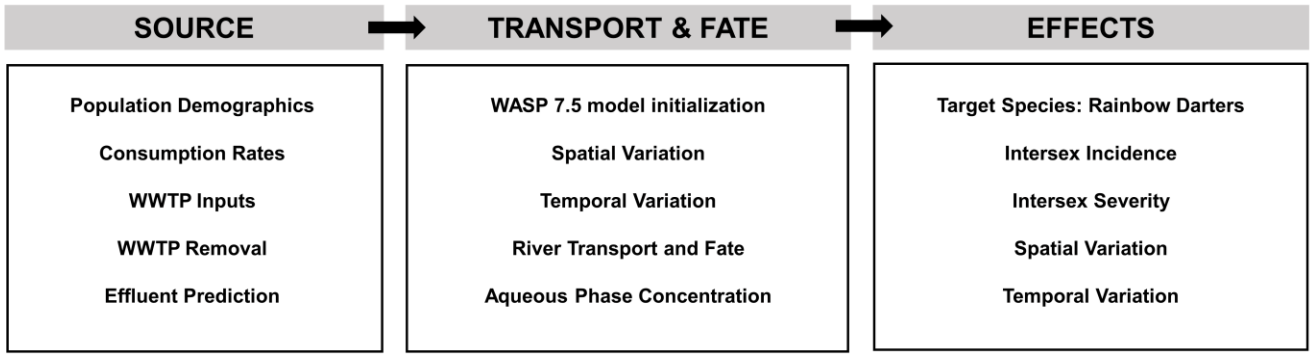

Figure 3.2 General components of the modeling strategy completed in this study.

3.3.3 Prediction of estrogen concentrations in the Grand River

A similar approach to Arlos et al. (2014) was employed to simulate estrogen concentrations in the Grand River. The WASP version 7.3 model, developed by the United States Environmental Protection Agency, was used as the model platform. This model was employed in a recent study that described the distribution of frequently detected pharmaceuticals with varying physical-chemical properties (triclosan, naproxen, venlafaxine, and carbamazepine) in the Grand River downstream of the Kitchener WWTP (~10 km reach). The model has already

been calibrated for compounds that spanned the properties of those examined in the current study and was found to provide robust mechanistic predictions of pharmaceutical fate and transport (Arlos et al., 2014).

Briefly, the following major steps were completed to predict the river concentrations: discretization of the river network; simulation of river transport mechanisms (i.e., advection); testing of the transport processes using a tracer compound (chloride); and integration of organic compound modeling through the addition of significant in-river fate mechanisms (e.g., biodegradation and photolysis). The first three steps were deemed to be crucial in establishing a baseline model that represented the mathematical structure of the system accurately. Completion of these steps was iterative in nature and involved the calibration of parameters specific to each step as detailed in Arlos et al. (2014).

3.3.3.1 Discretization of the river network

The study site was divided into 50 segments. Flows considered as inputs in the network included multiple tributaries and the four municipal WWTPs. To mimic the mixing conditions downstream of the Waterloo and Kitchener WWTPs, the reaches immediately downstream of these plants were discretized into multiple segments (Figure 3.1b). The Elora and Fergus WWTPs have a relatively minor contribution to the overall river flow so a complete mixing condition was assumed immediately below their outfalls. The segmentation is described in detail in the supplementary material (Table S3.1 in Appendix B). Only the aqueous phase was considered in the discretization (i.e., no bottom segments included).

3.3.3.2 Transport conditions

Advection is the primary transport process in rivers and is driven by water flows. The internal flows in WASP under the kinematic wave flow option were propagated using Manning's Equation (supplementary material, Appendix B-1). The model was initially setup to describe water movement and its accuracy was cross-checked against the measured hydro-geometry data such as water levels and flows. Measured water level data for segments 12 and 21 were used for river transport calibration. The finalized input parameters associated with the hydro-geometry and river transport are found in the supplementary material (Table S3.1, Appendix B).

3.3.3.3 Simulation of chloride in the modeled reaches

In addition to examining the model's accuracy in simulating water movement via measured water levels and flows, chloride was also used to determine the non-reactive constituent transport within the network. Since chloride is conservative, its assimilation in the river system is achieved via advection. Significant point sources of chloride in the river network come from urbanized creeks (Laurel and Schneider Creeks) and the WWTPs. Various segments with measured chloride data across the computational network were used as calibrating sites (Figure 3.1a). Observed chloride values at Segments 12, 21, 23, 42, and 50 were taken from Ontario's Provincial Water Quality Monitoring Network (PWQMN) database (https://www.ontario.ca/data) and previous monitoring work completed in the central Grand River (see supplementary material, Tables S3.2 and S3.3, Appendix B).

3.3.4 Modeling of target estrogens

The major inputs of target EACs into the studied reach of the Grand River were from the four WWTPs. Although the tributaries (1 river and 4 creeks) included in the modeled network may be receiving small amounts of estrogens from surrounding agricultural lands (i.e., municipal biosolids/manure applications), this has not been demonstrated in the Grand River as of this study period. Hence, it was assumed that the tributaries have negligible contributions of E1, E2, and EE2. The concentration profiles of the target estrogens in the Kitchener and Waterloo WWTP effluents were developed in a previously reported study (Arlos et al., 2018) that employed population demographics, usage and excretion rates, and removal through the plant to estimate effluent data. A similar approach was completed for the effluents from the Fergus and Elora WWTPs.

Estrogens can be assimilated into the aquatic environment via sorption, biodegradation, and photolysis in addition to transport mechanisms. The simulation of the transport and fate of the target EACs was completed by initially considering them as conservative contaminants (transport as a primary mechanism) and sequentially adding fate mechanisms responsible for their distribution in the aquatic environment. Chapra (1997) has suggested that sorption is minimal when the target compounds have log octanol-water partitioning coefficients (log Kow)

that are <4-5 and the suspended solids concentrations range from 1-50 mg/L. The estrogens examined in this study have log Kow's that are ~4.5 and the average suspended solids concentration in various segments ranged from 6 to 23 mg/L (PWQMN data set from 2007-2014). Hence, sorption was not simulated in this study. This decision was consistent with the results of Jurgens et al. (1999) who reported that estrogens in riverine environments are typically present in the dissolved phase. In addition, a previous modeling study by Arlos et al. (2014) in the Grand River found that inclusion of sorption had a minimal effect on the fate of modeled pharmaceuticals with log Kow of 3.2 to 4.8. Hence, only biodegradation and photolysis were deemed to be significant in the assimilation of estrogens in the aquatic environment (Balaam et al., 2010; Jürgens et al., 2002; Lin and Reinhard, 2005).

Biodegradation and photolysis processes were initialized and calibrated using the approach described by Arlos et al. (2014). Briefly, biodegradation was modeled as a first-order reaction and literature-derived kinetic rate constants (Table S3.4, Appendix B) were initially corrected based on the river temperature (Table S3.5). Temperature profiles for each segment were taken from the nearest PWQMN site (Table S3.5). Photolysis was also modeled as a first-order reaction and the range of reaction constants was derived from the literature (Table S3.4).

3.3.5 Model performance measures

The Nash-Sutcliffe Efficiency (NSE), index of agreement (d), and the percent bias (PBIAS) have been recommended by Moriasi et al. (2007) (Table 3.2) and were used to evaluate the performance of the hydrology portion of the model (i.e., water levels and flows). These performance criteria, however, are not applicable for simulations that have a limited number of measured data points (<50). Hence, a statistical test was completed using either the Pearson or Spearman correlation tests depending on the normality of the datasets (Table S3.9, Appendix B). An additional performance test using the percent difference criteria (Donigian, 2002) was also used to support the results of the correlation analysis (Table 3.2). These quantitative performance measures were used in addition to a subjective comparison of observed and predicted time series plots to assist with model development. Data was not available for all target estrogens in the modeled reach. Hence, the quality of the simulation of EAC fate mechanisms was conducted jointly with the assessment of the effects portion of the model (described in the next section).

Table 3.2 Definition of the performance criteria employed for this modeling study in addition to graphical measures.

Hydrology Component							
Statistic	**Equation**	**Range**	**Optimal Value**	**Very Good**	**Good**	**Satisfactory**	**Unsatisfactory**
NSE	$1 - \frac{\sum_{i=1}^{n}(O_i - P_i)^2}{\sum_{i=1}^{n}(O_i - \bar{O})^2}$	-∞ to 1.0	1.0	>0.80	0.70 to 0.80	0.50 to 0.70	<0.50
d	$1 - \frac{\sum_{i=1}^{n}(O_i - P_i)^2}{\sum_{i=1}^{n}(\lvert P_i - \bar{O}\rvert + \lvert O_i - \bar{O}\rvert)^2}$	0.0 to 1.0	1.0	>0.90	0.85 to 0.90	0.70 to 0.75	<0.75
PBIAS	$\frac{\sum_{i=1}^{n} O_i - P_i}{\sum_{i=1}^{n} O_i} \times 100$	-∞ to ∞	0	±5	±5 to ±10	±10 to ±15	>±15
Tracer contaminant (Chloride)							
PD		-∞ to ∞	0	<20	20-30	30-40	>40
Correlation Test	Pearson test for normal datasets and Spearman test for non-normal datasets	-1.0 to 1.0	-1.0 to 1.0	No performance criteria available but if there is a statistically significant correlation, then, the model performs its predictions well (alpha, $\alpha = 0.05$).			

Note: NSE = Nash-Sutcliffe Efficiency; *d*=index of agreement; PBIAS = percent bias; PD = percent difference.

3.3.6 Linking predicted concentrations (exposure) and intersex conditions (effects)

Although feminization of male rainbow darter has been observed at different levels of biological organization in the Grand River (Fuzzen et al., 2016; Hicks et al., 2017; Marjan et al., 2017c; Tanna et al., 2013; Tetreault et al., 2011), intersex has been found to be the most consistently observed endpoint related to reproductive changes downstream of municipal WWTPs (Fuzzen et al., 2016). Hicks et al. (2017) evaluated intersex incidence and severity from 2007 to 2015 at nine different sites within the study area (Figure 3.1), including periods prior to and after the Kitchener WWTP upgrades. This dataset was used as the primary biological response to which the predicted EAC concentrations were compared. It was assumed that the critical window of exposure for adult rainbow darter occurs during their gonadal recrudescence (late spring to summer) (Hicks et al., 2017). Hence, the predicted river estrogens concentrations from July to August were averaged at the 9 sites to provide the exposure conditions for the fish collected in the fall and spring sampling events of the following year.

The predicted concentrations were converted to total estrogenicity (EEQ) using:

$$EEQ = \sum C_i \times EEF_i \qquad \text{(Equation 3.1)}$$

where C_i is the predicted concentration. EEF_i is the estrogenicity equivalency factor that describes the potency of the estrogens relative to E2. EEFs of 0.3, 1, and 1.23 were used for E1, E2, and EE2 respectively (Jarošová et al., 2014). While several estrogens in municipal wastewater effluent such as estriol (E3), BPA, and octyl/nonylphenols may contribute to the total estrogenicity, a previous study employing an effects-directed analysis (EDA) of Kitchener and Waterloo WWTPs found that the estrogens E1, E2, and EE2 dominated the total estrogenicity (Arlos et al., 2018). Also, the average potency of estriol (E3) and BPA relative to E2 in most *in vitro* studies is only 2.4 to 3.5×10^{-4} and 3.9×10^{-4} respectively (Jarošová et al., 2014; Vega-Morales et al., 2013), suggesting that they do not substantially contribute to the total estrogenicity.

One of the simplest ways to describe the relationships between exposure conditions and effects is through a dose-response model (Barnthouse, 1992). The observed intersex incidence

and severity were related to the predicted EEQ values as per the concentration-response relationship (four-parameter Hill Equation) described by Equation 3.2:

$$Response = \min + \frac{(max - min)}{1 + 10^{(F - EEQ) * H)}} \quad \text{(Equation 3.2)}$$

where the response is either intersex incidence or severity, min and max are the lowest and highest expected responses, F is the response halfway between the min and max (often described as EC50), and H is the Hillslope parameter that describes the steepness of the curve.

The term intersex incidence refers to the percentage of fish with at least one oocyte (female ovarian tissue) in the male testis. For intersex incidence, the maximum response was set to 100% (i.e., all male fish collected were intersex) whereas the minimum was set to 0% (i.e., all male fish collected identified as normal males). By comparison, the intersex severity describes the degree of feminization in each animal and is scored from 0 to 7, with 0 describing a normal male whereas 7 is used for normal female (Bahamonde et al., 2015). The minimum and maximum levels of severity in rainbow darter (Grand River) were set to 0 and 6 respectively (although rare, the highest recorded severity was 6 (Hicks et al., 2017)). Prism 7 (GraphPad Software Inc.) was used to fit the regression model (Equation 3.2) and the goodness of fit (R^2) was employed to determine the quality of the fit between the predicted river estrogen concentrations and intersex data.

3.4 Results and discussion

3.4.1 River hydro-geometry and transport processes

The suitability of model discretization, hydrogeometry, and transport conditions was verified through the simulation of water levels and chloride concentrations at select sites. The results for three sites are shown in Figure 3.3 and the remainder is found in the supplementary material (Figures S3.1-S3.3, Appendix B). A graphical comparison of the calibrated model simulations with the measured data shows that the hydro-geometry and water movement within the network were adequately characterized by the model as depicted by its ability to describe both high and low flow conditions (Figure 3.3a). Also, the NSE, d, PBIAS metrics for the calibration sites had ratings ranging from “satisfactory” to “very good” (Table 3.3) which further

supported the accuracy of predictions. However, there were some periods in segment 12 (upper reach) when the water levels were under-predicted (resulting in "unsatisfactory" simulation, Table 3.3). However, visual and statistical comparisons of observed and predicted water flows were completed for segments 12, 21, and 37 and found to demonstrate an acceptable level of model performance ("satisfactory" to "very good" ratings for NSE, d, and PBIAS, Figure S3.1 in Appendix B).

The good agreement between the observed and simulated chloride concentrations (Figure 3.3 a/b, Table 3.3) further supported the conclusion that the hydro-geometry and transport conditions in the model adequately represented the conditions in the field. In particular, the model captured the different ranges of chloride concentrations measured in different segments (Figure S3.2). As similarly observed for water level simulation, there was no significant correlation between the measured and predicted concentrations for segment 12 when the model performance was evaluated statistically (Table 3.3). However, the mean percent differences (Table 3.3) for all the sites were within the calibration tolerances for water quality modeling, suggesting that the tracer contaminant simulation was acceptable for the purposes of this study (Donigian, 2002).

Table 3.3 Performance measures for water level and chloride concentrations at selected calibration sites.

Water Level			
Segment No.	**NSE (rating)**	***d* (rating)**	**PBIAS (rating)**
12	0.428 (US)	0.794 (G)	15% (S)
37	0.848 (VG)	0.953 (VG)	-3% (VG)
Chloride			
	Correlation Coefficient	**Mean PD (rating)**	
12[a]	no significant correlation	17 (VG)	
21[b]	0.758, $p<0.001$	30 (S)	
23[b]	0.531, $p<0.001$	25 (G)	
32[a]	0.895, $p<0.001$	33 (S)	
41[b]	0.223, $p=0.0515$	19 (VG)	
50[b]	0.836, $p<0.001$	32 (S)	

[a]Datasets are normal and the Pearson correlation test was used (parametric test statistics). [b]Datasets are non-normal so the Spearman non-parametric correlation test was used. Normality test results are found in Table S3.9 (Appendix B). "VG" =very good; "G" = good; "S" = satisfactory; "US" = unsatisfactory; "PD" = percent difference.

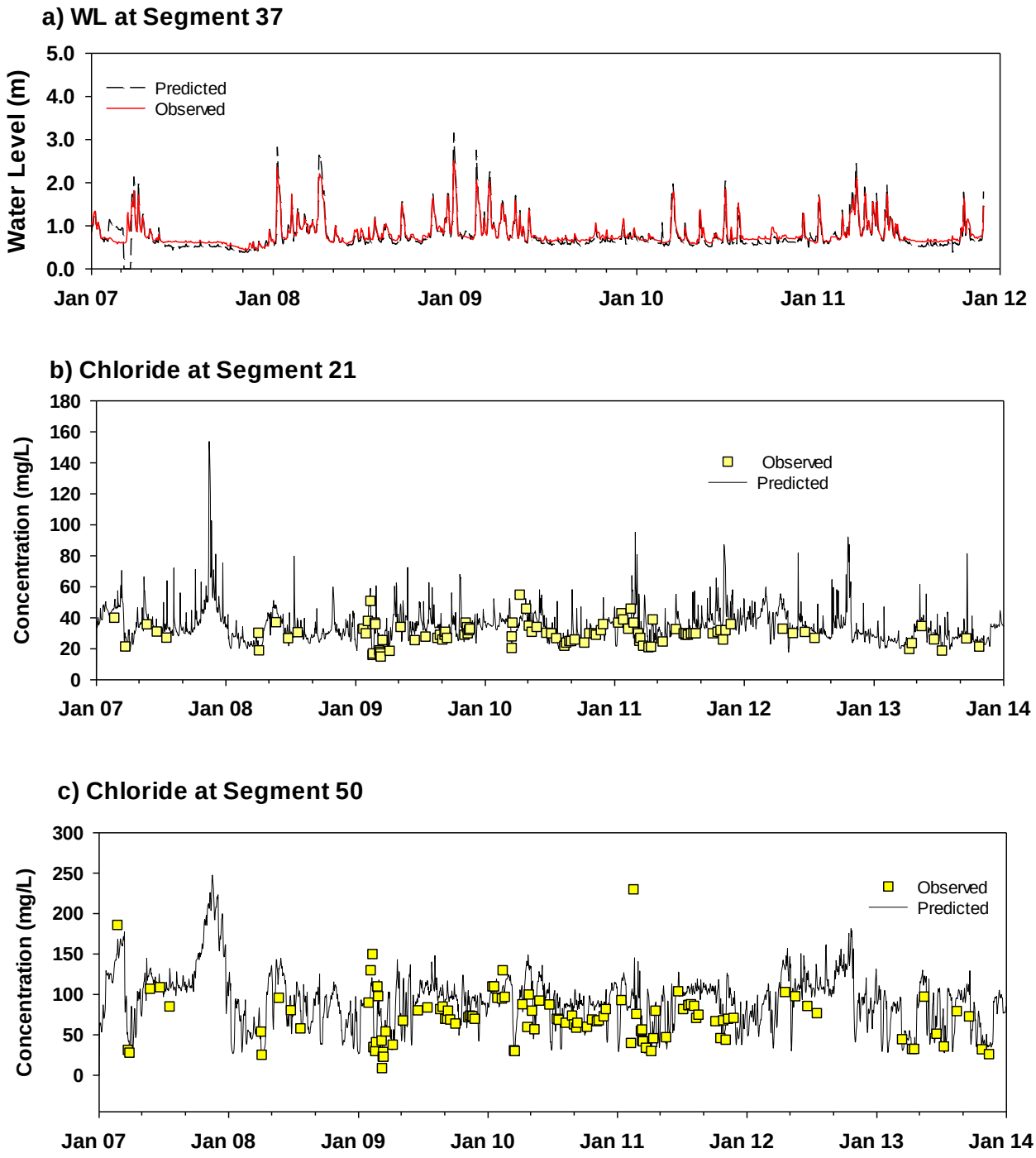

Figure 3.3 (a) Water level simulations and measured values for segments 37; Simulated and measured chloride concentrations at (b) Segment 21 and (b) Segment 50. See Figure 3.1 for relative locations in the modeled network.

3.4.2 Modeling the river concentrations of EACs

The concentrations of estrogens in the selected reaches were first simulated conservatively (assuming no degradation in the reach) (Figure 3.4) and biodegradation and photolysis loss mechanisms were subsequently added. As measured EAC concentrations in the river were not available, improvements in the R^2 value (a goodness of fit measure) derived from the relationship between simulated concentrations and the intersex response data (Equation 3.2) were used as the calibration target. Under the conservative approach, an R^2 value of 0.755 was derived when the concentrations predicted by the model were fitted against the field recorded intersex incidence (Figure 3.4a). A similar R^2 value (0.799) was also obtained for the intersex severity response Figure 3.4b).

While these results were deemed to be indicative of a good fit, the addition of biodegradation and photolysis mechanisms was examined to assess whether the predictions could be improved. It was found that the addition of these processes did not significantly change the results (see Table S3.8 for statistical analysis, Appendix B). The temperature-corrected biodegradation rate constants (literature-derived) were relatively low for all the target compounds (Table S3.4) and the model was found to be insensitive to any factors expected to impact the biodegradation (temperature correction coefficient, rate constants).

A similar trend was observed when photolysis was added to the model. Again, this was attributed to the relatively low photodegradation rate constants (literature-derived) that were employed for the target compounds. This observation was consistent with the environmental fate modeling study of pharmaceuticals in the Grand River during a low-flow condition (downstream of Kitchener WWTP) (Arlos et al., 2014). This prior study demonstrated that the first-order photolysis rate constant must be greater than 3 d^{-1} before photolysis became a significant mechanism in the fate and transport of pharmaceuticals within the modeled reach (with varying physical-chemical properties).

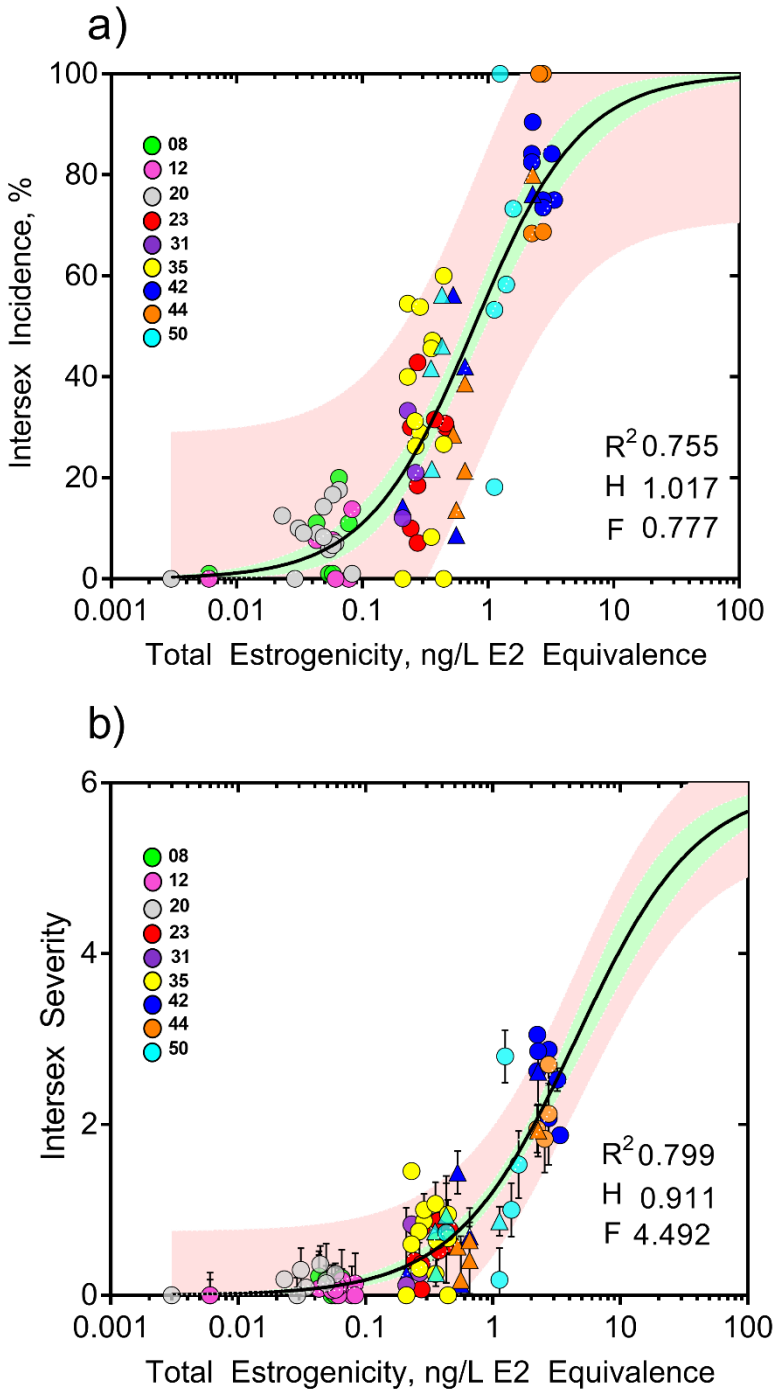

Figure 3.4 Relationship between predicted total estrogenicity and (a) intersex incidence and (b) intersex severity and associated standard errors. Shaded region represents the 95% prediction (red) and confidence (green) intervals. Circles represent the sites with biological data and the triangles represent the post-upgrade period datasets for segments 42, 44, and 50.

The highest direct photolysis rate constants reported for the estrogens in the literature were 3.5, 0.40, 0.58 d^{-1} for E1, E2, and EE2 respectively. As indicated by the magnitude of the rate constants, E1 would be most significantly removed via photolysis. However, its estradiol equivalency factor is only 0.3 compared to 1.25 for EE2. Hence, removals of E1 due to photolysis would result in minimal differences in the predicted estrogenicity. The simulations revealed that considerably large (and inconsistent with literature) values for biodegradation and photolysis rate constants would be required before substantial changes in estrogenicity were predicted (Figure S3.4, Appendix B).

The overall result of the simulations suggests that advection (transport) largely contributed to the distribution of estrogen concentrations in the Grand River as has been previously determined for a variety of pharmaceuticals (Arlos et al., 2014). Hence, the results of the conservative simulations (Figure 3.4) were employed for the subsequent interpretation of the exposure conditions and assessment of potential linkages between predicted estrogenicity and intersex responses.

3.4.3 Temporal patterns and relationship with flows

The predicted concentrations of the target EACs (2007 to 2015) at sites immediately downstream of the two major WWTPs (Waterloo and Kitchener) are presented in Figure 3.5. E1 was predicted to be the most abundant estrogen and contributed, on average, 51% and 65% of the total estrogenicity below the Kitchener (Segment 42) and Waterloo (Segment 23) WWTPs respectively. By contrast, EE2 (the most potent of the key estrogens) only contributed 17% and 18% of the total estrogenicity in the river segments below Kitchener and Waterloo WWTPs respectively. Historically, less attention has been given to E1 due to its lower potency relative to E2 and EE2. However, as observed by this modeling study and many field monitoring surveys worldwide (Blazer et al., 2014; Ma et al., 2016; Matthiessen et al., 2006; Sarmah et al., 2006), E1 can be present at much higher concentrations than its more potent counterparts. Ankley (2017) observed that caged fish (fathead minnows) with high levels of E2 in their tissue were found in river sites with elevated concentrations of E1. They further showed that fish can convert E1 to E2, suggesting that an exposure to high concentrations of E1 should also be considered when assessing risks to estrogen exposure.

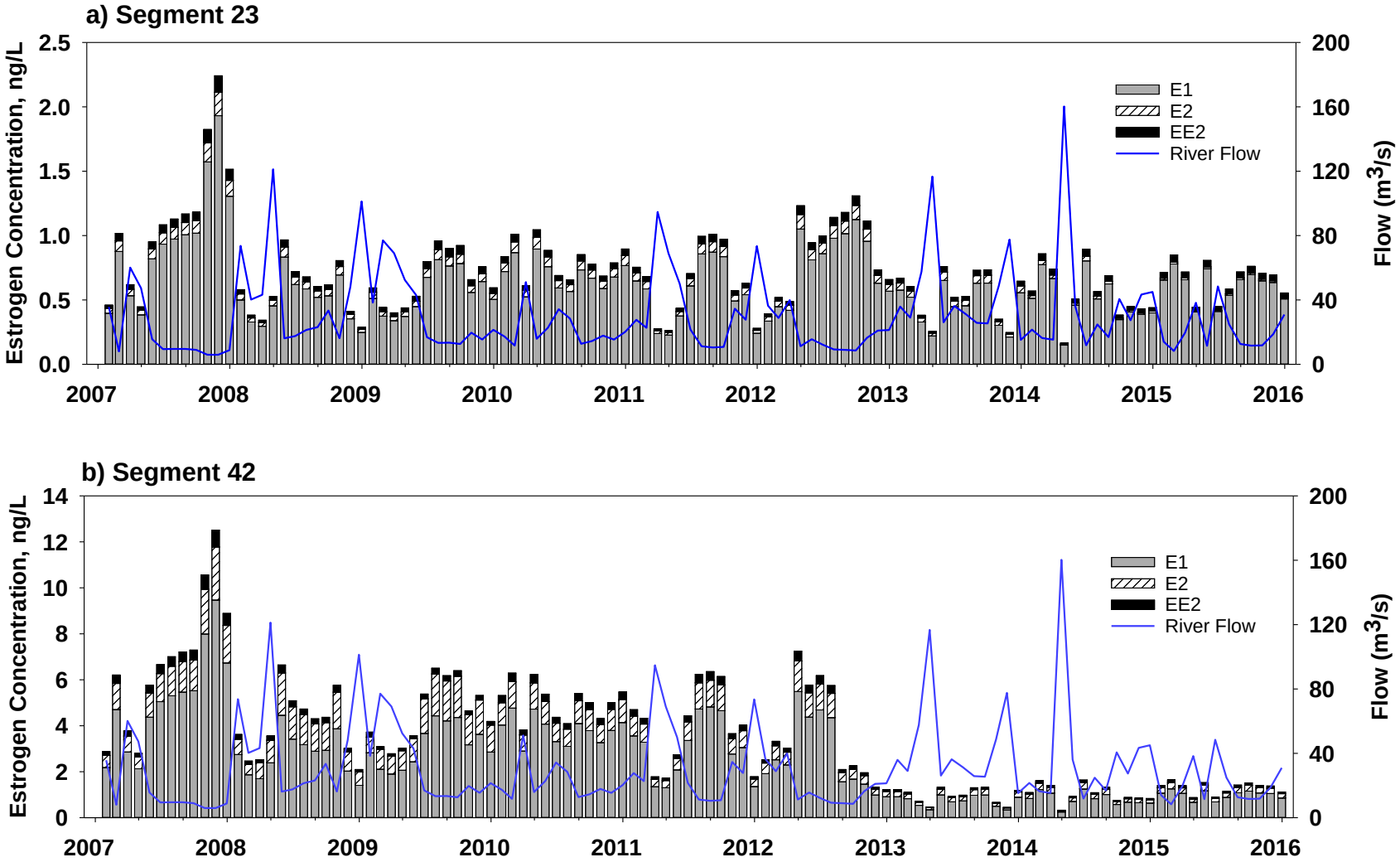

Figure 3.5 Temporal variation (monthly averaged) in estrogen concentrations in segments immediately downstream of (a) Waterloo and (b) Kitchener WWTPs.

Since only contaminant transport conditions were simulated in the model, the impact of river flow on predicted estrogenicity concentrations in the river is evident: low flow periods had high predicted concentrations and *vice-versa* (Figure 3.5). Furthermore, as the removal rates in the river via biodegradation and photolysis were determined to be minimal, the critical exposure conditions are controlled by dilution and will likely occur during low flows (Figure 3.5). The average predicted total estrogenicity that corresponded to flows that were less than or equal to the normal low-flow (11 m^3/s) was 0.45 ng/L (s=0.1 ng/L) E2 equivalents immediately downstream of Waterloo WWTP (Segment 23). The corresponding average predicted estrogenicity below the Kitchener WWTP (Segment 42) was 3.4 ng/L (s=0.9 ng/L) E2 equivalents prior to the WWTP upgrade and was reduced to 0.7 ng/L (s=0.1 ng/L) E2 equivalents post upgrade.

3.4.4 Spatial patterns

In addition to simulating temporally-varying conditions, the model was also employed to resolve the spatial patterns in EAC concentrations in response to the changes in the river (e.g., dilution, change in contaminant loadings due to WWTP upgrades). The analysis of spatial patterns was provided for low flow conditions as these could lead to critical exposures. A representative low flow event (<11 m^3/s) during the pre-upgrade period (May 20, 2012) was compared with a post-upgrade low flow condition (June 11, 2014). These dates were chosen such that the Waterloo WWTP operations and river flows were similar for both periods to avoid issues associated with river dilution (see Table S3.6).

Only low levels of estrogenicity were predicted in the first 50 km of the modeled section in response to the minimal release of estrogens from the two smaller upstream WWTPs (Fergus and Elora). By contrast, elevated estrogenicity concentrations were predicted below the Waterloo WWTP outfall and they persisted until Segment 50 (last modeled segment) at 1.6 ng/L E2 equivalents on May 20, 2012 (Figure 3.6a). The highest estrogenicity concentrations were predicted immediately below the Kitchener WWTP during this period (up to 3 ng/L E2 equivalents). However, the estrogenicity concentrations at all segments downstream of this plant were substantially reduced to 0.5 ng/L E2 (Segment 50) when the process upgrades were implemented (June 11, 2014, Figure 3.6b).

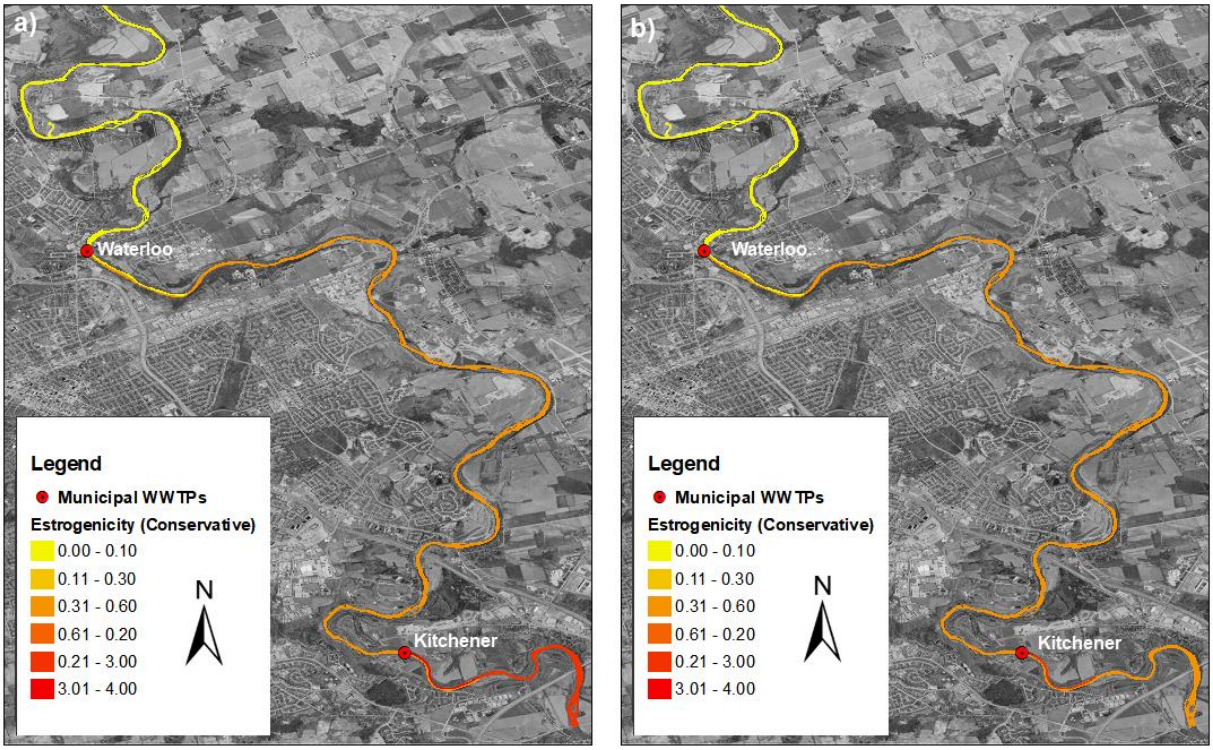

Figure 3.6 Spatial conditions of total estrogenicity during a low flow condition (river flow ≤ 11 m^3/s) (a) pre-upgrade (May 20, 2012) and (b) post-upgrade (June 11, 2014).

It can be observed that the 20-km distance between Waterloo and Kitchener WWTP provided limited dilution of EACs discharged by the Waterloo WWTP during the low-flow period (evident by the unchanged spatial profile between the two plants, Figure 3.6). If the Kitchener WWTP source was removed from the model, an estrogenicity concentration of approximately 0.3 ng/L E2 equivalents was predicted at Segment 50 (most downstream modeled segment) because of the inputs from the upstream Waterloo outfall. This simulation suggests that although some of the estrogenicity in the river below the Kitchener outfall was due to the Kitchener effluent post-upgrade, it appears that >60% of the exposure at Segment 50 was from the upstream Waterloo effluent (see Table S3.7, Appendix B). Hicks et al. (2017) showed low levels of incidence and severity of intersex in rainbow darter have persisted downstream of the Waterloo outfall, with similar levels below the Kitchener outfall after the upgrades. To determine the impact of future process upgrades at the Waterloo WWTP, a removal efficiency through the plant of 95% was implemented in the model and the concentrations of EAC were simulated. The

results of this simulation revealed that under a low flow scenario (June 11, 2014), the predicted estrogenicity would be reduced to ~0.2 ng/L E2 equivalents.

Overall, the modeling of the transport and fate of the key estrogens in the Grand River is useful in evaluating the efficiency of the current WWTP operation during a critical exposure condition (low flow). The significance of the temporally and spatially varied concentrations assessed with the field-recorded intersex conditions in the Grand River is discussed in the subsequent section.

3.4.5 Linkages to biological effects observed in the field

The concentration-response curve (Figure 3.4) is a fitted four-parameter Hill model that employs the predicted total estrogenicity derived from the river model and the intersex responses collected in the field (i.e., incidence and severity). Although this approach is not frequently employed, the study provides a useful relationship that can predict the effects associated with a given exposure (i.e., range of concentrations in the river). For instance, the concentration-response relationship (Figure 3.4a) suggests that the presence of 10 ng/L of total estrogenicity would feminize 93% (95% CI:89-97) of adult male rainbow darter, corresponding to a predicted mean intersex severity score of 4 (95% CI:3.6-4.4) (severely intersex fish have scores of 4-6 (Bahamonde et al., 2015). Although an estrogenicity of 10 ng/L E2 equivalents was never predicted at any sites in the Grand River, the high incidence of intersex (80% to 100%) that was mostly observed downstream of Kitchener WWTP (Segment 41, pre-upgrade) corresponded to a predicted total estrogenicity of 2.5 ng/L E2 equivalents (ranging from 0.8 to 6.1 ng/L E2 eq., Figure 3.4a).

The average background intersex conditions of the upstream (Segments 7, 12) and urban (Segment 19) reference sites were calculated to be 7.4% (s=6%) and 0.1 (s=0.1) for intersex incidence and severity (dataset from Hicks Hicks et al. (2017)). After the Kitchener WWTP upgrade (2013), the predicted estrogenicity at Segment 41 (immediately below the Kitchener outfall) ranged from 0.1 to 0.6 ng/L E2 equivalents. This concentration was predicted to cause 11% (95% CI:7-15) to 43% (95% CI:39-48) intersex incidence with a severity of 0.1 (95% CI :0.03-0.17) to 0.8 (95% CI:0.7-0.9) (Figure 3.4), suggesting that the levels are approaching the background conditions. This result also represented a major improvement in exposure conditions

associated with upgrades that were primarily intended for ammonia removal. The Waterloo WWTP will continue to contribute to the total estrogenicity but once upgrades at both plants have been implemented (i.e., 95% removal of estrogens is anticipated), the corresponding average estrogenicity concentration in the river below the Kitchener WWTP (Segment 41) was predicted to be ~0.2 ng/L E2 equivalents and this would correspond to low intersex incidence (20% with 95% CI:16-24) and severity scores (0.3 with 95% CI:0.2-0.4).

The model (Equation 3.2) predicts results that are consistent with a laboratory experiment by Fuzzen (personal communication, November 13, 2017) wherein 10 ng/L EE2 resulted in 100% female population was observed in larval fish (rainbow darter) exposed to 10 ng/L of EE2 (~12.5 E2 equivalents). In a separate experiment (Fuzzen, 2016), this concentration also significantly reduced the fertilization success in adult males. A similar observation (100% female population) was observed by Lange et al. (2009) when *Rutilus rutilus* (roach) were exposed to 4 ng/L EE2 for 2 years. Furthermore, Kidd et al. (2007) observed a population collapse in fathead minnows exposed to 5 ng/L EE2 (6 ng/L E2 equivalents) in a whole lake experiment whereas a life-cycle exposure of the same fish species to <1 ng/L of EE2 reduced male secondary characteristics (Parrott and Blunt, 2005).

Jobling et al. (2006) examined the relationship between the modeled total estrogenicity and observed intersex in wild fish population (roach) in the UK. They estimated that river sites with estrogenicities ranging from 1 to 10 ng/L E2 equivalents will cause an intersex incidence of 22% in a wild roach population. They categorized this exposure condition as medium risk whereas sites with >10 ng/L E2 equivalents were considered as having high-risk of exposure. By contrast the current study indicates that 1 to 10 ng/L of E2 equivalents will result in an intersex incidence between 53% to ~100%, with a predicted severity level ranging from moderate to highly severe conditions. The minor inconsistency between the Jobling et al. results and those of the current study may be attributed to the species difference (rainbow darter vs. roach) as well as the procedures employed in estimating the in-river estrogen concentrations (steady-state vs. time-variable hydrodynamic model).

Fernandez et al. (2007) assessed the estrogenicity in Canadian wastewaters using *in vitro* bioassays and detected total estrogenicities ranging from 9 to 106 ng/L E2 eq. After

incorporating a 100-fold dilution factor, it can be expected that low to moderate levels of intersex will still be associated with many effluents in Canada. However, the relatively steep concentration-response curve (Figure 3.4) also suggests that improved treatment can dramatically reduce intersex incidence and severity in watersheds as what has already been observed in the Grand River (Hicks et al., 2017).

3.4.6 Extrapolating the effects associated with thresholds recommended by other studies

Caldwell et al. (2012) determined the predicted no effects concentration (PNECs) of 6, 2, 0.1, and 60 ng/L for E1, E2, EE2, and E3 respectively based on the species sensitivity distribution (SSD) approach. Similarly, the EU derived an EQS of 0.4 and 0.035 ng/L for E2 and EE2 respectively. Considering only the recommended thresholds for E2 from both studies, an estrogenicity level of 2 ng/L and 0.4 ng/L E2 equivalents is predicted to cause 72% (95% CI:66-78) and 34% intersex incidence (95% CI:29-37) in rainbow darter respectively and corresponds to severity scores of 1.95 (95% CI:1.8,2.1) (moderate) and 0.60 (95% CI:0.5-0.7) (low). Although a relatively high incidence of intersex is predicted, the model is still supportive of the current E2 threshold recommendations (Caldwell and EU EQS) since adverse impacts on rainbow darter reproduction was estimated to occur only at very severe levels (severity score of 4-6) (Fuzzen et al., 2015). Hence, this study demonstrates the validity and usefulness of the recommended thresholds from the literature when assessing potential adverse impacts resulting from estrogen exposure.

When an *in vitro* bioassay is employed in water quality monitoring, Escher et al. (2015) proposed that total estrogenicities ranging from 0.2 to 12 ng/L E2 equivalents should trigger additional investigation so as not to compromise the potential adverse effects on exposed aquatic organisms. Alternatively, Jarošová et al. (2014) recommended a “safe” level of total estrogenicity of 0.1 to 0.4 ng/L E2 equivalents for effluent dominated streams (close to 100% effluent contribution). Based on our study, the upper limit trigger value proposed by Escher et al. (2015) was predicted to cause a high incidence of intersex and moderately severe to highly severe intersex conditions.

Furthermore, it appears that for both intersex incidence and severity, an estrogenicity of <0.1 ng/L will result in relatively lower intersex occurrence (up to 10%) and severity conditions in rainbow darter. Whether this level (<0.1 ng/L) should be set as a threshold for estrogenicity still requires additional studies employing both field and laboratory techniques that test several ecologically relevant endpoints. Nevertheless, this study has provided an *a priori* information that can assist with future hypothesis-driven studies related to estrogen exposure and may be used for other river systems with similar estrogenicity sources (i.e., point sources).

3.5 Conclusions

The concentrations of E1, E2, and EE2, compounds that contribute a large fraction of municipal wastewater-derived total estrogenicity in surface waters, were predicted using a mechanistic water quality model. It was determined that transport conditions play a major role in the spatial and temporal distribution of the target EACs in the case study (e.g. Grand River), while fate mechanisms such as biodegradation and photolysis had minimal influence. The relationships between the exposure concentrations (during the period of gonadal recrudescence for rainbow darter) and intersex incidence and severity were also developed using the four-parameter Hill concentration-response model. An estrogenicity level of <0.1 ng/L E2 equivalents is predicted to result in up to 10% intersex incidence and a low severity score of <1 which may unlikely impact the rainbow darter reproductive health. This work is consistent with the recommended thresholds for exposure and can support future risk assessments and subsequent regulation of natural and synthetic estrogens in surface waters.

Chapter 4

Influence of methanol when used as a water-miscible carrier of pharmaceuticals in TiO_2 photocatalytic degradation experiments

Modified from Journal of Environmental and Chemical Engineering, 5, M.J. Arlos, R. Liang, L.C.M. Li Chun Fong, N. Y. Zhou, C.J. Ptacek, S. A. Andrews, and M.R. Servos. Influence of methanol when used as a water-miscible carrier of pharmaceuticals in TiO_2 photocatalytic degradation experiments, 4497-4504, Copyright 2017, with permission from Elsevier.

4.1 Chapter summary

Research on the use of titanium dioxide (TiO_2) for water treatment has expanded to include the degradation of pharmaceuticals and personal care products (PPCPs). PPCPs are typically introduced in aqueous solutions during TiO_2 photocatalysis experiments using a water-miscible carrier solvent (e.g. methanol) to improve their solubility; however, carrier solvents may be detrimental to photocatalysis due to their scavenging effect. Although it is advisable to maintain the solvent at low concentrations, the influence of elevated concentrations of methanol or other solvents on photocatalysis has not been carefully explored. In this study, we examined the impacts of different methanol concentrations (0 to 0.2% v/v) on photocatalysis using P25 (commercial TiO_2) and TiO_2 nanomaterial synthesized via thermal and chemical oxidation (TCO). Scavenging of hydroxyl radicals by methanol was evident for both P25 and TCO but the effect was more prominent on TCO. Also, the photodegradation of some compounds using P25 was enhanced at low levels of methanol. Overall, this study highlights that trace amounts of methanol used as a carrier solvent can affect photocatalysis, especially in TiO_2 nanomaterials with low reactivity. This should be considered carefully in future experiments so that the results are not biased by the introduction of carrier solvents.

4.2 Introduction

Studies on the use of titanium dioxide (TiO_2) for environmental applications has grown rapidly since the discovery of its photocatalytic potential over four decades ago (Fujishima and Honda, 1972). Among the semiconductors that can initiate photocatalytic processes, TiO_2 is the most widely used material due to its relatively higher activity, non-toxic effects, inert qualities, resistance to corrosion, and low associated costs (Khataee and Kasiri, 2010). The use of TiO_2 for a variety of industrial applications began in the 1990s, mainly as a paint additive and glass coating because of its self-cleaning and anti-fogging functions (Hashimoto et al., 2005). With advances in nanoscience and nanotechnology, alternative synthesis methods and improvement in TiO_2 structural properties continue to progress. Alongside this development is the pressing need for advanced, low-cost, and efficient water treatment technologies to address the declining clean water sources worldwide (Chong et al., 2010). In addition, long-term droughts and increased

water demands have motivated the development of new water reuse, recycling, and reclamation strategies (i.e., indirect potable or non-potable reuse systems) that stress the need for robust treatment technologies to handle a diversity of contaminants emanating from unconventional water sources (Schimmoller et al., 2015). The ubiquity of the so-called emerging contaminants of concern in source waters, primarily pharmaceuticals and personal care products (PPCPs), has been a subject of water research for a number of years due to their potential risks to aquatic and human health (Daughton and Ternes, 1999). These combined challenges have encouraged several research and development studies that highlighted the potential use of TiO_2 photocatalysis for water treatment applications.

Numerous studies have suggested the use of TiO_2 photocatalysis in the effective degradation of PPCPs in water (Miranda-García et al., 2010; Miranda-García et al., 2011; Tong et al., 2012). Much of the current work has also employed methanol as a carrier solvent when conducting TiO_2 photocatalytic degradation experiments on PPCPs (Table 4.1). This practice facilitates the introduction of the compounds into aqueous matrices, as some are poorly soluble in water. However, the presence of methanol can be detrimental to PPCP removal due to its ability to scavenge the electron holes (Nosaka and Nosaka, 2013) and/or the hydroxyl radicals (Paul et al., 2007) produced during photocatalysis. When an organic compound is present, its degradation via TiO_2 photocatalysis occurs in two main pathways: (1) reactions via singlet electron transfer (SET) (i.e. hole-mediated and electron-donating processes); or, (2) reactions with hydroxyl radicals and other generated reactive oxygen species (Jenks, 2013). Methanol degradation is typically initiated by SET chemistry (i.e. hole-mediated) (Jenks, 2013; Panayotov et al., 2012) and, in fact, it has been used as an efficient hole scavenger in photocatalytic experiments (Jenks, 2013). However, there is still a mixed interpretation of the degradation pathway of alcohols as studies have utilized methanol as a hydroxyl radical scavenger rather than a hole scavenger (Paul et al., 2007; Sun and Pignatello, 1995). This practice was derived from experiments that did not observe the presence of ketone- and aldehyde-type intermediates which are indicator compounds for SET reactions (Jenks, 2013). Regardless of the mechanism, only a few studies discussed the effects of the carrier solvent on their photocatalysis experiments (Arlos et al., 2016a; Molinari et al., 2015; Skaf et al., 2016; Sun et al., 2010; Woo et al., 2009).

Although methanol and other carrier solvents are typically maintained at low concentrations from 0.002% to 0.5% v/v (Table 4.1), it is still important to assess the scavenging effects of these low concentrations of solvents when determining the overall efficiency of TiO_2 photocatalysis in degrading pharmaceuticals or other similar chemicals.

Table 4.1 Selected studies that employed carrier solvents during experimental investigations of photocatalytic decomposition of pharmaceuticals.

Carrier Solvent	No. of compounds	Carrier solvent concentration (v/v)	Reference
Methanol	15	0.004%[a]	Miranda-García et al. (2010)
Methanol	1	0.17%	Sun et al. (2010)
Acetonitirile	4	0.953%[a]	Li Puma et al. (2010)
Methanol	15	0.004%[a]	Miranda-García et al. (2011)
Methanol	2	0.5%[b]	Nasuhoglu et al. (2012)
Methanol	1	0.01%	Kralchevska et al. (2012)
Methanol	3	N/A	Marinho et al. (2013)
Methanol	33	0.4%[a]	Fernández et al. (2014)
Methanol	15	0.004%[a]	Miranda-García et al. (2014)
Methanol	2	0.1%	Yang et al. (2015)
Ethanol	2	0.075%[a]	Colina-Márquez et al. (2015)
Methanol	14	0.002%	Arlos et al. (2016a)
Methanol	5	0.002%	Arlos et al. (2016b)

[a]Calculated based on the data provided in the study. [b]Calculated based on the highest concentration of the target chemical in the mixture (~5 mg/L). N/A = not available nor cannot be calculated from the information provided.

In this study, we explored the influence of low levels of methanol additions (0%, 0.002%, 0.02% and 0.2% v/v) on photocatalytic degradation of 15 target compounds typically discharged in wastewater streams (Kasprzyk-Hordern et al., 2009; Nikolaou et al., 2007). The photocatalysis of these representative contaminants using commercially available TiO_2 nanopowder (P25) was compared to a TiO_2 material synthesized using the thermal-chemical oxidation of titanium powder (TCO). The study examines the overall confounding effects of the use of methanol when conducting TiO_2 photocatalysis tests on PPCPs.

4.3 Materials and methods

4.3.1 Reagents and chemicals

Titanium powder (~325 mesh, 99.95%), hydrochloric acid (HCl), sodium hydroxide (NaOH), and hydrogen peroxide (H_2O_2) were purchased from Sigma-Aldrich while the

commercial P25 powder (Aeroxide) was purchased from Evonik Industries. HPLC grade methanol (BDH) was purchased from VWR (Mississauga, ON) while ultrapure water was obtained from a MilliQ water purification system (MilliQ, EMD Millipore, Mississauga, ON). The 15 compounds included in this study have varying solubility and physical-chemical properties (Table 4.2) and were purchased from Sigma-Aldrich. Their chemical structures are presented in Figure S4.4 (Appendix C). Designated isotopically labeled standards were used for LC-MS/MS analysis and quantitation (except for monensin) and lorazepam was used as an internal standard (Table S4.2, Appendix C). These standards were purchased from CDN Isotopes Inc. (Pointe-Claire, QC, Canada), except for atorvastatin-d_5, which was purchased from Toronto Research Chemicals (Toronto, ON, Canada). The complete list of the deuterated standards employed in this study is provided in Table S4.2 (Appendix C). All compounds (regular and deuterated standards) were dissolved in methanol as 1 g/L stock solutions and stored in amber glass vials in a -20^{o}C freezer.

4.3.2 Thermal-chemical oxidation method (TCO) for nanomaterial synthesis

Titanium powder (1 g) was soaked in 50 mL of 30% H_2O_2 in a 500-mL clear glass jar which was capped and heat treated for 4 h at 80^{o}C producing a titanium-titanium dioxide complex in solution. The remaining liquid (yellowish in appearance) was transferred into a second glass jar and dried at 80^{o}C for 12 h. The powdered material that remained after evaporation was pulverised and heat treated again at 600^{o}C for 4 h. After the heat treatment, the material was stored in a glass vial and kept in the dark at room temperature.

4.3.3 Nanomaterial characterization

The surface morphology of TiO_2 nanomaterials was characterized by a high-resolution transmission electron microscope (HRTEM, JEOL 2010F) at the Canadian Centre for Electron Microscopy (CCEM). TEM samples were prepared by drop casting powder dispersions onto carbon grids. The X-ray photoelectron spectroscopy (XPS) was carried out to verify the presence of TiO_2. The measurement was conducted using VG Scientific ESCALab 250 system with an aluminum radiation source (hv = 1486.6 eV) under ultra-high vacuum. A survey scan was collected at 50 eV pass energy, whereas individual scans (Ti2p and O1s) were collected at 20 eV

Table 4.2 Selected physico-chemical properties of target compounds in this study.

Compound	Abbreviation	Use	Molecular Weight (g/mol)	Log Kow[a]	pKa_1, pKa_2, pKa_3[b]	Solubility in water (at 25°C, mg/L) [a]
Atenolol	ATEN	Beta-blocker	266.34	-2.5 to 0.31	9.60, 14.08, 15.95	24.24×10^3
Atorvastatin	ATOR	Lipid lowering	558.64	1.03 to 4.46	4.33	1.23×10^3
Atrazine	ATZ	Herbicide	215.68	2.20	1.68	33 (20°C)
Carbamazepine	CBZ	Anti-epileptic	236.27	1.34 to 2.5	13.90	18[c]
Diclofenac	DCF	Anti-inflammatory	296.15	-0.81 to 4.5	4.00	1.13×10^3 (32°C)
Fluoxetine	FLX	Antidepressant	309.33	0.59 to 4.65	9.80	50×10^3 [c]
Gemfibrozil	GEM	Lipid lowering	250.33	1.77 to 4.4	4.42	125
Ibuprofen	IBU	Anti-inflammatory	206.28	2.97 to 4.5	4.80	156
Monensin	MON	Antibiotic	692.85	4.82	4.3	NS
Naproxen	NAP	Anti-inflammatory	230.60	3.06 to 3.22	4.12	15.9
Sulfamethoxazole	SULF	Antibiotic	253.28	-1.54 to 0.95	1.60,5.70	550 (30°C)
Triclosan	TCS	Antimicrobial	289.54	3.82 to 4.8	7.60	11
Triclocarban	TCB	Antimicrobial	315.58	4.71	12.70	2.37×10^{-3}
Trimethoprim	TRIM	Antibiotic	290.32	-2.05 to 0.91	7.3	400
Venlafaxine	VEN	Antidepressant	277.40	1.95	8.91,14.42	267[c]

Notes: pKa = acid dissociation constant; Kow = octanol-water partition coefficient; [a]Values were taken from https://www.reaxys.com (a range of values were identified to reflect database derived from multiple studies); [b]pKa was taken from http://chemicalize.org; [c]value was taken from https://pubchem.ncbi.nlm.nih.gov; NS = not soluble in water.

pass energy. The atomic concentration was calculated using the CasaXPS software (Casa Software Ltd.).

The specific surface area was determined using Brunauer-Emmett-Teller (BET) surface analyzer (Quantachrome Autosorb iQ) using $N_{2(g)}$ adsorption data. The band gap of TiO_2 samples was determined by the diffuse reflectance spectra (DRS) using a Shimadzu UV-2501PC UV-Visible-NIR spectrophotometer equipped with an integrating sphere accessory, using $N_{2(g)}$ as the reference. The details regarding the band gap analysis are described by Hu et al. (2011). A Raman spectrometer (Renishaw Ramanscope) equipped with a He-Ne laser (5 mW incident power, 633 nm wavelength) was used to obtain spectra associated with different TiO_2 crystalline phases. Specific information on the TiO_2 Raman mode description is found elsewhere (Arlos et al., 2016a).

4.3.4 Experimental setup

Two types of TiO_2 nanomaterials were tested in this study: (1) P25, a commercially available TiO_2 powder and (2) TCO, a powder derived from the thermal-chemical oxidation of titanium powder. Different concentrations of methanol were selected based on the range of values observed in published studies that used methanol as a carrier solvent (Table 4.1). For each set of experiments, an empty 1 L amber glass solvent bottle was spiked with 200 µL of the 10 mg/L pharmaceutical stock solution in methanol (diluted from 1 g/L solution) and dried at room temperature using $N_{2(g)}$. For P25 experiments, the pharmaceutical compounds were re-solubilized in 1 L ultrapure water and stirred at 1100 rpm for 5 min. Aliquots (300 mL) of this solution containing 2 µg/L of pharmaceuticals were transferred into three beakers for replication and magnetically stirred (600 rpm) on a four-position stir plate equipped with an in-house designed UV-LED light source casing. Pre-measured P25 powder (30 mg) was added into each beaker and methanol was spiked immediately at different volumes (6, 60, and 600 µL) to obtain 0.002%, 0.02%, and 0.2% of methanol concentration (v/v). The experimental specifications of the photocatalytic batch reactors, including the light intensity, wavelength, and relative distance of the LED source to the reactors, are provided elsewhere (Arlos et al., 2016a).

An equilibration period of 60 min in the dark was completed prior to exposure to the UV-LED light source. Water samples (5 mL) were collected using a glass pipette into test tubes

every 30 min until the exposure reached 210 min. The test tubes were then centrifuged (Sorvall XTR Centrifuge, ThermoFisher) at 3500 rpm for 15 min to separate the TiO_2 particles from the aqueous phase. For TCO powder, 100 mg was initially dispersed for 5 min in 1 L ultrapure water through sonication (Fisherbrand Ultrasonic Cleaner). The solution was transferred to the 1 L amber glass solvent bottle containing the dried pharmaceuticals and the compounds were re-solubilized by stirring for 5 min at 1100 rpm. The same steps for P25 experiments were followed thereafter. All the samples were stored in the dark at 4^{o}C until sample preparation. Additional control experiments (dark and photolysis experiments, 0% methanol) were also completed. Finally, experiments (n=3) that determined the formation of hydroxyterephthalic acid (HTPA) upon the reaction of its parent compound (terephthalic acid [TPA]) to hydroxyl radicals were done using the method described in Arlos et al. (2016b). This step provided an indication of the photocatalytic activity of the two nanomaterials and the level of hydroxyl radical scavenging by methanol in aqueous solutions.

4.3.5 Sample preparation and analysis

The samples were spiked with a deuterated standard stock solution (final concentration of 20 µg/L) and followed a concentration and purification process via solid phase extraction (SPE) using the same method detailed in Arlos et al. (2016a). The analysis of compounds was completed using an Agilent 1200 HPLC (Agilent Technologies) coupled to a mass spectrometer (3200 QTRAP, ABSciex, Concord, ON). The optimized parameter values, including the chromatographic and ionization parameters, data acquisition, and quantitation are also detailed in Arlos et al. (2016a). The parameters of additional compounds that were not included in that study are presented in the Supplementary material (Tables S4.1 and S4.2, Appendix C). Measured degradation rate constants were fitted using SigmaPlot (Jandel Scientific).

4.4 Results and discussion

4.4.1 Nanomaterial characterization

The two types of TiO_2 nanomaterials were characterized: P25 and TCO powder. The SEM images of the nanomaterials are shown in Figure 4.1. P25 has clustered particles that are 10

to 30 nm. TCO has micron-sized agglomerated structures that contain crystalline anatase nanorod structures shown in Figure 4.1. The band gap energies of P25 and TCO are 3.05 and 3.00 eV respectively, suggesting that wavelengths below 400 nm are required to create electron-hole pairs Figure 4.2a. The Raman spectra of the materials presented in Figure 4.2b show that anatase is the primary crystalline phase for the TCO powder but there are some indications that rutile structures were also produced. The commercially available P25 powder is made up of pure TiO_2 mainly with anatase and rutile content at ~80% and ~20% by weight (Evonik, 2015). The lower bandgap of TCO is due to the higher amount of rutile content in the TCO sample compared to P25. The surface areas of P25 and TCO determined by BET measurements are 57.39 g/m^2 and 27.21 g/m^2 respectively.

XPS spectra were collected and the atomic concentration of Ti and O were determined for P25 and TCO powders as shown in Figure 4.3. P25 contained 89.54 at.% of O and 10.46 at.% of Ti, whereas TCO contained 91.05 at.% of O and 8.95 at.% of Ti. The $Ti2p_{3/2}$ peak of the TCO spectrum exhibited greater peak broadening than P25 suggesting more surface defects are present in TCO compared to P25 (Göpel et al., 1984).

Based on the physical properties of P25 and TCO, it can be inferred that P25 may be a more effective catalyst than the newly synthesized TCO powder due to high purity TiO_2 content, reported synergetic effect of anatase and rutile configurations found in P25, and relatively higher BET surface area. The mixed crystalline phase of P25 provides hotspots for catalytic reactions, particularly at the anatase-rutile interface (Hurum et al., 2003), and TiO_2 nanomaterials with the higher surface area are better photocatalysts due to the availability of more active sites that interact with the target compounds. In addition, the surface defects in TCO contribute to the increased charge carrier recombination which renders the material less active.

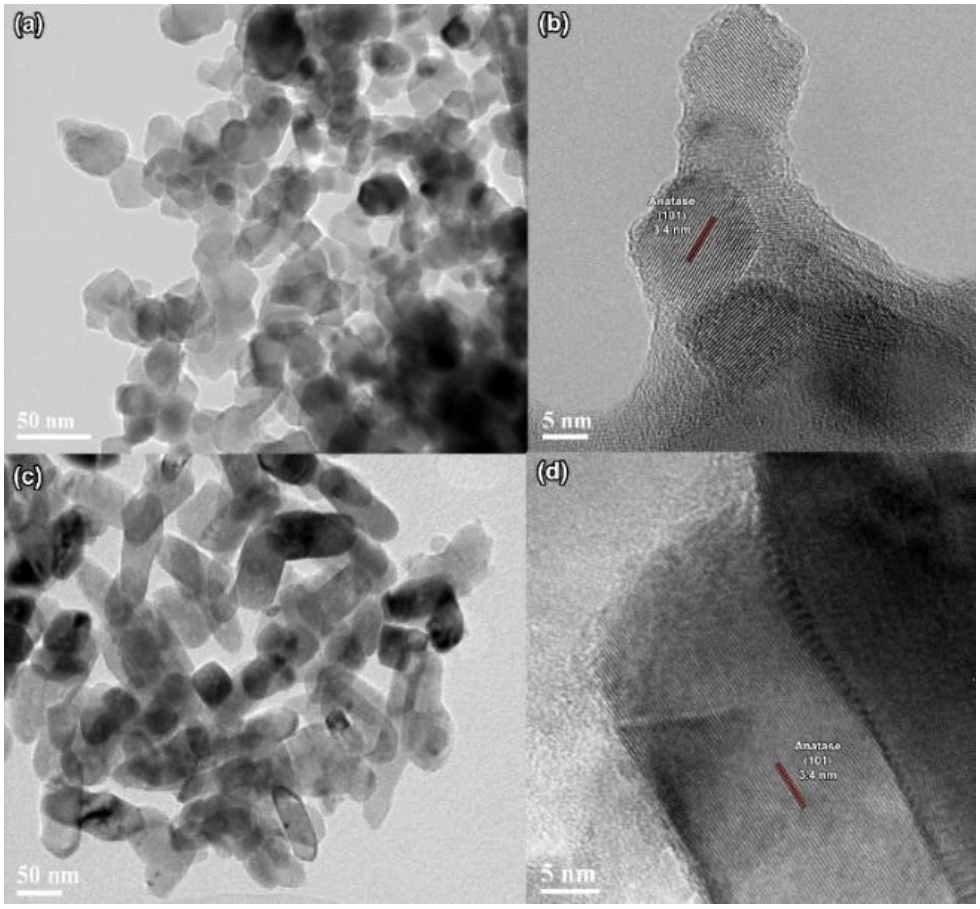

Figure 4.1 TEM/HRTEM images of (a,b) P25 and (c,d) TCO powder

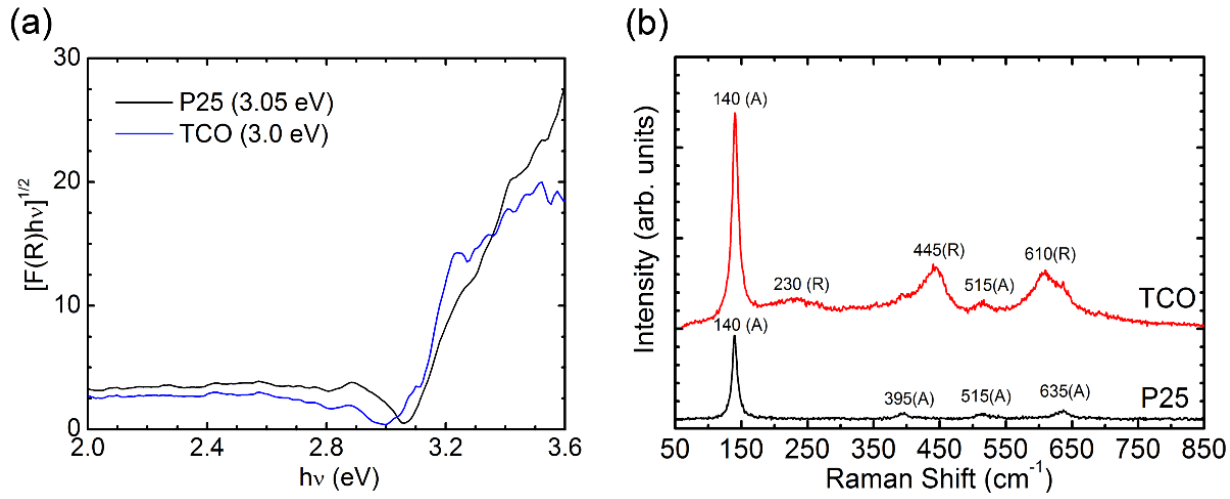

Figure 4.2 Additional material characteristics for P25 and TCO powder. (a) Band gap energies; (b) Raman spectra.

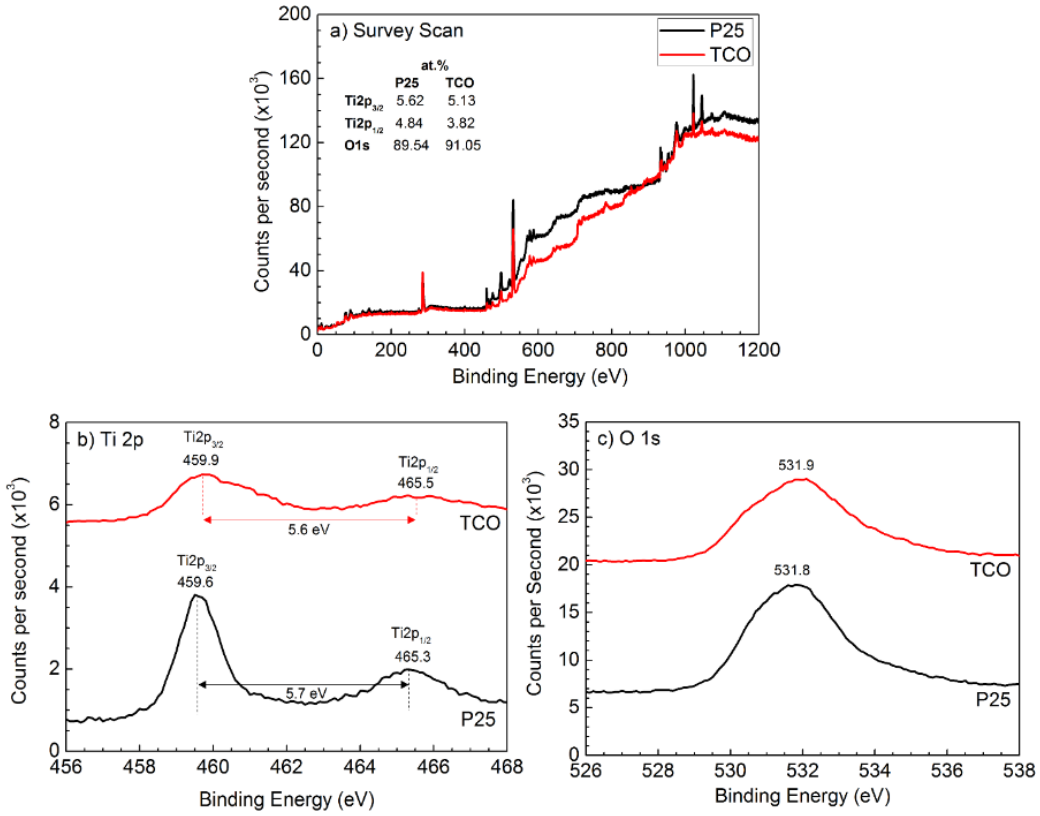

Figure 4.3 XPS (a) Survey, (b) Ti2p, (c) O1s scan of P25 and TCO powders

4.4.2 Probing the formation and scavenging of hydroxyl radicals

The probing of the HTPA formation was used as an indirect measurement of the nanomaterial's photocatalytic activity via hydroxyl radical production. HTPA formation at 0% methanol was at least 46 times higher for P25 compared to TCO (Figure 4.4, Table S4.8 in Appendix C). P25 was indeed more effective than the newly synthesized TCO. The mixed crystalline phase of P25 provided hotspots for catalytic reactions, particularly at the anatase-rutile interface (Hurum et al., 2003). Optimization may be required in the future to achieve the potential of TCO powder synthesis for water treatment applications. Nevertheless, it is evident that the presence of methanol impacts the photocatalytic activity of both nanomaterials by scavenging of hydroxyl radicals (i.e. inhibiting HTPA formation) formed during the photo-activation of P25 and TCO (Figure 4.4). There was a significant difference in the inhibition of HTPA formation among the methanol treatments for both P25 and TCO ($p<0.001$, ANOVA,

Tukey Test, post ad-hoc, α=0.05), indicating that even low levels of methanol may be impacting the results of TiO_2 photocatalytic studies. In particular, adding 0.002% in the experiment reduced the rate of HTPA formation by 20% and 30% for P25 and TCO respectively while 0.2% methanol in the solution inhibits the activity by 98% for both materials.

To gain an improved understanding of the potential mechanisms under the above-mentioned scenarios, the mechanisms of photocatalytic degradation via TiO_2 need to be carefully examined. When TiO_2 is activated, electron-hole pairs are generated and the fate of these high-energy charge carriers is dependent on the availability of molecules that can scavenge and/or trap them. Essentially, electrons can be easily scavenged by electron acceptors (e.g. oxygen) producing hydroxyl radicals and/or other ROS while the holes are quenched by electron donors such as water. An organic compound can be degraded directly by the holes or hydroxyl radicals. In circumstances when methanol concentration is low (<0.5 M), the oxidation via hydroxyl radical is the likely degradation route (Sun and Bolton, 1996). In this study, there is a substantial inhibition of HTPA formation when methanol concentrations in the solutions were increased, likely suggesting that methanol acts as hydroxyl radical scavenger more than a hole scavenger.

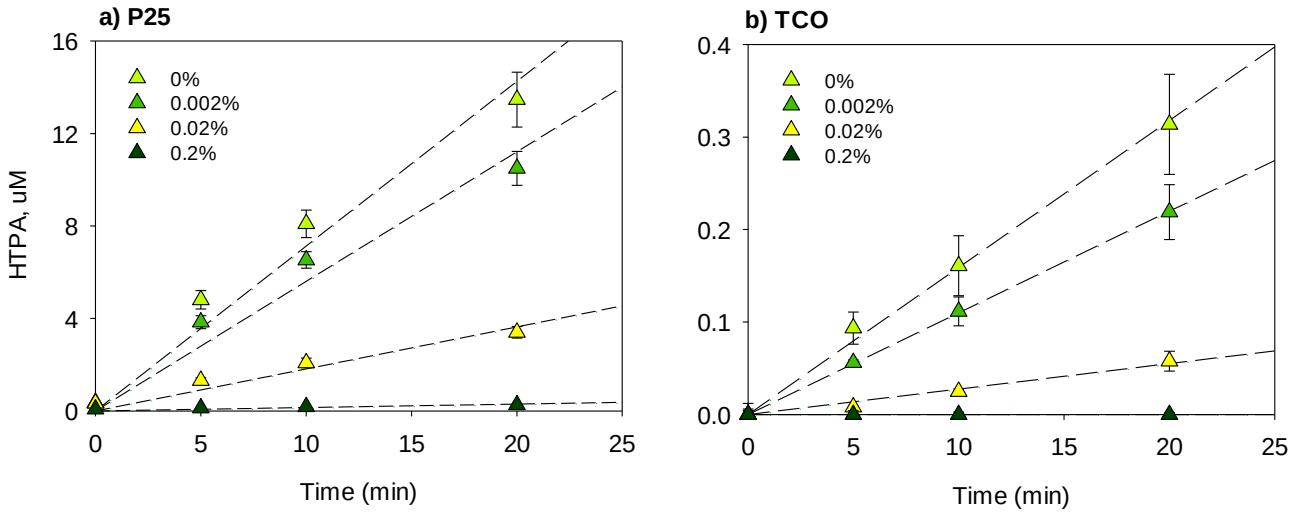

Figure 4.4 HTPA formation for (a) P25 and (b) TCO at different concentrations of methanol. The average rates of HTPA formation are found in the supplementary material (Table S4.8, Appendix C).

4.4.3 Effect of methanol on PPCP photocatalysis

To determine the influence of a carrier solvent during photocatalysis of PPCPs, different amounts of methanol (0%, 0.002%, 0.02%, and 0.2% v/v) were spiked into a solution containing a mixture of target PPCPs and 100 mg/L of TiO_2 nanomaterials (P25 or TCO). The observed degradation rate constants of most compounds in the presence of UV-LED irradiated P25 were indicative of a pseudo-first order exponential decay: $C = C_o e^{-k_p t}$ where C_o is the initial concentration (µg/L), t is time (min), and k_p (1/min) is the pseudo first-order decay rate constant (Figures S4.1 and S4.2, Appendix C). The rate constants derived from this equation are shown in Figure 4.5 for P25 and Figure 4.6 for TCO to illustrate the observed trends (also listed in Tables S4.3 and S4.4, Appendix C). The following discussion highlights the potential mechanisms for methanol scavenging of hydroxyl radicals and other ROS and its overall influence in each of the photocatalytic treatment investigation.

4.4.4 P25 experiments

The behavior of the target compounds at different levels of methanol under P25 treatment conditions (Figure 4.5) can be categorized into three groups: (1) no effect (Figure 4.5a); (2) scavenging effect (Figure 4.5b); and, (3) enhanced effect at low levels of methanol (Figure 4.5c). The compounds atorvastatin, atrazine, and naproxen (Figure 4.5a) showed statistically similar degradation at all methanol levels (SigmaPlot, One-way ANOVA, α=0.05, p=0.698 and 0.089 respectively). This is a favorable result as these compounds can be introduced in the aqueous solution using methanol (up to 0.2% v/v) without any major consequences. Carbamazepine, diclofenac, fluoxetine, and triclocarban showed reaction inhibition either at 0.002% or 0.02% methanol (Figure 4.5b). Above these thresholds, the scavenging effects become evident (see Table S4.5 for *p*-values, Appendix C). Hence, it is safe to suggest that methanol may be used to deliver these compounds in the solution during the experiments up to 0.002% or 0.02% v/v.

It appears that for some compounds (atenolol, trimethoprim, venlafaxine, ibuprofen, monensin, and sulfamethoxazole), small amounts of methanol can lead to an enhancement of PPCP degradation (Figure 4.5c) but methanol scavenging of hydroxyl radicals or other ROS was still evident at concentrations above these "optimal" conditions (either at 0.002% or 0.02% v/v,

Figure 4.5c). The rate constants for atenolol, trimethoprim, and venlafaxine at 0.002% methanol were statistically greater than the rate constants observed at 0% methanol (p=0.003, 0.004, and 0.002 respectively) but were statistically lower at 0.02% (p<0.001 for all). A similar pattern was detected for ibuprofen, monensin, and sulfamethoxazole but the "optimal" condition was observed at 0.02% rather than at 0.002%. A sporadic pattern for triclosan and gemfibrozil decay rate constants at different methanol concentrations was observed but the highest degradation rate constant was observed at 0.02% and the lowest occurred at 0.2%, when there was the highest amount of methanol in the solution.

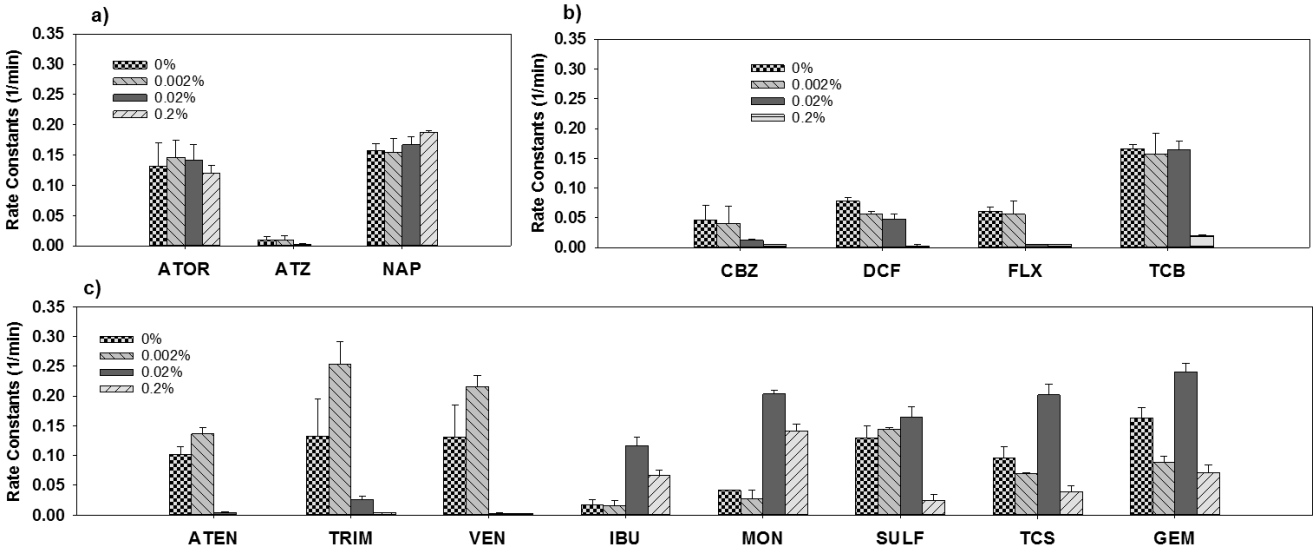

Figure 4.5 Pseudo first-order rate constants for all target compounds using UV-LED irradiated P25 powder at different methanol concentrations. a) Compounds that were not affected by the presence of methanol. b) Compounds with rate constants decreasing at increasing methanol concentration. c) Compounds with rate constants enhanced by some levels of methanol in the solution.

The dark control experiments conducted without methanol showed no significant loss of compounds via adsorption onto TiO_2 or glass walls (except for atorvastatin and monensin, Figure S4.3, Appendix C). The results for photolysis experiments (UV-LED only) were also similar, with only three compounds (atorvastatin, monensin, and triclocarban) showing susceptibility to degradation after UV-LED irradiation only (Figure S4.3, Appendix C). Note that improvements in the photocatalytic degradation behavior were observed for those compounds that were prone to both adsorption (dark control) and photolysis (UV-LED exposure only).

The results showing that some compounds (atorvastatin, atrazine, and naproxen) were not affected by methanol at any of the methanol concentrations evaluated under P25 treatment suggest that either these compounds have (1) better reactivity towards P25 than methanol or (2) undergo a degradation pathway (e.g., via SET mechanism) that is not exacerbated by methanol. Other factors such as exposure to UV-LED alone or adsorption onto TiO_2 may play a role in the non-observable effects of methanol on their degradation. This process is primarily illustrated by atorvastatin, a compound which is susceptible to both TiO_2 adsorption and photolysis reactions (Figure S4.3, Appendix C). By contrast, compounds that have been affected by methanol may have competed with the carrier solvent for reaction sites on TiO_2 surfaces and/or hydroxyl radicals generated after the photo-activation.

Some studies have suggested that the presence of scavengers (radical, electron, or hole scavengers) can enhance photocatalysis by preventing the recombination of charge carriers (Syoufian and Nakashima, 2008) or by producing highly reactive by-products that can additionally "attack" the target compounds (e.g. photosensitizers) (Rengaraj and Li, 2007; Zhu et al., 2012). A previous work on the photocatalytic decomposition of polycyclic aromatic hydrocarbons (PAHs) further indicated an efficient degradation due to the enhanced solubility of PAHs under the presence of a carrier solvent (acetone) (Woo et al., 2009). Zhu et al. (2005) observed an improvement in the photocatalytic degradation of pyridaben (pesticide, water solubility of 1.2×10^{-2} mg/L, 25°C) when the amounts of acetone were slightly increased. Skaf et al. (2016) also found a similar result when 1,3-dinitrobenzene, a compound with comparable solubility to our target chemicals (533 mg/L, 25°C), was introduced to the solution with a carrier solvent during TiO_2 photocatalysis. We recognize that additional studies are needed to confirm these results (especially for gemfibrozil and triclosan) and to identify the fundamental mechanisms of photocatalytic enhancement by scavengers.

4.4.5 TCO experiments

Unlike the variable behavior of target compounds under P25 treatments, the rate constants calculated for TCO treatments showed a decreasing trend as the concentrations of methanol in solution increased (Figure 4.6). This observation demonstrates the "classic" scavenging effect of methanol during TiO_2 photocatalysis as per the inhibition of HTPA

formation shown earlier (Figure 4.4). A significant difference was detected even when the methanol concentration was added at the lowest level evaluated in the study (0.002% v/v) for some compounds, especially atorvastatin, diclofenac, and naproxen. Other compounds, in contrast, showed a significant drop in the first order kinetic rate constants when methanol was at 0.02% or 0.2% v/v (*p*-values are presented in Table S4.6, Appendix C). A few compounds (atrazine, carbamazepine, ibuprofen, and venlafaxine) showed no degradation during the irradiation period, even without methanol. For TCO, it may be better to eliminate the use of a carrier solvent such as methanol as the scavenging effect was very pronounced even at low levels of methanol.

Additional studies could be done in the future to understand the differences in the results observed for P25 and TCO. For example, application of structure-activity relationships (SAR) for hydroxyl radical reactions could help clarify the patterns detected (e.g. why certain compounds have higher reactivity towards P25). It is clear in this present study that the use of carrier solvent has consequences for future experimental design and the interpretation of the results. For example, the use of excess methanol may confound the subsequent comparisons among new materials or among different water sources/quality.

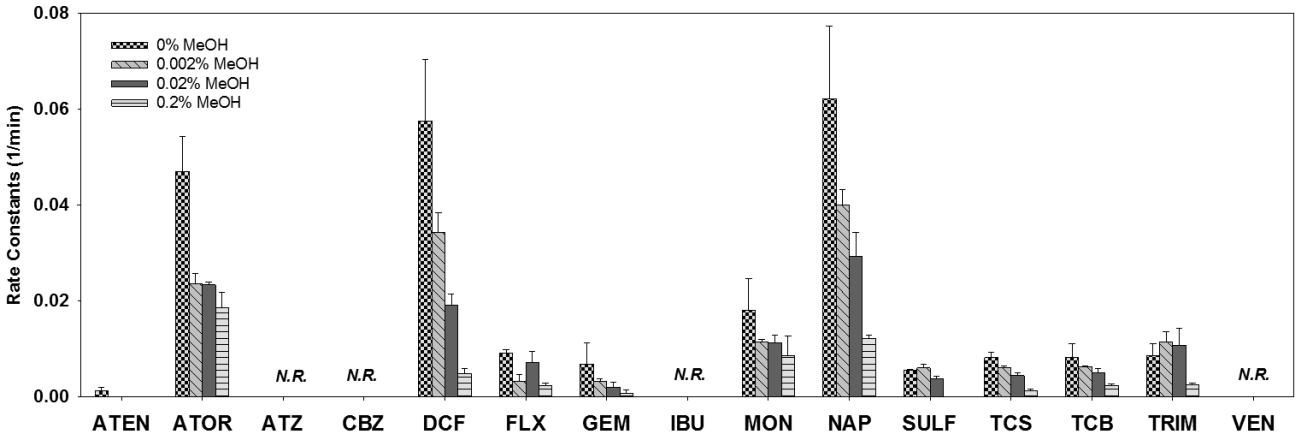

Figure 4.6 Pseudo first-order rate constants for all target compounds using UV-LED irradiated TCO powder. Pseudo first-order rate constants for all compounds decreased with increasing methanol concentration. N.R. = no response in the treatment.

4.4.6 Implications of the use of methanol for designing treatment experiments

The varying behavior of PPCPs under the presence of a carrier solvent, such as methanol as outlined above, has consequences in the design of experiments that evaluate the photocatalytic degradation of organic compounds in mixtures. When it comes to comparing the reaction or treatment efficiency of two or more nanomaterials, it is intuitively important to complete the experiments under the same conditions (e.g. same methanol concentration all throughout). However, as was demonstrated in this study, not all TiO_2 nanomaterials (or chemicals) behave similarly in the presence of methanol as a carrier solvent (i.e. scavenging effect in TCO, but not necessarily for P25). It appears that materials with lower reactivity such as TCO are easier targets for methanol scavenging. An investigator without *a priori* knowledge on the treatment efficiency of a new catalyst may conduct the experiments at different starting points (e.g. deliver target compounds using a carrier solvent at a relatively higher concentration). This is particularly important for investigators that are optimizing new materials, as future results may be misinterpreted.

Early investigations on the degradation of organic compounds in aqueous solutions using TiO_2 did not require the use of carrier solvents such as methanol because the model chemicals being investigated were very soluble in water (e.g. dye, organic acids, or phenolic compounds such as 4-chlorophenol). However, efforts to examine the use of TiO_2 for water treatment applications have expanded beyond the use of these highly water-soluble chemicals because they are not necessarily representative of the compounds being addressed by water treatment systems currently. Investigations have now included very diverse groups of compounds with varying types and levels of physical and chemical properties, including water solubility. While it may be more beneficial to conduct experiments without the use of a carrier solvent such as methanol, caution must be undertaken if it is used.

Westerhoff et al. (2005) suggested the use of acetone to introduce the pharmaceuticals in aqueous solutions instead of methanol as the radical scavenging effect is not as pronounced. Other organic solvents may also be used but recognizing the pathway they scavenge is beneficial for the interpretation of the experimental results. For instance, dimethysulfoxide (DMSO) is a commonly used carrier solvent but is also known to scavenge electrons. If the degradation

pathway of the target compound(s) is via SET, then DMSO may not impact the overall photocatalytic process. Regardless of the direction chosen, investigators must carefully assess the influence of the carrier solvent in the overall photocatalytic degradation and, at the very least, explicitly report its use during the experiment.

4.5 Conclusions

The use of a carrier solvent to deliver PPCPs and other similar compounds into aqueous solutions is a common practice used for preparing solutions for radical-mediated degradation experiments using photocatalytic materials such as TiO_2. However, the presence of a carrier solvent such as methanol can greatly reduce the chemical degradation rates during TiO_2 photocatalysis due to its inherent scavenging effect. In this study, we examined four levels of methanol concentrations that are representative of what has been used in the literature: 0%, 0.002%, 0.02% and 0.2% v/v methanol. The lowest level, 0.002% v/v, did not influence the rates of photocatalytic degradation of some target compounds when treated with a more photoactive TiO_2 nanomaterial such as P25. This result suggests that future studies using P25 alone may be able to use trace amounts of methanol as a carrier, but higher levels may confound the results. However, the influence of methanol when using a less reactive material such as the newly synthesized material included in this study (i.e. TiO_2 produced under thermal-chemical oxidation of titanium powder) was more pronounced than when using P25. It would be ideal to conduct experiments without a solvent carrier as even as little as 0.002% v/v methanol had some confounding effects. The results of this study illustrate that the effect of methanol as a carrier solvent must be assessed in radical-mediated testing especially for comparisons of newly synthesized TiO_2 nanomaterials (e.g. TCO) to avoid unbiased interpretation of experimental results.

Chapter 5

Photocatalytic decomposition of organic micropollutants using immobilized TiO_2 having different isoelectric points

Modified from Water Research, 101, M.J. Arlos, M.H. Hatat-Fraile, R. Liang, L.M. Bragg, N.Y. Zhou, S. A. Andrews, and M.R. Servos. Photocatalytic decomposition of organic micropollutants using immobilized TiO_2 having different isoelectric points, 351-361, Copyright 2016, with permission from Elsevier.

5.1 Chapter summary

Organic micropollutants found in the environment are a diverse group of compounds that includes pharmaceuticals, personal care products, and endocrine disruptors. Their presence in the aquatic environment continues to be a concern as the risk they pose towards both the environment and human health is still inconclusive. Removal of these compounds from water and wastewater is difficult to achieve and often incomplete, but UV-TiO_2 is a promising treatment approach. In this study, the efficiency of titanium dioxide (TiO_2) immobilized on porous supports was tested for treatment of target pharmaceuticals and their metabolites under UV-LED exposure, a potential low energy and cost-effective alternative to conventional UV lamps. Immobilization was completed using two different methods: (1) dip coating of TiO_2 onto quartz fiber filters (QFT) or (2) thermal-chemical oxidation of porous titanium sheets (PTT). Comparison against experimental controls (dark QFT, dark PTT, and photolysis using UV-LED only) showed that UV-LED/PTT and UV-LED/QFT treatments have the potential to reduce the concentrations of the target compounds. However, the treatments were found to be selective, such that individual pharmaceuticals were removed well using QFT and PTT but not both. The complementary treatment behavior is likely driven by electrostatic interactions of charged compounds with the membranes. QFT membranes are negatively charged at the experimental pH (4.5 to 5) while PTT membranes are positively charged. As a result, cationic compounds interact more with QFT while anionic compounds with PTT. Neutral compounds, however, were found to be recalcitrant under any treatment conditions suggesting that ionic interactions were important for reactions to occur. This behavior can be advantageous if specificity is required. The behavior of pharmaceutical metabolites is similar to the parent compounds. However, isomeric metabolites of atorvastatin with functional groups in *para* and *ortho* configurations behave differently, suggesting that the positioning of functional groups can have an impact on their interaction with the immobilized TiO_2. It was also apparent that PTT can be reused after cleaning by heat treatment. Overall, these newly synthesized membrane materials have potential applications for treatment of trace organic contaminants in water.

5.2 Introduction

Following municipal wastewater treatment, effluents are typically discharged into receiving aquatic environments such as rivers and lakes. These natural systems can act as buffers that assimilate residual contaminants through physical (e.g., sorption and photolysis) and biological (i.e., biodegradation) processes. However, many pharmaceuticals and personal care products (PPCPs) entering sewer systems through human excretion or hygienic practices remain recalcitrant for both wastewater treatment and natural attenuation (Brausch and Rand, 2011; Liu et al., 2009; Luo et al., 2014; Verlicchi et al., 2012). These compounds occur at trace levels but because of their therapeutic properties, long-term chronic exposure to PPCPs can have impacts on the aquatic organisms (Cleuvers, 2004; Thomaidi et al., 2015). Drinking water sources are often taken from effluent-impacted surface waters or aquifers (AWWA, 2014). Although human health risks are considered to be low or even negligible (Christensen, 1998; Schwab et al., 2005), high uncertainty exists because of insufficient monitoring and toxicological data (Kumar et al., 2010) and a lack of understanding of potential mixture effects to support the risk assessment. The public's negative perception and concern surrounding the presence of these compounds in water sources have also been growing. Some jurisdictions such as Switzerland have already started implementing advanced treatment upgrades in their wastewater plants as a strategy to reduce PPCP discharge into the environment (Eggen et al., 2014).

Immense effort has been expanded in the last decade to determine effective treatment options for PPCPs in drinking water. It is now well known that conventional systems are not capable of removing all PPCPs as they were not primarily designed for the removal of these compounds. Treatment plants with advanced oxidation processes (AOPs) such as either ozonation or ultraviolet (UV) irradiation with the addition of hydrogen peroxide (H_2O_2) oxidation have been shown to transform a broader range of PPCPs (Klavarioti et al., 2009). Recent studies completed by Fernández et al. (2014); Giri et al. (2010); Hu et al. (2011); Miranda-García et al. (2010) have additionally suggested the effectiveness of UV-irradiated titanium dioxide (TiO_2) in removing a number of pharmaceuticals such as steroidal estrogens, antibiotics, and analgesics.

TiO_2 has been receiving more attention in water treatment studies due to the nonspecific nature of reactive oxygen species produced by UV irradiation. TiO_2 acts as a photocatalyst where upon activation by light, an electron from the valence band moves up to the conduction band, adding a free electron (e^-) in the conduction band but leaving an electron hole (h^+) in the valence band (Linsebigler et al., 1995; Schneider et al., 2014). Overall, this excitation creates an ideal condition for redox reactions upon contact with oxygen and water which consequently generates active oxygen species that can attack organic molecules. The energy carriers (e^- and h^+) are also capable of redox reactions directly with pollutants (Schneider et al., 2014). In the absence of e^- and h^+ scavengers, the carriers can recombine and release the energy as heat.

TiO_2 is readily available in powder form, usually particles at nanoscale sizes to maximize photo-activity through increased surface area. However, the potential of TiO_2 nanoparticle suspensions in large scale water treatment is limited to the exhaustive efforts required for particle recovery. In addition to potential reuse, nanoparticles must be recovered to avoid human and environmental exposure to TiO_2 or to substances adsorbed to it as studies concerning their toxicity to human and aquatic ecosystem health have not been very conclusive (Clemente et al., 2011). A number of studies have minimized this problem by immobilizing TiO_2 on/in a variety of membrane supports, such as ceramic (e.g., alumina), polymeric (e.g., polyethersulfone) and metallic (e.g., aluminum) materials (Leong et al., 2014)

The potential application of UV-LED/TiO_2 during water treatment may provide another promising option in the removal of organic micropollutants in the environment, particularly in drinking water sources. This study assessed the treatment of PPCPs and pharmaceutical metabolites with UV-LED irradiated TiO_2 immobilized on porous supports via (1) dip-coating of quartz (SiO_2) fiber filters with sol-gel synthesized TiO_2 nanoparticle suspensions and (2) thermal and chemical oxidation of porous titanium sheets producing self-assembled TiO_2.

5.3 Materials and methods

5.3.1 Reagents and chemicals

Quartz fiber filters (Type A/E, 50 mm diameter, pore size 1 µm) were purchased from Pall Corporation (VWR International) while porous titanium sheets (50% porosity, 0.254 mm

thick) were purchased from Accumet Materials (Ossining, NY, USA). All solvents and chemicals (99 % purity) mentioned under the membrane preparation section were purchased from Sigma-Aldrich. Ultrapure water was obtained from a Milli-Q System with 18 MΩ·cm resistivity at 25 ^{o}C (EMD Millipore, Mississauga, ON). The parent compounds and selected metabolites (Table 5.1) were purchased from Sigma-Aldrich. Their associated isotopically labeled standards were purchased from CDN Isotopes Inc. (Pointe-Claire, QC, Canada) with the exception of atorvastatin-d_5, *o*-hydroxyatorvastin-d_5, and *p*-hydroxyatorvastin-d_5 which were purchased from Toronto Research Chemicals (Toronto, ON, Canada). The suppliers for all the reagents and chemicals associated with the sample preparation and chemical analysis are described in detail elsewhere (Arlos et al., 2015).

5.3.2 TiO_2 immobilization

5.3.2.1 Quartz fiber-TiO_2 (QFT) synthesis

Quartz fiber-TiO_2 (QFT) composite materials were prepared using the sol-gel method as described by Mendret et al. (2013). Briefly, TiO_2 nanoparticles were synthesized by mixing two solutions of (a) ultrapure water/isopropyl alcohol (IPA) and (b) titanium tetraisopropoxide (TTIP)/IPA at 20 ^{o}C. The concentrations of water (C_w) and TTIP (C_{TTIP}) in IPA were 0.265 M and 0.126 M respectively which was equivalent to a hydrolysis ratio (C_w/C_{TTIP}) of 2.1. Equal volumes of these reactant solutions (100 mL) were pumped into a static T-mixer using two peristaltic pumps at a flow rate of 0.6 L min^{-1}. T-mixer detailed design and hydrodynamics are found elsewhere (Hatat-Fraile et al., 2013).

Quartz fiber filters were first soaked in sulphuric acid (98%) for one hour, rinsed with ultrapure water, and dried at 70 ^{o}C overnight. The supports were submerged for 90 s in TiO_2 nanoparticle suspension and were withdrawn at a speed of 2 cm min^{-1} using a PTL-MMBO1 dip-coating apparatus (MTI Corporation, Richmond, CA, USA). This process was repeated six times and the coated filters were dried again at 70 ^{o}C overnight. After drying, the membranes were calcined at 400 ^{o}C set point temperature for one hour with a heating rate of 2 ^{o}C min^{-1}. The membranes were washed with ultrapure water to remove unbound nanoparticles.

Table 5.1 Physical and chemical properties of target compounds in this study.

Compound	Deuterated standard	Use	Abbr.	Molecular Weight (g mol^{-1})	Log Kow	[Dose] (nM)	pKa_1, pKa_2, pKa_3[b]	Dominant species at pH 4.5 to 5[b]	Ionisable functional group/s
Pharmaceuticals									
carbamazepine	carbamazepine- d_5	anti-epileptic	CBZ	236.27	1.89	8.46	13.90	neutral	amide
venlafaxine	venlafaxine- d_6	antidepressant	ATOR	277.40	3.20	7.21	8.91,14.42	+	amine, hydroxyl
fluoxetine	fluoxetine- d_5	antidepressant	FLX	309.33	3.93	6.47	9.80	+	amine
atenolol	atenolol- d_7	beta-blocker	ATEN	266.34	0.33	7.51	9.60, 14.08, 15.95	+	amine, hydroxyl, amide
sulfamethoxazole	sulfamethoxazole- d_4	antibiotic	SULF	253.28	0.66	7.90	1.60,5.70	neutral[c]	amide, amine
ibuprofen	ibuprofen- d_3	anti-inflammatory	IBU	206.28	3.97	9.70	4.80	−	carboxyl
atorvastatin	atorvastatin- d_5	lipid lowering	ATOR	558.64	4.24	3.59	4.33, 14	−	carboxyl, amide
naproxen	naproxen- d_3	anti-inflammatory	NPX	230.60	2.88	8.67	4.12	−	carboxyl
Personal care products									
triclosan	triclosan- d_3	antimicrobial	TCS	289.54	5.34	6.91	7.60	neutral	phenol
triclocarban	triclocarban- d_4	antimicrobial	TCCB	315.58	4.90	6.34	12.70	neutral	amide
Metabolites		*Parent compound*							
carbamazepine-10,11-epoxide	carbamazepine-10,11-epoxide - d_{10}	carbamazepine	E-CBZ	252.7	1.89	7.91	4.4	neutral	imidic acid[d]
norfluoxetine[a]	norfluoxetine- d_5	fluoxetine	NFLX	295.30	3.93	6.77	9.8	+	amine
p-hydroxy atorvastatin[a]	p-hydroxtatorvastatin- d_5	atorvastatin	P-ATOR	573.65	4.37	3.49	4.33	−	carboxyl, amide, phenol
o-hydroxy atorvastatin[a]	o-hydroxtatorvastatin- d_5	atorvastatin	O-ATOR	573.65	4.37	3.49	4.33	−	carboxyl, amide, phenol

[Dose]=dose molar concentration of compounds (prepared as 2 µg L^{-1}); pKa = acid dissociation constant; Kow = octanol-water partition coefficient; "+" positively charged; "−" negatively charged; [a]Properties of the parent compounds were used; [b]pKa properties and charge conditions were taken from http://chemicalize.org; [c]Mostly neutral but ~10% are negatively charged; [d]Due to the presence of hydroxyl and amine groups in imidic acid (-C(OH)=NH-), the compound can be positively and negatively ionized at the same time rendering the availability of four species: neutral, positive, negative, and zwitterionic (neutral but with both positive and negative charges).

5.3.2.1 Porous Titanium-TiO_2 (PTT) membrane synthesis through

Porous titanium (PTi) sheets (2.54 mm thick) were cut using a customized punch and die disc cutter into 50 mm-diameter filters. These filters were washed and sonicated in ethanol, acetone, and ultrapure water prior to oxidation treatment. PTT filters were placed in 500 mL glass jars and 50 mL of 30 % H_2O_2 was poured into the jar. The jars were capped and heat treated at 80 ^oC for 2 h to oxidize the surface of the PTi filters. After the reaction period, the liquid content of the jar was removed and the oxidized PTi filters were washed with ultrapure water. The filters were then dried overnight at 80 ^oC and calcined at 450 ^oC with the same temperature settings as the QFT synthesis. This process overall forms TiO_2 that self-assembled onto PTi sheets.

5.3.2.2 Porous Titanium-TiO_2 (PTT) cleaning

The potential of the PTT to be reused was determined using a cleaning test. The test was conducted by heating the membranes at 400 ^oC for 3 h. The behavior of selected target compounds was then re-examined after one cycle of membrane cleaning. Only PTT membranes were subjected to a cleaning test since PTi sheets can be expensive due to a complex metallurgy process associated with their production. Note that elaborate cleaning tests were not the major objective of this paper. Hence, only a single round of cleaning was completed to show the potential for the membranes to be reused.

5.3.3 Material characterization

The microscopic structure of QFT and PTT was characterized under a field emission scanning electron microscope (FE-SEM LEO 1550, Carl Zeiss Microscopy). An image of the naked supports was also compared to the TiO_2 coated quartz fiber filters and self-assembled TiO_2 on thermally-chemically oxidized PTi sheets. The effective coating of the TiO_2 sol-gel on the surface of quartz fibers and the formation of TiO_2 particles on the surface of PTi sheets were also confirmed under SEM. The crystal structures of the TiO_2 were verified by micro-Raman spectroscopy (Renishaw) that was operated with a He-Ne laser at an excitation wavelength of 632.8 nm. Bang gap energies of the immobilized TiO_2 were estimated using the Tauc plots derived from the diffuse reflection spectra (DRS) which was measured by a UV-NIR

spectrometer. Details regarding the operational procedures for band gap determination are presented in Hu et al. (2011).The membranes were also submitted to Anton-Paar (Ashland, VA) for isoelectric point determination using their SurPASS^{TM} Electrokinetic Analyser for solid surfaces.

5.3.4 Photocatalytic batch experiments

5.3.4.1 Target compounds

A variety of pharmaceuticals and personal care products were selected for the experiments based on their occurrence in the aquatic environment (Arlos et al., 2015; Kleywegt et al., 2011), available analytical methods, and published UV/TiO_2 treatment studies (Tong et al., 2012) (Table 5.1). Some pharmaceuticals such as carbamazepine and atorvastatin have known human metabolites and selected metabolites of these compounds were included in the study. Stock solutions (1 g L^{-1}) were prepared in methanol and stored in the freezer (-20 ^{o}C).

5.3.4.2 Standardization and setup

The experimental setup (Figure 5.1) consisted of a multi-position stir plate each with a collimated UV-LED (length$_{beam}$= 6 cm, θ_{beam}= 4 cm, λ=365 nm, 4.1 V and 1 A) situated 10.5 cm above the water level. The average power output of the UV-LED lamps measured by a Thorlabs power and energy meter (PM100-USB) was 1.67 mW ± 0.72 % which can be translated to an irradiance of 0.390 mW/cm^2 at 10.5 cm. In-house fabricated holders (63.5 mm in diameter) were additionally used to contain the immobilized TiO_2 during the experiment. The distance of the immobilized TiO_2 to the water level was 1.5 cm.

The pharmaceutical stock solution was spiked into each glass beaker containing 300 mL of ultrapure water to achieve the required dose concentration (Table 5.1) and a resulting methanol concentration of 5×10^{-3} mM. The authors were aware that methanol could have a detrimental effect on photocatalysis due to its hydroxyl radical scavenging ability. This consideration is subsequently addressed by including the results from a simple test of the effects of varying the methanol concentration (5×10^{-3} and 50×10^{-3} mM) during the UV-LED/QFT treatments.

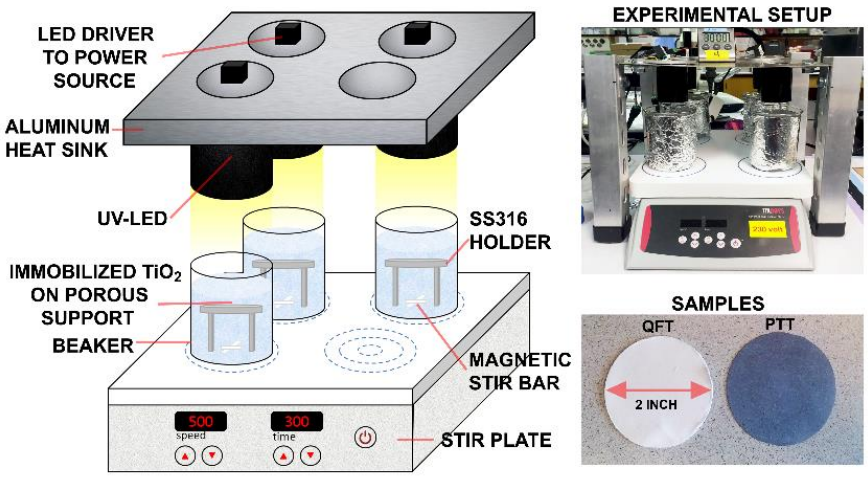

Figure 5.1 Experimental set up employed for this stu**dy**

The pH conditions (approximately 4.5 to 5) were not adjusted after the batch solutions were made and the experiments were conducted without the specific addition of reagents that enhance photocatalysis (e.g., hydrogen peroxide, oxygen, or air) in order to provide a set of benchmark conditions for future testing. However, for water in equilibrium with the atmosphere as in the case of our batch solutions, the dissolved oxygen concentration can be estimated using Henry's Law. At room temperature, the maximum oxygen saturation is around 9 mg L^{-1}.

In a separate study conducted by Hu et al. (2012), 20 µg pharmaceuticals reached equilibrium with TiO_2 powder (100 mg) in 20 to 40 min. Due to the lower amount of pharmaceuticals and TiO_2 used in this experiment (in the low mg range), experiments were equilibrated with the membrane in the dark for 60 min. This was immediately followed by UV-LED irradiation for another 300 min. Dark and photolysis (i.e., UV-LED irradiation only) control experiments were also conducted for the same duration as photocatalytic experiments. The water temperature was 24 ^{o}C ± 2 ^{o}C for these experiments. Four mL samples were taken every 60 min in glass test tubes using a glass pipette that was rinsed with methanol and ultrapure water three times before each sampling to avoid contamination. The total volume removed from each batch reactor was 24 mL and represented approximately 8% volume loss. Samples were stored in the dark at 4 ^{o}C until sample extraction. All the treatment investigations were done in triplicate.

A reference experiment (n=3) using commercially available TiO_2 powder purely in anatase form (Sigma Aldrich, 99.7 % purity) was conducted to determine the relative activity of immobilized TiO_2. The goal was to use a loading that was approximately within the expected amount of TiO_2 that deposited/self-assembled onto the porous supports. However, the combination of low TiO_2 loading and low initial contaminant concentration renders the TiO_2 powder photocatalysis very inefficient (Herrmann, 1999). Therefore, it was decided to use 5 mg L^{-1} of anatase which is the lowest loading found in the literature that showed some positive effect on the treatment of pharmaceuticals (Miranda-García et al., 2010).

5.3.5 Sample preparation and analysis

The 4 mL samples were first spiked with a deuterated standard stock solution (listed in Table 5.1) to a final concentration of 20 µg L^{-1} deuterated standard. Solid phase extraction (SPE) was initiated by conditioning the Bond Elut Plexa cartridges (30 mg, 1 mL, Agilent Technologies, Canada) with 1 mL of 100% methyl tert-butyl ether (MTBE) followed by 1 mL 100% methanol. Samples were introduced into the cartridges by pipetting 1 mL at a time (no vacuum), washed with ultrapure water, and dried for approximately 15 min. Elution was done with 2 × 2 mL methanol and 2 × 2 mL 90:10 methanol: MTBE. These extracts were evaporated to dryness using a Dionex SE 500 evaporator and reconstituted with 160 µL of methanol containing lorazepam and chloramphenicol (75 µg L^{-1}) as instrument injection standards. SPE recoveries were determined by spiking two test tubes of 4 mL ultrapure water with 32 µL each of the 100 µg L^{-1} deuterated and regular standard stock solution. Another 4-mL sample was prepared with only ultrapure water as SPE sample blanks. Method matrix recoveries during the analysis where higher than 90%. The extracts were stored in a -20 ^{o}C freezer and were analysed within two weeks. The analysis of compounds was completed using liquid chromatography and tandem mass spectrometry (LC-MS/MS) using an Agilent 1200 HPLC coupled to an Applied Biosystems 3200 QTRAP mass spectrometer (ABSciex, Concord, ON, Canada). LC-MS/MS analysis was previously described in Wang et al. (2011). Additional parameters including the optimized parameter values and chromatographic and ionization parameters are found in the supplementary material (Tables S5.1 to S5.3, Appendix D).

5.4 Results and discussion

5.4.1 Material characterization

TiO_2 was immobilized on two different substrates: (i) quartz filter and (ii) porous titanium substrates (Figure 5.2). The naked features of these substrates are shown in Figure 5.2a and Figure 5.2c. TiO_2 was coated on quartz filters consisting of fibers less than 2 μm in width and lengths that range from 10 to 100 μm using the sol-gel technique. TiO_2 agglomerates (nanoparticles) can be seen on the surface of these fibers (Figure 5.2b). Thermal chemical oxidation of PTi using H_2O_2 produced self-assembled TiO_2 nanowire fractal networks on the surface as shown in Figure 5.2d.

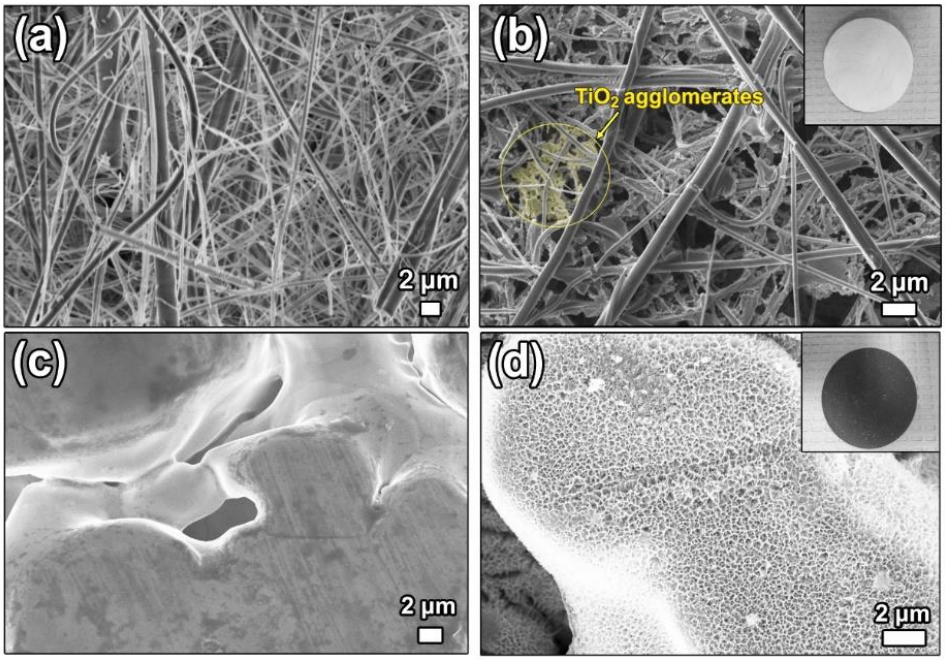

Figure 5.2 Scanning electron microscope images of (a) naked quartz fiber filters; (b) dip-coated TiO_2 on quartz fiber filters (QFT); (c) naked PTi sheets; and (d) self-assembled TiO_2 on thermally-chemically oxidized PTi sheets (PTT). The photographs of the immobilized TiO_2 are shown in the top-right hand corner of (b) and (d).

The average TiO_2 loading onto quartz filters which was determined by subtracting the weight before and after the dip-coating was found to be ~3.7 ±0 .004 mg. However, the majority of the TiO_2 that were activated by UV-LED would have been from the top surface coating only.

The amount of TiO_2 coated on the surface of quartz filter was estimated using equation 5.1 (Hatat-Fraile, 2013):

$$m = S \times t \times d(1 - \varepsilon) \qquad \text{(Equation 5.1)}$$

where m is the mass of the coating (g), S is the coated area ($\pi r^2_{quartz\ filter}$) in cm^2), t is the thickness of the TiO_2 coating (cm), d is the TiO_2 density (3.89 g/cm^3) and ε is the porosity (0.74).

The thickness of TiO_2 coating determined through SEM observations was 382.6 ± 57.1 nm. Therefore, the estimated TiO_2 activated during the UV-LED/QFT treatment was ~0.76 mg per filter. There is no direct way of determining the amount of TiO_2 produced after the thermal-chemical oxidation of porous Ti sheets as it is difficult to determine the percentage of the precursor material (titanium sheets) that has been transformed into TiO_2. Rutile and anatase are the two primary TiO_2 crystal structures that have been used in many studies, with the latter showing higher photocatalytic activity (Linsebigler et al., 1995). In addition to a more open structure and a larger band gap than rutile, the indirect band gap of anatase provides longer lifetimes for charge carriers, e^- and h^+ , allowing them to more likely participate in surface reactions (Luttrell et al., 2014). The typical Raman modes of anatase are at 144 cm^{-1}, 197 cm^{-1} 399 cm^{-1}, 516 cm^{-1}, and 639 cm^{-1} (Ohsaka et al., 1978). The Raman spectra illustrated in Figure 5.3 indicate that the TiO_2 morphology is primarily in the anatase form for both QFT and PTT. The spectra also confirmed that the quartz fiber and PTi naked supports have no crystalline phases. Additionally, the estimated band gap energies of TiO_2 on QFT and PTT are 3.0 eV and 3.5 eV respectively (Figure 5.4) suggesting that only wavelengths under 400-410 nm are capable of initiating the generation of charge carriers responsible for the TiO_2 photocatalytic process. Zeta potential is a quantitative measure of the electrostatic interaction between the charged surface and the bulk liquid phase. The measurement of zeta potentials at different pH conditions generally provides an overview of the material surface charge conditions. Positive zeta potentials suggest that the surface is mostly positively charged while negative zeta potentials suggest otherwise. The isoelectric point (IEP) occurs at a pH where the zeta potential is zero, that is, the pH where the concentrations of generally positive and negative charges are equivalent.

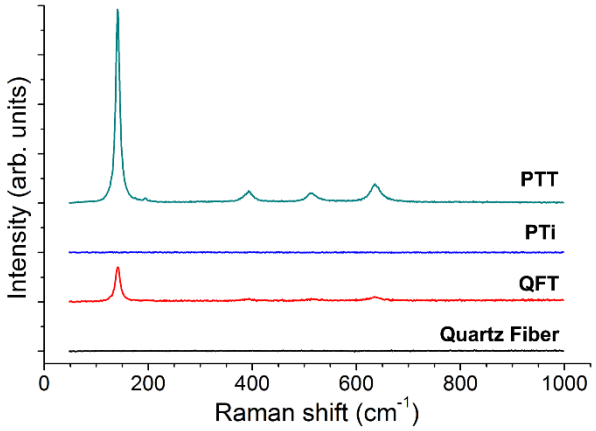

Figure 5.3 Raman spectra for PTT and QFT showing both the naked and immobilized TiO_2. The spectrum shows that the TiO_2 is found primarily in the anatase form.

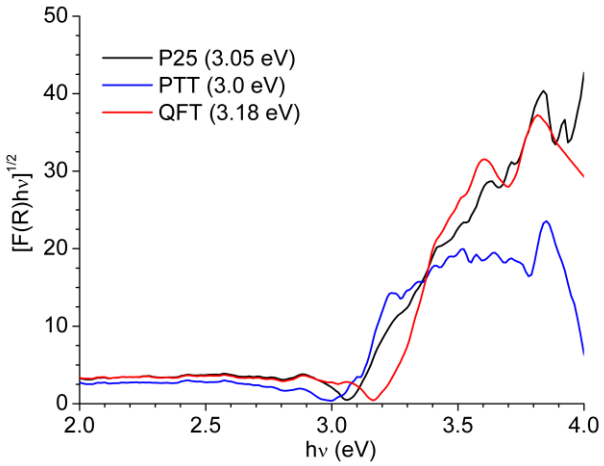

Figure 5.4 Tauc plot derived from UV-vis DRS spectra of the immobilized TiO_2 and their associated band gap energies.

The pIEPs for QFT and PTT were approximately at pH 4 and pH 6, respectively (Figure 5.5). Although TiO_2 was deposited or self-assembled onto different substrates, the pIEPs suggest that these substrates drive the surface chemistry, more so than the immobilized TiO_2 itself. When quartz (SiO_2) and titanium are hydrated, hydroxide ions form complexes with multivalent metal cations (Si^{IV} and Ti^{IV} in this case) and results in hydroxide or hydro-complex formation on the surface that have both acidic and basic properties. This interaction can form negative or positive charges on the surface depending on pH. Quartz has pIEP ranging from 2 to 3 (Júnior and Baldo,

2014) while titanium oxide's pIEP is around 5 to 6.7 (Cornell et al., 1975; Kurrat et al., 1998; Parks, 1965). There was a surface charge modification when TiO_2 was coated on the quartz fiber filters as evident by an increase in the final QFT product's pIEP to approximately 4 (Figure 5.5). The porous titanium's pIEP remained within its expected range of values after the thermal and chemical oxidation process for PTT synthesis. Based on these values, the QFT is positively charged below pH 4 and negative above this value, while the PTT is positively charged below pH 6 and negative for any pH above this.

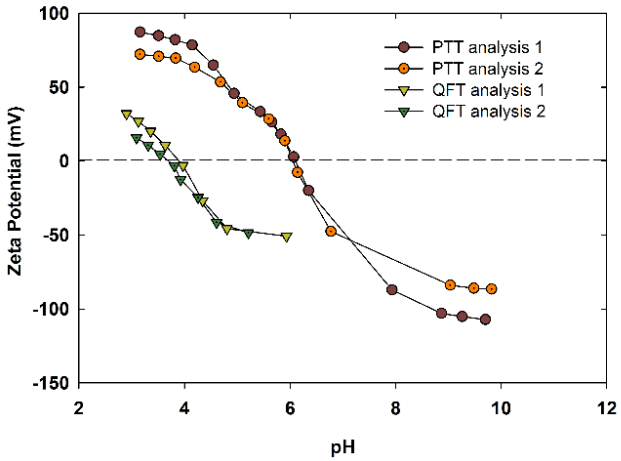

Figure 5.5 Zeta potential readings for PTT and QFT (n=2). pIEP is the point with a zero zeta potential (approximately at pH 4 for QFT and pH 6 for PTT).

5.4.2 Compound removals during equilibration

Compound removal through adsorption during the equilibration period (i.e., pre-irradiation during first 60 min in the dark) was calculated using the equation 5.2:

$$\frac{C_o - C_{60}}{C_o} \times 100 \qquad \text{(Equation 5.2)}$$

where C_0 is the initial concentration (Table 5.1) and C_{60} is the concentration at t=60 min. Only three compounds showed statistically significant removal via adsorption during equilibration with QFT (Figure 5.6): fluoxetine (71%, $p<0.001$), venlafaxine (29%, $p=0.009$), and norfluoxetine (72%, $p=0.002$) (Sigma Plot, one sample t-test, one-tailed, $\alpha=0.05$). Although most compounds showed minor to moderate adsorption on PTT, only atorvastatin (15%), fluoxetine (15%), naproxen (24%), and *o*-hydroxyatorvastatin (33%) showed significant removal during the equilibration period ($p=0.003$, $p=0.002$, $p=0.023$, and $p=0.007$ respectively).

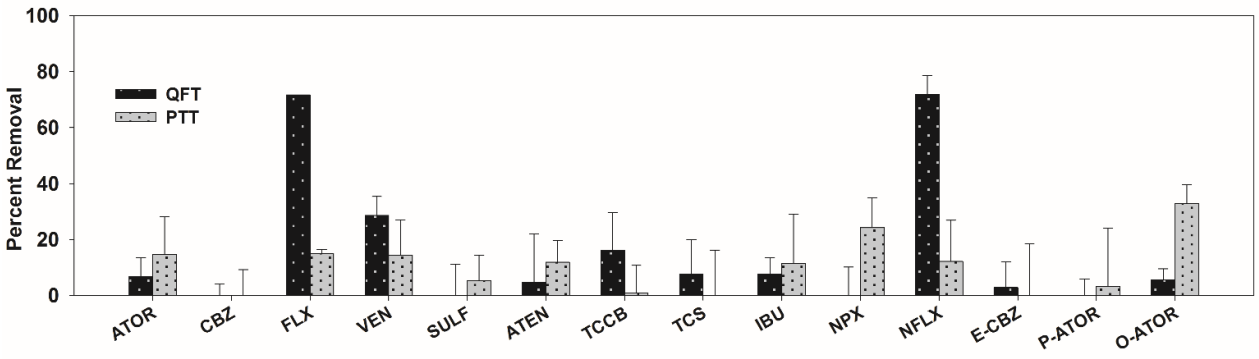

Figure 5.6 Average contribution of adsorption on the removal of target pharmaceuticals under UV-LED/QFT and UV-LED/PTT treatments during the equilibration period (60 min in the dark at pH=4.5-5 and a temperature of 24 ± 2°C).

It appears that charged compounds interacted well with oppositely charged materials but were repelled from a surface that is similarly charged. Pharmaceuticals can have functional groups that become ionized/charged depending on the pH of the solution (Table 5.1). As previously mentioned, the QFT surface is negatively charged at experimental pH (~4.5 to 5), hence the interaction of the cationic compounds such as venlafaxine and fluoxetine is favored. Using a similar analysis, the PTT is positively charged at experimental pH and negatively charged compounds such as naproxen and atorvastatin are well adsorbed by PTT (i.e., compounds that are mostly anionic above pH 4). Adsorption onto the surface is ideal in photocatalysis as redox reactions are generally more efficient when species have been pre-adsorbed (Linsebigler et al., 1995). This type of interaction, as described in subsequent sections, increases the specificity of the materials towards targeted compounds.

5.4.3 Photocatalytic treatments – specificity to charged compounds

The data collected at time steps following the equilibration period (i.e., 60 to 360 min under UV-LED) were used to determine the photocatalytic behavior of the target compounds using the concentration at t=60 min as the initial condition. The photocatalytic degradation of almost all organic compounds can be described by Langmuir-Hinshelwood kinetics (Sanchez et al., 1997) denoted by equation 5.3:

$$\frac{dC}{dt} = \frac{-k_r KC}{KC+1} \qquad \text{(Equation 5.3)}$$

where k_r is the rate constant of the surface adsorbed substrate (mol L^{-1} min^{-1}), K an equilibrium constant of adsorption (L mol^{-1}), and C is concentration (mol L^{-1}). Since C in this case is very low (<<mM), KC in the equation is negligible (KC<<1). Therefore, the analysis was simplified using the pseudo-first-order reaction equation:

$$\frac{dC}{dt} = -k_{app}t \qquad \text{(Equation 5.4)}$$

as described in many photocatalytic degradation studies of most organic compounds found in the literature (Lu and Pichat, 2013; Zhang et al., 2012b). The integration of this equation leads to

$$\ln\left(\frac{C_t}{C_{60}}\right) = -k_{app}t \qquad \text{(Equation 5.5)}$$

where k_{app} (min^{-1}) is the apparent first-order reaction rate constant.

Results for dark and photolysis treatments (Figure 5.7) indicate that there was little to no reductions in concentrations under experimental control conditions except for atorvastatin and triclocarban where minimal disappearance via dark and/or photolysis treatments was observed. The apparent first-order decay of pharmaceuticals (Table 5.2) was observed in both treatments. Similar to adsorption results, there is a distinct difference in the treatment performance of the two materials. For instance, venlafaxine and atenolol disappeared rapidly under UV-LED/QFT treatment but remained recalcitrant under UV-LED/PTT treatment. The reverse was observed for sulfamethoxazole, ibuprofen, and atorvastatin where compound disappearance was only observed in UV-LED/PTT treatment. Once more, it was mostly the cationic compounds that reacted with QFT while it was mostly anionic compounds that showed the effects when treated with PTT.

The dissimilarity in the treatment efficiency as observed in this study can be very advantageous when targeting specific types of contaminants. Specificity of TiO_2 photocatalysis in a mixed contaminant feed is particularly difficult to achieve due to the nonselective nature of hydroxyl radicals and other reactive oxygen species. However, this problem can be overcome by controlling the interaction between the photocatalytic sites and target compounds via surface charge modification (Shaham-Waldmann and Paz, 2013). Controlling pH conditions is a straightforward approach to achieving specificity as pH changes the surface characteristics of the materials and subsequently impacts the adsorptive behavior of contaminants. Some studies have also looked at improving the specificity of photocatalysis in a variety of ways. For example,

coating the surface of TiO_2 with organic layers can create better interaction towards hydrophobic compounds (Inumaru et al., 2004) and doping with metals and oxides delays the treatment of one compound while maintaining the decay rate constant of another (Muradov et al., 1996).

Atenolol, sulfamethoxazole, and ibuprofen showed insignificant adsorption onto the materials during the equilibration period but reductions in concentrations during the photocatalytic treatments were evident. Although these compounds poorly adsorbed during the equilibration period, they can still diffuse in close proximity to the surface of the material due to their inherent ionized conditions. Turchi and Ollis (1990) also suggest that hydroxyl radicals are mobile radicals that can diffuse from the surface and interact with compounds that do not adsorb on the material. Hence, adsorption during the equilibration period may not necessarily be a pre-requisite for efficient photocatalysis but as long as the compounds can interact with the material, and in this case, through surface charge interactions, efficient photocatalysis can still be achieved.

Fluoxetine displays a behavior that is different from the rest of the compounds that were removed by QFT. Adsorption results during the equilibration period (Figure 5.6) indicate that ~75% of fluoxetine was already removed during this period but remained recalcitrant under UV-LED/QFT exposure. This is substantiated by the dark control experiment showing a very similar behavior with UV-LED/QFT treatment (Figure 5.8), except that there was a gradual increase in concentrations after 60 min. It is well established that adsorption onto solid materials is a dynamic process where species adsorb and desorb at any given time (Schobert, 2013). At equilibrium, the rate of adsorption equals the rate of desorption. However, adsorbed molecules can desorb from the solid surface and diffuse back into the bulk solution when properties in the liquid phase such as concentration, temperature, and pH are altered (Worch, 2012). It is difficult to specify the exact mechanism as adsorption-desorption isotherms were not completed since the investigation of this process is not the main objective of the study. Nevertheless, the result showed that some compounds can strictly have sorption-related behavior towards the materials and may not necessarily be transformed via photocatalysis.

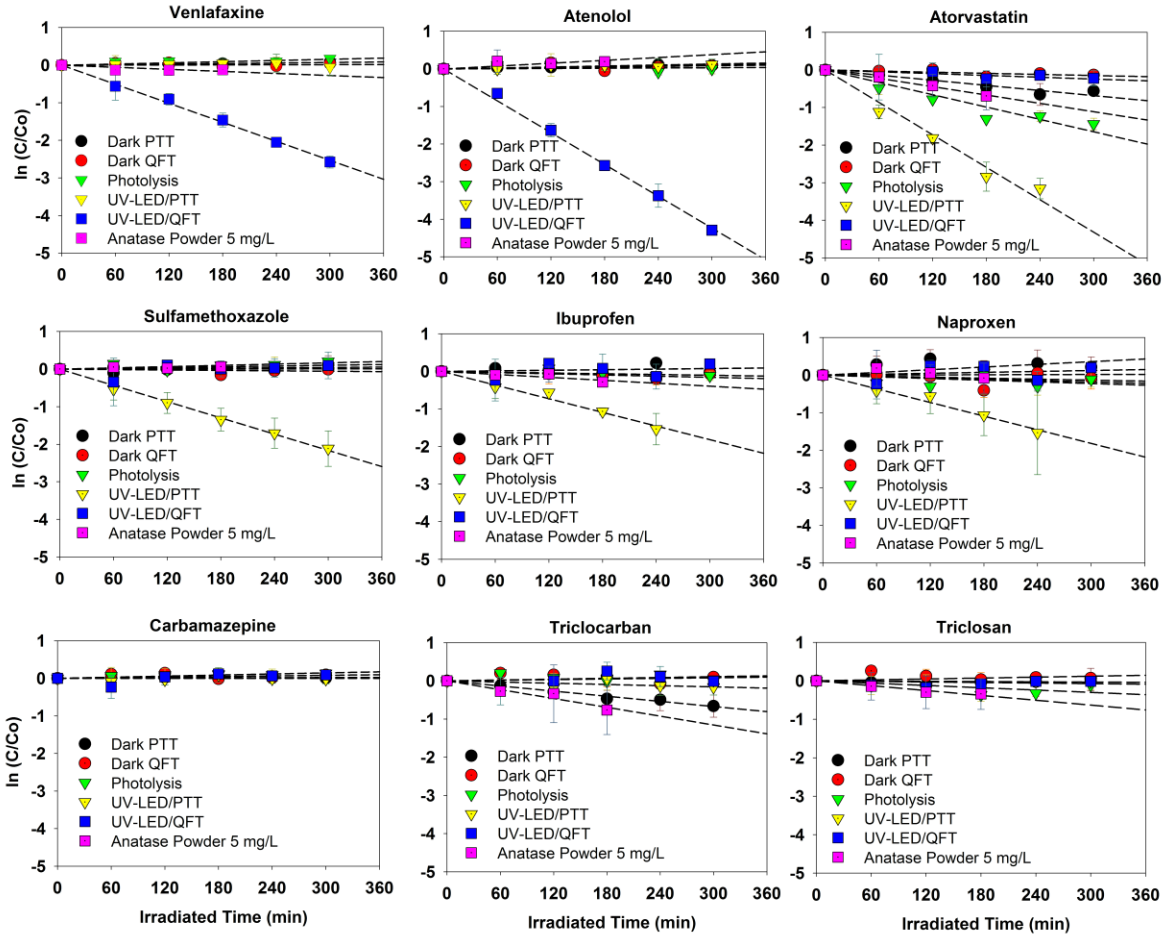

Figure 5.7 Removal of nine target compounds using UV-LED/QFT and UV-LED/PTT treatments. Experimental controls included dark and photolysis using UV-LED only experiments (300 min under UV-LED irradiation at pH=4.5-5 and a temperature of 24 ± 2ºC)

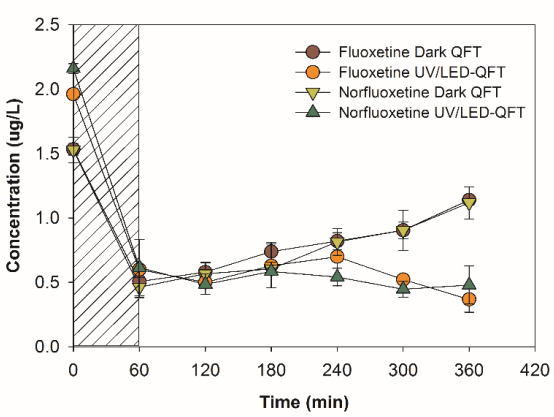

Figure 5.8 Fluoxetine and norfluoxetine concentrations from t=0 to t=360 min with samples taken every hour. The shaded region is the equilibration period (60 min in the dark).

Table 5.2 First-order decay rate constants of compounds using UV-LED/QFT or PTT treatments and from TiO_2 immobilization studies.

Compound	Reference Experiment	Concentration ($\mu g\ L^{-1}$)	UV conditions (Type, Power[W], Irradiance [$mW\ cm^{-2}$])	Batch reactor conditions (volume, TiO_2 immobilization)	Reported $k_{app} \times 10^{-3}$	R^2
FLX[a]	This work	2.0	UV-LED, 1.7×10^{-3}, 0.13	0.3 L, quartz fiber filters	-	-
	Fernández et al. (2014)	0.5	LP mercury lamp, 1.3, 5.7	5 L, submerged MPR	8.4	0.973
	Hu et al. (2011)	100	LP mercury lamp, 100, 0.27	0.08 L, free-standing nanowires	40.8	0.995
VEN	This work	2.0	UV-LED, 1.7×10^{-3}, 0.13	0.3 L, quartz fiber filters	8.5	0.993
	Hu et al. (2011)	100	LP mercury lamp, 100, 0.27	0.08 L, free-standing nanowires	31.9	0.997
ATEN	This work	2.0	UV-LED, 1.7×10^{-3}, 0.13	0.3 L, quartz fiber filters	14.5	0.998
	Fernández et al. (2014)	0.5	LP mercury lamp, 1.3, 5.7	5 L, submerged MPR	7.4	0.969
ATOR[b]	This work	2.0	UV-LED, 1.7×10^{-3}, 0.13	0.3 L, porous Ti sheets	13.4	0.974
	Hu et al. (2011)	100	LP mercury lamp, 100, 0.27	0.08 L, free-standing nanowires	68.8	0.999
SFX	This work	2.0	UV-LED, 1.7×10^{-3}, 0.13	0.3 L, porous Ti sheets	6.9	0.997
	Fernández et al. (2014)	0.5	LP mercury lamp, 1.3, 5.7	5 L, submerged MPR	≥160.5	-
	Miranda-García et al. (2010)	100	Natural sunlight, -, 3	1 L, glass spheres	85	0.900
	Hu et al. (2011)	100	LP mercury lamp, 100, 0.27	0.08 L, free-standing nanowires	42.2	0.989
IBU	This work	2.0	UV-LED, 1.7×10^{-3}, 0.13	0.3 L, porous Ti sheets	6.1	0.974
	Fernández et al. (2014)	0.5	LP mercury lamp, 1.3, 5.7	5 L, submerged MPR	≥188.8	-
	Giri et al. (2010)	1000	LP mercury lamp, 10, n.m.	1.5 L, coated module	22.17	-
	Miranda-García et al. (2010)	100	Natural sunlight, n.m.., 3	1 L, glass spheres	127	0.900
	Hu et al. (2011)	100	LP mercury lamp, 100, 0.27	0.08 L, free-standing nanowires	0.5	0.945
NAP	This work	2.0	UV-LED, 1.7×10^{-3}, 0.13	0.3 L, porous Ti sheets	8.72	0.979
	Fernández et al. (2014)	0.5	LP mercury lamp, 1.3, 5.7	5 L, submerged MPR	≥232.2	-
	Giri et al. (2010)	1000	LP mercury lamp, 10, n.m.	1.5 L, coated module	62.1	-
CBZ	This work	2.0	UV-LED, 1.7×10^{-3}, 0.13	0.3 L, porous Ti sheets	No deg	-
	Fernández et al. (2014)	0.5	LP mercury lamp, 1.3, 5.7	5 L, submerged MPR	18.2	0.986
	Hu et al. (2011)	100	LP mercury lamp, 100, 0.27	0.08 L, free-standing nanowires	0.8	0.971
TCS	This work	2.0	UV-LED, 1.7×10^{-3}, 0.13	0.3 L, porous Ti sheets	No deg	-
	Fernández et al. (2014)	0.5	LP mercury lamp, 1.3, 5.7	5 L, submerged MPR	86.9	0.975
	Hu et al. (2011)	100	LP mercury lamp, 100, 0.27	0.08 L, free-standing nanowires	42.2	0.989
TCCB	This work	2.0	UV-LED, 1.7×10^{-3}, 0.13	0.3 L, porous Ti sheets	No deg	-

R^2 = linear regression coefficient. [a]Compound showed no removal but was found to adsorb on QFT significantly. [b]Compound also showed disappearance in the dark and photolysis experiments with decay rates at 2.1×10^{-3} (0.913) and 4.7×10^{-3} (0.910) min^{-1} respectively. "-" not available. "no deg" = no degradation. CBZ, TCS, and TCCB showed no disappearance for both treatments under this study. There were no available studies that employed immobilized TiO_2 for TCCB.

5.4.4 Photocatalytic treatment of neutral compounds

While there are compounds that can be treated by QFT and PTT, carbamazepine, triclosan, and triclocarban showed very little to no removal via adsorption (dark control), photolysis (UV-LED only), or UV-LED/PTT and QFT (Figure 5.6 and Figure 5.7). Fernández et al. (2014) conducted a study on the disappearance of thirty-three trace organic contaminants at environmentally relevant concentrations (500 ng L^{-1}) using a submerged membrane in the presence of UV/TiO_2. They found that carbamazepine also adsorbed poorly on the membrane and slowly degraded under the UV/TiO_2 experimental condition. They further suggested that charge of pharmaceuticals greatly affect their adsorption on TiO_2 and subsequent photocatalytic treatment at low concentrations due to electrostatic interactions that involve repulsion and attraction with the membranes. Neutral compounds have weak electrostatic interactions on charged surfaces as observed by Vohra and Tanaka (2001) when they studied the removal of ionic and neutral compounds on nafion-coated TiO_2 (organic membrane). All three compounds that remained recalcitrant in this study are neutral.

5.4.5 Comparison to reference studies and experiments

Kinetic rate constants from some studies that employed different light sources (conventional UV or natural sunlight) and immobilized TiO_2 was reviewed to provide a brief comparison with the results presented in this work. There is a variation in the kinetic rate constants among the studies listed in Table 5.2 that is primarily due to different operational conditions employed across different studies. The authors recognized this limitation, hence an additional reference experiment was conducted that involves the use of commercially produced TiO_2 powder that is purely in anatase form. The results from this reference experiment are also presented in Figure 5.7. None of the compounds that were degraded by UV-LED/QFT were removed by the commercial TiO_2 anatase powder. This observation can be related back to surface charge interactions between the target contaminant and the photocatalyst. Various studies have determined the pIEP of anatase to be ~6 which is similar to that of the PTT (Parks, 1965). As a result, positively charged compounds (e.g., venlafaxine and atenolol) that are present during the experiment are least likely to interact with the positively charged anatase powder.

Atorvastatin which was well removed by UV-LED/PTT also showed an observable first-order decay rate constant (3.93×10^{-3}) under the reference experiment. However, under the UV-LED/PTT treatment, atorvastatin had a decay rate constant that was ~3.5 times higher than what was observed for commercial anatase powder experiment. For a 300-mL batch reactor volume, 1.5 mg of anatase powder is required to obtain 5 mg L^{-1} TiO_2 loading. Assuming that the light only penetrates at ~2mm and commercial anatase is uniformly distributed within the reactor, only ~47 µg of TiO_2 are activated at a time. This may be less than the amount activated in PTT, hence the reaction rate constant under the immobilization process is higher than that of the TiO_2 powder experiment. Nevertheless, it can still be reasonably generalized that the interaction between oppositely charged materials can likely enhance photocatalytic decomposition.

5.4.6 Scavenging effect of methanol

Because of solubility concerns of some pharmaceuticals in ultrapure water, the current experiments were conducted by spiking the chemicals with methanol as a carrier (5×10^{-3} mM in each batch reactor). The concentration was much lower than the calculated methanol concentration in the study by Fernández et al. (2014) (1.6 mM methanol in the solution). Methanol can act as a hydroxyl radical scavenger and can be detrimental to photocatalytic removal efficiency. As a result, we investigated the effect of methanol as a scavenger for hydroxyl radicals (Figure 5.9) by observing UV-LED/QFT treatment at 5×10^{-3} mM and 50×10^{-3} mM methanol concentrations. Only compounds that responded well to UV-LED/QFT treatments were carefully examined in this study (atenolol and venlafaxine). Carbamazepine was additionally examined as it was hypothesized that its recalcitrant behavior during both treatments could be explained by methanol radical scavenging. A few bench-scale experiments have shown that carbamazepine can be treated well via TiO_2 photocatalysis and another hydroxyl radical mediated processes such as ozonation, ozone/H_2O_2, due to its high reactivity with hydroxyl radicals (Ahmed and Chiron, 2014; Doll and Frimmel, 2004, 2005; Snyder et al., 2007; Vogna et al., 2004). For instance, Doll and Frimmel (2004) found carbamazepine to follow first-order decay with rates that ranged from 1.4×10^{-4} to 3.6×10^{-1} min^{-1} depending on the concentration and type of TiO_2 nanomaterial used.

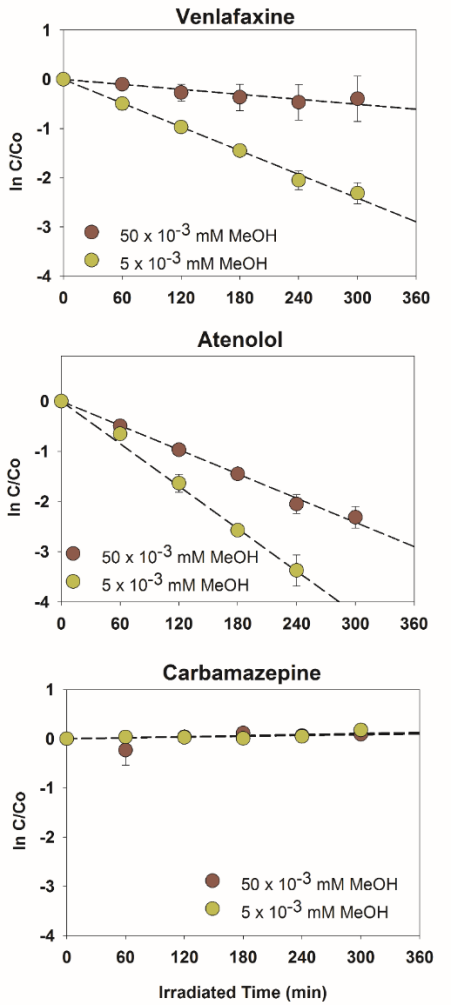

Figure 5.9 Effects of high and low methanol concentrations on the removal rates of selected pharmaceuticals vs. UV-LED/QFT membrane treatment. MeOH=methanol.

Methanol impacted the disappearance of atenolol and venlafaxine, with low methanol concentrations exhibiting higher decay rates. Kinetic rates for venlafaxine improved by a factor of five and atenolol decay rate increased by almost twice as much. However, compound disappearance at both conditions was not observed for carbamazepine suggesting that even a low concentration of a hydroxyl radical scavenger is detrimental to its photocatalytic treatment. The scavenging effect of methanol on carbamazepine treatment using solar photo-Fenton conditions was also investigated by Ahmed and Chiron (2014) and found that 192 mM methanol inhibited the treatment of 49.9 µM (11.8 mg L^{-1}) carbamazepine up to 90%.

The presence of other radical scavengers is inevitable in an actual water matrix (e.g., drinking water sources and wastewater). Natural source waters may contain carbonate and bicarbonate ions as well as other inorganic ions (phosphates and nitrates) that can have significant scavenging effect in any hydroxyl radical mediated processes (Mehrvar et al., 2001). The results of this study nevertheless suggest that TiO_2 immobilized on different porous supports can reduce the concentrations of some target pharmaceuticals in the presence of a radical scavenger. However, the effects of other scavengers in target water matrix must be addressed appropriately prior to pilot- or full-scale applications in order to determine the membrane or system modifications required for enhancing treatment efficiency.

5.4.7 Photocatalytic treatment of pharmaceutical metabolites

The uptake of drugs is followed by a metabolic process mediated by a number of enzymes that transform these compounds into more soluble metabolites. The body easily eliminates these metabolites that eventually end up, along with their parent compound, in wastewater treatment plants and their associated effluent discharge points. Hence, the behavior of selected pharmaceutical metabolites under UV-LED/QFT and UV-LED/PTT membrane treatments was also included in this study to illustrate the ability of the membranes to eliminate metabolites.

The first-order decay constant of the four metabolites and their treatment behaviors is comparable to their respective parent compounds (Table 5.3). Again, metabolites that are positively charged have an affinity towards QFT and negatively charged with PTT. Norfluoxetine adsorbs well on QFT membranes but it remained recalcitrant during the photocatalytic treatment, similar to its parent compound, fluoxetine (Figure 5.6). The carbamazepine metabolite, 10-11, epoxide carbamazepine was persistent in all treatment conditions. Hydroxylated compounds, such as the o-hydroxyatorvastatin, are generally prone to ring opening attacks by hydroxyl radicals (Vinu and Madras, 2008). This is illustrated well by atorvastatin metabolite, o-hydroxyatorvastatin, that showed significantly higher decay rate (SigmaPlot, one-tailed student's t-test, $p=0.009$, $\alpha=0.05$) than its parent compound under UV-LED/PTT treatment. However, this was not observed in its para-isomer (p-hydroxyatorvastatin) where the first-order rate constant was not found to be significantly higher than atorvastatin

(SigmaPlot, one-tailed student's t-test, p=0.130, α=0.05). Suresh et al. (2012) and Kumar et al. (2003) have indicated that the ortho-position of functional groups has enhanced adsorption ability in various adsorbent materials. Hence, this observed difference in treatment efficiency of *ortho* and *para* metabolites suggest that the position of functional groups can have an impact on the photocatalytic process and must be considered when targeting treatment of metabolites in the feed solution.

Table 5.3 First-order decay rate constants associated with UV-LED/PTT treatments, photolysis, and dark PTT control experiments of selected pharmaceutical metabolites.

Removal Rate, k_{app} (min^{-1}, × 10^{-3})	**Dark PTT k (R^2)**	**Photolysis k (R^2)**	**UV-LED/PTT k (R^2)**
carbamazepine 10,11-epoxide	-	-	-
p-hydroxyatorvastatin	1.39 (0.929)	2.56 (0.950)	10.01 (0.918)
o-hydroxyatorvastatin	2.18 (0.979)	6.07 (0.992)	28.08 (0.998)

R^2=linear regression coefficient. "-" suggests that rate cannot be determined as apparent reductions in concentrations were not observed.

5.4.8 Potential reusability of PTT

The three pharmaceuticals that were treated well by PTT were re-examined using the same material after one cycle of cleaning (Figure 5.10). There was no statistical difference (Sigma Plot, two-tailed student's t-test, α=0.05) in the first-order decay rates of sulfamethoxazole (p=0.753), ibuprofen (p=0.603) and atorvastatin (p=0.518) for both new and re-used materials suggesting that PTT maintained its photo-activity after one cycle cleaning test. Other tests for membrane filtration application include the analysis of flux during and after multiple cycles. Although this was not the main focus of the study, the authors would like to emphasize that through this cleaning, reusability has important future implications by extending the lifespan of the materials synthesized.

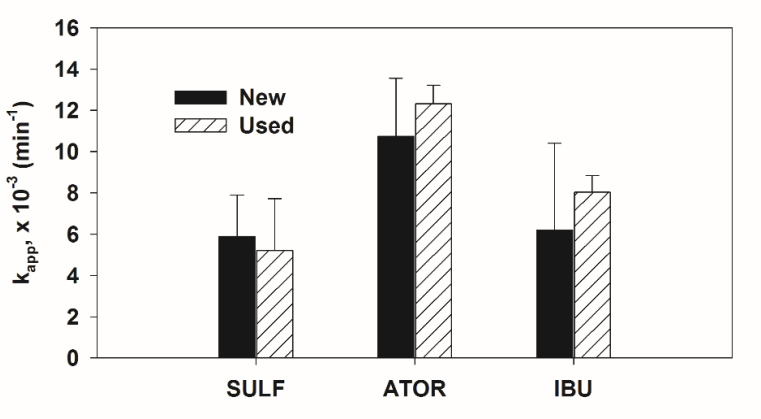

Figure 5.10 First-order removal rates of new and used PTT membranes. Used membranes were cleaned by heat treatment at 400 ºC for 3 h prior to re-testing. Information regarding the statistical tests are detailed in the results section.

5.5 Conclusions

TiO_2 was successfully immobilized on two types of supports: (1) quartz fiber filters and (2) porous titanium sheets. In addition, UV-LED exposure of TiO_2 immobilized on these supports reduced the concentrations of target PPCPs and their metabolites in ultrapure water. QFT and PTT, however, displayed specificity towards particular compounds such that anionic species showed preference to QFT treatment and cationic compounds to PTT. The electrostatic interactions between the newly synthesized materials and the target compounds were an influential factor in the overall treatment efficiency. Pharmaceutical metabolites behaved similarly to their parent compounds during the photocatalytic treatments. However, the *ortho* and *para* arrangements of atorvastatin metabolite isomers can have an impact during their treatment. Direct comparison of the rate constants to the reference experiment and studies that employed different light sources and immobilized TiO_2 is very difficult to establish. However, the trend on surface charge interactions mostly holds true for immobilized and powder experiments. Although not tested extensively, it was apparent that the newly synthesized materials can also be cleaned and reused, which may be an important factor in their implementation for real world applications.

Chapter 6

Photocatalytic decomposition of selected estrogens and their estrogenic activity by UV-LED irradiated TiO_2 immobilized on porous titanium sheets via thermal-chemical oxidation

Modified from Journal of Hazardous Materials, 318, M.J. Arlos, R. Liang, M.H. Hatat-Fraile, L.M. Bragg, N.Y. Zhou, M.R. Servos, and S. A. Andrews. Photocatalytic decomposition of selected estrogens and their estrogenic activity by UV-LED irradiated TiO_2 immobilized on porous titanium sheets via thermal chemical oxidation, 541-550, Copyright 2016, with permission from Elsevier.

6.1 Chapter summary

The removal of endocrine disrupting compounds (EDCs) remains a big challenge in water treatment. Risks associated with these compounds are not clearly defined and it is important that the water industry has additional options to increase the resiliency of water treatment systems. Titanium dioxide (TiO_2) has potential applications for the removal of EDCs from the water. TiO_2 has been immobilized on supports using a variety of synthesis methods to increase its feasibility for water treatment. In this study, we immobilized TiO_2 through the thermal-chemical oxidation of porous titania sheets. The efficiency of the material to degrade target EDCs under UV-LED irradiation was examined under a wide range of pH conditions. A yeast-estrogen screen assay was used to complement chemical analysis in assessing removal efficiency. All compounds but 17β-estradiol were degraded and followed pseudo first-order kinetics at all pH conditions tested, with pH 4 and pH 11 showing the most and the least efficient treatments respectively. In addition, the total estrogenic activity was substantially reduced even with the inefficient degradation of 17β-estradiol. Additional studies will be required to optimize different treatment conditions, UV-LED configurations, and membrane fouling mitigation.

6.2 Introduction

Endocrine disrupting compounds (EDCs) are chemicals that are known to interfere with the endocrine system, a system that is responsible for regulating the body's chemical equilibrium, stress response, sexual development, and reproduction (Kime, 1999). These chemicals alter the endocrine function by interacting with hormone receptors as agonists (mimics), antagonists (blocks), or both and interfering with enzyme activity responsible for biosynthesis, metabolism, and hormone circulation (Linsebigler et al., 1995). EDCs are also a diverse group of molecules but of prominent concern is the presence of environmental estrogens from municipal wastewater effluents that can mimic female hormone function known to cause feminization of wild fish (Hinck et al., 2009; Jobling et al., 1998; Tanna et al., 2013; Tetreault et al., 2011; Woodling et al., 2006).

Although human exposure to low concentrations of environmental estrogens is predicted to represent a minimal human health risk (Schwab et al., 2005), the diversity of estrogens and

their potential mechanisms of action create large uncertainties. Thus, it is important that the exposure to these contaminants be minimized (Jones et al., 2005). Estrogenic compounds are also poorly removed in conventional drinking water treatment systems (Huerta-Fontela et al., 2011; Stackelberg et al., 2007). However, bench- and pilot-scale experiments with advanced oxidation processes that employ UV, ozone, and hydrogen peroxide (H_2O_2) independently or in combination have shown promising results in the treatment of estrogens and other trace organic contaminants such as pharmaceuticals (Snyder et al., 2007). Innovative technologies have also emerged such as photocatalysis in drinking water treatment, particularly the combination of UV and titanium dioxide (TiO_2) (Tong et al., 2012).

Photocatalysis follows a series of elementary steps that occur inside the irradiated catalyst (e.g., charge carrier production) and also on the surface where interfacial redox reactions subsequently produce reactive species that oxidize compounds that are at or near the surface (Friedmann et al., 2010). Therefore, good reaction kinetics is achieved when the target compounds are well-adsorbed on the photocatalyst surface. This adsorptive process is highly influenced by both the target compounds, the surface properties of the photocatalytic materials, and the pH of the solution (Friedmann et al., 2010).

Since the semiconductor surface is the site of photocatalytic reactions, materials with a higher surface area have better photocatalytic performance (Varshney et al., 2016). As a result, photocatalysts such as TiO_2 have been widely applied in nanosize forms. This configuration has several disadvantages including the challenges related to separation and the recovery of TiO_2 during treatment applications. Recent developments, however, have explored a variety of methods to immobilize TiO_2 in films, porous supports, or membranes (Varshney et al., 2016). The Sol-gel/dip-coating process remains the most widely used method due to its simplicity and method reliability. Other methods include tape-casting, hydrothermal synthesis, electrophoretic, chemical vapor, and sputter deposition, and flame aerosol coating (Varshney et al., 2016). Each of these techniques has their own advantages including highly uniform TiO_2 coating and also some disadvantages such as high operating costs and flammability (Varshney et al., 2016). The thermal-chemical oxidation of titanium substrates is a method that has not been explored well in TiO_2 thin film synthesis. It is a simplistic process that involves the soaking of titanium substrates

in chemical oxidants (e.g., H_2O_2) at temperatures around 80-100°C. Tan et al. (2014) have recently synthesized TiO_2 thin films using a similar method and have shown the potential of these materials for organic compound degradation (dye). To our knowledge, TiO_2 thin films produced by this method have not been tested for the photocatalytic decomposition of estrogens in water.

The energy needed for photocatalysis when using conventional UV lamps is another potential challenge for UV/TiO_2 application in water treatment. It is therefore very desirable to find more energy efficient alternatives. The LED light source is a promising potential option that also has the additional advantage of having more flexible design configurations (Natarajan et al., 2011).

In this study, we explored the use of UV-LED as a cost-effective and design-adaptive alternative to conventional UV lamps during TiO_2 photocatalytic treatment. A photocatalytically active material was synthesized via thermal and chemical oxidation of porous titanium sheets, producing self-assembled TiO_2 particles on the surface. The efficiency of UV-LED and TiO_2 immobilized on porous titanium sheets in the degradation of target estrogens was then evaluated in controlled batch experiments under a range of different pH conditions. A biological assay for total estrogenicity in the form of yeast estrogen screen (YES) was conducted to complement chemical analysis. This study characterizes the potential application of these novel TiO_2 thin film materials for the removal of potentially hazardous estrogenic compounds from water.

6.3 Materials and methods

6.3.1 Reagents and chemicals

Solvents and chemicals listed in the material synthesis section were purchased from Sigma Aldrich and the 0.254 mm thick porous titanium sheets were purchased from Accumet Materials (Ossining, NY, USA). Ultrapure water (18 MΩ·cm resistivity at 25°C) was obtained from a MilliQ Water Purification System (EMD Millipore, Mississauga, ON). Hydrochloric acid (HCl), sodium hydroxide (NaOH), methyl tert-butyl ether (MTBE), ammonium fluoride, and HPLC grade methanol were purchased from Fisher Scientific. Estrone (E1), 17β-estradiol (E2), 17α-ethinylestradiol (EE2), estriol (E3), and bisphenol A (BPA) were purchased from Sigma

Aldrich (Oakville, ON) while their corresponding deuterated standards (E1-d_2, E2-d_4, EE2-d_4, E3-d_3, BPA-d_{16}) was purchased from CDN Isotopes (Pointe-Claire, QC). The compounds used to detect the presence of hydroxyl radicals (terephthalic acid and 2-hydroxyterephthalic acid) were also purchased form Sigma Aldrich.

6.3.2 Material synthesis and characterization

The porous titania sheets (PTi) were cut into 50 mm diameter filters. The filters were then washed and sonicated in ethanol, acetone, and ultrapure water. The oxidation process was initiated by the heat treatment of the filters immersed in 50 mL of 30% H_2O_2 for 2 h at 80^{o}C. The filters were then removed from the solution, washed with ultrapure water, and dried overnight at 80^{o}C. This process was followed by the calcination of filters at 450^{o}C which consequently allows for the self-assembly of TiO_2 on the PTi sheets, producing porous titania-TiO_2 thin film material (PTT).

The material morphology was characterized using a field emission scanning electron microscope (FE-SEM LEO 1550, ZEISS International). The surface topography was determined using an optical profilometer (Nanovea ST400, Irvine, California). Three-dimensional topographical surface maps of PTT were determined by rastering an optical head over a 1.2 × 1.2 mm^2 area using a step size of 1 μm. The arithmetic mean (R_a) and root-mean square (R_{RMS}) surface roughness was obtained from the surface profile using the methodology described elsewhere (ASME, 2009). Raman spectroscopy (Renishaw Ramanscope) with a resolution of ≤ 1 cm^{-1} was used to confirm TiO_2 structure (anatase or rutile). The Raman spectra were obtained using a He-Ne laser operating at a wavelength of 633 nm with an incident power of 5 mW. The material was also submitted to Anton-Paar (Ashland, VA) for isoelectric point analysis (see Supplementary Material, section D).

6.3.3 Experimental setup

The target compounds included in this study are moderately soluble weak acids with pKa generally around 10 (Table 6.1). Although the chemical structure of many EDCs varies, the target estrogens have phenol moieties as illustrated in Figure 6.1. These compounds also have maximum photon absorption at wavelengths occurring between 279-293 nm (see Figure S6.1).

Batch reactors (500 mL beakers wrapped with aluminum foil) contained 300 mL of ultrapure water that was pH adjusted to either 4, 8, or 11 using 0.1 N HCl and 0.1 N NaOH. Since preliminary results were suggestive of the surface charge interaction between the synthesized material and target compounds, the pH values chosen represent the following conditions: (a) pH 4 where the material is mostly positive while the target compounds are mostly neutral; (b) pH 8 where the material is negatively charged and the compounds are still mostly neutral; and (c) pH 11 where the material continues to stay negatively charged and the compounds have mostly been ionised into negatively charged compounds.

Table 6.1 Selected physical and chemical properties of target estrogenic compounds[a].

Compound	Use	Symbol	Molecular Weight (g/mol)	Log Kow at pH 5	pKa	Solubility[b] at 25°C in pure water (mg/L)
17α-ethinylestradiol	birth control pill ingredient	EE2	296.40	3.63	10.33	9.20
17β-estradiol	primary female sex hormone	E2	272.38	3.75	10.33	1.51
Estrone	least abundant female hormone	E1	270.37	3.30	10.33	1.30
Estriol	abundant during pregnancy	E3	288.38	2.54	10.33	0.12
Bisphenol A	plasticizer	BPA	228.29	3.8	9.78, 10.39	300

Notes: pKa = acid dissociation constant; Kow = octanol-water partition coefficient; [a]http://www.drugbank.ca; [b]Shareef et al. (2006)

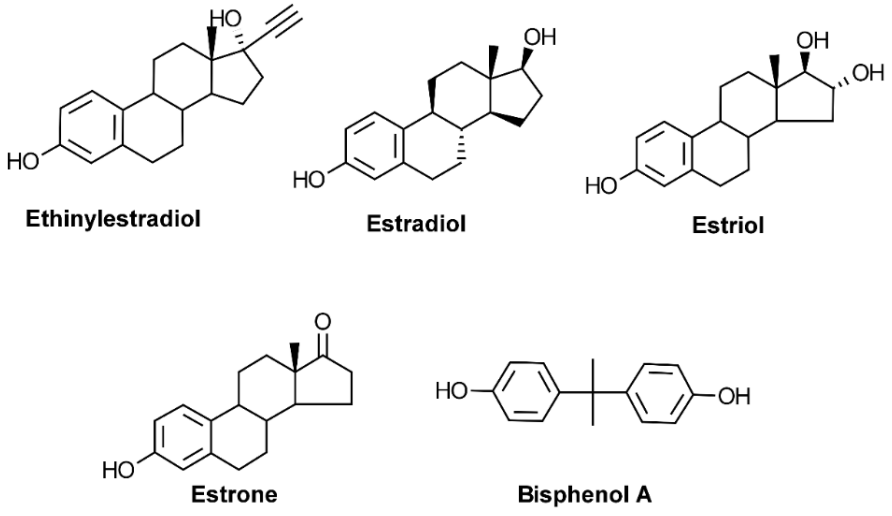

Figure 6.1 Chemical structure of the target estrogens included in this study.

The materials were mounted on an in-house fabricated holder and positioned inside the batch reactors (Figure 6.2). The reactors were placed in a four-position magnetic stir plate, three of which have an in-house assembled six-cm collimated UV-LED beam (θ_{beam}= 4 cm; at λ=365 nm) while the fourth one was reserved for dark control experiments (Figure 6.2). The bandgap energy for TiO_2 is typically ~3.2 eV suggesting that UV light with λ<387nm can be used for excitation (Bhatkhande et al., 2004). The distance of the UV-LEDs to the water level in the reactor was 10.5 cm while the distance of the immobilized TiO_2 (sitting on the holder) to the water level was 1.5 cm. The UV-LED power output (in mW) was measured using Thorlabs Power and Energy meter (PM100-USB) (New Jersey, USA) with a distance from the UV-LED to the sensor of 18 cm. The average irradiance estimated at 10.5 cm is 0.390 mW/cm^2.

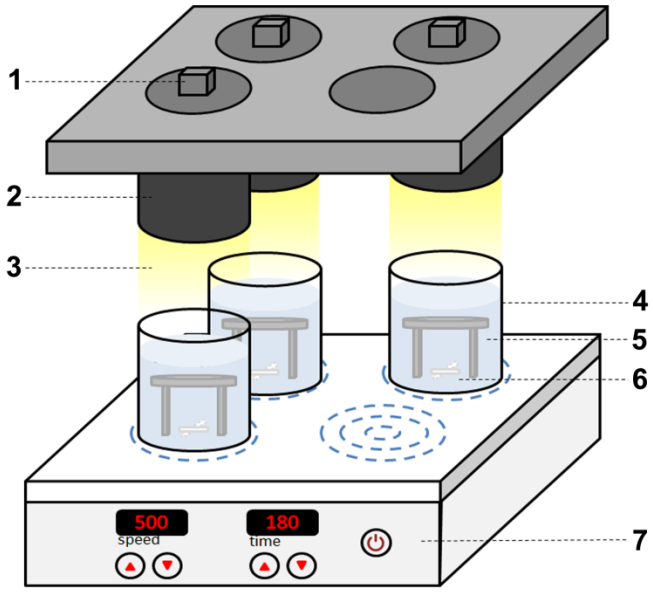

Figure 6.2 Experimental set up for this study. (1) LED constant current driver; (2) collimating tube; (3) UV-LED source (4) glass beaker batch reactor (covered in aluminum foil); (5) immobilized TiO_2 material and holder (6) magnetic stir bar; and (7) four position magnetic stir plate.

Each reactor was spiked with 60 µL of 20 mg/L of estrogen stock solution in methanol to achieve a final concentration of 4 µg/L. The reactors were allowed to equilibrate in the dark for 60 min followed by the immediate exposure to UV-LED for another 300 min (stirred at 800 rpm for the entire experiment period). Samples were collected (2.5 mL) in glass test tubes every hour

and were allocated for chemical analysis (2 mL) and YES assay (0.5 mL). A total of 15 mL were collected by the end, which corresponded to a 0.5 cm drop of water level in the reactor. All tests were completed in triplicate. Dark and photolysis (UV-LED only) experiments were also performed to serve as control tests.

An additional experiment with EE2 was conducted using a low-pressure UV lamp (UVP GL-58, 0.12 A, 6 W) operated in longwave mode (Ultraviolet Products Ltd., Upland, CA) and powdered TiO_2 suspensions (Evonik P25). This experiment was completed to compare the treatment efficiency of using conventional TiO_2 nanomaterials with the UV-LED/PTT experiments. This experiment was also conducted in triplicate using 500 µg/L of both EE2 and P25 suspension (500 mL) with an equilibration period of 30 min at the beginning followed by another 60 min of irradiation. The concentrations of both EE2 and P25 were purposely made higher than for the UV-LED experiments to represent the conditions typically chosen for these types of experiments found in the literature (Tong et al., 2012).

6.3.4 Detecting the presence of hydroxyl radicals

Hydroxyl radicals are very short-lived and direct determination of their concentration in the solution can be very challenging. Hence, a separate experiment was conducted to detect the formation of hydroxyl radicals in the solution using terephthalic acid (TPA) as a probe molecule (Ishibashi et al., 2000). This compound reacts with hydroxyl radicals with high specificity forming a 2-hydroxyterephthalic acid (HTPA), a product that is stable and highly fluorescent when excited at λ=315 nm (peak emission at λ=420 nm). The concentration of hydroxyl radicals can be inferred from the concentration of HTPA produced during the irradiation period. Specific details on the experimental preparation are found in Appendix E-5.

6.3.5 Sample preparation and chemical analysis

A sample clean-up was completed using solid phase extraction (SPE) in a 24-port Visiprep™ vacuum manifold (Supelco, Bellefonte, PA). Bond Elut Plexa cartridges with 1 mL volume and 30 mg bed mass (Agilent Technologies, Mississauga, ON) were preconditioned sequentially with 1 mL of MTBE, 1 mL of methanol, and 1 mL of ultrapure water. Samples were introduced 1 mL at a time by gravity only (i.e., no vacuum applied). Elution was completed with

2 mL of methanol followed by 2 mL of 10:90 methanol: MTBE. Samples were evaporated to dryness using the Dionex Rocket Evaporator (Thermo Scientific, Mississauga, ON) employing the built-in low boiling point standard method. The samples were reconstituted to 100 µL methanol and stored in 2 mL amber glass vials (with glass inserts) at -20^{o}C until analysis.

Chemical analysis for target estrogens was completed using an Agilent 1200 HPLC coupled to Agilent 6460 Triple QQQ equipped with an Agilent Jet Stream electrospray ion source (AJS-ESI). The chromatographic ionization parameters are presented in the Table S6.1 (Appendix E). The estrogens were analysed under negative ionization using unit resolution multiple reaction monitoring (MRM) with parameters listed on Table S6.2 (Appendix E). The chromatographic separation of analytes was completed on a 4.6 mm × 150 mm × 5 µm Agilent Eclipse XDB-C18 column (Agilent Technologies, Mississauga, ON). Data collection and quantitation were completed using Agilent MassHunter Workstation Software. Details on the quantitation are also found in the Appendix E-1.

6.3.6 Yeast estrogen screen (YES) assay preparation and analysis

The samples allocated for YES analysis were transferred into methanol to ensure the stability of compounds prior to analysis. This was done by evaporating the aqueous samples to dryness using the Dionex Rocket Evaporator (Thermo-Scientific, Mississauga, ON) and reconstituting to 320 µL of methanol. The samples were stored in 2 mL amber glass vials at 20^{o}C until analysis. The YES assay procedure, including culture media formulation was adapted from Smith (2013) but was originally developed by Gaido et al. (1997) using yeast cells that were stably transfected with human estrogen responsive element. Specific details on this assay are explained in Appendix E-2.

6.4 Results and discussion

6.4.1 Material characterization

The thermal-chemical oxidation of photocatalytic thin-film synthesis is a straightforward approach, utilizing a potentially scalable one-step synthesis that does not require the use of many organic solvents, acids, or bases. The 3D topographical profiles for PTT are shown in Figure

6.3a. The average R_a and R_{RMS} surface roughness values are 6.45 µm and 10.7 µm, respectively. R_a or R_{RMS} value close to zero indicates that the surface has no roughness and has a mirror-like finish, while higher R_a or R_{RMS} value is indicative of high surface roughness. The materials synthesized are rougher than other supports TiO_2 deposited on polymeric membranes (roughness in the nanometer range (Cao et al., 2006)) Rough surfaces have been found to be conducive for filtration applications due to enhanced permeability resulting from more contact with water (Kwak et al., 2001a). Although roughness can be detrimental during the filtration process because it increases the material's fouling potential, a few studies have shown that UV-irradiated TiO_2 thin films have self-cleaning mechanisms that can overcome the effects of common fouling agents (Cao et al., 2006; Damodar et al., 2009; Kwak et al., 2001b). Membrane fouling test was not the main objective of this study but the authors recognize that this can have implications for the potential use of the newly synthesized thin film materials.

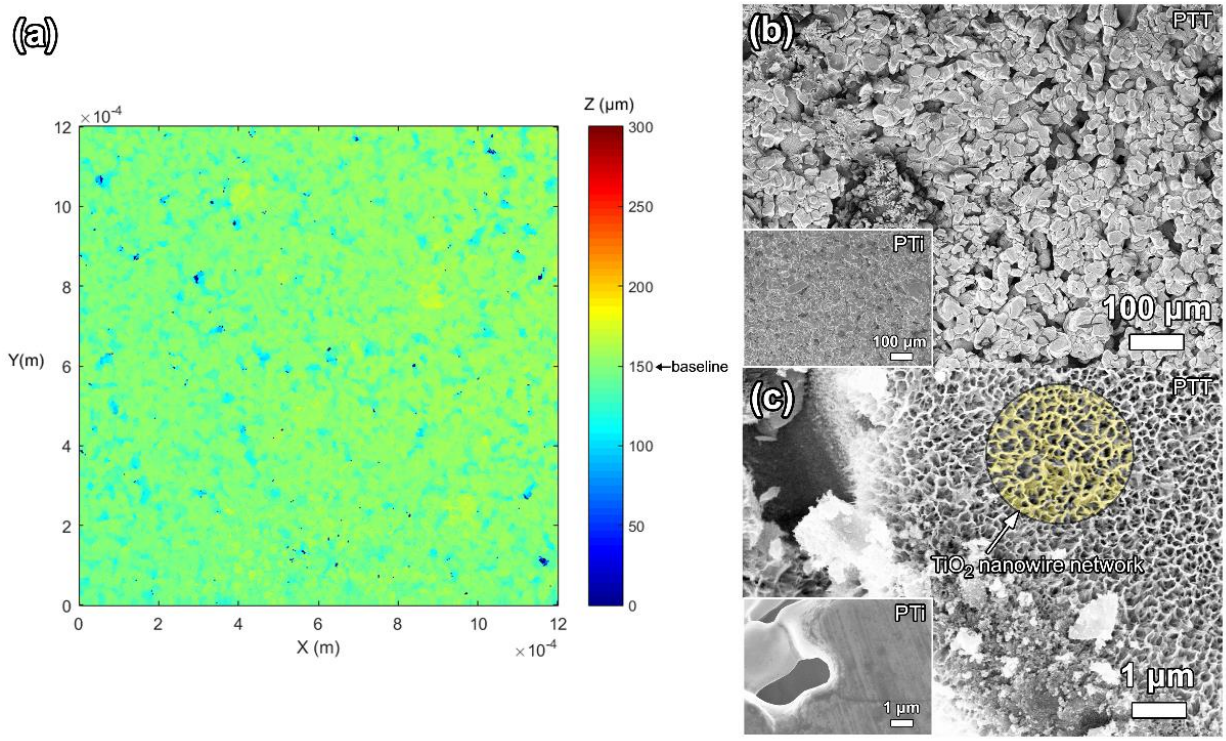

Figure 6.3 Surface morphology of PTT showing (a) surface roughness profile; (b) SEM image of PTT and PTi sheets (inset) at 100× magnification; and (c) SEM image of PTT with TiO_2 nanowire networks (highlighted) and PTi sheet at 5000× magnification.

The surface morphology was imaged using SEM as shown in Figure 6.3b and Figure 6.3c. The PTi was oxidized in the H_2O_2 solution which produced PTT containing TiO_2 neural networks that have formed on the surface of sintered Ti agglomerates upon heat treatment. The TiO_2 immobilized are of anatase phase as seen in the Raman peaks in Figure 6.4. The peaks were cross referenced for anatase and rutile from the RRUFF online database using the spectra IDs, R060277 and R050417, respectively (Database of Raman spectroscopy, X-ray diffraction and chemistry of minerals at http://rruff.info/). Anatase has higher photocatalytic activity than rutile and is generally more preferred than the latter (Luttrell et al., 2014).

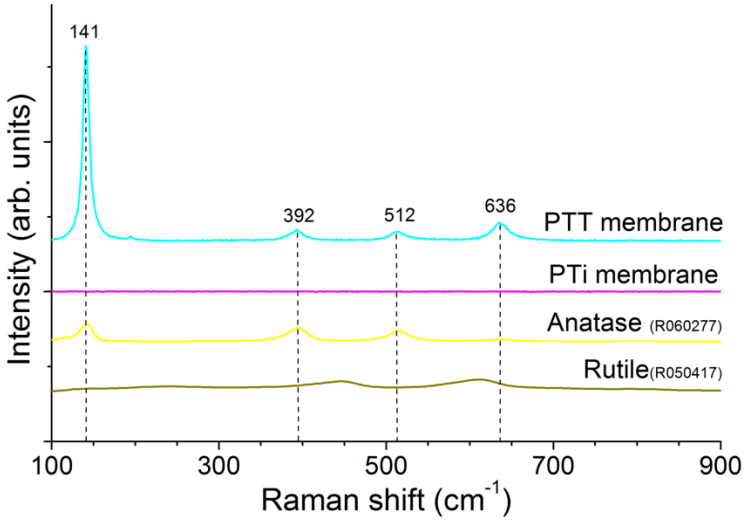

Figure 6.4 Raman spectra for PTT and porous titanium sheet in comparison to anatase and rutile Raman shift intensities.

6.4.2 Evidence of hydroxyl radical formation

The probe molecule, TPA, was used to investigate the generation of hydroxyl radicals. The formation of the hydroxylated and highly fluorescence product, HTPA, suggests the presence of hydroxyl radicals in the solution (Ishibashi et al., 2000). Furthermore, the increase in intensities of the fluorescence spectra of HTPA at various time points (Figure 6.5a) was indicative that hydroxyl radicals are being generated by the immobilized TiO_2 during UV-LED irradiation. The HTPA production was additionally found to be linear over the 300 min of UV-LED irradiation (Figure 6.5b).

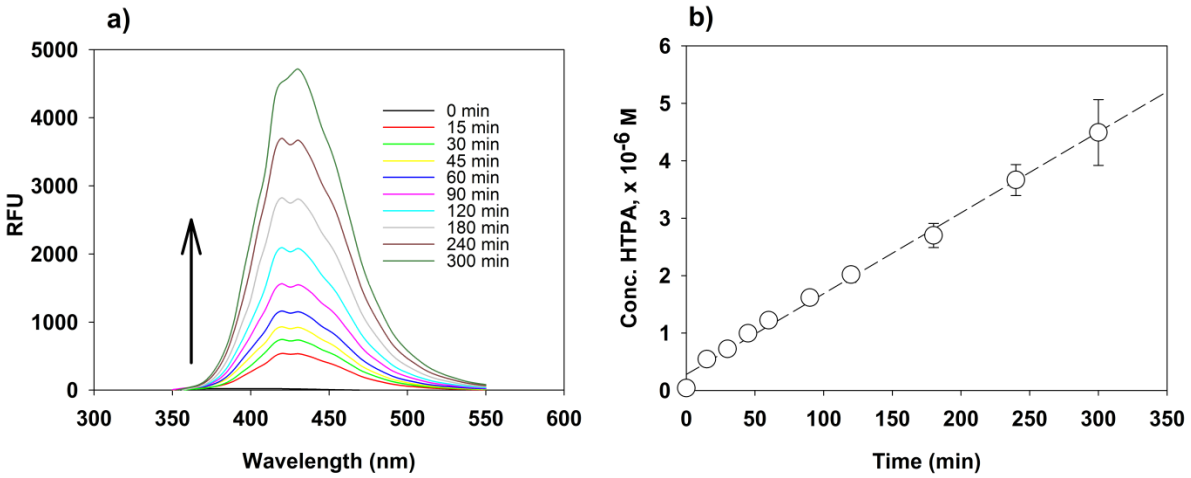

Figure 6.5 (a) HTPA formation at increasing exposure times and (b) hydroxyl radical concentrations increasing linearly over time. HTPA excitation wavelength at 315 nm and peak emission at 420 nm. RFU = relative fluorescent units.

6.4.3 Photocatalytic treatment of target estrogens – effect of pH

The Langmuir-Hinshelwood (L-H) mechanism is commonly used to describe the kinetics of photocatalytic oxidation (Konstantinou and Albanis, 2004). When the initial concentration (C_o) is in the millimolar range, L-H is simplified into a pseudo first-order decay equation:

$$\ln \frac{C_o}{C} = k_{app} \times t \qquad \text{(Equation 6.1)}$$

where C is the concentration (µg/L), k_{app} is the decay rate constant (1/min), and t is time (min) (Zhang et al., 2012a). The plot of $\ln \frac{C_o}{C}$ vs t is a straight line with the slope representing k_{app}.

The photocatalytic activity of the UV-LED irradiated PTT was investigated in batch mode under different pH conditions. There was no removal observed via adsorption onto immobilized TiO_2 or onto the porous titania support during the 60-min equilibration period (dark) for all pH conditions. The data collected after this period, however, followed the simplified L-H kinetics (Figure 6.6). A comparison against the dark and photolysis (UV-LED only) experiments showed that the disappearances of target estrogens were mainly attributed to the photocatalytic effect of UV-LED/PTT (Figure 6.6). These results suggest that a major mechanism of compound degradation is the oxidative attack of reactive oxygen species (e.g., hydroxyl radicals) generated by the UV irradiation of immobilized TiO_2. The decay rate constants for each compound are additionally shown in Table 6.2.

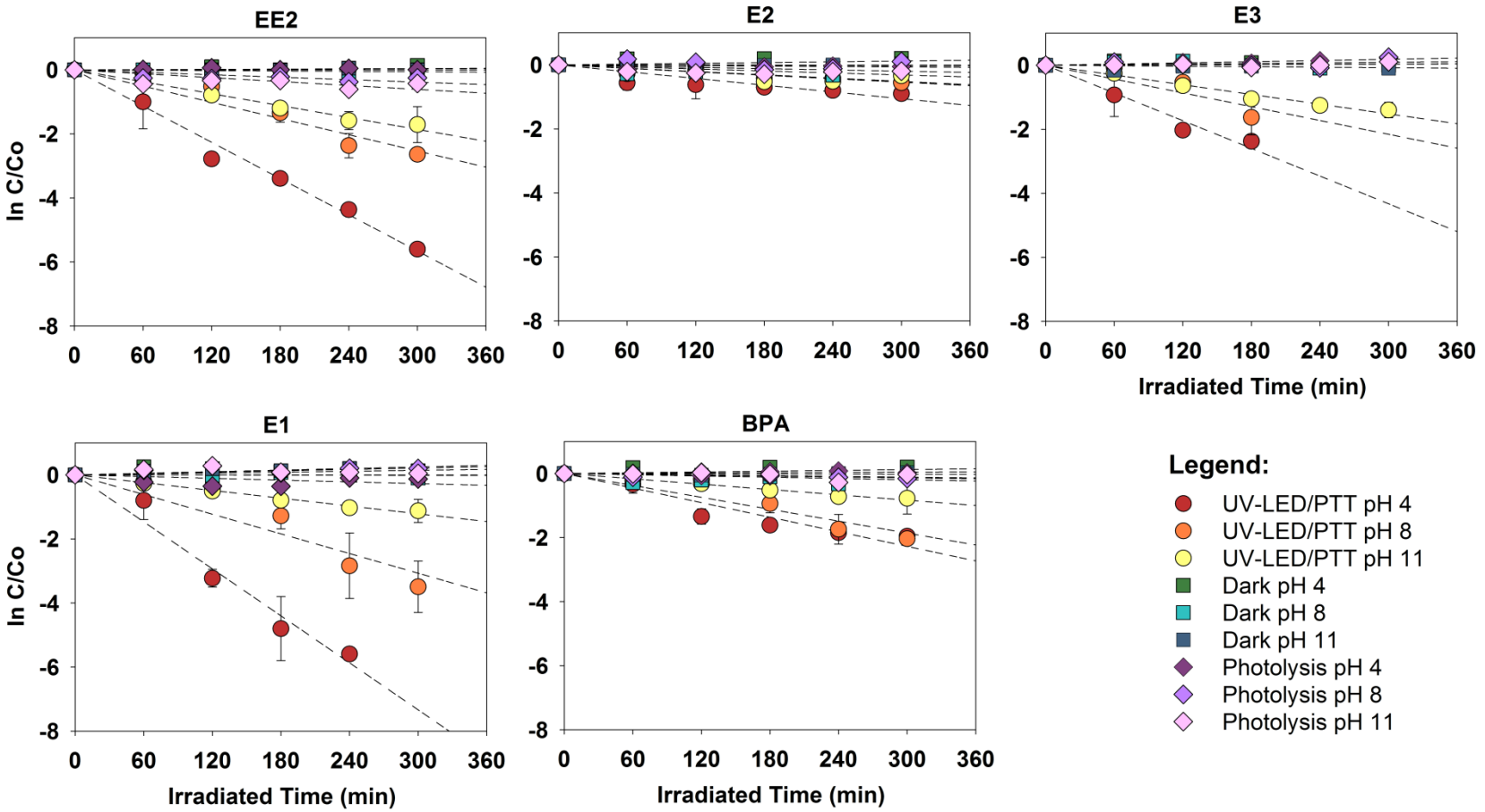

Figure 6.6 Concentration profiles of target estrogens under the control (dark and photolysis) and UV-LED/PTT treatments.

Table 6.2 First-order decay rate constants for target compounds at different pH conditions.

	pH 4		pH 8		pH 11	
Compound	**$k \times 10^{-3}$ (1/min)**	**R^2**	**$k \times 10^{-3}$ (1/min)**	**R^2**	**$k \times 10^{-3}$ (1/min)**	**R^2**
E1	24.5	0.968	11.5	0.975	4.1	0.984
E2	3.4	0.866	1.8	0.834	2.4	0.782
E3	14.4	0.960	7.2	0.801	5.1	0.976
EE2	18.9	0.986	8.4	0.915	6.2	0.982
BPA	7.3	0.952	6.6	0.954	2.8	0.981

There are statistically significant differences in the decay rate constants among different pH conditions for E1 (p=0.007), EE2 (p<0.001), E3 (p=0.002), and BPA (p=0.006) (Sigma Plot, one-way ANOVA, α=0.010). The rate constants at pH 4 were also found to be significantly different from pH 11 for all compounds but not from pH 8 (p values ranging from 0.002 to 0.006, Tukey test), except for EE2 where the pH 4 treatment is significantly different from both pH 8 and pH 11 treatments (p<0.001).

To explain the differences in the kinetic behavior of target estrogens at different pH conditions, it is important to understand that photocatalysis can be generalized as a two-step process, starting with adsorption of contaminants on the surface of activated TiO_2 followed by their reaction with hydroxyl radicals and/or direct oxidation by holes. Adsorption on the surface is a crucial process that is driven by the surface charge interaction between TiO_2 and the contaminant. In addition, the role of pH is critical in addressing adsorption as changing pH can considerably modify TiO_2 surface charge thereby achieving a certain specificity that limits the interaction of target compounds with TiO_2. The effect of pH during the removal of estrogenic compounds via UV-LED/PTT photocatalysis is very noticeable (Figure 6.6). The pH dependence is highly attributed to the charge of TiO_2 and the degree of ionization of estrogens at different pH values. TiO_2 surface is amphoteric and as a result, differently charged species occur at different pH conditions. The isoelectric point (pIEP) of TiO_2 is a good indicator of the expected surface charge conditions at different pH values as it describes when it is mostly negatively charged (pH>pIEP), positively charged, (pH<pIEP) or neutral (pH=pIEP). The pIEP of PTT is approximately 6 (see Arlos et al. (2016a) or Figure S6.2 in the supplementary material for details). Hence, it can be inferred that TiO_2 is positively charged in acidic media and mostly

negative in alkaline conditions while the EDCs in this study are mostly neutral in acidic conditions and mostly negative in alkaline environments based on their pKa (pH>10).

These conditions create charge interactions that resulted in a relatively poor treatment observed at pH 11 in response to the electrostatic repulsion between the negatively charged TiO_2 surface and target compounds. This non-interaction consequently lowers the chances of oxidation of organic molecules by different species involved in TiO_2 photocatalysis. Although there is evidence that hydroxyl radicals can disperse away from the surface, it is still believed that the close proximity of organic molecules to the TiO_2 surface increases treatment efficiency (Shaham-Waldmann and Paz, 2013).

While it is easier to visualize the interaction of charged compounds with the TiO_2 surface, interactions of neutral compounds with TiO_2 are driven by both pH of the solution and their potential to donate electrons (i.e., nucleophilicity). When a neutral compound is a strong Lewis base (strong nucleophile) and the pH of the solution is close to pIEP of TiO_2, adsorption onto the surface of charged TiO_2 is very likely (Rodríguez et al., 2008). Most organic compounds have Lewis base functional groups (e.g., alcohols [-OH], amines [-NH_2], thiols [-SH]) that form ionic bonds with metal oxides such as TiO_2 (Tang, 2003). As a result, the oxidation of neutral species is still possible during TiO_2 photocatalysis. This is well demonstrated in this study where more efficient removals were observed when target estrogens were mostly neutral rather than when they were mostly negatively charged.

The natural and synthetic hormones (E1, E2, EE2, and E3) have very similar molecular structures (Figure 6.1). Hence, their interaction with the TiO_2 will likely be comparable. A statistical analysis on the first-order decay rate constants has further suggested this, where no significant differences among the decay behavior of E1, E3, and EE2 at all pH conditions were observed (SigmaPlot, One-way ANOVA, p=0.309 to 0.999). The degradation of BPA was found to be different than E1 and EE2 at pH 4 (SigmaPlot, One-way ANOVA, p=0.017 & 0.027 respectively) but not for pH 8 and pH 11 treatments (p>0.05). Although considered an estrogenic compound, BPA has a different molecular structure than the hormonal estrogens, potentially resulting to a different photocatalytic degradation pathway.

While there were simultaneous disappearances of E1, E3, EE2, and BPA, the fast disappearance of E2 (17β-estradiol) was not as evident in any of the treatments, although there was some reduction in E2 concentrations at pH 4 (see rate constants in Table 6.3). A study conducted by Banjac et al. (2015) also found that the presence of other estrogens, E1 and EE2, can have inhibitory effects towards the degradation of E2 under UV/H_2O_2 oxidation process. Bahnemann et al. (1997) suggested that competition of molecules with the same charge conditions on adsorption sites, as in the case of the estrogens, is possible as highly competitive molecules can block other compounds thereby reducing their probability to undergo photocatalytic oxidation.

It is also important to note that the batch experiments were completed with the presence of methanol (0.02% v/v) to aid in the dissolution of estrogens in water. This is a common practice as observed in other studies where their carrier concentration (ethanol or methanol) ranged from 0.02 to 0.3% v/v (Table 6.3). The authors recognized the scavenging effect of methanol but the degradation observed with the presence of a scavenger still suggests that UV-LED/PTT treatment has a potential application in EDC degradation.

6.4.4 Impact of UV-LED use

The rate constants from pH 4 experiments were additionally compared to other studies that evaluated the efficiency of immobilized TiO_2 (Table 6.3). The decay rate constants derived from this study were lower than that from literature as those experiments were conducted using high powered lamps that were operated at 2.4×10^3 to 7.4×10^4 times more power than the UV-LEDs from this study. However, UV-LEDs can easily be adapted to suit a design configuration that improves the ability of UV/TiO_2 to degrade EDCs. Other characteristics of UV-LEDs over conventional UV lamps include its portability, robustness, and their potential to be implemented under pulsed illumination (known to be more effective in biofouling mitigation than continuous UV exposure) (Song et al., 2016). This study shows that UV-LEDs still remain a potential substitute to high powered lamps and investigations on optimized configurations of UV-LED light sources is still required.

Table 6.3 Reported decay kinetics by other studies that employed immobilized TiO_2.

Compound	Study	Concentration (mg/L)	Immobilization	UV conditions (Wavelength, Type, Power, Irradiance)	Removal kinetics[c] (1/min)	Percent carrier in solution	Estrogenic Activity
E1	Coleman et al. (2004)	0.010	Titanium alloy	UV-A (315-400 nm), HP mercury lamp, 125 W, NM.	0.086	0.01 EtOH	Estrogenicity loss after 60 min
	Mitamura et al. (2004)	0.288	Glass beads	365 nm, Fluorescent lamp, 4 W, NM.	0.015	<0.3 EtOH	NM
	Nakashima et al. (2003)	0.250	PTFE mesh sheet	NM, 8 fluorescent lamps, 15 W, 1.2 mW/cm^2	0.120	NM	NM
	This study[a]	0.004	Porous titanium	365 nm, UV-LED ,1.67 mW, 1.3×10^{-1} mW/cm^2	0.025	0.02 MeOH	Non-detectable estrogenicity ~120 min
E2	Coleman et al. (2004)	0.010	Titanium alloy	UV-A (315-400 nm), HP mercury lamp, 125 W, n.m.	0.106	0.01 EtOH	Loss after 55 min
	Coleman et al. (2005)	0.817	Coated TiO_2 on quartz coil reactor	UV-A, B, C (100-400 nm), MP mercury lamp, 125 W, n.m.	0.174	ACN, amount not mentioned	NM
	Mitamura et al. (2004)	0.272	Glass beads	365 nm, Fluorescent lamp, 4 W, n.m.	0.017	<0.3	NM
	Nakashima et al. (2003)	0.250	PTFE mesh sheet	NM, 8 fluorescent lamps, 15 W, 1.2 mW/cm^2	0.150	NM	NM
	This study[a]	0.004	Porous titanium	365 nm, UV-LED ,1.67 mW, 1.3×10^{-1} mW/cm^2	0.003	0.02 MeOH	Non-detectable estrogenicity ~120 min
E3	(Coleman et al., 2005)	0.865	Coated TiO_2 on quartz coil reactor	UV-A, B, C (100-400 nm), MP mercury lamp, 125 W	0.156	ACN, amount not mentioned	NM
	This study[a]	0.004	Porous titanium	365 nm, UV-LED, 1.67 mW, 1.3×10^{-1} mW/cm^2	0.014	0.02 MeOH	Non-detectable estrogenicity ~120 min
EE2	Coleman et al. (2004)	0.010	Titanium alloy	UV-A (315-400 nm), HP mercury lamp, 125 W, n.m.	0.086	0.01 EtOH	Estrogenicity loss after 60 min
	Coleman et al. (2005)	0.888	Coated TiO_2 on quartz coil reactor	UV-A, B, C (100-400 nm), MP mercury lamp, 125 W, n.m.	0.231	ACN, amount not mentioned	NM
	This study[a]	0.004	Porous titanium	365 nm, UV-LED ,1.67 mW, 1.3×10^{-1} mW/cm^2	0.019	0.02 MeOH	Non-detectable estrogenicity ~120 min
BPA	Wang et al. (2009)[b]	10	Porous PF foam cube	254 nm, LP mercury lamp, 25 W in horizontal circulating bed reactor, 18 mW/cm^2	9.7×10^{-4}	NM	NM
	This study[a]	0.004	Porous titania	365 nm, UV-LED ,1.67 mW, 1.3×10^{-1} mW/cm^2	0.007	0.02 MeOH	Non-detectable estrogenicity ~120 min

Note: ACN = acetonitrile; PTFE = polytetrafluorethylene; PF = phenol formaldehyde; LP, MP, HP = low, medium, high pressure; "NM" not mentioned or performed in the study; [a]Information presented is from the pH 4 test; [b]Authors conducted many tests under different conditions but only the optimal rate constant was reported here for comparison; [c]pseudo first order kinetics

6.4.5 Removal of estrogenic activity

The YES assay is a useful tool in investigating the potential of anthropogenic compounds and mixtures of chemicals to mimic human estrogen hormones. Hormones interact with the receptors in the body using a 'key and lock' mechanism. Hence, compounds with similar structures to natural hormones can interfere with this system by mimicking the processes that only endogenous hormones are responsible for initiating. In this study, the most efficient degradation was observed at lower pH conditions (Figure 6.6) and the estrogenic activity removal is reflective of this result (Figure 6.7). The total estrogenic activity measured by the YES assay was removed to below the detection limits within 120 min at pH 4. The pH 8 and pH 11 treatments showed the slower removal of total estrogenicity, similar to those observed for the disappearance of individual estrogens (Figure 6.7).

Estrogens additionally have different levels of potency relative to the natural receptor ligand E2. Beck et al. (2006) determined that EE2 has an estradiol equivalency factor (EEF) in YES assay that is 1.25 times more potent than E2, while E1, E3, and BPA are 2.5×10^{-1}, 5.9×10^{-3} and 1.2×10^{-4} times less potent than E2. Hence, the chemical concentrations (analytical data) of an estrogenic mixture can be converted into E2 equivalents (EEQ) as a sum of the individual concentrations, C_i, multiplied by their EEFs: $EEQ_{mixture} = \sum C_i \times EEF$. EEQs derived from the analytical data supports the results of the YES assay (Figure 6.7). As observed earlier, E2 was poorly degraded by the material but the total estrogenic activity still continued to decrease over time for all pH conditions. The large portion of the total estrogenic activity at the beginning of the experiment was mainly derived from EE2 (~52%) while the weaker estrogens (E1, E3, and BPA) contribute ~10%. Hence, the removal of these compounds still reduced the activity even with the poor degradation of E2.

Various estrogen removal studies via UV-TiO_2 have suggested that the degradation of phenol-containing estrogens can be attributed to hydroxylation (i.e., OH addition) and direct hole oxidation followed by subsequent ring opening mechanisms in the molecule. Mai et al. (2008) additionally predicted that the two carbon atoms in the phenol moieties are more susceptible to attack via OH radical and direct hole oxidation. It is important to note the phenol moiety in endogenous hormones is also responsible for their agonistic activity towards estrogen receptors

(Anstead et al., 1997; Klopman and Chakravarti, 2003). Therefore, once the phenol group is attacked, estrogenic activity decreases as there are no longer enough of that moiety that can bind to the estrogen receptors. Hence, the YES assay results reflected that of the chemical analysis.

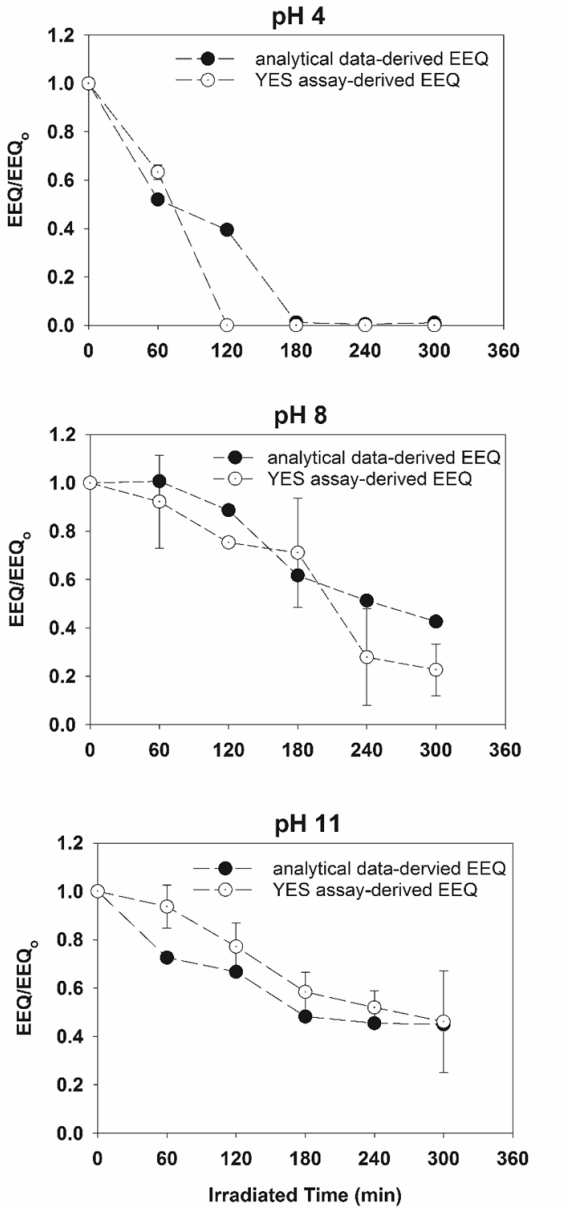

Figure 6.7 The biological activity removal as expressed by the YES assay and predicted chemical concentrations using the estradiol equivalents (EEQ) concept. The EEQs were normalized to the initial EEQ.

6.4.6 Comparison of EE2 removal with P25 suspension

The treatment of EE2 using commercially available TiO_2 suspensions (P25) with a conventional UV lamp was compared to that of the UV-LED/PTT. Both chemical (EE2) and estrogenic activity (YES) removals using P25 suspensions indicate first-order kinetics with rate constants corresponding to 62×10^{-3} 1/min and 58×10^{-3} 1/min respectively (Figure 6.8). The similarity in the removal kinetics of both chemical and biological analyses is further suggestive that the photocatalytic degradation of EE2 likely starts with the phenol moiety attack, the functional group responsible for interacting with the estrogen receptor.

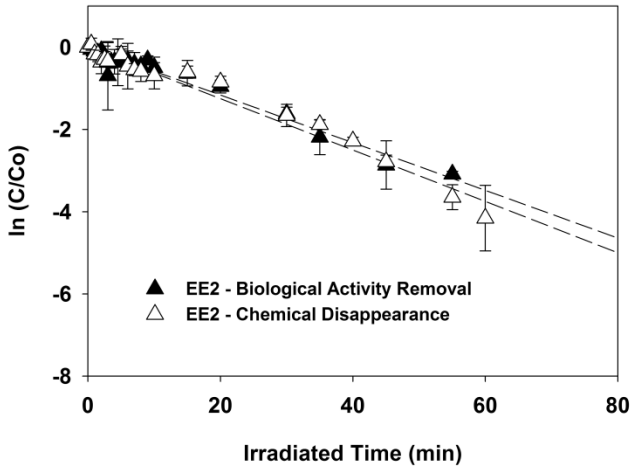

Figure 6.8 Chemical and estrogenic activity removal of EE2 using a separate experiment with 500 mg/L P25 suspensions.

When the rate constants for EE2 at pH 4 under UV-LED/PTT treatment (18.9×10^{-3} 1/min) was compared to this experiment, it was found that the UV-LED/PTT treatment rate constant was statistically lower than the rate constants with suspended P25 (62×10^{-3} 1/min) (SigmaPlot, two-tailed t-test, $p=0.026$, $\alpha=0.05$). The difference between UV-LED/PTT and P25 experiments was expected due to more photocatalytically favorable conditions employed in the suspension study. For instance, the concentrations of TiO_2 in slurry suspension was 500 mg/L, which is a few orders of magnitude higher than what would be expected in immobilized TiO_2 materials (typically in the µg/L range). In addition, the mass transfer dependent processes would be expected to be slower for an immobilized photocatalyst than for a suspension. Nevertheless,

the results of this study are still promising and we further reiterate that process optimization is a key to improving degradation kinetics.

6.5 Conclusions

In this study, photocatalytically active TiO_2 materials were synthesized via a one-step process of thermal and chemical oxidation of commercially available porous titanium sheets. The synthesis method was a straightforward approach that did not require the use of harmful organic solvents, acids or bases. The materials under UV-LED irradiation were tested for their ability to photocatalytically degrade target estrogenic compounds. The study showed that the UV-LED irradiated immobilized TiO_2 on porous titanium sheets have the potential for treatment (removal) of these compounds. Lower pH conditions (pH 4) favored the photocatalytic process due to the greater electrostatic interaction of target compounds with the charged TiO_2 surface. The materials were also capable of removing the biological activity (total estrogenicity) of the estrogenic mixture in a similar manner to that predicted by the chemical measurements. In addition, the use of UV-LED is very promising as it is not only a low energy substitute but can be very adaptive to various photo-reactor designs.

Chapter 7
Conclusions and Recommendations

This thesis demonstrated the utility of water quality models in exposure assessment (Chapters 2-3) and evaluated the potential use of UV/TiO_2 for organic micropollutant (OMP) removal (Chapters 4-6). This chapter specifically discusses the major conclusions and provides additional recommendations for future research.

7.1 The use of modeling in exposure assessment

Exposure assessment quantifies the magnitude, frequency, and duration of exposure in an environmental compartment and is a key element in the risk characterization of OMPs. The assessment is often completed using advanced analytical chemistry techniques and bioassays that detect the total biological activity such as estrogenicity. These methods can be limited by sampling logistics, analytical methods, and cost. Hence, water quality modeling can be useful to fill the data gaps on spatial and temporal distribution of OMPs and can be employed to make predictions under different future scenarios. Chapters 2 and 3 of this thesis focused on the emission-transport-fate (ETF) modeling of several key estrogens in the Grand River. This thesis further demonstrated the feasibility of modeling (1) by providing multi-year predictions (2007-2015) of estrogens released by the Kitchener and Waterloo WWTPs; (2) by simulating the temporal variation and spatial extent of estrogen presence downstream of the source; and finally, (3) by implementing the model to address the questions specific to proposed management strategies (i.e., efficiency of WWTP process upgrades). Also, the model was determined to be robust in representing the characteristics of a complex environmental system and can be employed by researchers and watershed managers as a tool for future investigations associated with exposure and remediation.

Model assumptions were explicitly presented when the predictions were made. A few assumptions include the use of constant daily loading rates in the influent and a single WWTP removal rate constant (Chapter 2). However, the loadings into the WWTP and compound removals are highly variable and are often described by daily (e.g., hourly, diurnal variations) and seasonal fluctuations (e.g., summer vs. winter). The availability of chemical measurements

would have helped to validate some of these assumptions and/or refine the predictions. Unfortunately, there are few reliable data available on estrogens in effluents or receiving environments. There are current issues with the analytical detection using LC/MS-MS due to the high matrix interferences in "dirty" municipal wastewater samples. The target estrogens in the river are at extremely low concentrations which is a significant challenge in the chemical analysis (e.g. detection limits). Although modeling is not a substitute for chemical and bioassay measurements, modeling is a viable option to complement the current lack of exposure data.

7.1.1 Estrogens as model compounds

Endocrine active chemicals such as E1, E2, and EE2 have gained the attention of many regulators worldwide due to their high potency to induce reproductive health effects. Also, field-observed effects such as intersex in wild fish (e.g., rainbow darter in the Grand River) have been associated with the presence of these estrogens in surface water. However, no data were available on the Grand River to support this claim. Hence, the ETF modeling was extended to dose-response (D-R) modeling (Chapter 3). The D-R model provides a useful field-based "exposure-effects" relationship over a wide range of environmentally relevant concentrations (0.01 ng/L to 100 ng/L E2 eq.). This model additionally predicted that concentrations >10 ng/L E2 eq. would result in high intersex incidence with very severe conditions in rainbow darter (severity score of 4-6). Severely intersex fish have reduced reproductive success and may become an issue at the population level (Fuzzen et al., 2015). Some locations near wastewater outfalls in the Grand River were historically exposed to relatively high levels of estrogenic chemicals that approached the levels that may have had adverse reproductive effects on fish. The implementation of WWTP process upgrades improved the water quality and led to reduced presence and severity of intersex downstream. Further upgrades are expected to provide additional improvements.

Caldwell et al. (2012) suggested a predicted no effects concentration (PNEC) of 2 ng/L for E2, whereas the EU proposed lower annual environmental quality standard (EQS) of 0.4 ng/L. Although these values were determined using the species sensitivity distribution (SSD) approach, the studies differ in the number and the type of no observed effects concentration (NOEC) data employed to generate the SSD. The EU included a NOEC that is 10 times lower

than most of the reported chronic effects data on reproductive endpoints, driving a lower value for the EQS. Note that PNECs and EQSs are also not equivalent. PNEC is a risk assessment tool used to calculate the risk quotient (PNEC: PEC) whereas the EQS is a threshold value employed in monitoring and regulatory compliance. Regardless of which value is applied in the assessment, PNECs and EQSs perform a similar role – to protect the ecological integrity of freshwater or marine ecosystems.

Do these recommended thresholds truly fit this purpose? The appropriateness of these recommendations can be assessed using the Grand River data as an example. The D-R model predicts a relatively high intersex incidence (40% to 70%) when exposed to concentrations of 0.4 and 2 ng/L E2 eq., respectively (Figure 7.1). Although these predictions may sound alarming and contradict the protective nature of PNECs and EQSs, intersex fish in the wild can still reproduce (Hamilton et al., 2014) and only very severe cases (severity score of 4-6) can potentially lead to adverse effects in rainbow darter population (Fuzzen et al., 2015). The intersex severity associated with the 0.4 and 2 ng/L E2 eq. exposure is low (severity score of 0.6 to 1.9). Hence, the D-R model validates and supports the PNEC and EQS derived for E2, suggesting that adverse effects will likely occur if the environment is exposed to concentrations above these thresholds. However, the EQS is a more conservative threshold which likely resulted from the EU's strict adherence to precautionary principle. Nevertheless, the predictions from the ETF and the D-R models have the potential benefits and utility to assist with the management decisions associated with the impacts of emerging pollutants.

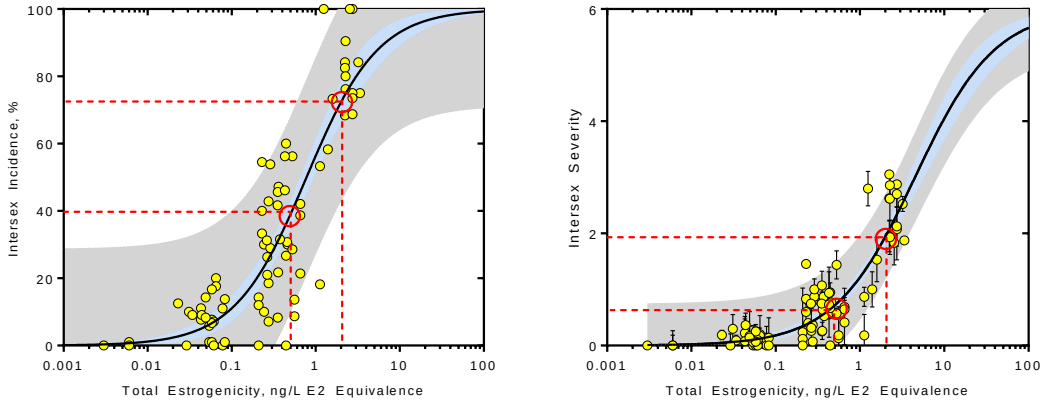

Figure 7.1 D-R model for intersex incidence and severity with 95% confidence (blue) and prediction intervals (grey). (---) effect levels associated with the recommended PNEC (2 ng/L) and EQS (0.4 ng/L) for E2.

7.1.2 Future model improvements

Additional investigations are required to verify the assumptions used in the ETF and D-R models. For instance, data on WWTP removal rates must be collected and assessed for their temporal variability (daily and seasonally) (Chapter 2). Also, the current model simulation is highly conservative (i.e., no fate mechanism). Therefore, model validation including the transport and fate of estrogens (Chapter 3) is required. This process can be completed when analytical methods improve or become available. A laboratory study is also currently underway to determine whether the period of gonadal recrudescence in rainbow darter (June – August) was a critical exposure condition as assumed within the D-R model (Chapter 3). Hence, the model should be updated once the results of this experiment are available. These suggestions will refine the predictions and may be important for future model implementation.

7.2 UV-irradiated TiO_2 as a promising option for OMP removal

UV/TiO_2 for water treatment application is still in relative infancy, but its potential use for water treatment applications is evident, particularly in the removal of OMPs (Chapters 4-6). Upon the absorption of UV, TiO_2 generates hydroxyl radicals and other reactive oxygen species that play an important role in the photocatalytic oxidation of organic compounds. In this thesis, newly synthesized TiO_2 nanomaterials were tested for their potential to remove a mixture of personal care products, pharmaceuticals, and their associated metabolites (Chapters 4 and 5). The specific removals of endocrine active chemicals (E1, E2, E3, EE2, and BPA) and their biological activity (Chapter 6) was also investigated.

Due to solubility issues, many studies that test the removal of pharmaceuticals using UV/TiO_2 employ carrier solvents (e.g., methanol, acetonitrile) during bench-scale testing. This process may confound the results since some carrier solvents can act as hydroxyl radical scavengers. In this thesis, the influence of different levels of methanol (a commonly used carrier solvent) during TiO_2 photocatalysis experiments was also assessed (Chapter 4). While eliminating the carrier solvents from the experiments is recommended, they are necessary to enhance the dissolution of target compounds, and it has been determined that trace amounts of methanol can be used (up to 0.002 v/v). It was also observed that the presence of methanol had

different effects on the reactivity of UV/TiO_2 with different pharmaceuticals (Chapter 4). A consistent low level of methanol (0.002% v/v) was employed in the photocatalysis experiments (Chapters 5) to ensure complete dissolution of the OMPs. Under the presence of 0.002% v/v, only 2 (venlafaxine and atenolol) out of the 11 pharmaceuticals tested in Chapter 5 showed kinetic rate constants that are statistically significant from 0% (P25 tests, Chapter 4). Hence, this methanol concentration was deemed a reasonable compromise between solubility requirements and hydroxyl radical scavenging activity. Regardless, it is advised that the implications of the use of carrier solvents must be carefully considered before being employed in experimentation.

Two types of TiO_2-based membrane materials were synthesized: quartz-fiber membranes dip-coated with sol-gel TiO_2 (QFT) and membrane materials produced from the thermal-chemical oxidation of Ti sheets (PTT) (Chapter 5). The resulting differences in surface charges heavily influenced the treatment of pharmaceuticals when using these materials. Although not a frequently measured parameter in bench-scale testing, the isoelectric points (IEP) of the materials were measured and compared with the compound pKa's to explain differences in the affinities of the compounds for the membrane. It was also observed that pH had an impact on the removal of estrogens, with low pH showing better removals than higher pH conditions (Chapter 6). The chemical removal of estrogens also followed the same pattern as the removal of biological activity suggesting that the structures responsible for the estrogenicity were also being oxidized, and that no new estrogenic compounds were formed (Chapter 6).

7.2.1 Outlook on UV/TiO_2 for water treatment

To fully realize the potential of UV/TiO_2, further material science and water treatment studies are required to resolve many technical issues. A few examples are discussed below:

1. **Material synthesis optimization**. Each synthesis method can be optimized to improve the photocatalytic activity of TiO_2. Specific experiments that investigate the parameters impacting the TiO_2 annealing onto supports such as immobilization temperature, TiO_2 suspension dosage, and solvents can be further explored. Specific attention during synthesis must also be given to material stability during water treatment (e.g., resistance to fluctuating water quality). The membrane materials can also be prone to fouling and appropriate strategies to reduce this issue must be identified.

2. **The configuration of photocatalytic membrane reactors (PMR)**. The immobilization of the TiO_2 proves to be more superior to nanopowder forms due to its operational feasibility in water treatment applications (i.e., no separation process required). Several PMR configurations are currently available (Chapter 1), and it is important to determine the optimal conditions for which the PMRs can be operated (e.g., dead-end vs. cross-flow filtration). A standardized approach to testing should also be completed when comparing different reactor designs. Most studies employ the first-order reaction rate constant (*k*) to assess the efficiency of PMRs. However, *k* is dependent on reactor volume and relies on light intensity and catalyst loading. As a result, comparison across many studies may not result in a more objective analysis of efficiency. The work of Leblebici et al. (2015) proposed the use of the photocatalytic space-time yield (PSTY), a parameter that is normalized against the effects of many photocatalysis parameters including the reaction kinetics, mass and photon transfer rates, and light utilization efficiency on the volumetric yield of PMRs.
3. **Application to representative water samples**. An area that was not explored in this thesis is the direct application of the newly synthesized material to treating actual source water or wastewater samples. Specific water quality parameters can have an impact on treatment (Chong et al., 2010). For example, turbidity can inhibit the UV light required for photocatalytic activation, and inorganic ions can compete with the target compounds during treatment. The water quality also fluctuates and it is crucial to identify a range of parameters for which the photocatalytic activity of the newly synthesized TiO_2 nanomaterials is not compromised. Naturally occurring hydroxyl radical scavengers such as carbonate and bicarbonate ions can also affect treatment and must be addressed appropriately prior to large-scale applications. This issue can be exacerbated when using carrier solvents in the experiments and therefore must be appropriately assessed when interpreting the results.
4. **Light source**. A drawback of using TiO_2 is that it requires UV to function. Although known as less powerful than the commercially available UV lamps, this study employed UV-LED as the light source due to its design adaptability and potential energy savings.

However, the use of visible light for photocatalytic activation has been considered an attractive option for water treatment applications. The doping of TiO_2 materials with metals or non-metals can alter their optical properties, crystallinity, and surface features that improve the responsiveness of TiO_2 to visible light (Dong et al., 2015). Material doping can be explored during the fabrication/synthesis step.

5. **Incorporating photoelectrical chemical processes.** After TiO_2 photoactivation, the electrons and the holes can recombine. Photoelectrical chemical techniques can be incorporated during the process to efficiently prevent the fast recombination of charge carriers. As a result, efficient degradation of target pollutants is very likely due to the improvement in carrier lifetimes and their increased likelihood to participate in redox reactions (Daghrir et al., 2012). The process can consequently improve the production of reactive oxygen species that can directly oxidize recalcitrant organic compounds.

In summary, this study advanced two separate areas of OMP research: (1) the assessment of their exposure via modeling and (2) the evaluation of their removal using UV/TiO_2. Further studies are essential to validate the assumptions and the model predictions (e.g.., chemical measurements of estrogens in the river). However, the model can be applied to assist with the decisions on OMP control strategies or assess new environmental conditions. Finally, this thesis contributes to a diversity of prior studies that investigated the use of UV/TiO_2 to degrade OMPs. Further studies are required to administer the use of this technology in large-scale operations effectively.

Letter of Copyright Permissions

Chapter 2

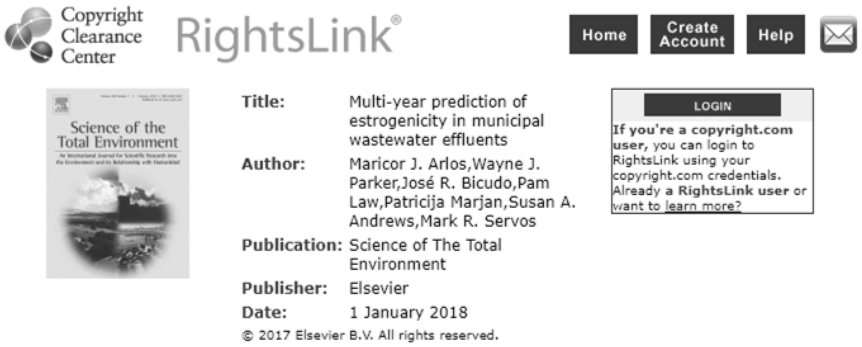

Please note that, as the author of this Elsevier article, you retain the right to include it in a thesis or dissertation, provided it is not published commercially. Permission is not required, but please ensure that you reference the journal as the original source. For more information on this and on your other retained rights, please visit: https://www.elsevier.com/about/our-business/policies/copyright#Author-rights

Chapter 4

Please note that, as the author of this Elsevier article, you retain the right to include it in a thesis or dissertation, provided it is not published commercially. Permission is not required, but please ensure that you reference the journal as the original source. For more information on this and on your other retained rights, please visit: https://www.elsevier.com/about/our-business/policies/copyright#Author-rights

Chapter 5

Chapter 6

Permission to use Table 1 of Varshney et al. 2016 (Chapter 1, Table 1.2, p. 15)

Copyright Clearance Center RightsLink®

Home | Account Info | Help

Title: Nanoscale TiO2 films and their application in remediation of organic pollutants

Author: Gaiven Varshney,Sushil R. Kanel,David M. Kempisty,Vikas Varshney,Abinash Agrawal,Endalkachew Sahle-Demessie,Rajender S. Varma,Mallikarjuna N. Nadagouda

Publication: Coordination Chemistry Reviews

Publisher: Elsevier

Date: 1 January 2016

Published by Elsevier B.V.

Logged in as:
Maricor Arlos
LOGOUT

Order Completed

Thank you for your order.

This Agreement between University of Waterloo ("You") and Elsevier ("Elsevier") consists of your license details and the terms and conditions provided by Elsevier and Copyright Clearance Center.

Your confirmation email will contain your order number for future reference.

printable details

License Number	4276431457754
License date	Jan 26, 2018
Licensed Content Publisher	Elsevier
Licensed Content Publication	Coordination Chemistry Reviews
Licensed Content Title	Nanoscale TiO2 films and their application in remediation of organic pollutants
Licensed Content Author	Gaiven Varshney,Sushil R. Kanel,David M. Kempisty,Vikas Varshney,Abinash Agrawal,Endalkachew Sahle-Demessie,Rajender S. Varma,Mallikarjuna N. Nadagouda
Licensed Content Date	Jan 1, 2016
Licensed Content Volume	306
Licensed Content Issue	n/a
Licensed Content Pages	22
Type of Use	reuse in a thesis/dissertation
Portion	figures/tables/illustrations
Number of figures/tables/illustrations	1
Format	both print and electronic
Are you the author of this Elsevier article?	No
Will you be translating?	No
Original figure numbers	Table 1
Title of your thesis/dissertation	Modeling the emission, transport, and fate of key micropollutants and their treatment using novel TiO2 nanomaterials
Expected completion date	Jan 2018
Estimated size (number of pages)	200
Requestor Location	University of Waterloo 2 Biology 2 Waterloo, ON N2L 3G1

Bibliography

Agunbiade, F.O., Moodley, B., 2016. Occurrence and distribution pattern of acidic pharmaceuticals in surface water, wastewater, and sediment of the Msunduzi River, Kwazulu-Natal, South Africa. Environmental Toxicology & Chemistry 35, 36-46.

Ahmed, M.M., Chiron, S., 2014. Solar photo-Fenton like using persulphate for carbamazepine removal from domestic wastewater. Water Research 48, 229-236.

Andersen, H., Siegrist, H., Halling-Sørensen, B., Ternes, T.A., 2003. Fate of estrogens in a municipal sewage treatment plant. Environmental Science & Technology 37, 4021-4026.

Andreozzi, R., Raffaele, M., Nicklas, P., 2003. Pharmaceuticals in STP effluents and their solar photodegradation in aquatic environment. Chemosphere 50, 1319-1330.

Ankley, G.T., Bennett, R.S., Erickson, R.J., Hoff, D.J., Hornung, M.W., Johnson, R.D., Mount, D.R., Nichols, J.W., Russom, C.L., Schmieder, P.K., 2010. Adverse outcome pathways: a conceptual framework to support ecotoxicology research and risk assessment. Environmental Toxicology & Chemistry 29, 730-741.

Anstead, G.M., Carlson, K.E., Katzenellenbogen, J.A., 1997. The estradiol pharmacophore: Ligand structure-estrogen receptor binding affinity relationships and a model for the receptor binding site. Steroids 62, 268-303.

Arlos, M.J., Bragg, L.M., Parker, W.J., Servos, M.R., 2015. Distribution of selected antiandrogens and pharmaceuticals in a highly impacted watershed. Water Research 72, 40-50.

Arlos, M.J., Bragg, L.M., Servos, M.R., Parker, W.J., 2014. Simulation of the fate of selected pharmaceuticals and personal care products in a highly impacted reach of a Canadian watershed. Science of the Total Environment 485–486, 193-204.

Arlos, M.J., Hatat-Fraile, M.M., Liang, R., Bragg, L.M., Zhou, N.Y., Andrews, S.A., Servos, M.R., 2016a. Photocatalytic decomposition of organic micropollutants using immobilized TiO_2 having different isoelectric points. Water Research 101, 351-361.

Arlos, M.J., Liang, R., Hatat-Fraile, M.M., Bragg, L.M., Zhou, N.Y., Servos, M.R., Andrews, S.A., 2016b. Photocatalytic decomposition of selected estrogens and their estrogenic activity by UV-LED irradiated TiO_2 immobilized on porous titanium sheets via thermal-chemical oxidation. Journal of Hazardous Materials 318, 541-550.

Arlos, M.J., Parker, W.J., Bicudo, J.R., Law, P., Marjan, P., Andrews, S.A., Servos, M.R., 2018. Multi-year prediction of estrogenicity in municipal wastewater effluents. Science of the Total Environment 610–611, 1103-1112.

Arnold, K.E., Boxall, A.B.A., Brown, A.R., Cuthbert, R.J., Gaw, S., Hutchinson, T.H., Jobling, S., Madden, J.C., Metcalfe, C.D., Naidoo, V., Shore, R.F., Smits, J.E., Taggart, M.A., Thompson, H.M., 2013. Assessing the exposure risk and impacts of pharmaceuticals in the environment on individuals and ecosystems. Biology Letters 9, 20130492.

Arnold, K.E., Brown, A.R., Ankley, G.T., Sumpter, J.P., 2014. Medicating the environment: assessing risks of pharmaceuticals to wildlife and ecosystems. Philosophical Transactions of the Royal Society of London, Series B: Biological Sciences 369, 20130569.

Ashauer, R., Wittmer, I., Stamm, C., Escher, B.I., 2011. Environmental risk assessment of fluctuating diazinon concentrations in an urban and agricultural catchment using toxicokinetic–toxicodynamic modeling. Environmental Science & Technology 45, 9783-9792.

ASME, 2009. Surface Texture: Surface Roughness, Waviness and Lay. American Society of Mechanical Engineers, New York, NY.
AWWA, 2014. Groundwater - Manual of Water Supply Practices, M21 (4th Edition), Fourth ed. American Water Works Association (AWWA), Denver, CO.
Bahamonde, P., Tetreault, G., McMaster, M., Servos, M., Martyniuk, C., Munkittrick, K., 2014. Molecular signatures in rainbow darter (*Etheostoma caeruleum)* inhabiting an urbanized river reach receiving wastewater effluents. Aquatic Toxicology 148, 211-220.
Bahamonde, P.A., Fuzzen, M.L., Bennett, C.J., Tetreault, G.R., McMaster, M.E., Servos, M.R., Martyniuk, C.J., Munkittrick, K.R., 2015. Whole organism responses and intersex severity in rainbow darter (*Etheostoma caeruleum*) following exposures to municipal wastewater in the Grand River basin, ON, Canada. Part A. Aquatic Toxicology 159, 290-301.
Bahnemann, D.W., Hilgendorff, M., Memming, R., 1997. Charge carrier dynamics at TiO_2 particles: Reactivity of free and trapped holes. Journal of Physical Chemistry B 101, 4265-4275.
Balaam, J.L., Grover, D., Johnson, A.C., Jürgens, M., Readman, J., Smith, A.J., White, S., Williams, R., Zhou, J.L., 2010. The use of modelling to predict levels of estrogens in a river catchment: How does modelled data compare with chemical analysis and in vitro yeast assay results? Science of the Total Environment 408, 4826-4832.
Banjac, Z., Ginebreda, A., Kuzmanovic, M., Marcé, R., Nadal, M., Riera, J.M., Barceló, D., 2015. Emission factor estimation of ca. 160 emerging organic microcontaminants by inverse modeling in a Mediterranean river basin (Llobregat, NE Spain). Science of the Total Environment 520, 241-252.
Barnthouse, L.W., 1992. The role of models in ecological risk assessment: A 1990's perspective. Environmental Toxicology and Chemistry 11, 1751-1760.
Baronti, C., Curini, R., D'Ascenzo, G., Di Corcia, A., Gentili, A., Samperi, R., 2000. Monitoring natural and synthetic estrogens at activated sludge sewage treatment plants and in a receiving river water. Environmental Science & Technology 34, 5059-5066.
Bean, T.G., Boxall, A.B.A., Lane, J., Herborn, K.A., Pietravalle, S., Arnold, K.E., 2014. Behavioural and physiological responses of birds to environmentally relevant concentrations of an antidepressant. Philosophical Transactions of the Royal Society B: Biological Sciences 369, 20130575.
Beaudet, M., Walop, W., Le Petit, C., 1997. Characteristics of women on hormone replacement therapy: The health benefits associated with hormone replacement therapy do not reflect the self-selection of healthy women with health-promoting lifestyles. Health Reports - Statistics Canada 9, 9-18.
Beck, I., Bruhn, R., Gandrass, J., 2006. Analysis of estrogenic activity in coastal surface waters of the Baltic Sea using the yeast estrogen screen. Chemosphere 63, 1870-1878.
Benotti, M.J., Stanford, B.D., Wert, E.C., Snyder, S.A., 2009. Evaluation of a photocatalytic reactor membrane pilot system for the removal of pharmaceuticals and endocrine disrupting compounds from water. Water Research 43, 1513-1522.
Benotti, M.J., Trenholm, R.A., Vanderford, B.J., Holady, J.C., Stanford, B.D., Snyder, S.A., 2008. Pharmaceuticals and endocrine disrupting compounds in U.S. drinking water. Environmental Science & Technology 43, 597-603.

Bhatkhande, D.S., Kamble, S.P., Sawant, S.B., Pangarkar, V.G., 2004. Photocatalytic and photochemical degradation of nitrobenzene using artificial ultraviolet light. Chemical Engineering Journal 102, 283-290.
Blazer, V., Iwanowicz, D., Walsh, H., Sperry, A., Iwanowicz, L., Alvarez, D., Brightbill, R., Smith, G., Foreman, W., Manning, R., 2014. Reproductive health indicators of fishes from Pennsylvania watersheds: association with chemicals of emerging concern. Environmental Monitoring and Assessment 186, 6471-6491.
Boreen, A., Arnold, W., McNeill, K., 2003. Photodegradation of pharmaceuticals in the aquatic environment: a review. Aquatic Sciences 65, 320-341.
Bound, J.P., Voulvoulis, N., 2005. Household disposal of pharmaceuticals as a pathway for aquatic contamination in the United Kingdom. Environmental Health Perspectives 113, 1705-1711.
Boxall, A.B.A., Rudd, M.A., Brooks, B.W., Caldwell, D.J., Choi, K., Hickmann, S., Innes, E., Ostapyk, K., Staveley, J.P., Verslycke, T., Ankley, G.T., Beazley, K.F., Belanger, S.E., Berninger, J.P., Carriquiriborde, P., Coors, A., DeLeo, P.C., Dyer, S.D., Ericson, J.F., Gagné, F., Giesy, J.P., Gouin, T., Hallstrom, L., Karlsson, M.V., Larsson, D.G.J., Lazorchak, J.M., Mastrocco, F., McLaughlin, A., McMaster, M.E., Meyerhoff, R.D., Moore, R., Parrott, J.L., Snape, J.R., Murray-Smith, R., Servos, M.R., Sibley, P.K., Straub, J.O., Szabo, N.D., Topp, E., Tetreault, G.R., Trudeau, V.L., Van Der Kraak, G., 2012. Pharmaceuticals and personal care products in the environment: What are the big questions? Environmental Health Perspectives 120, 1221-1229.
Brausch, J.M., Rand, G.M., 2011. A review of personal care products in the aquatic environment: Environmental concentrations and toxicity. Chemosphere 82, 1518-1532.
Brian, J.V., Harris, C.A., Scholze, M., Backhaus, T., Booy, P., Lamoree, M., Pojana, G., Jonkers, N., Runnalls, T., Bonf, xe, Angela, Marcomini, A., Sumpter, J.P., 2005. Accurate prediction of the response of freshwater fish to a mixture of estrogenic chemicals. Environmental Health Perspectives 113, 721-728.
Brodin, T., Piovano, S., Fick, J., Klaminder, J., Heynen, M., Jonsson, M., 2014. Ecological effects of pharmaceuticals in aquatic systems—impacts through behavioural alterations. Philosophical Transactions of the Royal Society B: Biological Sciences 369, 20130580.
Busch, W., Schmidt, S., Kühne, R., Schulze, T., Krauss, M., Altenburger, R., 2016. Micropollutants in European rivers: A mode of action survey to support the development of effect-based tools for water monitoring. Environmental Toxicology and Chemistry 35, 1887-1899.
Caldwell, D.J., Mastrocco, F., Anderson, P.D., Länge, R., Sumpter, J.P., 2012. Predicted-no-effect concentrations for the steroid estrogens estrone, 17β-estradiol, estriol, and 17α-ethinylestradiol. Environmental Toxicology and Chemistry 31, 1396-1406.
Cao, Q., Yu, Q., Connell, D., 2008. Degradation rate constants of steroids in sewage treatment works and receiving water. Environmental Technology 29, 1321-1330.
Cao, X., Ma, J., Shi, X., Ren, Z., 2006. Effect of TiO_2 nanoparticle size on the performance of PVDF membrane. Applied Surface Science 253, 2003-2010.
Carballa, M., Omil, F., Lema, J.M., Llompart, M.a., García-Jares, C., Rodríguez, I., Gómez, M., Ternes, T., 2004. Behavior of pharmaceuticals, cosmetics and hormones in a sewage treatment plant. Water Research 38, 2918-2926.
Čelić, M., Insa, S., Škrbić, B., Petrović, M., 2017. Development of a sensitive and robust online dual column liquid chromatography-tandem mass spectrometry method for the analysis

of natural and synthetic estrogens and their conjugates in river water and wastewater. Analytical and Bioanalytical Chemistry 409, 5427-5440.
Chapra, S.C., 1997. Surface water quality modeling. McGraw-Hill, New York, NY.
Charanpahari, A., Umare, S.S., Gokhale, S.P., Sudarsan, V., Sreedhar, B., Sasikala, R., 2012. Enhanced photocatalytic activity of multi-doped TiO_2 for the degradation of methyl orange. Applied Catalysis A: General 443, 96-102.
Chong, M.N., Jin, B., Chow, C.W., Saint, C., 2010. Recent developments in photocatalytic water treatment technology: a review. Water Research 44, 2997-3027.
Chow, V.T., 1959. Open channel hydraulics. McGraw-Hill, New York, NY.
Christensen, F., 1998. Pharmaceuticals in the environment—a human risk? Regulatory Toxicology and Pharmacology 28, 212-221.
Clara, M., Kreuzinger, N., Strenn, B., Gans, O., Kroiss, H., 2005. The solids retention time—a suitable design parameter to evaluate the capacity of wastewater treatment plants to remove micropollutants. Water Research 39, 97-106.
Clemente, Z., Castro, V., Jonsson, C., Fraceto, L., 2011. Ecotoxicology of nano-TiO_2–an evaluation of its toxicity to organisms of aquatic ecosystems. International Journal of Environmental Research 6, 33-50.
Cleuvers, M., 2004. Mixture toxicity of the anti-inflammatory drugs diclofenac, ibuprofen, naproxen, and acetylsalicylic acid. Ecotoxicology & Environmental Safety 59, 309-315.
Coleman, H.M., Abdullah, M.I., Eggins, B.R., Palmer, F.L., 2005. Photocatalytic degradation of 17β-oestradiol, oestriol and 17α-ethynyloestradiol in water monitored using fluorescence spectroscopy. Applied Catalysis B: Environmental 55, 23-30.
Coleman, H.M., Routledge, E.J., Sumpter, J.P., Eggins, B.R., Byrne, J.A., 2004. Rapid loss of estrogenicity of steroid estrogens by UVA photolysis and photocatalysis over an immobilised titanium dioxide catalyst. Water Research 38, 3233-3240.
Colina-Márquez, J., Machuca-Martínez, F., Li Puma, G., 2015. Modeling the photocatalytic mineralization in water of commercial formulation of estrogens 17-β estradiol (E2) and nomegestrol acetate in contraceptive pills in a solar powered compound parabolic collector. Molecules 20, 13354-13373.
Corcoran, J., Winter, M.J., Tyler, C.R., 2010. Pharmaceuticals in the aquatic environment: a critical review of the evidence for health effects in fish. Critical Reviews in Toxicology 40, 287-304.
Cornell, R.M., Posner, A.M., Quirk, J.P., 1975. A titrimetric and electrophoretic investigation of the pzc and the iep of pigment rutile. Journal of Colloid & Interface Science 53, 6-13.
D'Ascenzo, G., Di Corcia, A., Gentili, A., Mancini, R., Mastropasqua, R., Nazzari, M., Samperi, R., 2003. Fate of natural estrogen conjugates in municipal sewage transport and treatment facilities. Science of the Total Environment 302, 199-209.
Daghrir, R., Drogui, P., Robert, D., 2012. Photoelectrocatalytic technologies for environmental applications. Journal of Photochemistry and Photobiology A: Chemistry 238, 41-52.
Dale, A.L., Casman, E.A., Lowry, G.V., Lead, J.R., Viparelli, E., Baalousha, M., 2015. Modeling nanomaterial environmental fate in aquatic systems. Environmental Science & Technology 49, 2587-2593.
Damodar, R.A., You, S.-J., Chou, H.-H., 2009. Study the self cleaning, antibacterial and photocatalytic properties of TiO_2 entrapped PVDF membranes. Journal of Hazardous Materials 172, 1321-1328.

Dang, Z., 2010. Comparison of relative binding affinities to fish and mammalian estrogen receptors: The regulatory implications. Toxicology Letters 192, 298-315.
Daughton, C.G., Ternes, T.A., 1999. Pharmaceuticals and personal care products in the environment: agents of subtle change? Environmental Health Perspectives 107, 907-938.
de Witte, B., van Langenhove, H., Demeestere, K., Dewulf, J., 2011. Advanced oxidation of pharmaceuticals: Chemical analysis and biological assessment of degradation products. Critical Reviews in Environmental Science &Technology 41, 215-242.
Desbrow, C., Routledge, E.J., Brighty, G.C., Sumpter, J.P., Waldock, M., 1998. Identification of Estrogenic Chemicals in STW Effluent. 1. Chemical Fractionation and in Vitro Biological Screening. Environmental Science & Technology 32, 1549-1558.
Doll, T.E., Frimmel, F.H., 2004. Kinetic study of photocatalytic degradation of carbamazepine, clofibric acid, iomeprol and iopromide assisted by different TiO_2 materials—determination of intermediates and reaction pathways. Water Research 38, 955-964.
Doll, T.E., Frimmel, F.H., 2005. Photocatalytic degradation of carbamazepine, clofibric acid and iomeprol with P25 and Hombikat UV100 in the presence of natural organic matter (NOM) and other organic water constituents. Water Research 39, 403-411.
Dong, S., Feng, J., Fan, M., Pi, Y., Hu, L., Han, X., Liu, M., Sun, J., Sun, J., 2015. Recent developments in heterogeneous photocatalytic water treatment using visible light-responsive photocatalysts: a review. RSC Advances 5, 14610-14630.
Donigian, A., 2002. Watershed model calibration and validation: The HSPF experience. Proceedings of the Water Environment Federation 2002, 44-73.
Dotan, P., Tal, A., Arnon, S., 2017. A simple model for estimating the concentrations of natural estrogens in raw wastewater. Science of the Total Environment 575, 588-594.
Eggen, R.I.L., Hollender, J., Joss, A., Schärer, M., Stamm, C., 2014. Reducing the discharge of micropollutants in the aquatic environment: The benefits of upgrading wastewater treatment plants. Environmental Science & Technology 48, 7683-7689.
Elmolla, E.S., Chaudhuri, M., 2010. Photocatalytic degradation of amoxicillin, ampicillin and cloxacillin antibiotics in aqueous solution using UV/TiO_2 and $UV/H_2O_2/TiO_2$ photocatalysis. Desalination 252, 46-52.
Escher, B., Leusch, F., 2012. Bioanalytical tools in water quality assessment. IWA publishing, London, UK.
Escher, B.I., Allinson, M., Altenburger, R., Bain, P.A., Balaguer, P., Busch, W., Crago, J., Denslow, N.D., Dopp, E., Hilscherova, K., 2013. Benchmarking organic micropollutants in wastewater, recycled water and drinking water with in vitro bioassays. Environmental Science & Technology 48, 1940-1956.
Escher, B.I., Neale, P.A., Leusch, F.D., 2015. Effect-based trigger values for in vitro bioassays: Reading across from existing water quality guideline values. Water Research 81, 137-148.
European Commission, 2012. Proposal for a directive of the European Parliament and of the council amending Directives 2000/60/EC and 2008/105/EC as regards priority substances in the field of water policy (COM(2011) 876). European Commission, Brussels.
Evonik, 2015. AEROXIDE®, AERODISP® and AEROPERL®Titanium Dioxide as Photocatalyst: Technical Information 1243. Evonik Industries, Parsipanny, NJ.
Fernandez, M.P., Buchanan, I.D., Ikonomou, M.G., 2008. Seasonal variability of the reduction in estrogenic activity at a municipal WWTP. Water Research 42, 3075-3081.

Fernandez, M.P., Ikonomou, M.G., Buchanan, I., 2007. An assessment of estrogenic organic contaminants in Canadian wastewaters. Science of the Total Environment 373, 250-269.
Fernández, R.L., McDonald, J.A., Khan, S.J., Le-Clech, P., 2014. Removal of pharmaceuticals and endocrine disrupting chemicals by a submerged membrane photocatalysis reactor (mpr). Separation and Purification Technology 127, 131-139.
Fleming, M., Achari, G., Hassan, Q.K., Ng, C.A., 2016. Modeling the loading and fate of estrogens in wastewater treatment plants. Cogent Environmental Science 2, 1-15.
Friedmann, D., Mendive, C., Bahnemann, D., 2010. TiO_2 for water treatment: Parameters affecting the kinetics and mechanisms of photocatalysis. Applied Catalysis B: Environmental 99, 398-406.
Frontistis, Z., Daskalaki, V.M., Hapeshi, E., Drosou, C., Fatta-Kassinos, D., Xekoukoulotakis, N.P., Mantzavinos, D., 2012. Photocatalytic (UV-A/TiO_2) degradation of 17α-ethynylestradiol in environmental matrices: Experimental studies and artificial neural network modeling. Journal of Photochemistry and Photobiology A: Chemistry 240, 33-41.
Fujishima, A., Honda, K., 1972. Electrochemical photolysis of water at a semiconductor electrode. Nature 238, 37-38.
Fuzzen, M., 2016. Does intersex matter? A case study of rainbow darter in the Grand River, Department of Biology. University of Waterloo, Waterloo, ON.
Fuzzen, M.L.M., Bennett, C.J., Tetreault, G.R., McMaster, M.E., Servos, M.R., 2015. Severe intersex is predictive of poor fertilization success in populations of rainbow darter (*Etheostoma caeruleum*). Aquatic Toxicology 160, 106-116.
Fuzzen, M.L.M., Bragg, L.M., Tetreault, G.R., Bahamonde, P.A., Tanna, R.N., Bennett, C.J., McMaster, M.E., Servos, M.R., 2016. An assessment of the spatial and temporal variability of biological responses to municipal wastewater effluent in rainbow darter (*Etheostoma caeruleum*) collected along an urban gradient. PLOS ONE 11, e0164879.
Gaido, K.W., Leonard, L.S., Lovell, S., Gould, J.C., Babaï, D., Portier, C.J., McDonnell, D.P., 1997. Evaluation of chemicals with endocrine modulating activity in a yeast-based steroid hormone receptor gene transcription assay. Toxicology & Applied Pharmacology 143, 205-212.
Gaworecki, K.M., Klaine, S.J., 2008. Behavioral and biochemical responses of hybrid striped bass during and after fluoxetine exposure. Aquatic Toxicology 88, 207-213.
Giri, R., Ozaki, H., Ota, S., Takanami, R., Taniguchi, S., 2010. Degradation of common pharmaceuticals and personal care products in mixed solutions by advanced oxidation techniques. International Journal of Environmental Science & Technology 7, 251-260.
Göpel, W., Anderson, J., Frankel, D., Jaehnig, M., Phillips, K., Schäfer, J., Rocker, G., 1984. Surface defects of TiO_2 (110): a combined XPS, XAES and ELS study. Surface Science 139, 333-346.
Grechi, L., Franco, A., Palmeri, L., Pivato, A., Barausse, A., 2016. An ecosystem model of the lower Po river for use in ecological risk assessment of xenobiotics. Ecological Modelling 332, 42-58.
Grill, G., Khan, U., Lehner, B., Nicell, J., Ariwi, J., 2016. Risk assessment of down-the-drain chemicals at large spatial scales: Model development and application to contaminants originating from urban areas in the Saint Lawrence River Basin. Science of the Total Environment 541, 825-838.

Hamilton, P.B., Nicol, E., De-Bastos, E.S., Williams, R.J., Sumpter, J.P., Jobling, S., Stevens, J.R., Tyler, C.R., 2014. Populations of a cyprinid fish are self-sustaining despite widespread feminization of males. BMC Biology 12, 1-13.

Hashimoto, K., Irie, H., Fujishima, A., 2005. TiO_2 photocatalysis: a historical overview and future prospects. Japanese journal of applied physics 44, 8269-8285.

Hatat-Fraile, M., Mendret, J., Rivallin, M., Brosillon, S., 2013. Effect of hydrodynamics during sol–gel synthesis of TiO_2 nanoparticles: From morphology to photocatalytic properties. Chemical Engineering Research & Design 91, 2389-2400.

Hatat-Fraile, M.M., 2013. Etude des méthodes d'élaboration et de la mise en oeuvre de photocatalyseurs pour le traitement de la micro pollution bio-réfractaire dans l'eau. Université de Montpellier, Montpellier, France.

Hicks, K., 2017. Response of wild fish to municipal wastewater treatment plant upgrades, Department of Biology. University of Waterloo, Waterloo, ON.

Hicks, K., Servos, M., 2017. Site fidelity and movement of a small-bodied fish species, the rainbow darter (*Etheostoma caeruleum*): Implications for environmental effects assessment. River Research and Applications 33, 1016-1025.

Hicks, K.A., Fuzzen, M.L.M., McCann, E.K., Arlos, M.J., Bragg, L.M., Kleywegt, S., Tetreault, G.R., McMaster, M.E., Servos, M.R., 2017. Reduction of intersex in a wild fish population in response to major municipal wastewater treatment plant upgrades. Environmental Science & Technology 51, 1811-1819.

Hinck, J.E., Blazer, V.S., Schmitt, C.J., Papoulias, D.M., Tillitt, D.E., 2009. Widespread occurrence of intersex in black basses (*Micropterus spp.*) from US rivers, 1995–2004. Aquatic Toxicology 95, 60-70.

Hosseini, N.A.A., Parker, W.J.J., Matott, L.S.L., 2012. Modelling concentrations of pharmaceuticals and personal care products in a Canadian watershed. Canadian Water Resources Journal 37, 191-208.

Houtman, C.J., Kroesbergen, J., Lekkerkerker-Teunissen, K., van der Hoek, J.P., 2014. Human health risk assessment of the mixture of pharmaceuticals in Dutch drinking water and its sources based on frequent monitoring data. Science of the Total Environment 496, 54-62.

Hu, A., Zhang, X., Luong, D., Oakes, K., Servos, M., Liang, R., Kurdi, S., Peng, P., Zhou, Y., 2012. Adsorption and photocatalytic degradation kinetics of pharmaceuticals by TiO_2 nanowires during water treatment. Waste and Biomass Valorization 3, 443-449.

Hu, A., Zhang, X., Oakes, K.D., Peng, P., Zhou, Y.N., Servos, M.R., 2011. Hydrothermal growth of free standing TiO2 nanowire membranes for photocatalytic degradation of pharmaceuticals. Journal of Hazardous Materials 189, 278-285.

Huerta-Fontela, M., Galceran, M.T., Ventura, F., 2011. Occurrence and removal of pharmaceuticals and hormones through drinking water treatment. Water Research 45, 1432-1442.

Huggett, D., Benson, W., Chipman, K., Cook, J., Gray, L., Kinter, L., Meyerhoff, R., Trudeau, V., 2005. Role of mammalian data in determining pharmaceutical responses in aquatic species. SETAC Press: Pensacola, FL.

Huggett, D.B., Foran, C.M., Brooks, B.W., Weston, J., Peterson, B., Marsh, K.E., La Point, T.W., Schlenk, D., 2003. Comparison of in vitro and in vivo bioassays for estrogenicity in effluent from North American municipal wastewater facilities. Toxicological Sciences 72, 77-83.

Hurum, D.C., Agrios, A.G., Gray, K.A., Rajh, T., Thurnauer, M.C., 2003. Explaining the enhanced photocatalytic activity of Degussa P25 mixed-phase TiO_2 using EPR. Journal of Physical Chemistry B 107, 4545-4549.

Iglesias, O., Rivero, M.J., Urtiaga, A.M., Ortiz, I., 2016. Membrane-based photocatalytic systems for process intensification. Chemical Engineering Journal 305, 136-148.

Ings, J.S., Servos, M.R., Vijayan, M.M., 2011. Exposure to municipal wastewater effluent impacts stress performance in rainbow trout. Aquatic Toxicology 103, 85-91.

Ings, J.S., Vijayan, M.M., Servos, M.R., 2012. Tissue-specific metabolic changes in response to an acute handling disturbance in juvenile rainbow trout exposed to municipal wastewater effluent. Aquatic Toxicology 108, 53-59.

Inumaru, K., Murashima, M., Kasahara, T., Yamanaka, S., 2004. Enhanced photocatalytic decomposition of 4-nonylphenol by surface-organografted TiO_2: A combination of molecular selective adsorption and photocatalysis. Applied Catalysis B: Environmental 52, 275-280.

Ishibashi, K.-I., Fujishima, A., Watanabe, T., Hashimoto, K., 2000. Detection of active oxidative species in TiO_2 photocatalysis using the fluorescence technique. Electrochemistry Communications 2, 207-210.

Jager, T., 2016. Predicting environmental risk: A road map for the future. Journal of Toxicology and Environmental Health, Part A 79, 572-584.

Jarošová, B., Bláha, L., Giesy, J.P., Hilscherová, K., 2014. What level of estrogenic activity determined by in vitro assays in municipal waste waters can be considered as safe? Environment International 64, 98-109.

Jenks, W.S., 2013. Photocatalytic reaction pathways–effects of molecular structure, catalyst, and wavelength, in: Pichat, P. (Ed.), Photocatalysis and water purification: From fundamentals to recent applications. Wiley-VCH, Weinham, Germany, pp. 25-51.

Jeong, T.-Y., Kim, H.Y., Kim, S.D., 2015. Multi-generational effects of propranolol on Daphnia magna at different environmental concentrations. Environmental Pollution 206, 188-194.

Jin, S., Yang, F., Liao, T., Hui, Y., Xu, Y., 2008. Seasonal variations of estrogenic compounds and their estrogenicities in influent and effluent from a municipal sewage treatment plant in China. Environmental Toxicology & Chemistry 27, 146-153.

Jobling, S., Burn, R.W., Thorpe, K., Williams, R., Tyler, C., 2009. Statistical modeling suggests that antiandrogens in effluents from wastewater treatment works contribute to widespread sexual disruption in fish living in English rivers. Environmental Health Perspectives 117, 797-802.

Jobling, S., Nolan, M., Tyler, C.R., Brighty, G., Sumpter, J.P., 1998. Widespread sexual disruption in wild fish. Environmental Science & Technology 32, 2498-2506.

Jobling, S., Williams, R., Johnson, A., Taylor, A., Gross-Sorokin, M., Nolan, M., Tyler, C.R., van Aerle, R., Santos, E., Brighty, G., 2006. Predicted exposures to steroid estrogens in UK rivers correlate with widespread sexual disruption in wild fish populations. Environmental Health Perspectives 114, 32-39.

Johnson, A.C., Chen, Y., 2017. Does exposure to domestic wastewater effluent (including steroid estrogens) harm fish populations in the UK? Science of the Total Environment 589, 89-96.

Johnson, A.C., Sumpter, J.P., 2001. Removal of endocrine-disrupting chemicals in activated sludge treatment works. Environmental Science & Technology 35, 4697-4703.

Johnson, A.C., Sumpter, J.P., 2016. Are we going about chemical risk assessment for the aquatic environment the wrong way? Environmental Toxicology and Chemistry 35, 1609-1616.
Johnson, A.C., Williams, R.J., 2004. A model to estimate influent and effluent concentrations of estradiol, estrone, and ethinylestradiol at sewage treatment works. Environmental Science & Technology 38, 3649-3658.
Jones, O.A., Lester, J.N., Voulvoulis, N., 2005. Pharmaceuticals: a threat to drinking water? Trends in Biotechnology 23, 163-167.
Jordan, S.J., Benson, W.H., Foran, C.M., Bennett, E.R., Snyder, E.M., 2016. Endocrine-disrupting compounds in aquatic ecosystems, Endocrine Toxicology. Informa Healthcare USA, Inc., New York, NY, pp. 324-351.
Júnior, J.A.A., Baldo, J.B., 2014. The behavior of zeta potential of silica suspensions. New Journal of Glass and Ceramics 4, 29-37.
Jurgens, M., Williams, R., Johnson, A., 1999. Fate and behaviour of steroid oestrogens in rivers: a scoping study. UK Environment Agency R&D Dissemination Cenre, Swindon, Wilts, pp. 1-74.
Jürgens, M.D., Holthaus, K.I., Johnson, A.C., Smith, J.J., Hetheridge, M., Williams, R.J., 2002. The potential for estradiol and ethinylestradiol degradation in English rivers. Environmental Toxicology & Chemistry 21, 480-488.
Kanakaraju, D., Glass, B., Oelgemöller, M., 2014. Titanium dioxide photocatalysis for pharmaceutical wastewater treatment. Environmental Chemistry Letters 12, 27-47.
Kasprzyk-Hordern, B., Dinsdale, R.M., Guwy, A.J., 2009. The removal of pharmaceuticals, personal care products, endocrine disruptors and illicit drugs during wastewater treatment and its impact on the quality of receiving waters. Water Research 43, 363-380.
Kebarle, P., Tang, L., 1993. From ions in solution to ions in the gas phase - the mechanism of electrospray mass spectrometry. Analytical Chemistry 65, 972A-986A.
Kehrein, N., Berlekamp, J., Klasmeier, J., 2015. Modeling the fate of down-the-drain chemicals in whole watersheds: New version of the GREAT-ER software. Environmental Modelling & Software 64, 1-8.
Khataee, A.R., Kasiri, M.B., 2010. Photocatalytic degradation of organic dyes in the presence of nanostructured titanium dioxide: Influence of the chemical structure of dyes. Journal of Molecular Catalysis A: Chemical 328, 8-26.
Kidd, K.A., Blanchfield, P.J., Mills, K.H., Palace, V.P., Evans, R.E., Lazorchak, J.M., Flick, R.W., 2007. Collapse of a fish population after exposure to a synthetic estrogen. Proceedings of the National Academy of Sciences 104, 8897-8901.
Kime, D.E., 1999. Environmentally induced endocrine abnormalities in fish, in: Hester, R.E., Harrison, R.M. (Eds.), Endocrine Disrupting Chemicals. The Royal Society of Chemistry, pp. 27-48.
Klavarioti, M., Mantzavinos, D., Kassinos, D., 2009. Removal of residual pharmaceuticals from aqueous systems by advanced oxidation processes. Environment International 35, 402-417.
Kleywegt, S., Pileggi, V., Yang, P., Hao, C., Zhao, X., Rocks, C., Thach, S., Cheung, P., Whitehead, B., 2011. Pharmaceuticals, hormones and bisphenol A in untreated source and finished drinking water in Ontario, Canada—Occurrence and treatment efficiency. Science of the Total Environment 409, 1481-1488.
Klopman, G., Chakravarti, S.K., 2003. Structure–activity relationship study of a diverse set of estrogen receptor ligands (I) using MultiCASE expert system. Chemosphere 51, 445-459.

Konstantinou, I.K., Albanis, T.A., 2004. TiO_2-assisted photocatalytic degradation of azo dyes in aqueous solution: kinetic and mechanistic investigations: A review. Applied Catalysis B: Environmental 49, 1-14.

Kralchevska, R., Milanova, M., Bistan, M., Pintar, A., Todorovsky, D., 2012. The photocatalytic degradation of 17α-ethynylestradiol by pure and carbon nanotubes modified TiO_2 under UVC illumination. Central European Journal of Chemistry 10, 1137-1148.

Kumar, A., Chang, B., Xagoraraki, I., 2010. Human health risk assessment of pharmaceuticals in water: issues and challenges ahead. International Journal of Environmental Research & Public Health 7, 3929-3953.

Kumar, A., Kumar, S., Kumar, S., 2003. Adsorption of resorcinol and catechol on granular activated carbon: Equilibrium and kinetics. Carbon 41, 3015-3025.

Kumar, V., Johnson, A.C., Nakada, N., Yamashita, N., Tanaka, H., 2012. De-conjugation behavior of conjugated estrogens in the raw sewage, activated sludge and river water. Journal of Hazardous Materials 227, 49-54.

Kümmerer, K., 2008. Pharmaceuticals in the environment: sources, fate, effects and risks. Springer, Berlin.

Kurrat, R., Wälivaara, B., Marti, A., Textor, M., Tengvall, P., Ramsden, J., Spencer, N., 1998. Plasma protein adsorption on titanium: comparative in situ studies using optical waveguide lightmode spectroscopy and ellipsometry. Colloids and Surfaces B: Biointerfaces 11, 187-201.

Kwak, S.-Y., Jung, S.G., Kim, S.H., 2001a. Structure-motion-performance relationship of flux-enhanced reverse osmosis (RO) membranes composed of aromatic polyamide thin films. Environmental Science & Technology 35, 4334-4340.

Kwak, S.-Y., Kim, S.H., Kim, S.S., 2001b. Hybrid organic/inorganic reverse osmosis (RO) membrane for bactericidal anti-fouling. 1. Preparation and characterization of TiO_2 nanoparticle self-assembled aromatic polyamide thin-film-composite (TFC) membrane. Environmental Science & Technology 35, 2388-2394.

Lange, A., Paull, G.C., Coe, T.S., Katsu, Y., Urushitani, H., Iguchi, T., Tyler, C.R., 2009. Sexual reprogramming and estrogenic sensitization in wild fish exposed to ethinylestradiol. Environmental Science & Technology 43, 1219-1225.

Leblebici, M.E., Stefanidis, G.D., Van Gerven, T., 2015. Comparison of photocatalytic space-time yields of 12 reactor designs for wastewater treatment. Chemical Engineering & Processing: Process Intensification 97, 106-111.

Leong, S., Razmjou, A., Wang, K., Hapgood, K., Zhang, X., Wang, H., 2014. TiO_2 based photocatalytic membranes: A review. Journal of Membrane Science 472, 167-184.

Leopold, L.B., Maddock, T., 1953. The hydraulic geometry of stream channels and some physiographic implications. US Department of Interior: Geological Survey, Washington, DC.

Li Puma, G., Puddu, V., Tsang, H.K., Gora, A., Toepfer, B., 2010. Photocatalytic oxidation of multicomponent mixtures of estrogens (estrone (E1), 17β-estradiol (E2), 17α-ethynylestradiol (EE2) and estriol (E3)) under UVA and UVC radiation: Photon absorption, quantum yields and rate constants independent of photon absorption. Applied Catalysis B: Environmental 99, 388-397.

Lin, A.Y., Reinhard, M., 2005. Photodegradation of common environmental pharmaceuticals and estrogens in river water. Environmental Toxicology & Chemistry 24, 1303-1309.

Linsebigler, A.L., Lu, G., Yates, J.T., 1995. Photocatalysis on TiO_2 surfaces: Principles, mechanisms, and selected results. Chemical Reviews 95, 735-758.
Liu, Z.-h., Kanjo, Y., Mizutani, S., 2009. Removal mechanisms for endocrine disrupting compounds (EDCs) in wastewater treatment—physical means, biodegradation, and chemical advanced oxidation: a review. Science of the Total Environment 407, 731-748.
Loomer, H., Cooke, S., 2011. Water quality in the Grand River watershed: current conditions & trends (2003–2008). Grand River Conservation Authority, Cambridge, ON.
López-Roldán, R., de Alda, M.L., Gros, M., Petrovic, M., Martín-Alonso, J., Barceló, D., 2010. Advanced monitoring of pharmaceuticals and estrogens in the Llobregat River basin (Spain) by liquid chromatography–triple quadrupole-tandem mass spectrometry in combination with ultra performance liquid chromatography–time of flight-mass spectrometry. Chemosphere 80, 1337-1344.
Lu, M., Pichat, P., 2013. Photocatalysis and water purification: From fundamentals to recent applications. John Wiley & Sons, Weinham, Germany.
Luo, Y., Guo, W., Ngo, H.H., Nghiem, L.D., Hai, F.I., Zhang, J., Liang, S., Wang, X.C., 2014. A review on the occurrence of micropollutants in the aquatic environment and their fate and removal during wastewater treatment. Science of the Total Environment 473–474, 619-641.
Luttrell, T., Halpegamage, S., Tao, J., Kramer, A., Sutter, E., Batzill, M., 2014. Why is anatase a better photocatalyst than rutile?-Model studies on epitaxial TiO_2 films. Scientific Reports 4, 1-8.
Ma, L., Yates, S.R., Ashworth, D., 2016. Parent and conjugated estrogens and progestagens in surface water of the Santa Ana River: Determination, occurrence, and risk assessment. Environmental Toxicology & Chemistry 35, 2657-2664.
Mai, J., Sun, W., Xiong, L., Liu, Y., Ni, J., 2008. Titanium dioxide mediated photocatalytic degradation of 17β-estradiol in aqueous solution. Chemosphere 73, 600-606.
Mandaric, L., Celic, M., Marcé, R., Petrovic, M., 2016. Introduction on emerging contaminants in rivers and their environmental risk, Emerging Contaminants in River Ecosystems. Springer International Publishing, Switzerland, pp. 3-25.
Marinho, B.A., de Liz, M.V., Lopes Tiburtius, E.R., Nagata, N., Peralta-Zamora, P., 2013. TiO_2 and ZnO mediated photocatalytic degradation of E2 and EE2 estrogens. Photochemical & Photobiological Sciences 12, 678-683.
Marjan, P., Bragg, L.M., MacLatchy, D.L., Servos, M.R., Martyniuk, C.J., 2017a. How does reference site selection influence interpretation of omics data?: Evaluating liver transcriptome responses in male rainbow darter (*Etheostoma caeruleum*) across an urban environment. Environmental Science & Technology 51, 6470-6479.
Marjan, P., Martyniuk, C.J., Fuzzen, M.L.M., MacLatchy, D.L., McMaster, M.E., Servos, M.R., 2017b. Returning to normal? Assessing transcriptome recovery over time in male rainbow darter (*Etheostoma caeruleum*) liver in response to wastewater treatment plant upgrades. Environmental Toxicology & Chemistry 36, 2108-2122.
Marjan, P., Van Der Kraak, G.J., MacLatchy, D.L., Fuzzen, M.L., Bragg, L.M., McMaster, M.E., Tetreault, G.R., Servos, M.R., 2017c. Assessing recovery of in vitro steroid production in male rainbow darter (*Etheostoma caeruleum*) in response to municipal wastewater treatment plant infrastructure changes. Environmental Toxicology & Chemistry.

Matthiessen, P., Arnold, D., Johnson, A., Pepper, T., Pottinger, T., Pulman, K., 2006. Contamination of headwater streams in the United Kingdom by oestrogenic hormones from livestock farms. Science of the Total Environment 367, 616-630.
McCann, E.K., 2016. Evaluating contaminants of emerging concern in municipal wastewater effluents, Department of Biology. University of Waterloo, Waterloo, ON.
Mehrvar, M., Anderson, W.A., Moo-Young, M., 2001. Photocatalytic degradation of aqueous organic solvents in the presence of hydroxyl radical scavengers. International Journal of Photoenergy 3, 187-191.
Mendret, J., Hatat-Fraile, M., Rivallin, M., Brosillon, S., 2013. Hydrophilic composite membranes for simultaneous separation and photocatalytic degradation of organic pollutants. Separation & Purification Technology 111, 9-19.
Metcalfe, C.D., Chu, S., Judt, C., Li, H., Oakes, K.D., Servos, M.R., Andrews, D.M., 2010. Antidepressants and their metabolites in municipal wastewater, and downstream exposure in an urban watershed. Environmental Toxicology & Chemistry 29, 79-89.
Metz, F., Ingold, K., 2014. Sustainable wastewater management: is it possible to regulate micropollution in the future by learning from the past? A policy analysis. Sustainability 6, 1992-2012.
Miranda-García, N., Maldonado, M.I., Coronado, J.M., Malato, S., 2010. Degradation study of 15 emerging contaminants at low concentration by immobilized TiO_2 in a pilot plant. Catalysis Today 151, 107-113.
Miranda-García, N., Suárez, S., Maldonado, M.I., Malato, S., Sánchez, B., 2014. Regeneration approaches for TiO_2 immobilized photocatalyst used in the elimination of emerging contaminants in water. Catalysis Today 230, 27-34.
Miranda-García, N., Suárez, S., Sánchez, B., Coronado, J.M., Malato, S., Maldonado, M.I., 2011. Photocatalytic degradation of emerging contaminants in municipal wastewater treatment plant effluents using immobilized TiO_2 in a solar pilot plant. Applied Catalysis B: Environmental 103, 294-301.
Mitamura, K., Narukawa, H., Mizuguchi, T., Shimada, K., 2004. Degradation of estrogen conjugates using titanium dioxide as a photocatalyst. Analytical Sciences 20, 3-4.
Mohagheghian, A., Nabizadeh, R., Mesdghinia, A., Rastkari, N., Mahvi, A.H., Alimohammadi, M., Yunesian, M., Ahmadkhaniha, R., Nazmara, S., 2014. Distribution of estrogenic steroids in municipal wastewater treatment plants in Tehran, Iran. Journal of Environmental Health Science & Engineering 12, 97-105.
Molinari, R., Lavorato, C., Argurio, P., 2015. Photocatalytic reduction of acetophenone in membrane reactors under UV and visible light using TiO_2 and Pd/TiO_2 catalysts. Chemical Engineering Journal 274, 307-316.
Moriasi, D.N., Arnold, J.G., Van Liew, M.W., Bingner, R.L., Harmel, R.D., Veith, T.L., 2007. Model evaluation guidelines for systematic quantification of accuracy in watershed simulations. Transactions of the American Society of Agricultural & Biological Engineers 50, 885-900.
Moriasi, D.N., Gitau, M.W., Pai, N., Daggupati, P., 2015. Hydrologic and water quality models: Performance measures and evaluation criteria. Transactions of the American Society of Agricultural & Biological Engineers 58, 1763-1785.
Mozia, S., 2010. Photocatalytic membrane reactors (PMRs) in water and wastewater treatment. A review. Separation & Purification Technology 73, 71-91.

Muller, M., Rabenoelina, F., Balaguer, P., Patureau, D., Lemenach, K., Budzinski, H., Barceló, D., López de Alda, M., Kuster, M., Delgenès, J.P., 2008. Chemical and biological analysis of endocrine-disrupting hormones and estrogenic activity in an advanced sewage treatment plant. Environmental Toxicology & Chemistry 27, 1649-1658.

Muradov, N.Z., Ali, T., Muzzey, D., Painter, C.R., Kemme, M.R., 1996. Selective photocatalytic destruction of airborne VOCs. Solar Energy 56, 445-453.

Muruganandham, M., Suri, R., Jafari, S., Sillanpää, M., Lee, G.-J., Wu, J., Swaminathan, M., 2014. Recent developments in homogeneous advanced oxidation processes for water and wastewater treatment. International Journal of Photoenergy 2014, 1-21.

Naddeo, V., Rizzo, L., Belgiorno, V., 2010. Water, wastewater and soil treatment by advanced oxidation processes. Università degli Studi di Salerno - Sanitary Environmental Engineering Division, Fisciano, Italy.

Nakashima, T., Ohko, Y., Kubota, Y., Fujishima, A., 2003. Photocatalytic decomposition of estrogens in aquatic environment by reciprocating immersion of TiO_2-modified polytetrafluoroethylene mesh sheets. Journal of Photochemistry and Photobiology A: Chemistry 160, 115-120.

Nash, J.P., Kime, D.E., Van der Ven, L.T., Wester, P.W., Brion, F., Maack, G., Stahlschmidt-Allner, P., Tyler, C.R., 2004. Long-term exposure to environmental concentrations of the pharmaceutical ethynylestradiol causes reproductive failure in fish. Environmental Health Perspectives 112, 1725.

Nasuhoglu, D., Berk, D., Yargeau, V., 2012. Photocatalytic removal of 17α-ethinylestradiol (EE2) and levonorgestrel (LNG) from contraceptive pill manufacturing plant wastewater under UVC radiation. Chemical Engineering Journal 185–186, 52-60.

Natarajan, T.S., Natarajan, K., Bajaj, H.C., Tayade, R.J., 2011. Energy efficient UV-LED source and TiO2 nanotube array-based reactor for photocatalytic application. Industrial & Engineering Chemistry Research 50, 7753-7762.

Neale, P.A., Altenburger, R., Aït-Aïssa, S., Brion, F., Busch, W., de Aragão Umbuzeiro, G., Denison, M.S., Du Pasquier, D., Hilscherová, K., Hollert, H., 2017a. Development of a bioanalytical test battery for water quality monitoring: Fingerprinting identified micropollutants and their contribution to effects in surface water. Water Research 123, 734-750.

Neale, P.A., Munz, N.A., Aït-Aïssa, S., Altenburger, R., Brion, F., Busch, W., Escher, B.I., Hilscherová, K., Kienle, C., Novák, J., Seiler, T.-B., Shao, Y., Stamm, C., Hollender, J., 2017b. Integrating chemical analysis and bioanalysis to evaluate the contribution of wastewater effluent on the micropollutant burden in small streams. Science of the Total Environment 576, 785-795.

Nikolaou, A., Meric, S., Fatta, D., 2007. Occurrence patterns of pharmaceuticals in water and wastewater environments. Analytical & Bioanalytical Chemistry 387, 1225-1234.

Nosaka, Y., Nosaka, A.Y., 2013. Identification and roles of the active species generated on various photocatalysts, in: Pichat, P. (Ed.), Photocatalysis and water purification: From fundamentals to recent applications. Wiley-VCH Verlag GmbH & Co. KGaA, Weinham, Germany, pp. 3-24.

Ohko, Y., Iuchi, K.-i., Niwa, C., Tatsuma, T., Nakashima, T., Iguchi, T., Kubota, Y., Fujishima, A., 2002. 17β-Estradiol degradation by TiO_2 photocatalysis as a means of reducing estrogenic activity. Environmental Science & Technology 36, 4175-4181.

Ohsaka, T., Izumi, F., Fujiki, Y., 1978. Raman spectrum of anatase, TiO_2. Journal of Raman Spectroscopy 7, 321-324.
Ottmar, K.J., Colosi, L.M., Smith, J.A., 2013. Evaluation of a prediction model for influent pharmaceutical concentrations. Journal of Environmental Engineering 139, 1017-1021.
Panayotov, D.A., Burrows, S.P., Morris, J.R., 2012. Photooxidation mechanism of methanol on rutile TiO_2 nanoparticles. Journal of Physical Chemistry C 116, 6623-6635.
Parks, G.A., 1965. The isoelectric points of solid oxides, solid hydroxides, and aqueous hydroxo complex systems. Chemical Reviews 65, 177-198.
Parrott, J.L., Blunt, B.R., 2005. Life-cycle exposure of fathead minnows (*Pimephales promelas*) to an ethinylestradiol concentration below 1 ng/L reduces egg fertilization success and demasculinizes males. Environmental toxicology 20, 131-141.
Paul, T., Miller, P.L., Strathmann, T.J., 2007. Visible-light-mediated TiO_2 photocatalysis of fluoroquinolone antibacterial agents. Environmental Science & Technology 41, 4720-4727.
Perreault, H.A., Semsar, K., Godwin, J., 2003. Fluoxetine treatment decreases territorial aggression in a coral reef fish. Physiology & Behavior 79, 719-724.
Petrovic, M., Sabater, S., Elosegi, A., Barceló, D., 2016. Emerging contaminants in river ecosystems. Springer International Publishing, Switzerland.
Pimentel, D., 2012. Silent Spring, the 50th anniversary of Rachel Carson's book. BMC Ecology 12, 1-2.
Quintana, J.B., Weiss, S., Reemtsma, T., 2005. Pathways and metabolites of microbial degradation of selected acidic pharmaceutical and their occurrence in municipal wastewater treated by a membrane bioreactor. Water Research 39, 2654-2664.
Rengaraj, S., Li, X.Z., 2007. Enhanced photocatalytic reduction reaction over Bi_3+–TiO_2 nanoparticles in presence of formic acid as a hole scavenger. Chemosphere 66, 930-938.
Rodríguez, A., Rosal, R., Perdigón-Melón, J., Mezcua, M., Agüera, A., Hernando, M., Letón, P., Fernández-Alba, A., García-Calvo, E., 2008. Ozone-based technologies in water and wastewater treatment. Springer, Berlin, Heidelberg.
Roig, B., D'Aco, V., 2016. Distribution of pharmaceutical residues in the environment, Pharmaceuticals in the Environment. The Royal Society of Chemistry, pp. 34-69.
Rotermann, M., Dunn, S., Black, A., 2015. Oral contraceptive use among women aged 15 to 49: Results from the Canadian Health Measures Survey. Health reports 26, 21.
Salveson, A., Rauch-Williams, T., Dickenson, E., Drewes, J.E., Drury, D., McAvoy, D., Snyder, S., 2012. Trace organic compound indicator removal during conventional wastewater treatment. Water Environment Research Foundation Alexandria, VA.
Sanchez, L., Peral, J., Domenech, X., 1997. Photocatalyzed destruction of aniline in UV-illuminated aqueous TiO_2 suspensions. Electrochimica Acta 42, 1877-1882.
Sarmah, A., Northcott, G., Leusch, F., Tremblay, L., 2006. A survey of endocrine disrupting chemicals (EDCs) in municipal sewage and animal waste effluents in the Waikato region of New Zealand. Science of the Total Environment 355, 135-144.
Schimmoller, L.J., Kealy, M.J., Foster, S.K., 2015. Triple bottom line costs for multiple potable reuse treatment schemes. Environmental Science: Water Research & Technology 1, 644-658.
Schneider, J., Matsuoka, M., Takeuchi, M., Zhang, J., Horiuchi, Y., Anpo, M., Bahnemann, D.W., 2014. Understanding TiO_2 photocatalysis: mechanisms and materials. Chemical Reviews 114, 9919-9986.

Schobert, H., 2013. Heterogenous catalysis, Chemistry of fossil fuels and biofuels. Cambridge University Press, New York, NY.
Schwab, B.W., Hayes, E.P., Fiori, J.M., Mastrocco, F.J., Roden, N.M., Cragin, D., Meyerhoff, R.D., D'Aco, V.J., Anderson, P.D., 2005. Human pharmaceuticals in US surface waters: A human health risk assessment. Regulatory Toxicology and Pharmacology 42, 296-312.
Schwarzenbach, R.P., Escher, B.I., Fenner, K., Hofstetter, T.B., Johnson, C.A., Von Gunten, U., Wehrli, B., 2006. The challenge of micropollutants in aquatic systems. Science 313, 1072-1077.
Scott, P.D., Bartkow, M., Blockwell, S.J., Coleman, H.M., Khan, S.J., Lim, R., McDonald, J.A., Nice, H., Nugegoda, D., Pettigrove, V., 2014. A national survey of trace organic contaminants in Australian rivers. Journal of Environmental Quality 43, 1702-1712.
Servos, M., Bennie, D., Burnison, B., Jurkovic, A., McInnis, R., Neheli, T., Schnell, A., Seto, P., Smyth, S., Ternes, T., 2005. Distribution of estrogens, 17β-estradiol and estrone, in Canadian municipal wastewater treatment plants. Science of the Total Environment 336, 155-170.
Shaham-Waldmann, N., Paz, Y., 2013. Modified photocatalysts, in: Pichat, P. (Ed.), Photocatalysis and water purification: From fundamentals to recent applications, Weinham, Germany, pp. 103-143.
Shareef, A., Angove, M.J., Wells, J.D., Johnson, B.B., 2006. Aqueous Solubilities of Estrone, 17β-Estradiol, 17α-Ethynylestradiol, and Bisphenol A. Journal of Chemical and Engineering Data 51, 879-881.
Silva, L.L., Moreira, C.G., Curzio, B.A., da Fonseca, F.V., 2017. Micropollutant removal from water by membrane and advanced oxidation processes—a review. Journal of Water Resource & Protection 9, 411-431.
Skaf, D., Grannas, A., Colotti, D., Bowes, E., 2016. The effects of photocatalyst and solution co-contaminants on photocatalytic oxidation of 1,3- dinitrobenzene in aqueous semiconductor oxide suspensions. Journal of Chemical Engineering & Processing Technology 7, 1-6.
Smith, B.M., 2013. Evaluating the estrogenicity of municipal wastewater effluents, Department of Biology. University of Waterloo, Waterloo, ON.
Snyder, S., Lei, H., Wert, E., Westerhoff, P., Yoon, Y., 2007. Removal of EDCs and pharmaceuticals in drinking water. AWWA Research Foundation, Denver, CO, p. 331.
Snyder, S.A., Villeneuve, D.L., Snyder, E.M., Giesy, J.P., 2001. Identification and quantification of estrogen receptor agonists in wastewater effluents. Environmental Science & Technology 35, 3620-3625.
Song, K., Mohseni, M., Taghipour, F., 2016. Application of ultraviolet light-emitting diodes (UV-LEDs) for water disinfection: A review. Water Research 94, 341-349.
Stackelberg, P.E., Gibs, J., Furlong, E.T., Meyer, M.T., Zaugg, S.D., Lippincott, R.L., 2007. Efficiency of conventional drinking-water-treatment processes in removal of pharmaceuticals and other organic compounds. Science of the Total Environment 377, 255-272.
Sumpter, J.P., 1998. Xenoendocrine disrupters—environmental impacts. Toxicology Letters 102, 337-342.
Sumpter, J.P., 2009. Protecting aquatic organisms from chemicals: the harsh realities. Philosophical Transactions of the Royal Society of London A: Mathematical, Physical & Engineering Sciences 367, 3877-3894.

Sumpter, J.P., Johnson, A.C., Williams, R.J., Kortenkamp, A., Scholze, M., 2006. Modeling effects of mixtures of endocrine disrupting chemicals at the river catchment scale. Environmental Science & Technology 40, 5478-5489.
Sun, L., Bolton, J.R., 1996. Determination of the Quantum Yield for the Photochemical Generation of Hydroxyl Radicals in TiO_2 Suspensions. The Journal of Physical Chemistry 100, 4127-4134.
Sun, W., Li, S., Mai, J., Ni, J., 2010. Initial photocatalytic degradation intermediates/pathways of 17α-ethynylestradiol: Effect of pH and methanol. Chemosphere 81, 92-99.
Sun, Y., Pignatello, J.J., 1995. Evidence for a surface dual hole-radical mechanism in the titanium dioxide photocatalytic oxidation of 2,4-D. Environmental Science & Technology 29, 2065-2072.
Suresh, S., Srivastava, V.C., Mishra, I.M., 2012. Adsorption of catechol, resorcinol, hydroquinone, and their derivatives: a review. International Journal of Energy & Environmental Engineering 3, 1-19.
Syoufian, A., Nakashima, K., 2008. Degradation of methylene blue in aqueous dispersion of hollow titania photocatalyst: Study of reaction enhancement by various electron scavengers. Journal of Colloid & Interface Science 317, 507-512.
Tan, B., Zhang, Y., Long, M., 2014. Large-scale preparation of nanoporous TiO_2 film on titanium substrate with improved photoelectrochemical performance. Nanoscale research letters 9, 1-6.
Tan, B.L., Hawker, D.W., Müller, J.F., Leusch, F.D., Tremblay, L.A., Chapman, H.F., 2007. Modelling of the fate of selected endocrine disruptors in a municipal wastewater treatment plant in South East Queensland, Australia. Chemosphere 69, 644-654.
Tang, W.Z., 2003. Physicochemical treatment of hazardous wastes. CRC Press, Boca Raton, Florida.
Tanna, R.N., Tetreault, G.R., Bennett, C.J., Smith, B.M., Bragg, L.M., Oakes, K.D., McMaster, M.E., Servos, M.R., 2013. Occurrence and degree of intersex (testis–ova) in darters (*Etheostoma spp.*) across an urban gradient in the Grand River, Ontario, Canada. Environmental Toxicology & Chemistry 32, 1981-1991.
ter Laak, T.L., Kooij, P.J.F., Tolkamp, H., Hofman, J., 2014. Different compositions of pharmaceuticals in Dutch and Belgian rivers explained by consumption patterns and treatment efficiency. Environmental Science & Pollution Research 21, 12843-12855.
Ternes, T., Joss, A., 2007. Human pharmaceuticals, hormones and fragrances: The challenge of micropollutants in urban water management IWA publishing, London, UK.
Ternes, T.A., Joss, A., Siegrist, H., 2004. Scrutinizing pharmaceuticals and personal care products in wastewater treatment. Environmental Science & Technology 38, 392A-399A.
Ternes, T.A., Stumpf, M., Mueller, J., Haberer, K., Wilken, R.-D., Servos, M., 1999. Behavior and occurrence of estrogens in municipal sewage treatment plants—I. Investigations in Germany, Canada and Brazil. Science of the Total Environment 225, 81-90.
Teske, S.S., Arnold, R.G., 2008. Removal of natural and xeno-estrogens during conventional wastewater treatment. Reviews in Environmental Science and Bio/Technology 7, 107-124.
Tetreault, G.R., Bennett, C.J., Shires, K., Knight, B., Servos, M.R., McMaster, M.E., 2011. Intersex and reproductive impairment of wild fish exposed to multiple municipal wastewater discharges. Aquatic Toxicology 104, 278-290.

Tetreault, G.R., Brown, C.J.M., Bennett, C.J., Oakes, K.D., McMaster, M.E., Servos, M.R., 2013. Fish community responses to multiple municipal wastewater inputs in a watershed. Integrated Environmental Assessment & Management 9, 456-468.

Thomaidi, V.S., Stasinakis, A.S., Borova, V.L., Thomaidis, N.S., 2015. Is there a risk for the aquatic environment due to the existence of emerging organic contaminants in treated domestic wastewater? Greece as a case-study. Journal of Hazardous Materials 283, 740-747.

Togunde, O.P., Oakes, K.D., Servos, M.R., Pawliszyn, J., 2012. Determination of pharmaceutical residues in fish bile by solid-phase microextraction couple with liquid chromatography-tandem mass spectrometry (LC/MS/MS). Envionmental Science & Technology 46, 5302-5309.

Tong, A.C., Braund, R., Warren, D., Peake, B., 2012. TiO_2-assisted photodegradation of pharmaceuticals — a review. Central European Journal of Chemistry 10, 989-1027.

Turchi, C.S., Ollis, D.F., 1990. Photocatalytic degradation of organic water contaminants: mechanisms involving hydroxyl radical attack. Journal of Catalysis 122, 178-192.

Tyler, C., Jobling, S., Sumpter, J., 1998. Endocrine disruption in wildlife: a critical review of the evidence. Critical Reviews in Toxicology 28, 319-361.

Tyler, C., Routledge, E., 1998. Natural and anthropogenic environmental oestrogens: the scientific basis for risk assessment. Pure Applied Chemistry 70, 1795-1804.

Vajda, A.M., Barber, L.B., Gray, J.L., Lopez, E.M., Woodling, J.D., Norris, D.O., 2008. Reproductive disruption in fish downstream from an estrogenic wastewater effluent. Environmental Science & Technology 42, 3407-3414.

Varshney, G., Kanel, S.R., Kempisty, D.M., Varshney, V., Agrawal, A., Sahle-Demessie, E., Varma, R.S., Nadagouda, M.N., 2016. Nanoscale TiO_2 films and their application in remediation of organic pollutants. Coordination Chemistry Reviews 306, 43-64.

Vega-Morales, T., Sosa-Ferrera, Z., Santana-Rodríguez, J.J., 2013. Evaluation of the presence of endocrine-disrupting compounds in dissolved and solid wastewater treatment plant samples of Gran Canaria Island (Spain). BioMed research international 2013, 1-15.

Verlicchi, P., Al Aukidy, M., Zambello, E., 2012. Occurrence of pharmaceutical compounds in urban wastewater: removal, mass load and environmental risk after a secondary treatment—a review. Science of the Total Environment 429, 123-155.

Vinu, R., Madras, G., 2008. Kinetics of simultaneous photocatalytic degradation of phenolic compounds and reduction of metal ions with nano-TiO_2. Environmental Science & Technology 42, 913-919.

Vogna, D., Marotta, R., Andreozzi, R., Napolitano, A., d'Ischia, M., 2004. Kinetic and chemical assessment of the UV/H_2O_2 treatment of antiepileptic drug carbamazepine. Chemosphere 54, 497-505.

Vohra, M.S., Tanaka, K., 2001. Enhanced photocatalytic activity of nafion-coated TiO_2. Environmental Science & Technology 35, 411-415.

Wang, R., Ren, D., Xia, S., Zhang, Y., Zhao, J., 2009. Photocatalytic degradation of bisphenol A (BPA) using immobilized TiO_2 and UV illumination in a horizontal circulating bed photocatalytic reactor (HCBPR). Journal of Hazardous Materials 169, 926-932.

Wang, S., Oakes, K.D., Bragg, L.M., Pawliszyn, J., Dixon, G., Servos, M.R., 2011. Validation and use of *in vivo* solid phase micro-extraction (SPME) for the detection of emerging contaminants in fish. Chemosphere 85, 1472-1480.

Westerhoff, P., Yoon, Y., Snyder, S., Wert, E., 2005. Fate of endocrine-disruptor, pharmaceutical, and personal care product chemicals during simulated drinking water treatment processes. Environmental Science & Technology 39, 6649-6663.
Williams, R.T., 2005. Human pharmaceuticals: assessing the impacts on aquatic ecosystems. Society of Environmental Toxicology & Chemistry (SETAC), Pensacola, Florida.
Wittmer, I.K., Bader, H.P., Scheidegger, R., Stamm, C., 2016. REXPO: A catchment model designed to understand and simulate the loss dynamics of plant protection products and biocides from agricultural and urban areas. Journal of Hydrology 533, 486-514.
Woo, O.T., Chung, W.K., Wong, K.H., Chow, A.T., Wong, P.K., 2009. Photocatalytic oxidation of polycyclic aromatic hydrocarbons: intermediates identification and toxicity testing. Journal of Hazardous Materials 168, 1192-1199.
Woodling, J.D., Lopez, E.M., Maldonado, T.A., Norris, D.O., Vajda, A.M., 2006. Intersex and other reproductive disruption of fish in wastewater effluent dominated Colorado streams. Comparative Biochemistry & Physiology Part C: Toxicology & Pharmacology 144, 10-15.
Worch, E., 2012. Adsorption technology in water treatment: fundamentals, processes, and modeling. Hubert & Co. GmbH & Co. KG, Gottingen, Germany.
Xu, J., Ao, Y., Fu, D., Yuan, C., 2009. Synthesis of Gd-doped TiO_2 nanoparticles under mild condition and their photocatalytic activity. Colloids and Surfaces A: Physicochemical and Engineering Aspects 334, 107-111.
Xu, W., Zhang, G., Li, X., Zou, S., Li, P., Hu, Z., Li, J., 2007. Occurrence and elimination of antibiotics at four sewage treatment plants in the Pearl River Delta (PRD), South China. Water Research 41, 4526-4534.
Yang, Y., Luo, L., Xiao, M., Li, H., Pan, X., Jiang, F., 2015. One-step hydrothermal synthesis of surface fluorinated TiO_2/reduced graphene oxide nanocomposites for photocatalytic degradation of estrogens. Materials Science in Semiconductor Processing 40, 183-193.
Zhang, Q.-Q., Ying, G.-G., Chen, Z.-F., Liu, Y.-S., Liu, W.-R., Zhao, J.-L., 2015. Multimedia fate modeling and risk assessment of a commonly used azole fungicide climbazole at the river basin scale in China. Science of the Total Environment 520, 39-48.
Zhang, W., Li, Y., Su, Y., Mao, K., Wang, Q., 2012a. Effect of water composition on TiO_2 photocatalytic removal of endocrine disrupting compounds (EDCs) and estrogenic activity from secondary effluent. Journal of Hazardous Materials 215–216, 252-258.
Zhang, W., Li, Y., Wu, Q., Hu, H., 2012b. Removal of endocrine-disrupting compounds, estrogenic activity, and Escherichia coliform from secondary effluents in a TiO_2-coated photocatalytic reactor. Environmental Engineering Science 29, 195-201.
Zhao, J.-L., Zhang, Q.-Q., Chen, F., Wang, L., Ying, G.-G., Liu, Y.-S., Yang, B., Zhou, L.-J., Liu, S., Su, H.-C., Zhang, R.-Q., 2013. Evaluation of triclosan and triclocarban at river basin scale using monitoring and modeling tools: Implications for controlling of urban domestic sewage discharge. Water Research 47, 395-405.
Zhu, X., Yuan, C., Bao, Y., Yang, J., Wu, Y., 2005. Photocatalytic degradation of pesticide pyridaben on TiO_2 particles. Journal of Molecular Catalysis A: Chemical 229, 95-105.
Zhu, X., Zhou, D., Cang, L., Wang, Y., 2012. TiO_2 photocatalytic degradation of 4-chlorobiphenyl as affected by solvents and surfactants. Journal of Soils & Sediments 12, 376-385.

Appendix A

Supplementary Data for Chapter 2

Table S2.1. Population Demographics

Profile	Kitchener	Waterloo
Total	219,155	98,780
Total Males	107,735	48,875
Total Females	111,420	49,905
Menstruating	69,170	26,280*
Menopause	15,250	31,575
HRT	6,556	3,009
Pregnant**	2,455	1,106
BCP	11, 493	11,735*

*Includes average female population at two major universities (University of Waterloo and Wilfrid Laurier University). See Tables S2.2 and S2.3.

**Crude live births in the Region of Waterloo is 11.2 per 1000 (1.12% per person). The number of women in reproductive age (ages 15-49) represents 29% of the total population. Therefore, the number of women pregnant represents ~4% of the total population of the women in reproductive age.

Table S2.2 Breakdown of female population at the University of Waterloo

Semester	Term	Total Population	Female Population
Fall	2008	26457	11229
Winter	2009	25867	11011
Spring	2009	15691	5779
Fall	2009	28387	12159
Winter	2010	27396	11754
Spring	2010	16396	6080
Fall	2010	29956	12862
Winter	2011	29070	12468
Spring	2011	17615	6565
Fall	2011	31121	13349
Winter	2012	30243	12994
Spring	2012	18403	6976
Fall	2012	32239	13877
Winter	2013	31144	13487
Spring	2013	19418	7436
Fall	2013	33140	14456
Winter	2014	32073	14004
Spring	2014	19734	7677
Fall	2014	33604	14840
Winter	2015	32444	14363
Spring	2015	20571	8176
Fall	2015	34040	15318
Average		**26591**	**11168**

Data from: https://uwaterloo.ca/institutional-analysis-planning/university-data-and-statistics/student-data/student-headcounts. Retrieved on December 28, 2016.

Table S2.3 Breakdown of female population at the University of Waterloo

Semester	Term	Total Population	Female Population
Fall	2008	15498	9162
Winter	2009	14757	8730
Spring	2009	4315	2364
Fall	2009	16512	9684
Winter	2010	15649	9196
Spring	2010	4687	2612
Fall	2010	17247	9985
Winter	2011	16364	9521
Spring	2011	4942	2745
Fall	2011	18115	10504
Winter	2012	17260	9972
Spring	2012	5583	2076
Fall	2012	18898	4065
Winter	2013	17931	3673
Spring	2013	5937	2191
Fall	2013	18877	3884
Winter	2014	18058	3607
Spring	2014	5979	2150
Fall	2014	18571	3931
Winter	2015	17663	3315
Spring	2015	6265	2236
Fall	2015	18553	3798
Average		**13530**	**5682**

Data from: https://legacy.wlu.ca/page.php?grp_id=1367&p=12308. Retrieved on December 28, 2016.

Table S2.4 Calculated performance criteria for the total estrogenicity predictions at Kitchener and Waterloo WWTPs.

Performance Measure	Description	Criteria	Kitchener WWTP	Waterloo WWTP
Percent bias[a]	$\frac{\sum_{i=1}^{n} O_i - P_i}{\sum_{i=1}^{n} O_i} \times 100$	Range: -∞ to ∞ Very good: <±15 Good: ±15 to ±20 Satisfactory: ±20 to ±30 Unsatisfactory: >±30	1% (very good)	-21% (satisfactory)

O=observed; P=predicted. [a]Based on the suggestions by Moriasi et al. (2015) for nutrient modeling.

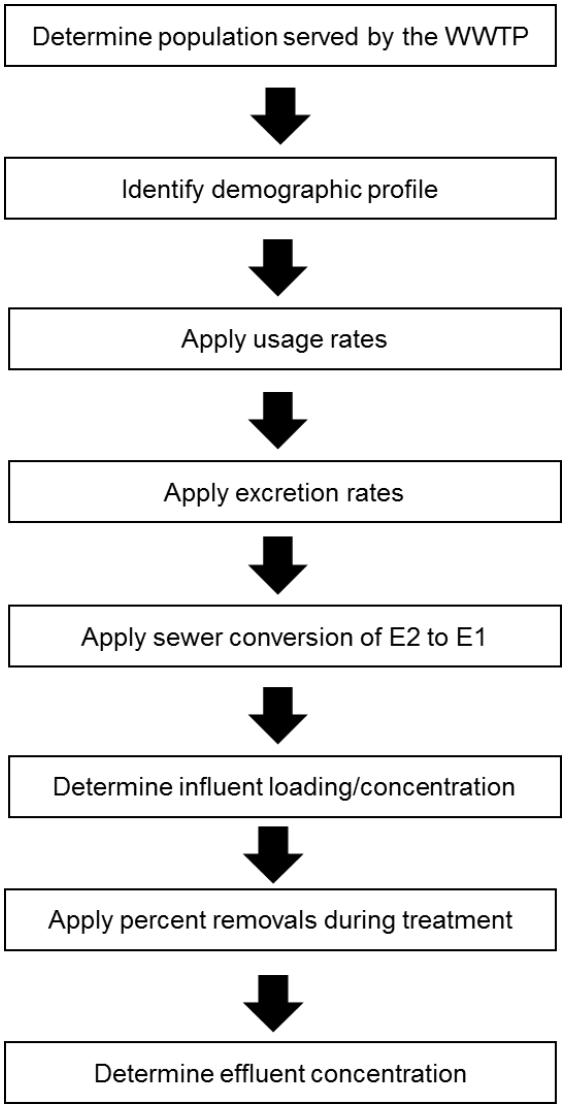

Figure S2.1 General process diagram used in the estimation of selected estrogens in the Kitchener and Waterloo WWTP effluents. Methodology adapted from Johnson and Williams (2004).

A-1 Effects Directed Analysis (EDA) for estrogen identification in WWTP effluent extracts

The wastewater sample collection and extraction for the EDA were completed according to the methods described in Smith (2013). Briefly, the effluents were collected onsite in 500 mL or 1 L amber glass bottles, preserved with 1 g/L sodium azide and 50 mg/L ascorbic acid and stored at 4ºC until extraction (within 24 h). The samples were extracted using solid phase extraction (SPE) in 12-port Visiprep manifold (Supelco, Bellefonte, PA). A 6 mL, 500 mg Oasis HLB SPE cartridge (Waters Corporation, Mississauga, ON) was used per 500 mL sample or 2 cartridges in series per 1 L. The cartridges were pre-conditioned using 5 mL each of methyl-tert-butyl ether (MTBE), methanol, and ultrapure water. Following sample introduction under vacuum, the cartridges were disassembled and rinsed with 5 mL ultrapure water and then eluted with 5 mL of methanol and 5 mL of 90:10 MTBE: methanol. The extracts were dried in Dionex Rocket Evaporator (Thermo Scientific, Mississauga, ON) using the built-in low boiling point standard method. The samples were then reconstituted in 50 µL methanol and stored in 2 mL vials with 150 µL glass inserts. The estrogenicity of the whole extracts was analysed using the yeast estrogen screen (YES) assay described in detail in (Tanna et al., 2013). These extracts were then fractionated to determine the key estrogens that contributed to the overall estrogenicity. The chromatographic separation and fractionation of the whole extracts were completed using the Agilent 1260 Infinity Quaternary LC system with diode array detector (DAD). Prior to the injection of the whole extracts, a 10^{-4} M standard containing 9 compounds (estrone, 17β-estradiol, estriol, 17α-ethinylestradiol, testosterone bisphenol A, octylphenol, nonylphenol and diethystilbesterol) were analyzed first to provide a reference for the order of compound elution and their associated retention times (Figure S2.2). The separation was completed using a 2.1 mm × 50 mm × 1.8 µm Agilent Eclipse XDB-C18 column (Agilent Technologies, Mississauga, ON) and detected in the DAD at 220 ± 4 nm and 254 ± 4 nm with reference wavelengths at 360 ± 100 nm. Initially, 60 fractions of the standard were collected in a 30 s fraction window from 2.5 min and 60 min. Each fraction was subsequently profiled for estrogenic activity using the YES assay (Figure S2.3-A).

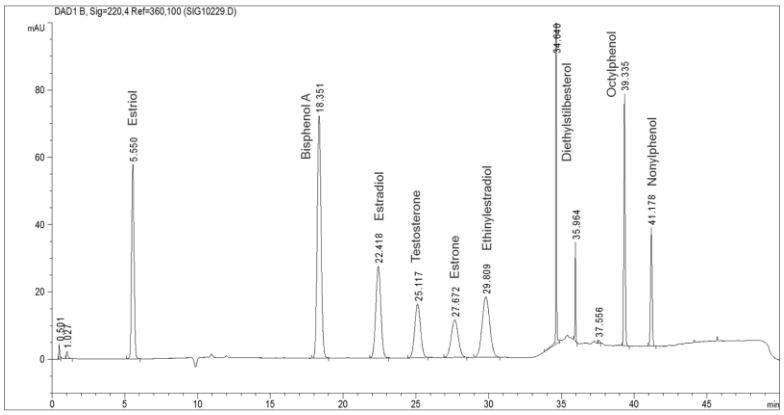

Figure S2.2 Separation of target estrogens. The elution times of each target compound were used as a reference

A similar process was completed for an unspiked extract of Kitchener WWTP (Figure S2.4, one each for pre-upgrade and post-upgrade period) and then contrasted against the spiked extract (Figure S2.3). The total estrogenicity (**ΣE2 Eq.)** contributed by each compound was calculated by adding the E2 equivalents of each fraction associated with the target compound. A similar procedure was completed for Waterloo WWTP (Figure S2.5).

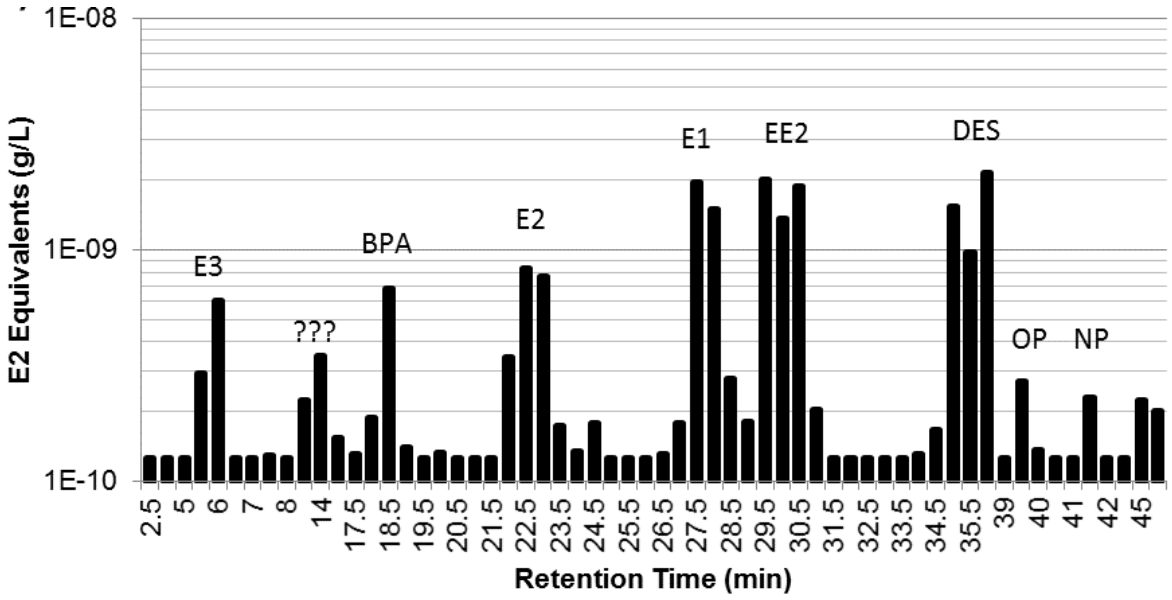

Figure S2.3 Estrogenicity profile of the fractionated standard.

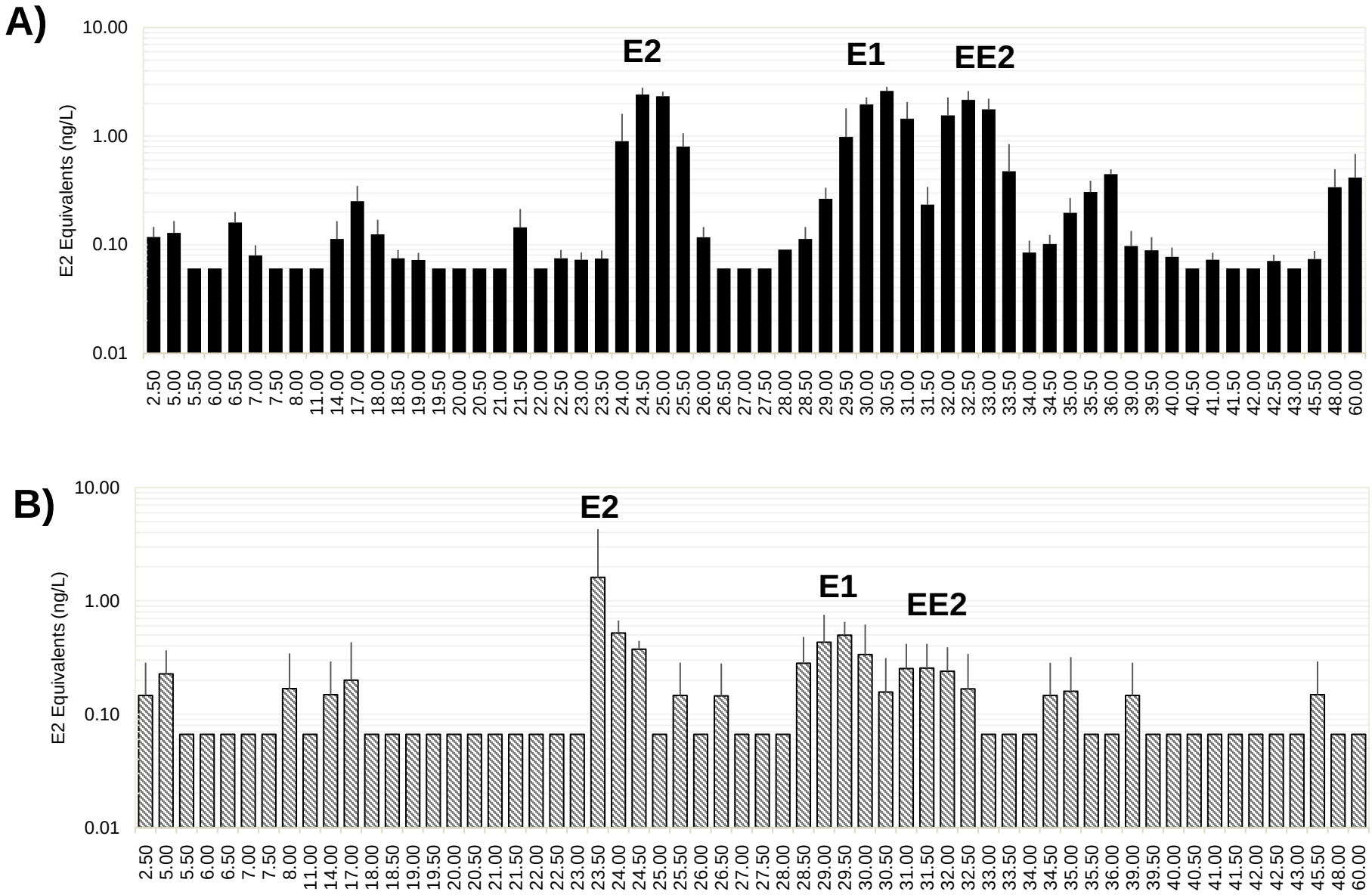

Figure S2.4 Estrogenic profile of Kitchener WWTP effluent sample (a) pre-upgrade, collected in 2010 and (b) post-upgrade, collected in 2012.

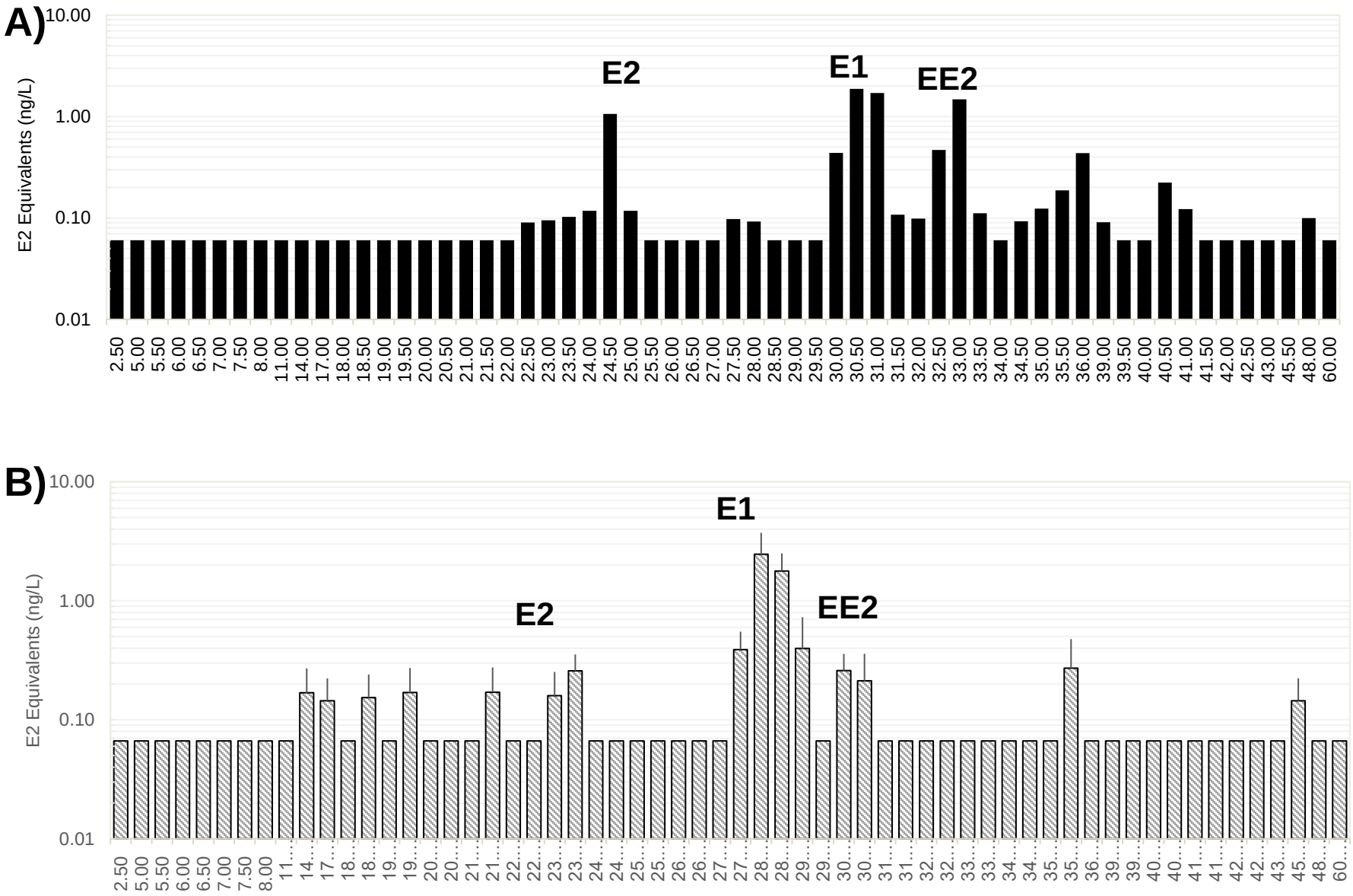

Figure S2.5 Estrogenic profile of Waterloo WWTP effluent sample collected in (a) 2010 and (b) 2012. There was a shift in the elution times of the extracts collected in 2012 and the compounds were identified based on elution order.

The concentration of the target estrogens (E1, E2, and EE2) in the effluent ($C_{e,\ EDA}$) was subsequently calculated by dividing the total estrogenicity exhibited by each compound to the potency factor detailed in Jarošová et al. (2014) Finally, the percent removal (r) associated during the pre- and post-upgrade conditions were calculated by:

$$r = \frac{C_i - C_{e,EDA}}{C_i} \times 100$$

where Ci is the influent concentration and Ce is the effluent concentration. Ci was derived from the average influent estimates using population demographics and excretion rates. For Kitchener WWTP, a different percent removal was used for the pre- and post-upgrade conditions.

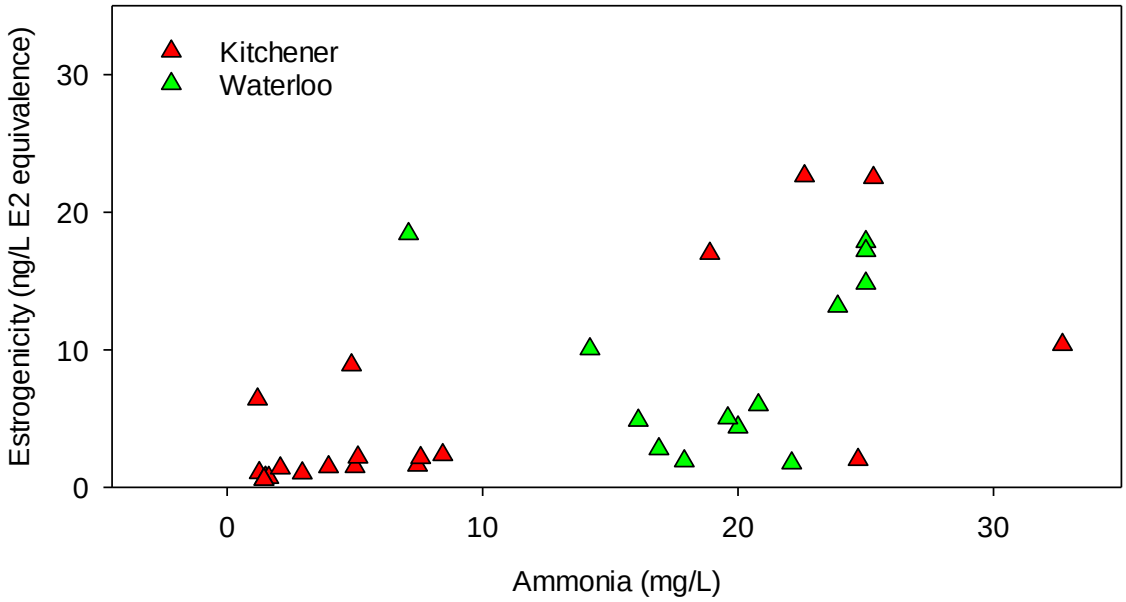

Figure S2.6 Scatter plot of measured ammonia concentrations and measured estrogenicity at the Kitchener and Waterloo WWTPs. Note that when the dates for sample collection of ammonia and estrogenicity did not match, the closest date to the estrogenicity sampling date was used as the ammonia concentration. The Pearson correlation coefficient for Kitchener WWTP and Waterloo WWTPs were 0.498 and 0.009 respectively.

Appendix B

Supplementary Data for Chapter 3

B-1. River hydro-geometry and transport processes

The cross-sections of the segments were initialized as rectangular. To represent the river configurations appropriately, the power functions within WASP were used to describe river hydro-geometry (velocity, channel width, and depth) as a function of flow. These equations were empirically developed by Leopold and Maddock (1953) and are described as:

$$v = aQ^d,$$
$$w = bQ^e;$$
$$h = aQ^f$$

where Q is flow (m^3/s); v, w, and h are velocity, channel width, and depth respectively; a, b, and c are the parameter specific hydraulic coefficients; and d, e, and f are the parameter specific hydraulic exponents. The river segment can either assume a U, V, or trapezoidal shape depending on the values of hydraulic constants used in the model. When one set of coefficients are specified, the rest can be internally calculated.

Advection is the primary transport process in rivers and is driven by water flows. Any dissolved constituents in the water column as well as other suspended materials can be transported subsequently in the river depending on flow conditions. The internal flows in WASP under the kinematic wave flow option is propagated using the Manning's equation:

$$Q = \frac{1}{n}\frac{A^{5/3}}{B^{2/3}}S^{1/2}$$

where A is the segment area, B is segment width and S is bed slope. Bed slopes were taken from ArcGIS mapping software which used the digital elevation model to estimate this parameter. Roughness coefficient value was initialized using the values described by Chow (1959) and eventually finalized to 0.035. One segment in the model was set up as a ponded reach (segment 33) due to the dam used for water taking (WASP accounts for this condition in its algorithms).

The Manning's equation is incorporated in a one-dimensional continuity equation that is evaluated using kinematic wave differential equation. The differential equation is solved using finite-difference formulations for flow and continuity (e.g., Euler and Runga-Kutta solution techniques). The model was first initialized for water transport and the accuracy of this process was cross-checked against the measured hydro-geometry data such as water level and flows. Measured water level available for segments 12 and 21 were primarily used for river transport calibration. The finalized input parameters associated with the hydro-geometry and river transport are found in the supplementary material (Table S3.1).

B-2. Calculating ECF

Recall that the dose-response curve for Hill equation (four parameters) is:

$$R = \min + \frac{(max - min)}{1 + 10^{(F - EEQ) * H)}}$$

where R is intersex incidence or severity, min and max are the highest and lowest expected responses, F is the response halfway between the min and max (EC50), and H is the hillslope parameter that describes the steepness of the curve. This equation can be rearranged such that:

$$EC_F = \left(\frac{F}{100 - F}\right)^{1/HillSlope} \times EC_{50}$$

where F is the fractional response of choice. In this study, EC10 was used.

Table S3.1. Finalized segment inputs entered in WASP. Volume was initiated by multiplying the lengths, widths, and minimum depths. Bed slopes were estimated from the ARC-GIS mapping software using the digital elevation (DEM) image available for the Grand River watershed. Depth multiplier (Mult), depth exponent, and roughness were the major parameters calibrated to achieve good simulation of water levels.

Segment	Description	Volume (m^3)	Depth Mult	Depth Exp	Length[a] (m)	Width[a] (m)	Min Depth[a] (m)	Slope (m/m)	Roughness
1	BSDFER_1	75000	4.75	0.35	3000	50	0.05	0.03	0.035
2	BSDFER_2	38610	4.75	0.35	2574	30	0.05	0.03	0.035
3	FERELO_1	82000	4.75	0.35	4100	40	0.05	0.03	0.035
4	INVWMR_1	34620	4.75	0.35	1731	40	0.05	0.012	0.035
5	INVWMR_2	13027.5	4.75	0.35	1737	15	0.05	0.012	0.035
6	INVWMR_3	38745	4.75	0.35	2214	35	0.05	0.012	0.035
7	INVWMR_4	77500	4.75	0.35	3100	50	0.05	0.012	0.035
8	INVWMR_5	3825	4.75	0.35	2125	36	0.05	0.012	0.035
9	INVWMR_6	3824	4.75	0.35	1912	40	0.05	0.0025	0.035
10	INVWMR_7	6466.6	4.75	0.35	2086	62	0.05	0.0075	0.035
11	INVWMR_8	3743.25	4.75	0.35	1610	46.5	0.05	0.04	0.035
12	INVWMR_9	4979.04	4.75	0.35	2024	49.2	0.05	0.02	0.035
13	WMR-LC_1	38305	4.75	0.35	1630	47	0.05	0.005	0.035
14	WMR-LC_2	44697.75	4.75	0.35	1954	45.75	0.05	0.005	0.035
15	WMR-LC_3	63084	4.75	0.35	2253	56	0.05	0.04	0.035
16	WMR-LC_4	75000	4.75	0.35	2686	50	0.05	0.01	0.035
17	WMR-LC_5	88227.2	4.75	0.35	2792	63.2	0.05	0.05	0.035
18	WMR-LC_6	50739.5	4.75	0.35	1862	54.5	0.05	0.025	0.035
19	WMR-LC_7	102198.375	4.75	0.35	2547	80.25	0.05	0.035	0.035
20	WMR-LC_8	70483.5	4.75	0.35	2043	69	0.05	0.05	0.035
21	WMR-LC_9	84588.875	4.75	0.35	2443	69.25	0.05	0.05	0.035
22	LC-WWTP	1348.75	4.75	0.35	325	83	0.05	0.009	0.035
23	WWTP_FPT_1a	2550	4.75	0.35	1700	30	0.05	0.009	0.035
24	WWTP_FPT_1b	2550	4.75	0.35	1700	30	0.05	0.03	0.035
25	WWTP_FPT_2	5250	4.75	0.35	1500	70	0.05	0.012	0.035
26	WWTP_FPT_3	5804.7	4.75	0.35	1759	66	0.05	0.012	0.035
27	WWTP_FPT_4	5731.85	4.75	0.35	1711	67	0.05	0.012	0.035
28	WWTP_FPT_5	4011	4.75	0.35	1337	60	0.05	0.07	0.035
29	WWTP_FPT_6	5827.5	4.75	0.35	1850	63	0.05	0.03	0.035
30	WWTP_FPT_7	5062.5	4.75	0.35	1350	75	0.05	0.03	0.035
31	WWTP_FPT_8	7500	4.75	0.35	2500	60	2	1.00E-06	0.035
32	WWTP_FPT_9	3750	4.75	0.35	1500	50	0.05	0.009	0.035
33	FPT_Doon_1	131840	4.75	0.35	824	80	0.05	0.009	0.035
34	FPT_Doon_2	2556	4.75	0.35	639	80	0.05	0.009	0.035
35	FPT_Doon_3	3500	4.75	0.35	1000	70	0.05	0.009	0.035
36	FPT_Doon_4	2019	4.75	0.35	673	60	0.05	0.03	0.035
37	FPT_Doon_5	1653.75	4.75	0.35	525	63	0.05	0.01	0.035
38	FPT_Doon_6	8728.9625	4.75	0.35	2521	69.25	0.05	0.01	0.035
39	Doon_PT1_1a	775	4.75	0.35	500	31	0.05	0.01	0.035
40	Doon_PT1_1b	775	4.75	0.35	500	31	0.05	0.01	0.035
41	PT1_SC1a	13020	4.75	0.35	400	31	0.05	0.01	0.035
42	PT1_SC1b	25420	4.75	0.35	400	31	0.05	0.01	0.035
43	SC1b_PT2_1a	1933.75	4.75	0.35	1190	32.5	0.05	0.01	0.035
44	SC1b_PT2_1b	1933.75	4.75	0.35	1190	32.5	0.05	0.01	0.035
45	PT2_Blair_1	1950	4.75	0.35	600	65	0.05	0.01	0.035
46	PT2_Blair_2	1662	4.75	0.35	554	60	0.05	0.01	0.035
47	PT2_Blair_3	1875	4.75	0.35	500	75	0.05	0.01	0.035
48	PT2_Blair_4	1907.5	4.75	0.35	545	70	0.05	0.01	0.035
49	PT2_Blair_5	3400	4.75	0.35	680	100	0.05	0.01	0.035
50	PT2_Blair_6	5694	4.75	0.35	876	130	0.05	0.01	0.035

Table S3.2. Summarized information on data sources for the boundary conditions required for river transport and chloride simulation from 2007-2015.

Segment No.	Description	Daily Flow (m^3/s)	pH and Temperature	Chloride (mg/L)
1	Below Shand Dam	WSC 02GA016	PWQMN 16018403702	PWQMN 16018403702
3	Fergus WWTP	Centre Wellington	Centre Wellington	Estimate from Servos Lab[a]
4	Elora WWTP	Centre Wellington	Centre Wellington	Estimate from Servos Lab[a]
5	Irvine Creek	WSC 02GA005	PWQMN 16018410402	PWQMN 16018410402
14	Canagigue Creek	WSC 02GA023	PWQMN 16018401602	PWQMN 16018401602
17	Conestogo River	WSC 02GA006	PWQMN 16018402902	PWQMN 16018402902
22	Laurel Creek	WSC 02GA024	PWQMN 16018413002	PWQMN 16018413002
23	Waterloo WWTP	Region of Waterloo	Region of Waterloo	Servos Lab monitoring data[a]
33	Water Taking	Bunt, 2001	N/A	N/A
39	Kitchener WWTP	Region of Waterloo	Region of Waterloo	Servos Lab monitoring data[a]
43	Schneider Creek	GRCA	PWQMN 16018411702	PWQMN 16018411702

Notes: [a]Sporadic wastewater sampling events show relatively constant chloride concentration of ~500 mg/L of chloride for Waterloo and Kitchener WWTPs. Hence, this concentration was also employed for Fergus and Elora WWPTS. The areas within the Waterloo WWTPs are highly urbanized leading to some chloride inputs which were not accounted for (i.e., storm sewer inputs). Hence, the chloride concentration in Waterloo WWTP was made into 1,000 mg/L to capture this. WSC = Water survey of Canada; ROW = Region of Waterloo, GRCA = Grand River Conservation Authority; PWQMN = Provincial Water Quality Monitoring Network

Table S3.3. Summarized information on the data used for water level and chloride calibration from 2007-2015.

Daily Water Level		
Segment No.	Site Name	Data Source
12	West Montrose	WSC
32	Bridgeport	WSC
37	Doon	GRCA
Chloride		
Segment No.	Site Name	Data Source (number of datapoints)
12	West Montrose	PWQMN 16018410302 (43)
22	Bridgeport	PWQMN 16018401502 & LGL Water Quality Reports[a] (106)
32	Freeport	PWQMN 16018404102 (37)
50	Blair	PWQMN 16018401202 & LGL Water Quality Reports[a] (79)

Note: [a]Surface water quality monitoring program for the Grand River for the Region of Waterloo 2009-2014 year-end report. WSC = Water Survey of Canada; GRCA = Grand River Conservation Authority.

Table S3.4. Rate constants employed in this study.

Biodegradation			
Compound	Average First order rate constant (1/d)	Range (1/d)	Study
E1	0.294	0.079-3.465	Jürgens et al. (2002)
E2	0.255	0.064-9.63	Jürgens et al. (2002)
EE2	0.041	-	Jürgens et al. (2002)
Temperature correction factor equation $k=k_{,20}\ Q^{(T-20/10)}$ with Q from 1.5-2.0			
Photodegradation			
Compound	Average First order rate constant (1/d)	Range (1/d)	Study
E1	1.804	0.069,3.538	Jürgens et al. (2002); Lin and Reinhard (2005)[a]
E2	0.234	0.069,0.397	Jürgens et al. (2002); Lin and Reinhard (2005)[a]
EE2	0.328	0.069,0.586	Jürgens et al. (2002); Lin and Reinhard (2005)[a]

Table S3.5. Temperature Profiles used for the modeled reach.

Segments 1-12[a]		Segments 24-38[b]		Segments 39-50[c]		Segments 13-22[d]	
Date	**Temp (C)**	**Date**	**Temp (C)**	**Date**	**Temp (C)**	**Date**	**Temp (C)**
3/26/2007	2.0000	2/20/2007	0.6000	2/21/2007	3.1000	3/26/2007	14.2
3/28/2007	2.0000	3/23/2007	3.1000	3/23/2007	2.3000	3/28/2007	13.3
5/22/2007	12.3000	5/23/2007	19.8000	3/27/2007	7.2000	4/4/2007	41.4
6/19/2007	13.9000	6/20/2007	21.1000	5/24/2007	24.0000	5/23/2007	3.5
7/16/2007	19.2000	7/17/2007	22.7000	6/21/2007	24.6000	6/20/2007	4.7
8/12/2008	5.3000	4/1/2008	2.4000	7/18/2007	21.9000	7/17/2007	3.8
9/15/2008	15.2000	4/3/2008	3.3900	4/1/2008	2.6500	5/21/2008	1.2
10/9/2008	19.4000	5/21/2008	9.9300	4/3/2008	2.2000	6/24/2008	3.8
3/18/2009	2.0000	6/24/2008	18.8000	5/21/2008	12.2000	7/21/2008	-
4/6/2009	2.3000	7/21/2008	20.7000	6/24/2008	22.3000	3/17/2009	9.6
5/5/2009	12.7000	3/17/2009	3.1000	7/21/2008	23.1000	4/6/2009	5.5
6/15/2009	15.7	4/6/2009	3.0000	1/29/2009	1.2000	5/7/2009	-
7/14/2009	17.1	5/7/2009	14.6000	2/12/2009	7.8000	6/16/2009	-
4/19/2010	10.1000	6/16/2009	19.0000	4/7/2009	2.3000	7/15/2009	-
5/25/2010	14.2000	7/16/2009	22.0000	5/6/2009	15.9000	4/21/2010	3.0
6/21/2010	14.1000	4/21/2010	15.2000	6/17/2009	19.9000	3/16/2010	23.3
7/19/2010	19.1000	3/16/2010	1.4000	7/14/2009	22.9000	5/26/2010	2.6
4/11/2011	4.7000	5/26/2010	25.7000	3/15/2010	2.9000	6/22/2010	4.2
4/20/2011	3.7000	6/22/2010	22.5000	4/22/2010	15.8000	7/20/2010	2.6
6/20/2011	16.6000	7/20/2010	24.9000	5/26/2010	25.4000	3/18/2011	74.6
7/18/2011	19.3000	3/11/2011	0.3000	6/23/2010	24.8000	4/13/2011	3.5
5/17/2011	10.5000	4/13/2011	6.5000	7/19/2010	24.8000	5/16/2011	7.3
4/16/2012	10.8	5/16/2011	9.7000	3/11/2011	0.5000	6/22/2011	2.7
5/15/2012	12.5	6/22/2011	20.8000	4/12/2011	10.2000	7/20/2011	3.5
6/18/2012	15.7	7/20/2011	25.5000	5/18/2011	12.5000	4/18/2012	1.4
7/16/2012	20.2	4/18/2012	12.8	6/21/2011	28.2000	5/17/2012	0.5
4/18/2013	5	5/17/2012	15.5	7/20/2011	23.5000	6/20/2012	5.3
5/16/2013	11.6	6/20/2012	27.2	3/13/2013	0.7	7/17/2012	7.5
6/17/2013	16.3	7/17/2012	26.9	4/10/2013	4.1	4/10/2013	78.4
7/9/2013	19.9	4/10/2013	3.6	4/16/2013	6.9	5/15/2013	0.8
8/13/2013	20.4	4/17/2013	6.2	5/14/2013	10.5	6/19/2013	4.3
9/16/2013	18.5	5/15/2013	14.9	6/18/2013	21.4	7/11/2013	6.8
10/22/2013	10.8	6/19/2013	19.9	7/9/2013	22.2	8/15/2013	2.7
4/11/2014	2.3	7/11/2013	21.5	8/14/2013	19.8	9/18/2013	2.6
4/30/2014	1.7	9/18/2013	18.4	9/18/2013	14.2	10/24/2013	7.3
5/12/2014	6.5	10/24/2013	8.1	10/24/2013	8.1	4/11/2014	61.6
6/16/2014	10.1	4/28/2014	9.9	11/13/2013	4.5	4/28/2014	4.5
8/25/2014	14.9	5/14/2014	17.1	4/10/2014	5.3	5/14/2014	4.6
9/18/2014	19.9	6/18/2014	22.5	4/15/2014	2.9	6/18/2014	4.3
10/20/2014	16.6	8/27/2014	23.1	4/29/2014	8.8	8/27/2014	4.3
11/24/2014	11.7	9/11/2014	17.8	5/13/2014	20.6	9/17/2014	4.9
4/11/2015	2.3	9/17/2014	16.2	6/17/2014	22.2	10/21/2014	10.5
4/30/2015	1.7	10/21/2014	10.1	8/26/2014	25.3	11/17/2014	3.2
5/12/2015	6.5	11/17/2014	2	9/11/2014	18.2	4/11/2015	2.5
6/16/2015	10.1	4/28/2015	9.9	9/17/2014	16.6	4/28/2015	9.2
8/25/2015	14.9	5/14/2015	17.1	10/21/2014	10.2	5/14/2015	15.1
9/18/2015	19.9	6/18/2015	22.5	11/18/2014	4.3	6/18/2015	20
10/20/2015	16.6	8/27/2015	23.1	4/10/2015	5.3	8/27/2015	21.4
11/24/2015	11.7	9/11/2015	17.8	4/15/2015	2.9	9/17/2015	15.8
		10/21/2015	16.2	4/29/2015	8.8	10/21/2015	9.8
		11/17/2015	10.1	5/13/2015	20.6	11/17/2015	2.5
				6/17/2015	22.2		
				8/26/2015	25.3		
				9/11/2015	18.2		
				9/17/2015	16.6		
				10/21/2015	10.2		
				11/18/2015	4.3		

[a]PWQMN ID 16018403702; [b]PWQMN ID 16018401502 [c]PWQMN ID 16018410202;[d]PWQMN ID 16018410302

Table S3.6. Information on the date selected to analyze spatial patterns.

Date	River Flow (m3/s)	Estrogenicity – Kitchener WWTP (ng/L E2 equivalents)[a]	Estrogenicity – Waterloo WWTP (ng/L E2 equivalents)[a]
May 20, 2012 (pre-upgrade)	9.62	17	8.92
June 11, 2014 (post-upgrade)	11.1	2.13	8.62

[a]predictions were taken from the simulation of Arlos et al (2017).

Table S3.7. Waterloo WWTP effluent contribution to total estrogenicity at Segment 50.

Changes in Kitchener WWTP operation, post-upgrade (June 11, 2014)	Estrogenicity at Segment 50	Contribution of Waterloo WWTP to total estrogenicity in Segment 50 ($Estrogenicity_{OFF}/Estrogenicity_{ON} \times 100$)
Estrogen Loading ON	0.51	62%
Estrogen loading OFF	0.32	

Table S3.8. Selected examples for different fate simulations for target estrogens.

	Biodegradation			Q10	Photolysis Rates			Occurrence Quality - Model Predictions			
	E1	**E2**	**EE2**		**E1**	**E2**	**EE2**	**Hillslope**	**EC50**	**EC10**	**R^2**
1	0	0	0	0	0	0	0	1.017	0.715	0.082	0.755
2	0.1575	0.365	0.0267	0	0	0	0	1.036	0.668	0.080	0.732
3	1	1	1	0	0	0	0	0.958	0.587	0.059	0.720
4	5	3	1	0	0	0	0	0.805	0.488	0.032	0.652
5	9	3.5	1	0	0	0	0	0.805	0.488	0.032	0.682
6	5	3	1	0	5.5	5.5	5.5	0.630	0.408	0.012	0.621
7	0.1575	0.365	0.0267	0	5.5	5.5	5.5	0.713	0.445	0.020	0.651
8	0.1575	0.365	0.0267	0.2	0	0	0	1.033	0.667	0.079	0.731
9	0.1575	0.365	0.0267	0.5	0	0	0	1.033	0.667	0.079	0.731
10	0.2941	0.255	0.0267	0.2	0	0	0	1.026	0.658	0.077	0.730
11	5	3	1	0.2	0	0	0	0.793	0.483	0.030	0.675
12	0.2941	0.255	0.0400	0.2	0	0	0	1.026	0.658	0.077	0.730
13	0.2941	0.255	0.0400	0.2	0.24	0.242	0.216	1.006	0.636	0.072	0.727
14	0.2941	0.255	0.0400	1.5 (but 1 for EE2)	0.24	0.242	0.216	1.006	0.636	0.072	0.727
15	0.2941	0.255	0.0400	1.5 (but 1 for EE2)	3.5	0.242	0.216	0.884	0.531	0.044	0.702

Shaded cells = base case conditions (conservative approach, transport conditions only). No statistical significant differences (ANOVA, p=0.596. α=0.05) were detected when the simulations were compared to the base case.

Table S3.9. Normality test results for the correlation coefficient study

Site	Measured data W-Statistic	*p* value, Normal (Y/N)	Predicted data W-Statistic	*p* value, Normal (Y/N)
BPT	0.967	0.009, N	0.933	<0.001, N
WMR	0.992	0.987, Y	0.958	0.117, Y
FPT	0.943	0.060, Y	0.953	0.124, Y
BLR	0.964	0.003, N	0.936	<0.001, N
EIT	0.954	0.006, N	0.752	<0.001, N
PT1	0.956*	0.010, N	0.978	0.192, Y

*non-normal correlation test was used for subsequent analysis.

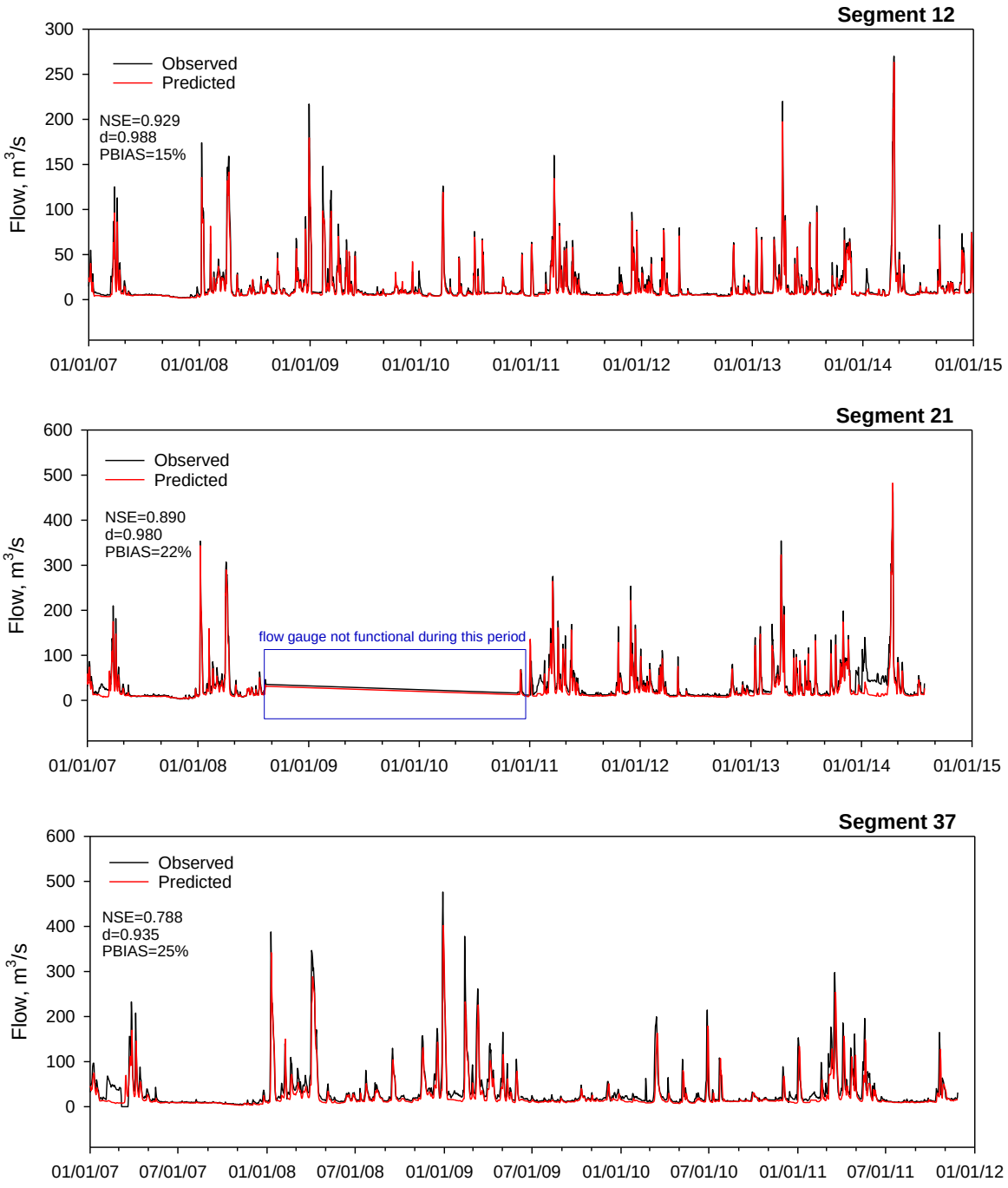

Figure S3.1. Comparison of observed and measured flows at three sites located in the upstream, middle and downstream reaches of the modeled river network.

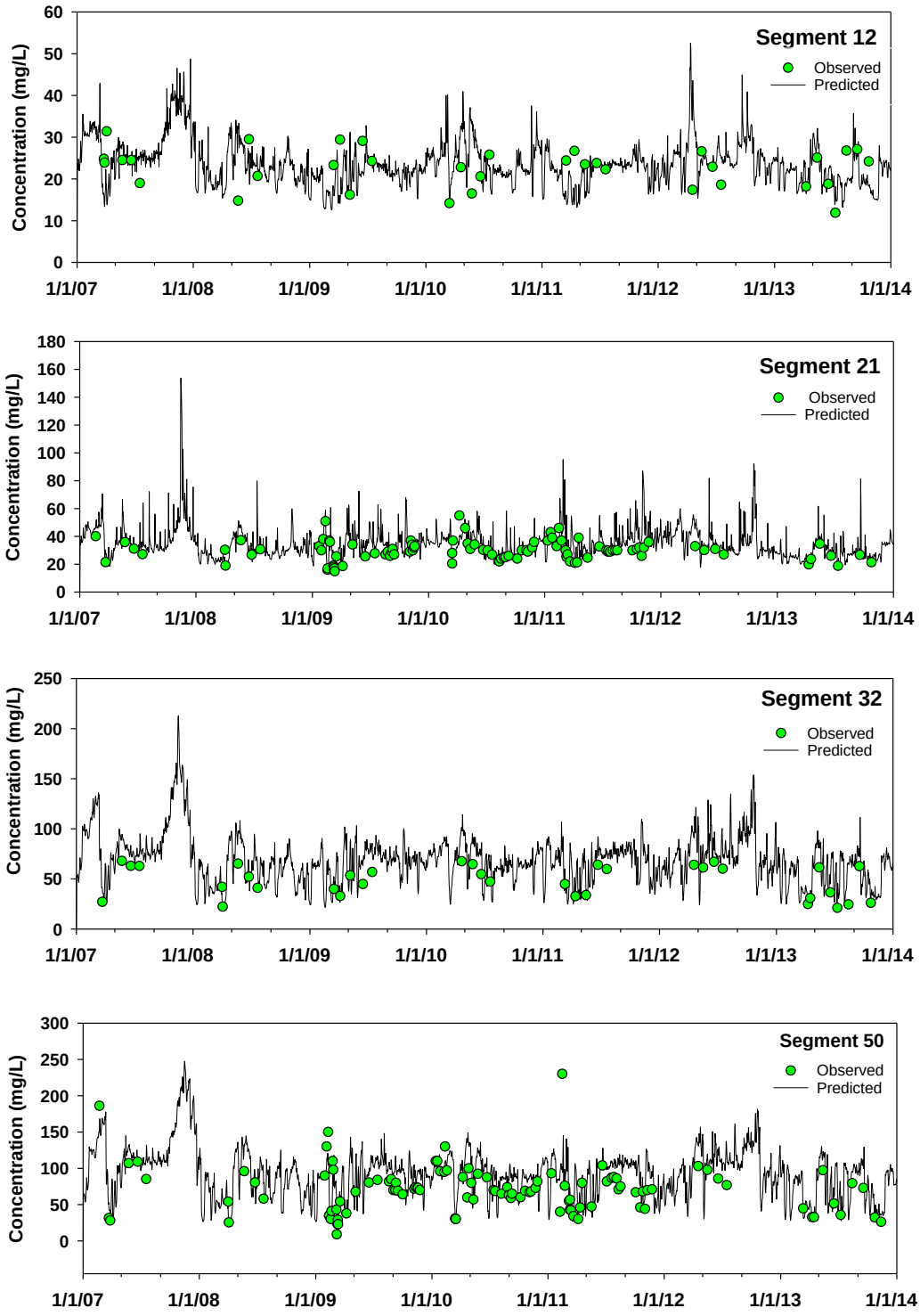

Figure S3.2. Predicted and measured chloride concentrations for four calibration sites (far-field locations).

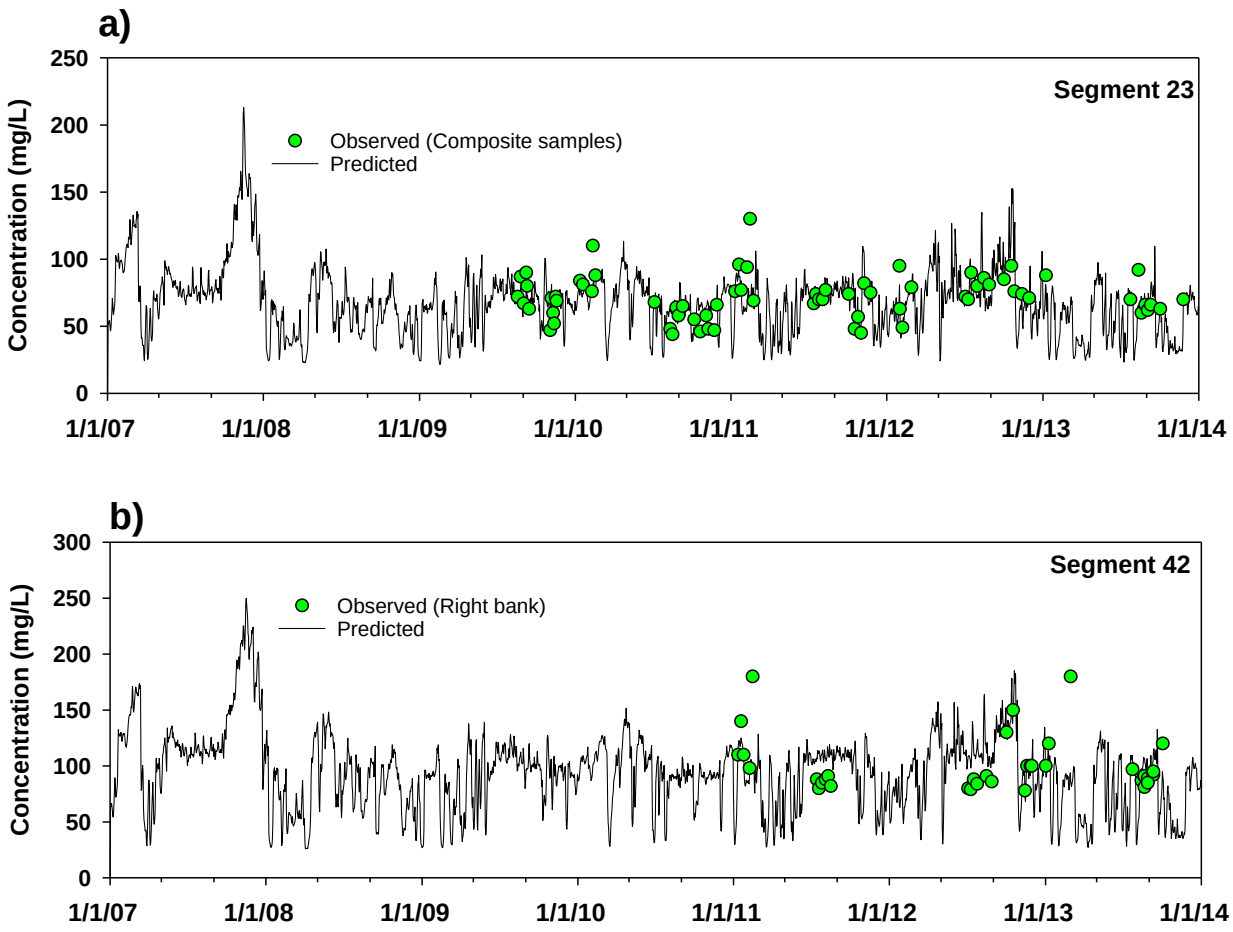

Figure S3.3. Predicted and observed concentrations for sites downstream of WWTPs (near-field sites). The observed data for segment 23 are composite samples that were collected by combining samples from the left, middle, and right regions of the river.

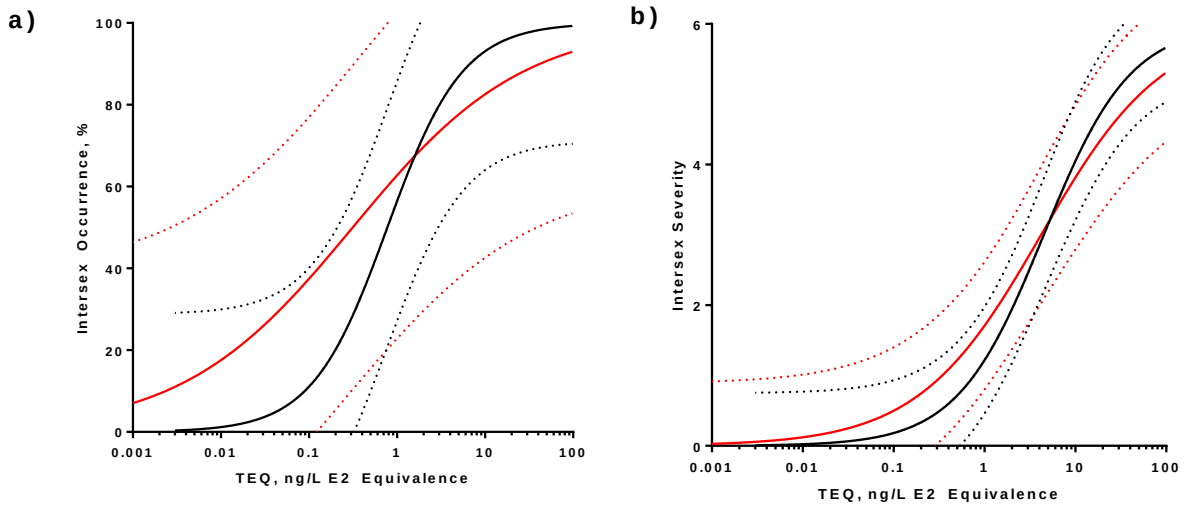

Figure S3.4. Predicted (a) incidence and (b) severity of base case simulation (black line) and the simulation using unrealistically high biodegradation and photolysis rate.

Appendix C

Supplementary Data for Chapter 4

Table S4.1 Optimized MS/MS parameters and detection limits for the analysis of target compounds (regular standards) in addition to values reported by Arlos et al. (2016a).

Compound	IDL* (µg/L)	Q1	Q3	Polarity	DP	EP	CEP	CE	CXP
Atrazine	1	216.00	174.300	+	66.9	3.8	13.500	27.00	2.4
Diclofenac	1	293.900	250.00	-	-46.0	-2.5	-22.530	-15.00	-1.7
Gemfibrozil	1	249.100	121.100	-	-55.0	-2.0	-20.873	-17.00	-3.0
Monensin	0.5	693.400	675.400	+	124.7	9.6	29.558	55.90	10.9
Trimethoprim	0.5	291.100	261.200	+	59.00	4.0	12.000	32.00	3.0

*Samples were concentrated via solid phase extraction based on the IDLs (concentration factor = 25). Q1=quadrant 1; Q2=quadrant 2; DP=declustering potential; EP=entrance potential; CEP=collision cell entrance potential; CE=collision energy; CXP=collision exit potential

Table S4.2 Optimized MS/MS parameters used for the analysis of target compounds (deuterated standards).

Compound	Q1	Q3	Polarity	DP	EP	CEP	CE	CXP
Atrazine-d_5	221.100	179.300	+	67.9	4.1	16.334	22.100	3.0
Diclofenac- d_4	298.200	253.800	-	-25.8	-6.9	-22.689	-16.900	-6.1
Gemfibrozil-d_6	255.000	120.700	-	-46.5	-11	-21.091	-19.240	-2.0
Lorazepam*	321.100	275.100	+	60.1	5.1	19.134	32.800	3.0
Trimethoprim-d_3	294.200	126.200	+	59.0	4.0	12.000	38.000	3.0

*Lorazepam was used as an internal standard for monensin.

Table S4.3 Calculated first-order kinetic rate constants for the target compounds (P25 treatment)

	Pseudo first-order kinetic rate constants x 10^{-2} (1/min)							
MeOH (v/v)	0%		0.002%		0.02%		0.20%	
Compound	Mean	STDEV	Mean	STDEV	Mean	STDEV	Mean	STDEV
Atenolol	10.183	1.320	13.657	1.065	0.448	0.127	0.000	0.000
Atorvastatin	13.200	3.874	14.600	2.800	14.133	2.650	12.033	1.210
Atrazine	0.998	0.552	0.968	0.737	0.254	0.094	0.000	0.000
Carbamazepine	5.700	2.404	5.600	1.414	1.200	0.265	0.500	0.100
Diclofenac	7.794	0.668	5.655	0.467	4.756	0.824	0.243	0.207
Fluoxetine	6.100	0.707	5.567	2.312	0.467	0.058	0.488	0.065
Gemfibrozil	16.300	1.782	8.856	1.004	24.023	1.478	7.108	1.293
Ibuprofen	1.719	0.804	1.635	0.860	11.627	1.399	6.643	0.846
Monensin	4.129	0.000	2.726	1.440	20.350	0.592	14.103	1.177
Naproxen	15.783	1.130	15.437	2.266	16.700	1.312	18.700	0.397
Sulfamethoxazole	12.950	1.970	14.470	0.207	16.503	1.633	2.398	1.005
Triclosan	9.596	1.844	6.970	0.121	20.177	1.782	3.968	0.914
Triclocarban	16.560	0.753	15.739	3.508	16.420	1.539	1.941	0.198
Trimethoprim	16.815	0.035	25.280	3.818	2.580	0.573	0.383	0.042
Venlafaxine	16.245	0.955	21.545	1.930	0.310	0.034	0.302	0.017

Note: STDEV = standard deviation

Table S4.4. Calculated first-order kinetic rate constants for the target compounds (TCO treatment)

	Pseudo first-order kinetic rate constants x 10^{-2} (1/min)							
MeOH (v/v)	0%		0.002%		0.02%		0.20%	
Compound	Mean	STDEV	Mean	STDEV	Mean	STDEV	Mean	STDEV
Atenolol	0.133	0.069	0.000	0.000	0.000	0.000	0.000	0.000
Atorvastatin	4.700	0.721	2.367	0.208	2.333	0.058	1.867	0.306
Atrazine	0.000	0.000	0.000	0.000	0.000	0.000	0.000	0.000
Carbamazepine	0.000	0.000	0.000	0.000	0.000	0.000	0.000	0.000
Diclofenac	5.750	1.291	3.435	0.396	1.905	0.239	0.481	0.104
Fluoxetine	0.908	0.076	0.332	0.141	0.723	0.219	0.238	0.049
Gemfibrozil	0.689	0.446	0.318	0.060	0.200	0.099	0.076	0.065
Ibuprofen	0.000	0.000	0.000	0.000	0.000	0.000	0.000	0.000
Monensin	1.796	0.677	1.148	0.050	1.133	0.149	0.856	0.409
Naproxen	6.218	1.511	3.997	0.326	2.936	0.491	1.220	0.074
Sulfamethoxazole	0.556	0.016	0.605	0.084	0.380	0.050	0.000	0.000
Triclosan	0.821	0.106	0.610	0.035	0.440	0.068	0.119	0.039
Triclocarban	0.830	0.276	0.631	0.006	0.503	0.089	0.237	0.031
Trimethoprim	0.860	0.255	1.153	0.204	1.076	0.347	0.245	0.039
Venlafaxine	0.000	0.000	0.000	0.000	0.000	0.000	0.000	0.000

Note: TCO = thermally-chemically oxidized TiO_2 powder; STDEV = standard deviation

Table S4.5 The *p*-values for One-Way ANOVA tests (SigmaPlot, α=0.05). for P25 treatment experiments. Post-hoc tests (multiple comparisons) were conducted when a statistical significance was detected using Holm-Sidak method with an overall statistical significance level of 0.05.

MeOH (%)	**0 vs 0.002**	**0 vs. 0.02**	**0 vs 0.2**	**0.002 vs. 0.02**	**0.002 vs. 0.2**	**0.02 vs. 0.2**
Compound	**Statistical Significance Testing Using One-Way ANOVA**					
Atenolol	Yes	Yes	Yes	Yes	Yes	No
p-value	0.003	<0.001	<0.001	<0.001	<0.001	0.37
Atorvastatin	No	No	No	No	No	No
p-value	0.698	0.698	0.698	0.698	0.698	0.698
Atrazine	No	No	No	No	No	No
p-value	0.066	0.066	0.066	0.066	0.066	0.066
Carbamazepine	No	Yes	Yes	Yes	Yes	No
p-value	0.734	0.021	0.015	0.017	0.014	0.934
Diclofenac	Yes	Yes	Yes	No	Yes	Yes
p-value	0.004	<0.001	<0.001	0.098	<0.001	<0.001
Fluoxetine	No	Yes	Yes	Yes	No	No
p-value	0.883	0.007	0.005	0.01	0.009	0.984
Gemfibrozil	Yes	Yes	Yes	Yes	No	Yes
p-value	0.004	0.003	0.002	<0.001	0.223	<0.001
Ibuprofen	No	Yes	Yes	Yes	Yes	Yes
p-value	0.932	<0.001	0.002	<0.001	0.002	0.002
Monensin	No	Yes	Yes	Yes	Yes	Yes
p-value	0.184	<0.001	<0.001	<0.001	<0.001	<0.001
Naproxen	No	No	No	No	No	No
p-value	0.089	0.089	0.089	0.089	0.089	0.089
Sulfamethoxazole	No	Yes	Yes	No	Yes	Yes
p-value	0.214	0.04	<0.001	0.205	<0.001	<0.001
Triclosan	Yes	Yes	Yes	Yes	No	Yes
p-value	0.046	<0.001	0.003	<0.001	0.053	<0.001
Triclocarban	No	No	Yes	No	Yes	Yes
p-value	0.945	0.935	<0.001	0.898	<0.001	<0.001
Trimethoprim	Yes	Yes	Yes	Yes	Yes	No
p-value	0.004	<0.001	<0.001	<0.001	<0.001	0.142
Venlafaxine	Yes	Yes	Yes	Yes	Yes	No
p-value	0.002	<0.001	<0.001	<0.001	<0.001	0.992

Note: “Yes” suggests significant difference while “No” suggests the opposite.

Table S4.6 The *p*-values for One-Way ANOVA tests (SigmaPlot, α=0.05) for TCO experiments. Post-hoc tests (multiple comparisons) were conducted when a statistical significance was detected using Holm-Sidak method with an overall statistical significance level of 0.05.

MeOH (%)	**0 vs 0.002**	**0 vs. 0.02**	**0 vs 0.2**	**0.002 vs. 0.02**	**0.002 vs. 0.2**	**0.02 vs. 0.2**
Compound	**Statistical Significance Testing Using One-Way ANOVA**					
Atenolol	only 0% showed degradation					
p-value	-	-	-	-	-	-
Atorvastatin	Yes	Yes	Yes	No	No	No
p-value	<0.001	<0.001	<0.001	0.922	0.425	0.355
Atrazine	NR	NR	NR	NR	NR	NR
p-value	-	-	-	-	-	-
Carbamazepine	NR	NR	NR	NR	NR	NR
p-value	-	-	-	-	-	-
Diclofenac	Yes	Yes	Yes	No	Yes	Yes
p-value	0.01	<0.001	<0.001	0.05	0.003	0.035
Fluoxetine	Yes	No	Yes	Yes	No	Yes
p-value	0.005	0.26	0.002	0.025	0.429	0.01
Gemfibrozil	No	No	No	No	No	No
p-value	0.055	0.055	0.055	0.055	0.055	0.055
Ibuprofen	NR	NR	NR	NR	NR	NR
p-value	-	-	-	-	-	-
Monensin	No	No	No	No	No	No
p-value	0.099	0.099	0.099	0.099	0.099	0.099
Naproxen	Yes	Yes	Yes	NO	Yes	NO
p-value	0.03	0.006	<0.001	0.148	0.012	0.063
Sulfamethoxazole	No	Yes	Yes	Yes	Yes	Yes
p-value	0.265	0.005	<0.001	0.002	<0.001	<0.001
Triclosan	Yes	Yes	Yes	Yes	Yes	Yes
p-value	0.011	<0.001	<0.001	0.016	<0.001	0.001
Triclocarban	No	No	Yes	No	No	No
p-value	0.251	0.097	0.007	0.312	0.052	0.16
Trimethoprim	No	No	No	No	Yes	Yes
p-value	0.433	0.51	0.053	0.706	0.01	0.014
Venlafaxine	NR	NR	NR	NR	NR	NR
p-value	-	-	-	-	-	-

Note: "Yes" suggests significant difference while "No" suggests the opposite. NR = no response

Table S4.7 Compound name abbreviations

Compound	Abbreviation
Atenolol	ATEN
Atorvastatin	ATOR
Atrazine	ATZ
Carbamazepine	CBZ
Diclofenac	DCF
Fluoxetine	FLX
Gemfibrozil	GEM
Ibuprofen	IBU
Monensin	MON
Naproxen	NAP
Sulfamethoxazole	SULF
Triclosan	TCS
Triclocarban	TCB
Trimethoprim	TRIM
Venlafaxine	VEN

Table S4.8 Rate of HTPA formation for P25 and TCO at different levels of methanol.

Compound	P25 (µM/min)	TCO (µM/min)
0%	0.713	0.016
0.002%	0.561	0.011
0.02%	0.182	3.0×10^{-3}
0.2%	0.015	0.0

HTPA= hydroxyterephthalic acid

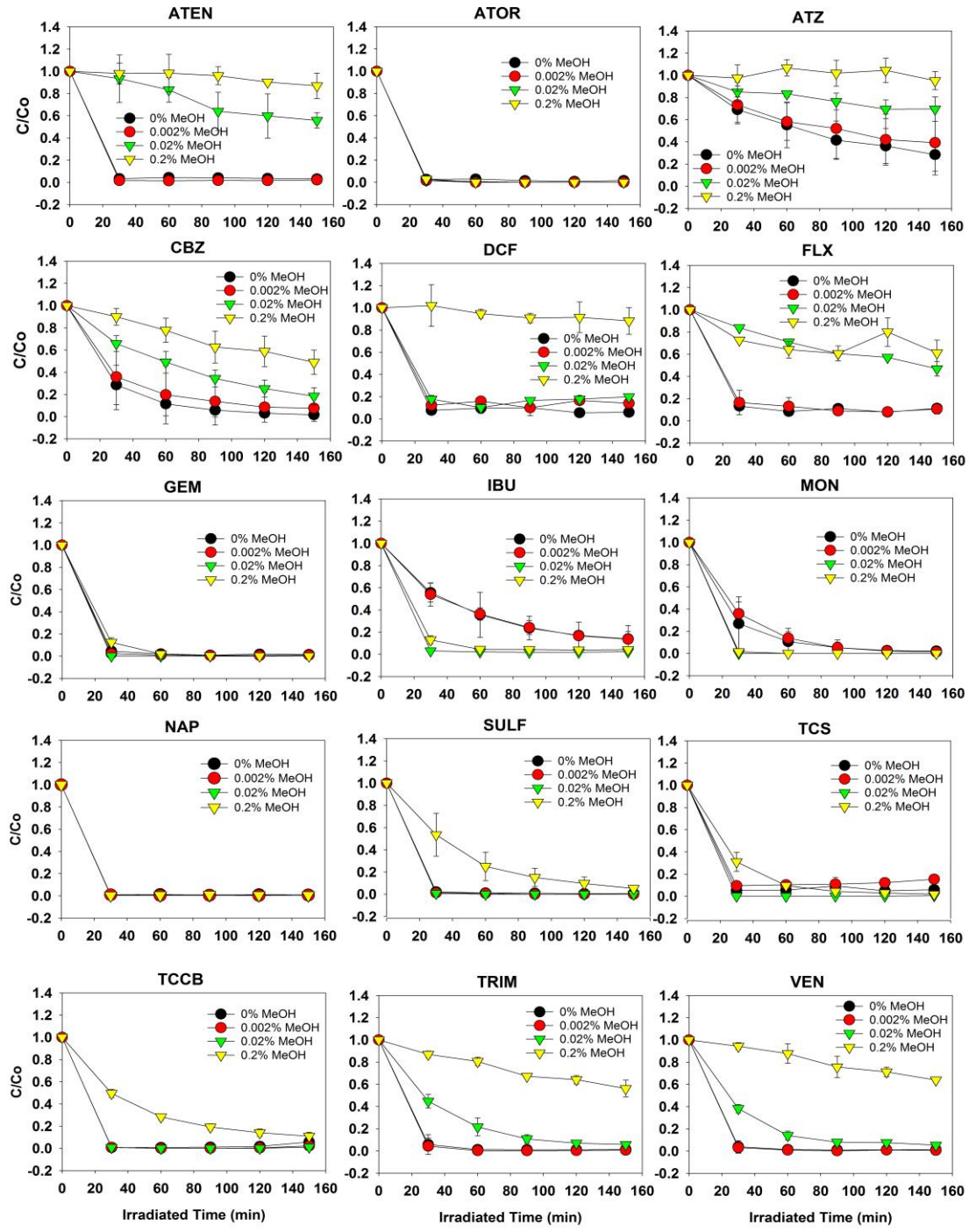

Figure S4.1 Kinetic behavior of all target compounds undergoing P25 treatment. See compound names in Table S4.7.

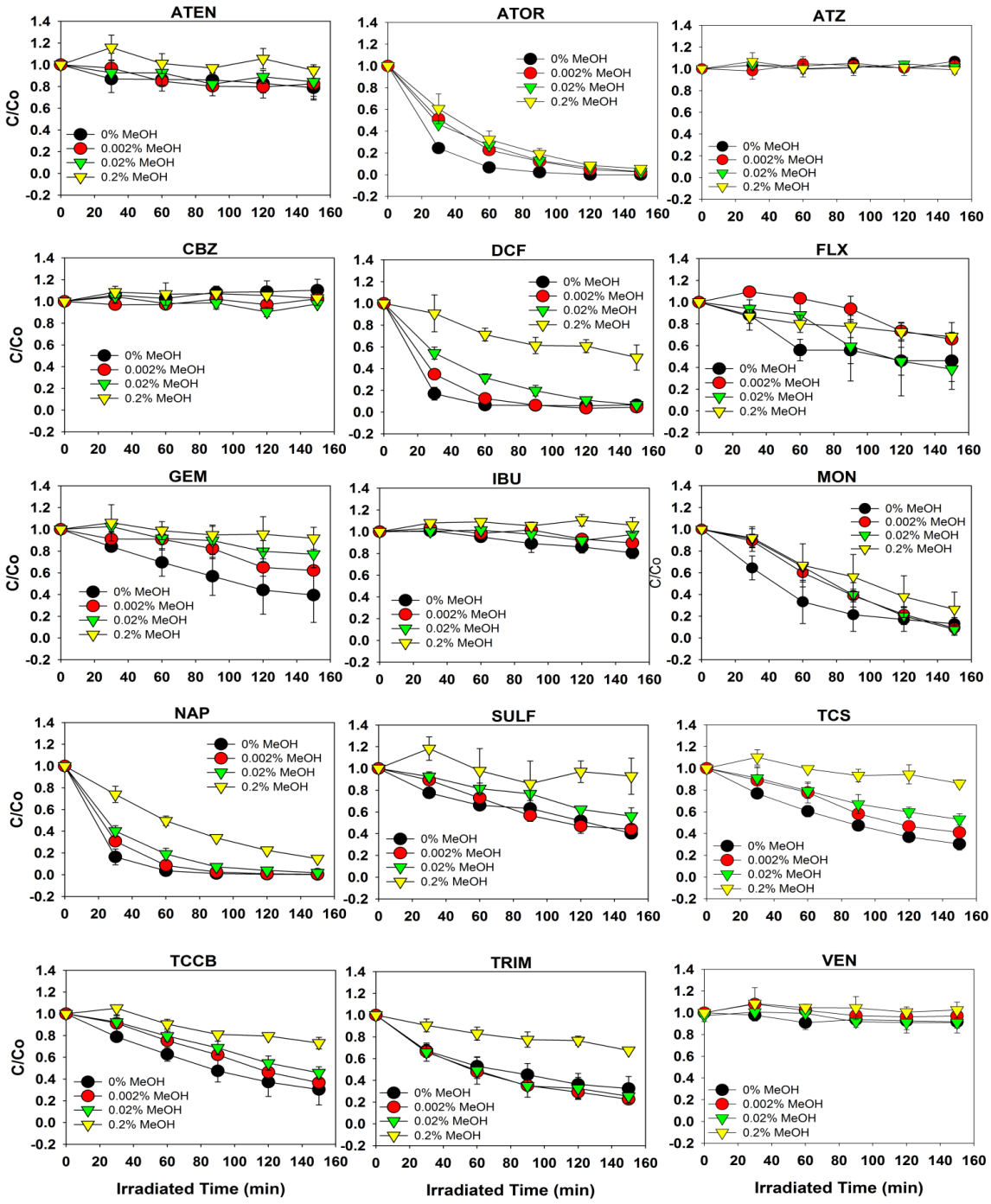

Figure S4.2 Rate of removal of all target compounds undergoing P25 treatment for different concentrations of MeOH. See compound names in Table S4.7.

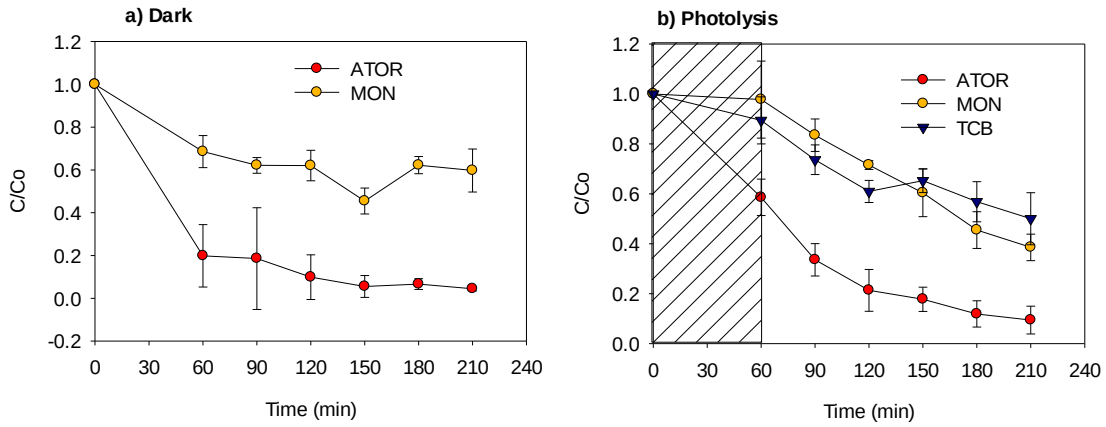

Figure S4.3 Behavior of compounds that were removed via adsorption in the dark and photolysis (UV-LED) only. Only two compounds showed removal in the dark and three for photolysis. Note that the rate constant for atorvastatin undergoing photolysis reactions are not significantly different (p=0.136, one-way ANOVA). The shaded region was the 60-min equilibration period before irradiation. See compound names in Table S4.7.

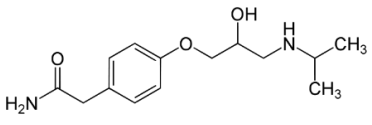
Atenolol

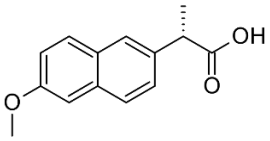
Naproxen

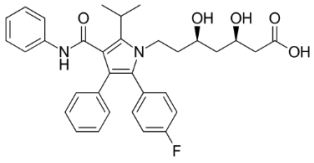
Atorvastatin

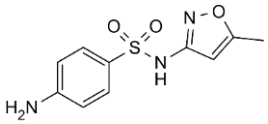
Sulfamethoxazole

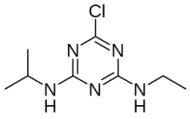
Atrazine

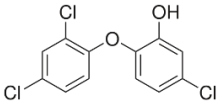
Triclosan

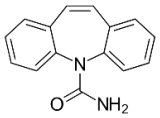
Carbamazepine

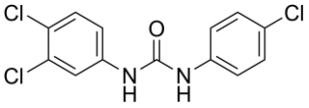
Triclocarban

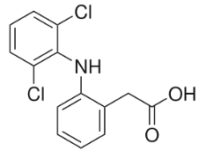
Diclofenac

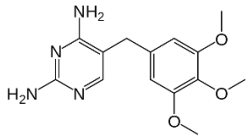
Trimethoprim

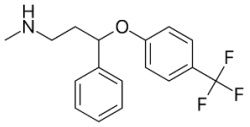
Fluoxetine

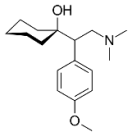
Venlafaxine

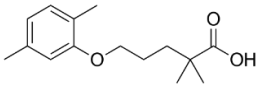
Gemfibrozil

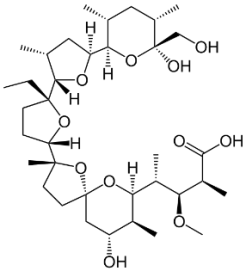
Monensin

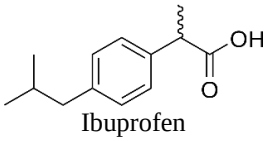
Ibuprofen

Figure S4.4 Chemical structure of compounds included in this study.

Appendix D

Supplementary Data for Chapter 5

Table S5.1 Optimized MS/MS parameters and detection limits for the analysis of target compounds (regular standards).

Compound	IDL* (µg/L)	Q1	Q3	Polarity	DP	EP	CEP	CE	CXP
Pharmaceuticals									
Carbamazepine	1	216.2	174.3	+	55	4.9	14.3	51	2.7
Venlafaxine	1	278.3	58.1	+	38.2	2.9	21.00	42	8
Fluoxetine	3	310.3	44.3	+	48	2.9	12.08	44	7
Atenolol	2	267.2	145.1	+	51	3	30.00	36	5
Sulfamethoxazole	1	254.1	156.2	+	41	3	9.00	22.1	3
Ibuprofen	2	204.9	160.9	−	-41	-2.6	-19.24	-11	-0.5
Atorvastatin	8	559.3	440.2	+	83	5.9	18.91	32	22
Naproxen	3	229.0	170.0	−	-29	-1.9	-20.13	-25	-3.8
Personal care products									
Triclosan	10	286.9	35.0	−	-33	-2	-7	-30	-3
Triclocarban	4	314.8	161.6	−	-50	-3	-12	-20	-13
Metabolites									
10,11 epoxide carbamazepine	1	253.2	180.3	+	26	3.5	20	34	5
Norfluoxetine	10	296.1	134.1	+	23	3	9.5	9	5
p-hydroxy atorvastatin	10	575.2	440.3	+	64	4	19	32	5
o-hydroxy atorvastatin	10	575.2	440.3	+	64	4	19	32	5

*the samples were consequently concentrated via solid phase extraction based on the IDLs (concentration factor = 25)

Table S5.2 Optimized MS/MS parameters used for the analysis of target compounds (deuterated standards).

Deuterated standards	**Q1**	**Q3**	**Polarity**	**DP**	**EP**	**CEP**	**CE**	**CXP**
Carbamazepine- d_5	247.200	204.400	+	60.9	4.3	17.07	28.0	3.3
Venlafaxine- d_6	284.271	64.100	+	44.8	3.3	18.22	45.0	2.4
Fluoxetine- d_5	315.200	44.200	+	50.0	4.0	18.97	38.2	3.1
Atenolol- d_7	274.300	145.200	+	49.8	3.7	41.40	35.6	3.7
sulfamethoxazole- d_4	258.122	160.100	+	54.0	4.0	25.00	37.0	3.0
ibuprofen- d_3	207.900	164.100	−	-24.1	-7.6	-19.35	-10.0	-3.0
atorvastatin- d_5	564.300	445.300	+	45.6	4.0	25.94	30.0	16.0
naproxen- d_3	233.000	16.900	−	-36.8	-2.0	-20.28	-25.7	-1.0
triclosan- d_3	289.900	35.000	−	-28.5	-2.0	-11.31	-25.3	-2.3
triclocarban- d_4	316.900	159.900	−	-50.0	-2.5	-23.38	-18.0	-2.0
10,11 epoxide carbamazepine - d_{10}	263.200	190.300	+	53.0	3.5	20.00	34.0	5.0
Norfluoxetine- d_5	301.200	139.200	+	23.0	3.0	10.00	9.0	5.0
p-hydroxtatorvastatin- d_5	580.200	445.200	+	64.0	4.0	19.00	32.0	5.0
o-hydroxtatorvastatin- d_5	580.200	445.200	+	64.0	4.0	19.00	32.0	5.0

Table S5.3 Chromatographic and ionization parameters used for LC-MS/MS analysis for target analytes.

Ionization conditions	**Positive**	**Negative**
Curtain Gas (psig)	30	10
Collision Gas (psig)	Low	Low
Ion Spray Voltage	5500	-4500
Temperature (°C)	750	750
Ion Source Gas 1	50	60
Ion Source Gas 2	30	40
Chromatographic conditions		
Injection volume (μL)	20	
Solvent A	5 mM ammonium acetate in water	
Solvent B	methanol	
Flow rate (mL/min)	0.8	

Mobile Phase Gradient

For pharmaceuticals in positive mode, the mobile phase gradient began at 80% B and was ramped to 100% B over a 4.5 min period where it was held constant for 1 min. The initial negative mobile phase for pharmaceuticals gradient was 60% B which was then increased to 100% B over an 8 min period where it was held constant for 0.5 min. Column re-equilibration was done for 8 min at the end of the run.

Appendix E

Supplementary Data for Chapter 6

Table S6.1. Optimized conditions for chromatographic separation and electron spray ionization.

Chromatography Conditions	
Flow Rate (mL/min)	0.3
Injection volume (µL)	5
Mobile Phase A	water with 0.5 mM ammonium fluoride
Mobile Phase B	acetonitrile
Re-equilibration time (min)	8 min included in 20 min method
Endtime (min)	20.1
Gradient	The mobile phase gradient began at 10% B and was ramped to 95% B over a 10 min period where it was held constant for 2 min. Column equilibration followed for 8 min with 10% B.
Ionization Conditions	
Gas Temp (°C)	250
Gas Flow (L/min)	10
Nebulizer (psi)	30
Sheath Gas Temp (°C)	350
Sheath Gas Flow (L/min)	11
Capillary Voltage (V)	4000
Nozzle Voltage(V)	2000

Table S6.2 Optimized MRM parameters for LC-MS/MS analysis of estrogenic compounds including their corresponding deuterated standards.

Compound Name	Precursor Ion	Product Ion	RT (min)	Frag (V)	CE (V)	CAV (V)
BPA	227.3	212.3	8.036	128	14	4
	227.3	133.2	8.036	128	26	4
BPA-d_{16}	241.3	223.3	8.036	140	16	4
	241.3	142.2	8.036	140	24	4
E1	269.4	145.1	8.722	155	38	4
	269.4	143.1	8.722	155	45	4
E1-d_2	271.2	145.1	8.722	200	42	4
	271.2	143.1	8.722	200	42	4
E2	271.4	145.1	8.189	200	40	4
	271.4	143.1	8.189	200	56	4
E2-d_4	275.5	187.2	8.189	147	34	4
	275.5	145.3	8.189	147	40	4
E3	287.4	171.2	6.360	170	30	4
	287.4	145.1	6.360	170	38	4
E3-d_3	290.2	287.4	6.360	147	38	4
	290.2	145.3	6.360	147	50	4
EE2	295.4	158.9	8.600	170	32	4
	295.4	144.9	8.600	170	38	4
EE2-d_4	299.4	161.2	8.600	135	34	4
	299.4	147.2	8.600	135	38	4

Note: Two product ions were monitored during quantitation; d = deuterated standard and the subscript corresponds to the substituted hydrogen; RT = retention time; Frag = fragmentor voltage; CE = collision energy voltage; CAV = cell accelerator voltage.

E-1. Quantitation of Analytes

A calibration curve was prepared with concentrations at 0, 0.5, 1, 50, 100, 200, and 500 µg/L using a linear fit with 1/x weighting and no inclusion of the origin. The calibration curves prepared had linear regression correlation coefficients, R^2, varying from 0.997 to 0.999. Analyte confirmation during the quantitation process was carried out by examining the retention times and qualifier/quantifier ratio within ±25 % of the value for each analyte. The instrument detection limit is approximately 0.5 µg/L for E1, E2, E3 and 1 µg/L for EE2 and BPA. SPE concentration factors were designed based on this value. Overall method recoveries ranged from 103 to 116 percent.

E-2. Specific details for the yeast estrogen screen (YES) assay

A colony of yeast cells from a prepared streak plate (less than two weeks old) was incubated at 30°C and shaken at 300 rpm for 18 to 24 h in 1 mL of GOLD media. The cells were then diluted 1:10 in minimal media and were incubated under the same conditions as previously mentioned. Another dilution (1:1 in minimal media) and incubation was completed for 6 hours. Cells were harvested and diluted to an optical density (OD) of 0.03 in 10 mM copper sulfate. At the same time, samples previously prepared (i.e., solvent-exchanged) were dispensed (10 µL) into 2 mL amber glass vials and dried prior to transfer of the diluted cells (200 µL, OD=0.03). A 12-point standard curve was also prepared similarly within each plate with concentrations starting at 1.25×10^{-8} M to 6.10×10^{-12} M. The plates were incubated at 30°C, 300 rpm and exposed to target estrogens from the samples for 18 to 24 hours. The exposed cells (25 µL) were transferred to a 96-well plate, topped with 75 µL minimal media, and read at 660 nm OD using a microplate reader (Molecular Devices, M3) with Softmax Pro Software programmed to a 5 min kinetic mode with readings completed at an interval of 0.25 min. Each well then received 100 µL of 1:1 β-galactosidase: YPER prepared solution of the β-galactosidase kit (Thermo Scientific) and the plate was read at 420 nm OD (30 min kinetic mode, 0.25 min readings). The β-galactosidase production was calculated using this equation: $(1000 \times \Delta OD_{420})/ (\Delta t \times V \times OD_{660})$, where Δt is reaction time (min) and V is the volume of cells plated (µL). Only ODs of 0.02 to 1.0 were included in the analysis as per the β-galactosidase kit's protocol. The standard curve was fitted to a four-parameter logistic equation (SigmaPlot) and was used to determine the corresponding E2 equivalents (µg/L) for all samples. The β-galactosidase response of the samples was ensured to be within the linear range of the logistic curve. The limit of detection of 1.95×10^{-11} M (0.58 µg/L E2 equivalents) was calculated from the lowest concentration in the standard curve that could be

statistically differentiated from the control. The concentration factor and well dilutions described previously were chosen based on this value.

E-3 UV-vis spectra of target estrogens

The UV-vis spectra of target estrogens (100 mg/L, 10:90 v/v methanol: water) were analysed using the Hewlett Packard 8453 UV-vis spectrophotometer and are shown in Figure S6.1. The maximum wavelength of absorption for ethinylestradiol, estrone, estradiol, estriol and bisphenol A were at 287, 293, 289, 278, and 276 nm. The spectra also show that E1, E2, and EE2 can absorb photons at the wavelength that the UV-LEDs are operating (λ=365 nm).

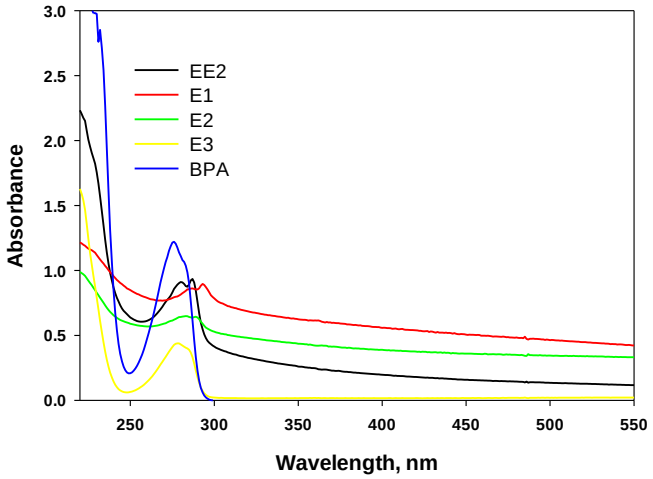

Figure S6.1 UV-vis spectra of target estrogens (100 mg/L).

E-4. Isoelectric point determination for PTT

The material was submitted to Anton-Paar (Ashland, VA) for isoelectric point analysis using their SurPASS solid surface electrokinetic analyzer. The cylinder cell for the SurPASS was used to measure the pIEP using 1 mM of potassium chloride solution as the electrolyte. The instrument provides an auto-titration measurement results (in zeta potential, mV) at different pH conditions (shown below). The pIEP is the pH where the zeta potential is zero (~approximately 6 for PTT).

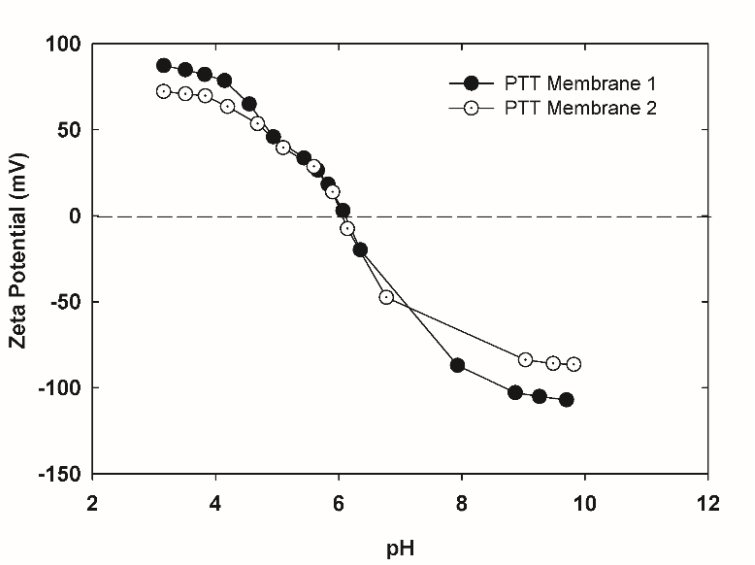

Figure S6.2. Zeta pIEP of PTT material

E-5. Detection of the presence of hydroxyl radicals

Terepthalic Acid (TPA) is an OH radical scavenger that does not react with other reactive oxygen species (superoxide, hydrogen peroxide). Under the presence of OH radicals, TPA can undergo a reaction producing 2-hydroxyterephthalic acid (HTPA) via:

$$C_6H_4(COOH)_2 + {}^{\bullet}OH \Longrightarrow C_6H_4(COOH)_2OH$$

HTPA fluoresces at around λ=420-425 nm and is independent of pH in the range of 6-11.

The same experimental set up described in the manuscript was used to conduct the test. Each beaker however contained 0.5 mM of TPA dissolved in 6 mM NaOH solution. Aliquots (1 mL) were taken at t=0, 15, 30, 45, 60, 90, 120, 180, 240 and 300 min. The formation of HTPA was monitored using fluorescence measured from the SpectraMax M3 plate reader (Molecular Devices). The samples were plated in a black 96 well plate (Costar, Corning) and were excited at 315 nm and the emission spectra were taken from 350-550 nm at 5 nm interval. A separate HTPA standard curve was included in the plate to quantify the amount of HTPA formed during the irradiation of PTT thin films. The standard curve (Figure S6.4) was generated using the intensities taken from the peak emission wavelength of each spectrum (Figure S6.3).

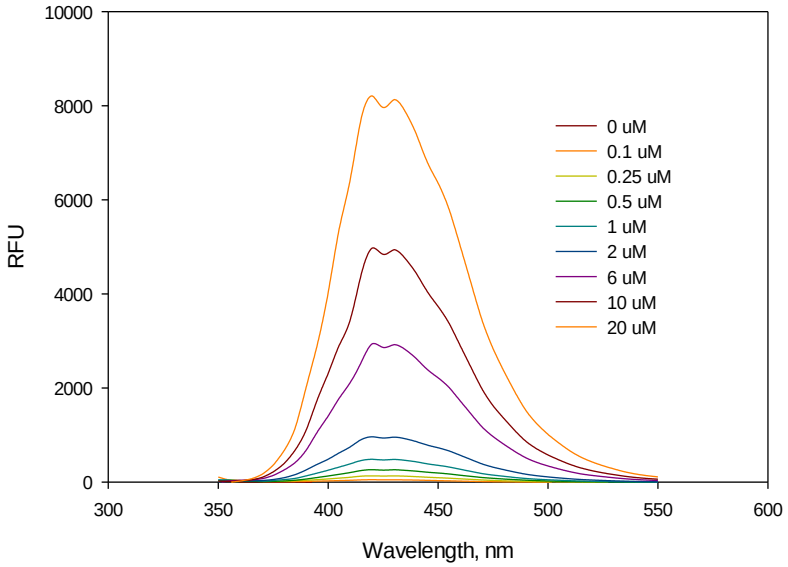

Figure S6.3. Fluorescence spectra of known HTPA concentrations (0 µM to 20 µM)

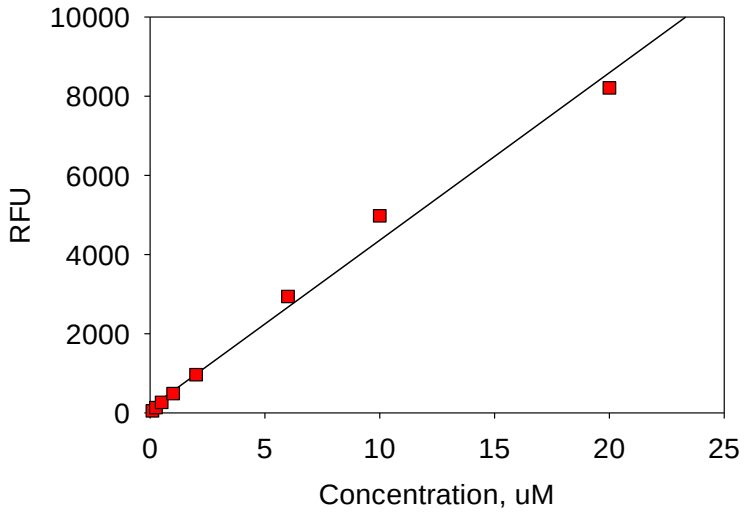

Figure S6.4. Standard Curve for HTPA.